THE UNIVERSITY *of* EDINBURGH

Liquid Acrylic Resin-Based Composites for Marine and Renewable Energy Applications

Machar Laurie Devine

THE UNIVERSITY
of EDINBURGH

A thesis presented for the degree of

Doctor of Philosophy

February 2025

Abstract

Rapid growth in the installation of wind and tidal turbines has caused increasing usage of polymer composite materials to manufacture the blades, but the current use of non-recyclable thermoset materials makes composite waste a growing problem. The development of recyclable alternatives to traditional thermoset matrices, or new techniques for recycling these materials, is therefore a necessity. While established high-performance thermoplastics such as polyether ether ketone (PEEK) are recyclable and have excellent mechanical properties, leading to their use in the aerospace industry, the high temperatures and pressures needed to process them make their use in wind and tidal turbine blades prohibitively expensive. Recyclable alternatives should therefore be processable via vacuum infusion, which is commonly used with thermoset resins in the manufacture of wind and tidal turbine blades. Room temperature infusible acrylic resins, known commercially as Elium®, are one such family of promising recyclable resins, and are currently the only commercially available 'drop-in' thermoplastic alternative for the marine and renewable energy sectors.

Since liquid acrylic resins are relatively new to the market, several aspects of their use remain uncertain. For example, if acrylic-matrix composites are to be used in the tidal stream energy and marine sectors, they must be able to withstand long-term immersion in seawater without significant losses in mechanical properties. While published studies on water absorption in acrylic-matrix composites often rely on multi-compatible or other non-tailored fibre sizing agents, it has been suggested that improvements to the mechanical properties and water absorption behaviour of these composites may be gained with a sizing agent tailored specifically to acrylic resins. Additionally, beyond being simply a recyclable replacement to traditional thermosets, acrylic resins create opportunities to improve the manufacturing of wind and tidal turbine blades. Since acrylic is a thermoplastic, it can be welded instead

of adhesively bonded, which may result in faster manufacturing with stronger, more resilient bonds.

Several aspects of acrylic resins relevant to marine and renewable energy applications are therefore explored in this thesis. Firstly, accelerated seawater ageing is applied to glass-fibre reinforced acrylic (GF/acrylic) and PPE-modified acrylic (GF/acrylic-PPE) composites, as well as to a traditional GF/epoxy baseline. The static mechanical properties (tensile, flexural, and short beam) are compared before and after ageing, and electron microscopy of the fracture surfaces to determine the effects of water ingress on fracture propagation. The diffusion coefficients of water in GF/acrylic (1.8×10^{-12} m^2 s^{-1}) and GF/acrylic-PPE (3.4×10^{-12} m^2 s^{-1}) were an order of magnitude larger than that of GF/epoxy (0.16×10^{-12} m^2 s^{-1}), and analysis showed this would correspond to greater penetration of water into acrylic-matrix tidal turbine blades.

The tension-tension fatigue resistance of 0° GF/acrylic coupons with an acrylic-tailored sizing is then characterised, both in dry and water-saturated conditions. Comparisons are made to the performance of GF/acrylic composites with a multi-compatible sizing agent to investigate the necessity of acrylic-tailored sizing agents. Water saturation was found to decrease the low-cycle fatigue performance of the composite, but performance was more similar in the high-cycle fatigue to which wind and tidal turbine blades are subject. For example, at 2×10^2 cycles, ageing reduced the fatigue strength by 21%, but this decrease was 14% at 2×10^5 cycles. Differences in static and low-cycle fatigue performance were also observed between the acrylic-tailored and multi-compatible composites—for example a 12% lower dry UTS with the tailored reinforcement—likely due to differences in the fibre diameter and tow size, but their performance was again similar in high-cycle fatigue.

A novel method of joining acrylic-matrix composites is also explored. The solubility of acrylic polymer in its own liquid monomer creates the opportunity to 'weld' acrylic-matrix (Elium®) composites without the application of heat. In this method, termed resin welding, acrylic monomeric resin is infused between acrylic-matrix composite parts. The resin dissolves and diffuses into the acrylic matrix and creates a continuous material, and a strong bond, when it polymerises, without the sensitivities of traditional welding methods to adherend or bondline thickness. Sin-

gle lap shear testing was conducted on resin-welded and adhesively bonded coupons with varying bondline thicknesses and filling fibres, and the bonding and fracture mechanisms were investigated using scanning electron microscopy and the diffusion of dyed acrylic resin. High strengths and low sensitivity to bondline thickness were observed, with the highest bond strength of resin-welded coupons reaching 27.9 MPa, which is 24% higher than the strongest weld reported in the literature. This indicates that resin welding is a promising alternative to traditional bonding and welding methods for acrylic-matrix composites.

Lay Summary

Wind and tidal turbine blades are the parts of the turbine which capture energy from the wind/tidal flow, and cause the turbine to turn and generate electricity. They need to be strong, stiff, lightweight, and corrosion resistant, which means that metals like steel cannot be used to make them. Instead, composite materials are used. These are materials which are made of a fibre reinforcement such as glass or carbon fibre mixed with a plastic, to combine the benefits of both materials. Readers may be familiar with composite materials as the 'fibreglass' which is used to make, for example, baths and leisure yachts.

The problem is that the plastics which are currently used to make the composite materials in turbine blades and yachts are not recyclable. Recyclable plastics—such as in plastic bottles or food packaging—can be melted and reshaped, but those currently used in blades cannot. This leads to old wind and tidal turbine blades being landfilled or incinerated, rather than recycled.

New recyclable composite materials have therefore been developed, and one of these is made using 'liquid acrylic resin'. Acrylic is a recyclable plastic which is chemically similar to Perspex windows and acrylic nails, but has been shown to perform very well when used in composite materials. However, since these acrylic composite materials are relatively new, there is much we don't know about them. For example, do they last as long as traditional materials when exposed to seawater? Do they need specialised fibre reinforcements, or do they bond well to the reinforcements already in use? And can we create new ways to join acrylic composite parts which could be used to manufacture wind turbine blades?

In this thesis, studies are performed to answer these three questions. Firstly, acrylic composite coupons are exposed to seawater, and its effects on their strength and stiffness are measured. Additionally, additives are mixed with the acrylic to

determine if its properties can be further improved. These results are compared with a traditional non-recyclable composite material, which would be found in wind turbines today, with positive results.

In another set of experiments, a new reinforcement specially made to be compatible with acrylic is compared to a multi-compatible reinforcement. This was performed by comparing the durability of acrylic composites made with each reinforcement, before and after exposure to seawater. The results showed that the multi-compatible reinforcement performed very well, and that specialised reinforcements may not be needed.

Finally, a new method of joining acrylic composite parts is developed, using liquid acrylic resin instead of adhesives to create a bond. These bonds were measured to be stronger than adhesives, and even conventionally welded bonds. The results also suggested that the method could be applied to large structures such as wind turbine blades.

Acknowledgements

I would firstly like to acknowledge my supervisor, Prof. Dipa Roy, who has been not only a source of expertise and guidance, but also support and encouragement. I would also like to thank my second supervisor, Prof. Conchúr Ó Brádaigh, for his sound advice. I am grateful to them both for making every meeting something to look forward to, which I do not take for granted.

I would like to acknowledge with thanks the EPSRC Centre for Doctoral Training in Wind and Marine Energy Systems and Structures (CDT-WAMSS, EP/S023801/1) for providing funding and support, the University of Edinburgh EPSRC IAA for funding received through block grant EP/R511687/1, and to the Supergen ORE Hub for funding received through the Flexible Fund Award FF2021-1014. I would also like to thank Arkema GRL and Johns Manville for the provision of materials and support, and TWI for performing ultrasonic welding and providing advice.

Finally I would like to thank the Edinburgh University Composites Group for being the collaborative community that it is—the work in this thesis would not be possible without these colleagues and friends. In particular I would like to thank Dr Ankur Bajpai, Dr James Maguire and Dr James Quinn for the support and training they provided, and Mr John Blackhurst and Mr Eddie Monteith for being able to solve any problem, technical or not. I would also like to thank Mx. Kit O'Rourke, Dr Helena Pérez Martín, Ms Ione Smith and Dr Catherine Megregian for being the brightest part of any day.

List of Publications

A list of published works, or manuscripts under review/preparation, is presented below. Work from the first-author publications make up Chapters 4 and 6, as indicated below, and the other publications are summarised in Appendix A. Elements from each paper have been included in the literature review in Chapter 2.

First Author Publications

Chapter 4

Devine, M., Bajpai, A., Obande, W., Ó Brádaigh, C. M., & Ray, D. (2023). Seawater ageing of thermoplastic acrylic hybrid matrix composites for marine applications. Composites Part B: Engineering, 263, 110879. https://doi.org/10.1016/j.compositesb.2023.110879

Chapter 6

Devine, M., Bajpai, A., Ó Brádaigh, C. M., & Ray, D. (2024). 'Resin welding': A novel route to joining acrylic composite components at room temperature. Composites Part B: Engineering, 272, 111212. https://doi.org/10.1016/j.compositesb.2024.-111212

Other Relevant Publications

Appendix A.1

Stankovic, D., Obande, W., Devine, M., Bajpai, A., Ó Brádaigh, C. M., & Ray, D. (2024). Accelerated seawater ageing and fatigue performance of glass fibre reinforced thermoplastic composites for marine and tidal energy applications. Composites Part C: Open Access, 14, 100470. https://doi.org/10.1016/j.jcomc.2024.100470

Appendix A.4

Bolluk, A., Devine, M., Quinn, J. A., & Ray, D. (2024). Repair of acrylic/glass composites by liquid resin injection and press moulding. Composites Part B: Engineering, 281, 111513. https://doi.org/10.1016/j.compositesb.2024.111513

Contents

List of Figures

List of Tables

Abbreviations

ANOVA analysis of variance.

AS acrylic sizing.

CF carbon fibre.

CT computed tomography.

DCB double cantilever beam.

DIC digital image correlation.

DMA dynamic mechanical analysis.

DSC differential scanning calorimetry.

FF flax fibre.

FVF fibre volume fraction.

GF glass fibre.

GF/acrylic glass fibre reinforced acrylic.

GF/acrylic-PPE glass fibre reinforced acrylic-PPE.

GF/epoxy glass fibre reinforced epoxy.

IFSS interfacial shear stress.

IPN interpenetrating polymer network.

MCS multi-compatible sizing.

MMA methyl methacrylate.

NMR nuclear magnetic resonance.

PA6 polyamide 6.

PALS positron annihalation lifetime spectroscopy.

PBT polybutylene terephthalate.

PDMS polydimethylsiloxane.

PEEK polyether ether ketone.

PMMA polymethyl methacrylate.

PPE poly phenylene ether.

PPS polyphenylsulfone.

QENS quasi-elastic neutron scattering.

RRV resin rich volume.

SBS short beam strength.

SEM scanning electron microscopy.

TRL technology readiness level.

UD unidirectional.

UTS ultimate tensile strength.

Chapter 1

Introduction

The late 1800s saw the advent of the generation of electricity from wind, with the first wind turbine in operation being created in 1887 by Scottish inventor James Blyth, and driven by canvas sails [1, 2]. Steel, or occasionally aluminium, was the next material of choice for wind turbine blades, but by the 1970s 'modern' wind turbines with blades made of fibre-reinforced polymer composite materials—hereafter referred to simply as *composites* or *composite materials*—became the norm [3, 4]. These blades were often manufactured via hand lay up with polyester resins, but manufacturing has since progressed, and the latest wind turbine blades are commonly manufactured via the vacuum infusion of epoxy resins [3–5].

A similar pattern can be seen in the marine industry, with composites being used in almost all leisure yachts, and interest is growing in the creation of composite cargo ships to lower weight and reduce maintenance costs [6, 7]. In the marine energy sector, tidal turbines occasionally had metallic blades in the initial stages of their development [8], but modern tidal turbines have followed in the footsteps of the wind industry and typically use composites [7]. Even some wave energy converters, such as CorPower's C4, are made from composite materials. This range of applications is illustrated in Figure 1.1, and shows the importance of composite materials to the renewable energy and marine sectors.

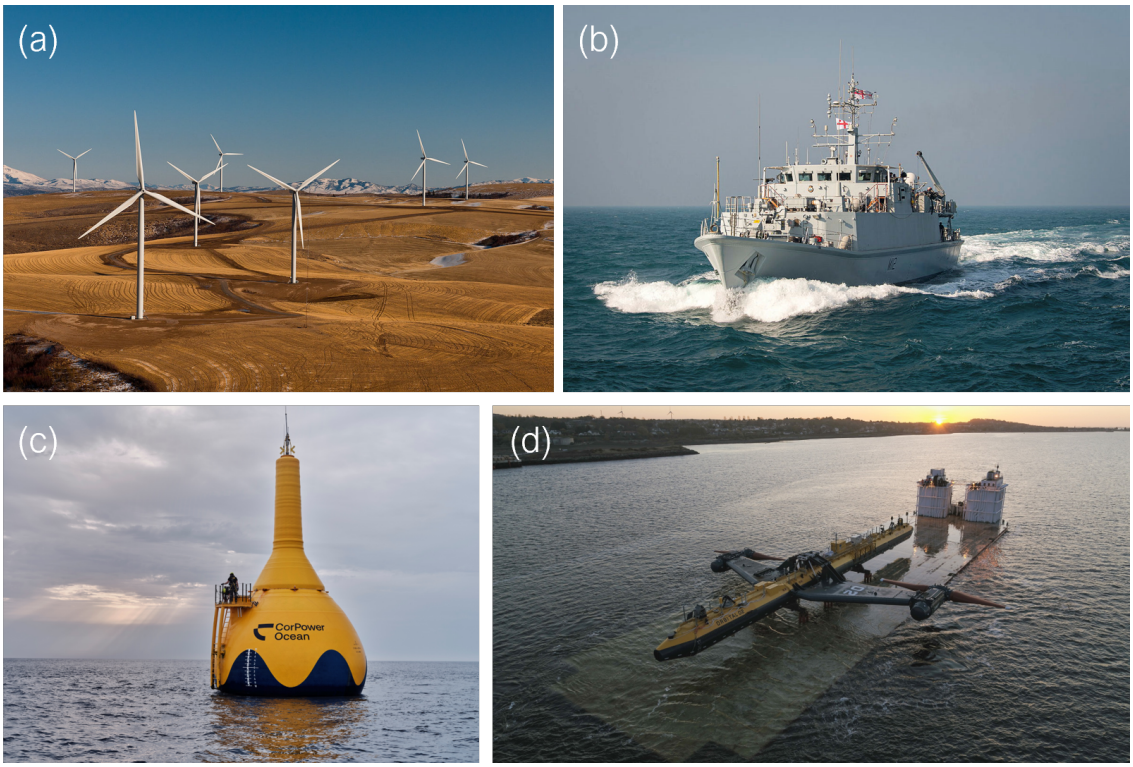

Figure 1.1: *Examples of the applications of composite materials in the marine and renewable energy industries. (a) Nordex N100 wind turbines with composite blades and a rotor diameter of 100 m. Source: U.S. Department of Energy. (b) HMS Shoreham Sandown-class minehunter with glass-fibre composite hull. Source: UK Ministry of Defence © Crown copyright. (c) CorPower C4 wave energy converter made from glass-fibre reinforced polymer. Source: CorPower. (d) Orbital O2 floating tidal turbine, with composite blades. Source: Orbital Marine Power.*

The use of these composite materials reduces weight and improves efficiency, but unlike steel the thermosetting composites in use today are not easily recyclable. Therefore, as the use of composites increases, so does the amount of composite waste produced [9]. Interest in recyclable composites is therefore growing due to a need for sustainability in the renewable energy and marine sectors. These environmental pressures have caused several wind turbine manufacturers and developers to investigate recyclable resins, and pledge to manufacture recyclable blades by as early as 2030 [10–12].

Of the recyclable resins that are available, one forerunner is the family of monomeric liquid acrylic resins marketed as Elium® by Arkema. Much research has been published on acrylic-matrix composites in recent years [13–15], and results have been

positive enough to test the resin in full-scale 62 m wind turbine blades [16]. These liquid acrylic resins are only a decade old at the time of writing, and aren't as well understood as the thermoset resins which have been used for decades. As a result, continued investigation of their behaviour in renewable energy and the marine environment is essential if these recyclable resins are to be adopted commercially. The properties of acrylic-matrix composites prepared using liquid acrylic resins are therefore studied in this thesis, with the aim of facilitating the use of recyclable composites.

1.1 Thesis Outline

This thesis investigates acrylic-matrix composites with a focus on marine and renewable energy applications such as tidal turbines, wind turbines and marine vessels, in which composites play a significant role. The use of acrylic-matrix composites in the renewable energy and marine industries is first discussed in a literature review. This is followed by three research chapters: a chapter on water absorption in acrylic-matrix composites, another on the effect of a specialised sizing agent on water absorption and fatigue performance, and a final research chapter on the joining of acrylic-matrix composites.

Together, these research chapters provide insight into the practical application of liquid acrylic resin at multiple stages across the product life cycle, from reinforcement selection and manufacturing methods to in-service performance. These chapters are partially based on published work, as detailed previously and in Appendix C. Work which was performed in parallel with the aforementioned studies, in collaboration with other researchers, is presented in Appendix A.

1.2 Chapter References

[1] Trevor J. Price. James Blyth — Britain's first modern wind power pioneer. *Wind Engineering*, 29(3):191–200, 2005. doi: 10.1260/030952405774354921.

[2] J. F. Manwell, J. G. McGowan, and A. L. Rogers. *Introduction: Modern Wind*

Energy and its Origins, pages 1–22. 2009. ISBN 9781119994367. doi: https://doi.org/10.1002/9781119994367.ch1.

[3] J. F. Manwell, J. G. McGowan, and A. L. Rogers. *Wind Turbine Materials and Components*, pages 257–309. 2009. ISBN 9781119994367. doi: https://doi.org/10.1002/9781119994367.ch6.

[4] L. Mishnaevsky, K. Branner, H. N. Petersen, J. Beauson, M. McGugan, and B. F. Sorensen. Materials for wind turbine blades: An overview. *Materials (Basel)*, 10(11), 2017. ISSN 1996-1944 (Print) 1996-1944 (Linking). doi: 10.3390/ma10111285.

[5] Oliver Nixon-Pearson, Peter Greaves, Dimitrios Mamalis, and Lewis Stevenson. Wind turbine blades design and manufacturing, current state-of-the art literature review. Report, 2022.

[6] N. H. Nash, A. Portela, C. I. Bachour-Sirerol, I. Manolakis, and A. J. Comer. Effect of environmental conditioning on the properties of thermosetting- and thermoplastic-matrix composite materials by resin infusion for marine applications. *Composites Part B: Engineering*, 177, 2019. ISSN 13598368. doi: 10.1016/j.compositesb.2019.107271.

[7] John Summerscales, Jasper Graham-Jones, and Richard Pemberton. *Marine Composites : Design and Performance*. Woodhead Publishing series in composites science and engineering. Woodhead Publishing, Cambridge, MA, 2018. ISBN 9780081019139.

[8] Verdant Power LLC. Pilot license application roosevelt island tidal energy project ferc no. 12611, 2010. URL `https://elibrary.ferc.gov/eLibrary`.

[9] P. Liu and C. Y. Barlow. Wind turbine blade waste in 2050. *Waste Management*, 62:229–240, 2017. ISSN 1879-2456 (Electronic) 0956-053X (Linking). doi: 10.1016/j.wasman.2017.02.007.

[10] Ørsted. Ørsted commits to sustainable recycling of wind turbine blades, 2021. URL `https://orsted.com/en/media/news/2021/06/702084352457649`.

[11] Vestas. Zero-waste, 2024. URL https://www.vestas.com/en/sustainability/environment/zero-waste.

[12] Siemens Gamesa. Commanding circularity: Siemens gamesa announces recyclableblade for onshore wind power projects, 2022. URL https://www.siemensgamesa.com/global/en/home/press-releases/092222-siemens-gamesa-press-release-onshore-recyclable-blade.html.

[13] Winifred Obande, Dimitrios Mamalis, Dipa Ray, Liu Yang, and Conchúr M. Ó Brádaigh. Mechanical and thermomechanical characterisation of vacuum-infused thermoplastic- and thermoset-based composites. *Materials and Design*, 175, 2019. ISSN 02641275. doi: 10.1016/j.matdes.2019.107828.

[14] Winifred Obande, Conchúr M. Ó Brádaigh, and Dipa Ray. Continuous fibre-reinforced thermoplastic acrylic-matrix composites prepared by liquid resin infusion – a review. *Composites Part B: Engineering*, 215, 2021. ISSN 13598368. doi: 10.1016/j.compositesb.2021.108771.

[15] David Snowberg, Derek Berry, Dana Swan, Zhang Mingfu, Steve Nolet, Douglas Adams, Johnathan Goodsell, Dayakar Penumadu, and Aaron Stebner. Iacmi project 4.2: Thermoplastic composite development for wind turbine blades. Report, Institute for Advanced Composites Manufacturing Innovation, 2021-12-07 2021.

[16] IRT Jules Verne. Zebra project achieves key milestone with production of the first prototype of its recyclable wind turbine blade, 2022. URL https://www.irt-jules-verne.fr/wp-content/uploads/zebra-pr-en-vdef.pdf.

Chapter 2

Literature Review

As discussed in Chapter 1, the development of recyclable alternatives to traditional thermoset composites is of growing importance in the renewable energy and marine sectors. Liquid acrylic resins are one such alternative, offering vacuum infusibility and room-temperature processing, which make them promising for use in large structures such as wind and tidal turbine blades or ships. These structures are subject to harsh environments, and so understanding the response of the composites used to construct them is crucial. For example, key considerations are water absorption and its effects on the static properties and fatigue life, and the optimum sizing agents for the resin.

Thermoset resins such as epoxy and polyester have been used in the renewable energy and marine industries for decades, and so these issues are well understood. However, the novelty of liquid acrylic resins means knowledge of their performance is more limited. This literature review therefore explores the potential of liquid acrylic resins in these demanding environments. It begins by discussing the construction of wind and tidal turbine blades, and the available recyclable resins which could feasibly replace thermosets in these structures. The review then discusses specific aspects of composite materials, such as sizing agents, water absorption, fatigue, and the joining of composite parts. For each of these topics, the extensive body of research on traditional composites is first discussed. This is followed by a detailed examination of how acrylic matrix composites perform under similar conditions, with a particular focus on their water ingress behavior, interfacial bonding, fatigue resistance, and bonding methods.

2.1 Composites in Renewable Energy

2.1.1 Manufacture of Wind and Tidal Turbine Blades

Modern, large wind and tidal turbine blades are typically made from glass-fibre reinforced thermoset resins such as epoxy or polyester, with a growing usage of carbon fibre [1–3]. A 'standard' method of manufacturing a wind or tidal turbine blade is to manufacture the high and low pressure blade skins separately via vacuum infusion in clamshell moulds. The skins are then joined together, and to a central composite spar or shear web, using adhesives [2, 4, 5]. This process is detailed in Figure 2.1.

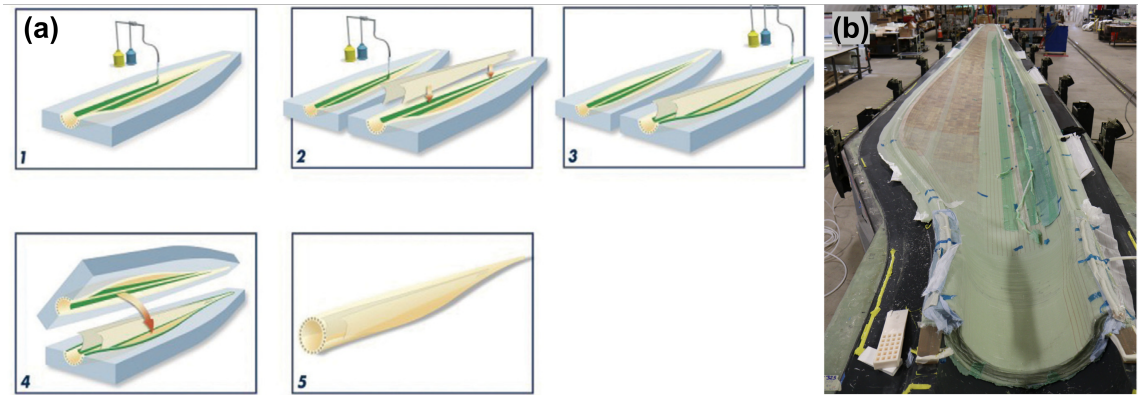

Figure 2.1: *Illustration of a typical blade manufacturing process. (a) Vacuum infusion of the blade skins, attachment of shear web with adhesive then bonding of the second skin. Image from [5]. (b) An image of the low-pressure skin from [4]*

.

Departures from this method are made by several manufacturers. For example, although vacuum infusion is the lowest-cost and most common method of manufacturing wind turbine blades [1], Vestas Wind Systems manufactures their blades from epoxy prepregs [2, 6], which are provided as rolls of reinforcement pre-impregnated with resin. Epoxy prepregs have similarly been used to manufacture tidal turbine blades, as in a 2.5 m long tidal turbine blade manufactured for Verdant Power using GF/epoxy prepregs [7], and tidal turbine blades manufactured in FastBlade, Rosyth from CF/epoxy prepregs [8]. Siemens also deviates from the 'standard' manufacturing method through its IntegralBlade® process, in which wind turbine blades are manufactured as a single piece, reducing weight by avoiding adhesive bonds [9].

There is therefore flexibility in the manufacturing of wind turbine blades, and perhaps even more in tidal turbine blades given their smaller size and less developed supply chains. However, large departures from established manufacturing techniques are likely to require significant investment which may not be acceptable to manufacturers [10].

2.1.2 Disposal of Blades

Increasing wind and tidal turbine installations cause increasing volumes of composite waste both during production and at end of life. A commonly-cited figure is of a total of 43 Mt of blade waste by 2050, according to Liu and Barlow [11], but it is important to note that this analysis is for onshore wind alone. Offshore wind currently generates more energy than onshore turbines in the UK, and significant offshore capacity is being installed across Europe [12, 13], so large quantities of waste from these sectors should also be expected.

The nature of thermoset composites means that they are difficult to recycle, and landfill or incineration are common methods of disposal [14, 15]. These practices have been banned in Germany, Austria, the Netherlands and Finland, and WindEurope has called for a ban across Europe by 2025 [13, 16]. Reuse of the blades in other structures has been demonstrated [14], for example the BladeBridge project in County Cork, Ireland (Figure 2.2) [17], but this may not be scalable to deal with all composite waste. Recycling is therefore of increasing importance from an environmental, economic and regulatory standpoint.

Figure 2.2: *A pedestrian bridge installed by BladeBridge [17] in 2022. Used wind turbine blades provide structural support. Image reproduced from [17].*

Thermoset composites can be recycled or recovered to a limited extent via various methods, many of which have been discussed in detail by WindEurope [13], Mishnaevsky [14] and Cooperman et al. [15]. These methods, as well as their technology readiness level (TRL) as of 2020, are summarised in Table 2.1. However, they do not result in full recovery of the matrix and reinforcement, with the possible exception of solvolysis, and so are not a closed-loop solution. The following section therefore discusses possible resins for truly recyclable composites.

Table 2.1: *Current methods of recovering/recycling thermoset composites. Some methods are at different stages of development for glass and carbon fibres (GF and CF). Data from [13] and [15].*

Method	Products	TRL
Cement co-processing	Energy & silica for cement	GF: 9
Mechanical grinding	Filler powders	GF: 9, CF: 6/7
Pyrolysis	Fibres & matrix feedstock or energy	9, Microwave: 4/5
High voltage pulse fragmentation	Short fibres & matrix fragments	6
Solvolysis	Fibres & matrix feedstock	5/6
Fluidised bed	Short fibres & heat	5/6

2.1.3 Resins for Recyclable Blades

This section will give a brief overview of available recyclable resins and their potential for use in wind and tidal turbine blades. For a resin to be used in both wind and tidal turbine blades it must have acceptable mechanical, fatigue and thermal properties, be feasibly processed and be resistant to water absorption. More specifically, for tidal turbine blades to conform to DNV-ST-0164—a standard which specifies requirements for the entire lifecycle of a tidal turbine blade—the resin must show resistance to distilled water, seawater, water condensation and salt spray, and mechanical tests must be performed on saturated coupons. DNV-ST-0164 also specifies that:

> *"The water absorption of the laminating resin shall be determined according to ISO 62 (specimen 50×50×2 mm³) and shall not exceed 50mg after 168h and 100mg after 28 days of immersion in water."*

For a resin density of 1200 kg m^{-3}, 100 mg of water would be a 1.7% increase in coupon mass, which should be taken into account when selecting the resin.

One class of recyclable composites are thermoplasics, which can be recycled via thermal reshaping, shredding and press forming, or separation of the matrix and fibres via e.g. dissolution [18, 19]. Thermoplastic polymers are often supplied as solid resins, prepregs, or co-mingled fibres, which are then reshaped using heat and pressure. These polymers range from high-performance polyaryletherketones such as PEEK, to commodity thermoplastics such as polypropylene [20].

The high temperatures and pressures needed to process thermoplastic polymers mean that their use is generally not scalable to large wind turbine blades [21, 22]. However, small, residential wind turbines often have blades made from injection moulded polymer or composites [23, 24], and Twintex® fabrics (co-mingled glass and polypropylene fibres) were also used in the manufacture of larger 6 kW and 15 kW thermoplastic wind turbine blades in a collaboration between ÉireComposites and SD Wind Energy [25, 26].

These difficulties in processing molten thermoplastic polymers have led to the development of reactive thermoplastic resins as infusible alternatives to polymeric resins. Many are supplied as a solid monomer with a low melt viscosity, which polymerises in-situ, allowing for their use in the manufacture of vacuum-infused composites [22]. Commercially available resins include polyamides such as nylon-6 (PA6); for example, AP-NYLON® from Brüggemann. PA6 composites can be produced by vacuum infusion of molten ε-caprolactam, a catalyst, and an initiator, which then polymerise via anionic ring opening polymerisation [21, 27, 28]. Anionically polymerised PA6 has been shown to have excellent properties in comparison with heat moulded PA6 and epoxy [29, 30].

Polybutylene terephthalate (PBT) is another thermoplastic which undergoes ring opening polymerisation from low viscosity precursors [27, 31], and reactive processing of PBT was used by ÉireComposites, Ireland to manufacture a 12.6 m long thermoplastic wind turbine blade [32] (Figure 2.3). The resin was previously sold by Cyclics® as CBT® resin [21], although the company has ceased trading and the resin appears to be no longer available [33, 34].

The reason that these resins have not been adopted by wind turbine manufac-

Figure 2.3: *A 12.6 m long recyclable wind turbine blade made by ÉireComposites from CBT® thermoplastic resin. Half of the heated concrete mould used to produce the blade is visible at the bottom. Reproduced from [32].*

turers may lie in their processing conditions. The polymerisation of polyamides and PBT requires elevated temperatures, of around 170°C and 190°C respectively, and specialised moulds [27, 31, 32, 35], so they have not been demonstrated in large wind turbine blades. Additional issues with PA6 include the hygroscopicity of the monomer, which creates difficulties in processing and storage [36, 37]. PA6 polymer is also hydrophilic, with coupons absorbing 0.68% water after just 24 hours immersion in water, and saturating at around 9.5% mass increase, which means it may not be suitable for tidal turbine blades [27].

A wide variety of other thermoplastic polymers, including polycarbonate and even PEEK [21], can be polymerised in-situ and may theoretically be vacuum infused, but these monomeric/oligomeric resins are not commercially available for composite applications. A summary of reactive thermoplastic resins is included in Table 2.2, as is an assessment by Qin et al. [22] of the 'essential criteria' for their use in marine composites—i.e. acceptable monomer viscosity, processing temperature, T_g and moisture absorption.

Table 2.2: *A list of reactive thermoplastic resins assessed by Qin et al. [22] for use in the marine environment. The essential criteria of monomer processing viscosity, processing temperature, polymer T_g and maximum moisture uptake are included. Cells are shaded green for an acceptable value, amber for a marginal value and red for an unsuitable value, and an overall 'pass or fail' decision is made by the authors of [22]. Reproduced from [22].*

	Essential Criteria				
Polymer	Viscosity (mPa s)	$T_{processing}$ (°C)	T_g (°C)	Moisture (%)	Pass? (Y/N)
PA6	~5	130–200	40–60	6–11	N
PA12	23	180–240	40–50	<2	N
PBT	20–150	180–260	25–60	0.09	N
PC	250–300	250–300	150	0.16	N
PLA	-	150–185	55–65	<2	Y
PMMA	100	20–100	107	0.5	Y
TPU	800	300	-8–17	0.1	N
PEK	340–390	340–390	228	0.07	N
PET	250–325	250–325	73	0.5	N
PPA	1000	200–290	121–138	0.36	N

Liquid acrylic resins, marketed by Arkema as Elium®, are unique in that they are thermoplastics which are processed almost exactly like traditional thermoset resins. They are vacuum infusible and polymerise at room temperature, their properties have been shown to be comparable to epoxies [38, 39], and they have been demonstrated in the manufacture of full-scale wind turbine blades [40]. In addition, a techno-economic analysis of acrylic-matrix wind turbine blades by Murray et al. [41] concluded that lower costs could be achieved by replacing epoxy with acrylic, due to the lack of a post-cure stage.

Liquid acrylic resins are largely composed of methyl methacrylate (MMA) monomers, making the polymer similar to PMMA, but with the addition of other acrylate monomers to control the polymer's properties, and acrylic polymer to control the resin's viscosity [42–44]. The resin polymerises via a free radical mechanism after the addition of a peroxide initiator, and can be depolymerised via pyrolysis for re-

covery of the monomer and reinforcement fibres, in addition to the other described recycling methods for thermoplastics [45].

Due to the reactive nature of the monomeric acrylic resin, it can be easily modified by reactive blending to tailor its properties. Acrylic resins have been modified by Obande et al. [46, 47] using a second polymer, poly phenylene ether (PPE), which was used to make GF/acrylic-PPE composites. The solvent resistance, ductility, transverse flexural properties and initiation fracture toughness were improved, while reshapability was retained. On the other hand, a decrease in propagation fracture toughness and an increase in resin viscosity were observed. A comprehensive review of liquid acrylic resins has been written by Obande et al. [39], which discusses various aspects of acrylic-matrix composites including processing considerations, mechanical properties and resin modification.

Non-thermoplastic recyclable resins are also commercially available. For example, vitrimers are polymers which have exchangeable crosslinks, meaning they behave as a thermoset at low temperatures but become malleable at higher temperatures [48]. Various chemistries can be used to create these exchangeable crosslinks, but the commercially available VITRIMAX™ resin from Mallinda has exchangeable imine crosslinks [49, 50]. The resins have been shown to have good mechanical properties, are repairable, and can be recycled via thermal reshaping or depolymerisation in various solvents [48, 50]. Water causes the polymer to become malleable, which is beneficial for recycling, but also causes significant swelling and calls into question its use in tidal turbine blades [48, 51].

Recyclable thermoset resins are available as cleavable epoxies, which are polymers with chemically reversible crosslinks. Recylamine® from Aditya Birla Advanced Materials is one such technology in which a variety of chemistries are used to make reversible crosslinking agents, which can be used with standard epoxy resins [52]. Composites made with these crosslinking agents are recycled via immersion in an acetic acid solution, which cleaves the crosslinks and allows the separation of the matrix and fibres. The matrix is then converted into a low performance thermoplastic polymer [52]. EzCiclo® from Swancor is another epoxy resin which can be depolymerised using its CleaVER technology to produce monomers and oligomers [53]. These products can then be used to manufacture new epoxy resin, and the

recovered fibres can also be reused.

Other recyclable non-thermoplastic resins are also under development, such as the PECAN (PolyEster Covalently Adaptable Network) resin developed at NREL [54]. This resin has exchangeable crosslinks—similar to the vitrimeric resins discussed above—meaning it is recyclable (see Figure 2.4), and it has the additional benefit of being bio-based. The PECAN resin has been demonstrated in a 9 m long wind turbine blade, and its properties compare favourably to traditional thermosets [54, 55].

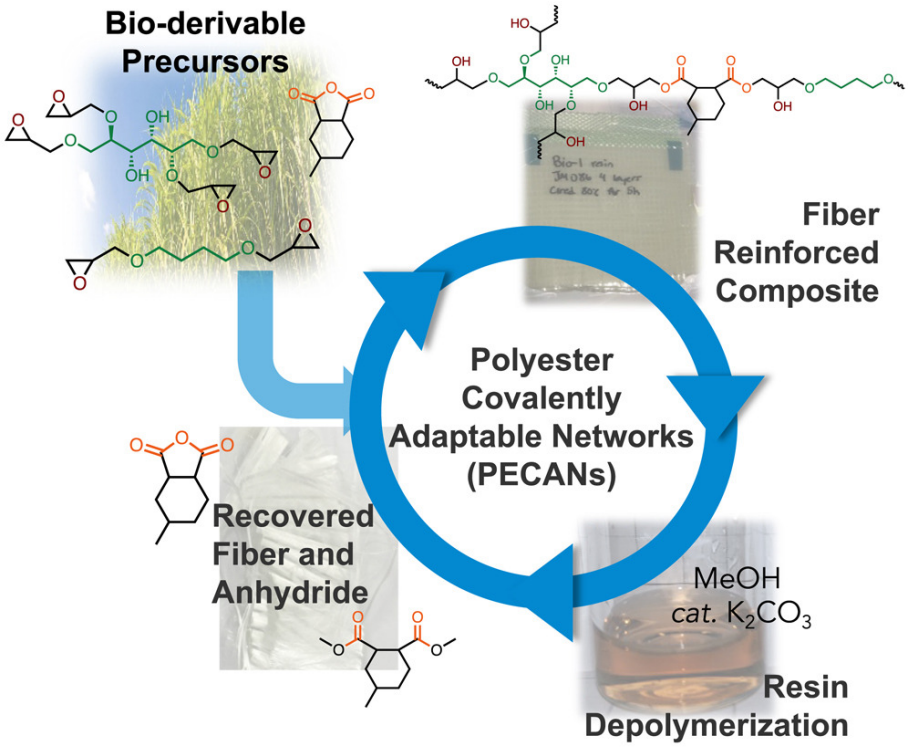

Figure 2.4: *Details of the synthesis and recycling of the PECAN resin. Reproduced from [54].*

Additionally, the CETEC (Circular Economy for Thermoset Epoxy Composites) consortium—a collaboration between Aarhus University, Vestas Wind Systems, Olin Corporation and the Danish Technical Institute—has developed a method for chemically cleaving standard epoxy resins, rather than requiring the use of specialised resins and hardeners, providing a route to recycling existing wind turbine blades

[56]. It also provides manufacturers the possibility of continuing to use their preferred resins, while still achieving recyclability.

2.1.4 The Future of Recyclable Blades

Numerous recyclable resins may therefore be theoretically used in the renewable energy and marine sectors, but few have been endorsed by major wind turbine manufacturers. A summary of the preferred recyclable resins or recycling processes of several major wind turbine manufacturers is presented in Table 2.3. There is a clear preference for resins which require minimal changes to existing manufacturing processes. Indeed, Vestas' approach is to develop new methods of recycling current resins—the method of catalytic cleavage of epoxy developed by the CETEC consortium, as discussed in Section 2.1.3—rather than changing the resin system itself.

Table 2.3: *The recyclable resins or recycling methods which are currently being explored by several large wind turbine manufacturers.*

Manufacturer	Recyclable Resin	References
Vestas	Catalysed epoxy cleavage	[56, 57]
GE/LM Wind Power	Arkema Elium	[40]
Siemens Gamesa	Swancor EzCiclo	[58]
	Aditya Birla Recyclamine	[59]
Mingyang Smart Energy	Swancor EzCiclo	[60]

2.2 Interfacial Bonding

After selecting a matrix resin, compatibility with the reinforcement fibres must be ensured as poor bonding can significantly reduce mechanical properties [61–63]. Interfacial bonding in glass-fibre reinforced composites is therefore explained in the following section, and work on interfacial bonding in acrylic-matrix composites is discussed.

2.2.1 Glass Fibre Sizing Agents

In glass fibre reinforcements, sizing agents are fibre coatings which improve handling and prevent fibre damage, but they also play a key role in interfacial bonding. Bonding is largely promoted by the inclusion of a coupling agent, which is usually an organosilane compound in the case of glass fibre reinforcements, but the majority of the sizing agent is made up of other components as will be discussed in the following paragraphs. Sizing agents' formulations and effects are complex, but they are covered in depth in a review by Thomason [64].

The general structure of a silane coupling agent is shown in Figure 2.5a. The sizing agent containing the silane coupling agent is typically applied to the fibre surface as an aqueous dispersion or emulsion immediately after fibre forming. The silane hydrolyses to a silanol in the solution, and the fibre is then heated so the silanol chemically bonds with the surface of the glass via a condensation reaction (Figure 2.5b). The organic group later reacts with the matrix, bonding it to the fibres [64–66].

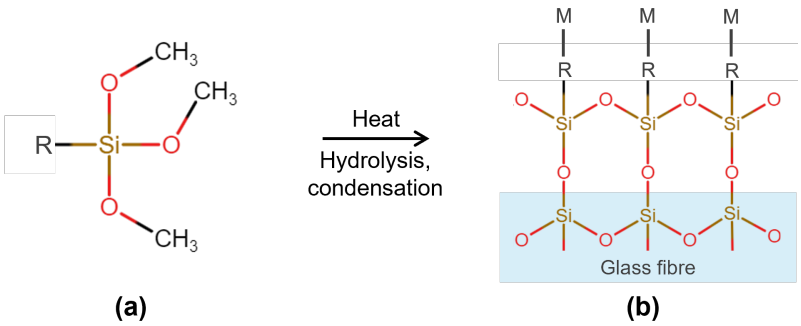

Figure 2.5: *(a) The general structure of a trimethoxy silane coupling agent. The R group is an organofunctional group which reacts with the matrix, M. (b) After hydrolysis of the silane, it bonds to the surface of the glass fibre via a condensation reaction.*

The complexity of sizing agent formulations is illustrated in Figure 2.6, which is a possible combination of components described in a patent from Owens Corning/3B Fibreglass [65]. As discussed by Thomason [64], the secrecy surrounding sizing agent formulations means patents such as this are one of the few sources for their composition, and for the purposes of each component. For example, the film former

protects the fibres during handling, and in Figure 2.6a it is an epoxy resin emulsion, with an optional addition of a polyurethane emulsion to improve toughness [65, 67]. These film formers must be compatible with the matrix resin for good adhesion, and surfactants are added to stabilise the emulsion (Figure 2.6a) [68].

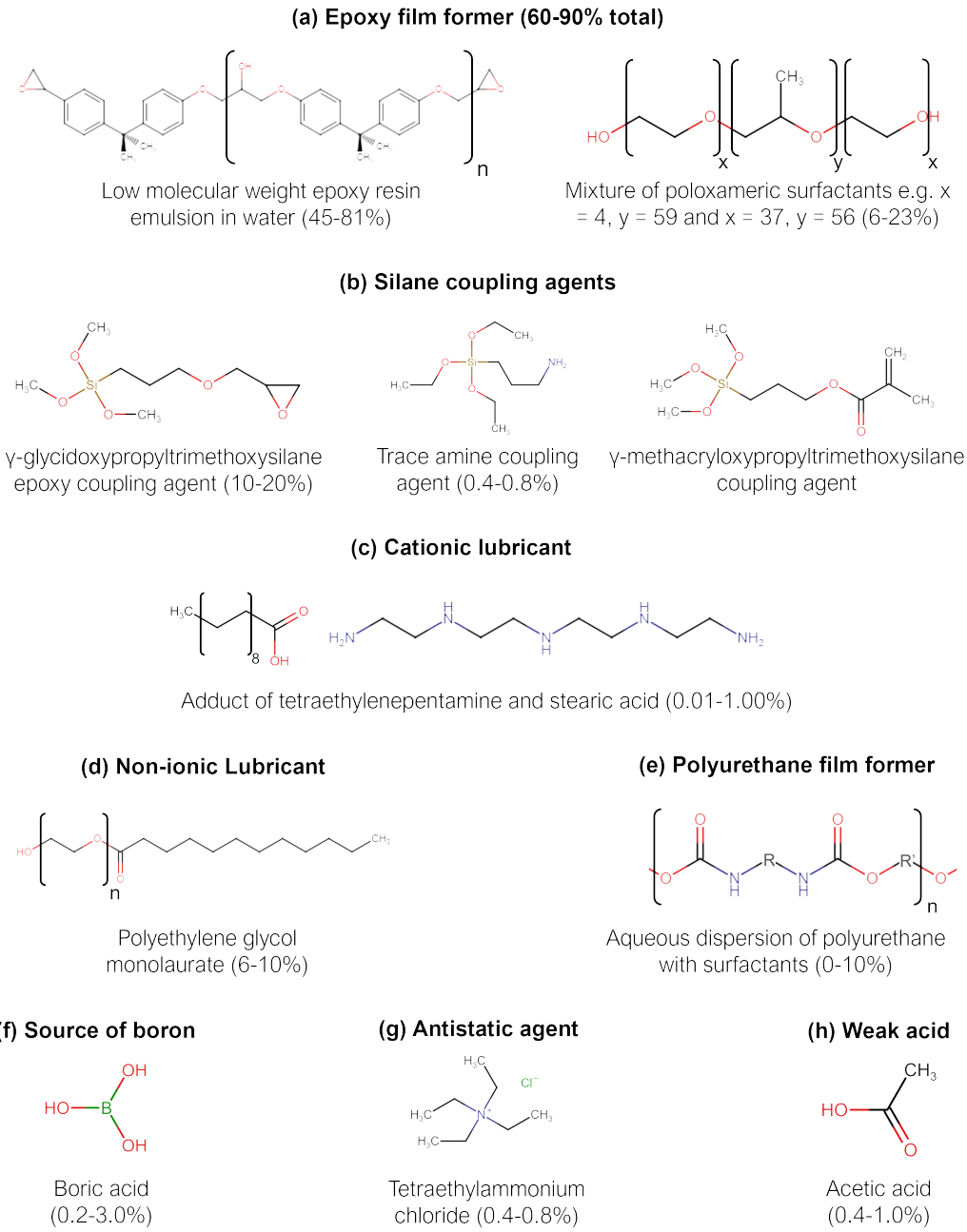

Figure 2.6: *Examples of components of a sizing agent, according to [65]. Many alternative components are possible, even within the cited patent [65, 67–69]. Percentages are given by weight of the solid fraction. Structures are from PubChem [70].*

Three possible silane coupling agents are illustrated in Figure 2.6b. The epoxy and amine coupling agents allow the fibres to bond with epoxy resins, but methacryloxy coupling agents may replace some or all of the epoxy sizing agent to add compatibility with vinylester and polyester resins. Other silane chemistries can be chosen for compatibility with e.g. polyurethane [65], although they generally have amino, epoxide, methacryloxy, or vinyl functionality according to Thomason [64]. Multi-compatible sized fabrics are commonly available, and these fabrics—which are simultaneously epoxy-, polyester- and vinylester-compatible—are the standard reinforcement from suppliers such as [71] and [72]. Reinforcements advertised for compatibility with liquid acrylic resins are not generally available, but since they polymerise via a free radical reaction—the same as polyester and vinylester resins—a vinylester-compatible sizing agent is recommended by the manufacturer [73]. The methacryloxy coupling agent in Figure 2.6b would therefore be expected to bond with acrylic resins.

The other components in Figure 2.6 also play important roles. Cationic and non-ionic lubricants (Figures 2.6c and d) are included in the formulation to further protect the fibres, prevent interfilament abrasion and reduce fuzz [65, 69]. A molecule containing boron and a weak acid (Figures 2.6f and h) both contribute to bonding between the coupling agent and the glass fibre [65, 74]. Finally, a small amount of an agent to prevent the buildup of static electricity is also added (Figure 2.6g). Each of these components is dispersed in water, which can make up 85-99% of the total weight in the patented composition described here [65].

2.2.2 Interfacial Strength in GF/Acrylic

As mentioned above, sizing agents for acrylic are recommended to be vinylester compatible, which is a common feature of multicompatible reinforcements, and so these non-specialised sizing agents have been extensively—and successfully—used with acrylic resins [4, 7, 19, 38, 75, 76]. Limited studies on sizing agents and interfacial strength in acrylic-matrix composites are available, and are discussed below.

Beguinel et al. [77] compared an acrylic-tailored sizing agent to a polypropylene-tailored sizing agent in GF/acrylic, and to an epoxy-tailored sizing agent in CF/acrylic. The wettability of the fibres was characterised via contact angle measure-

ments, and the IFSS was measured via microbond testing. It should be noted that the acrylic matrix was made from both reactive and non-reactive acrylic *latexes*—dispersions of acrylic polymer in water—rather than the acrylic resins discussed so far. The acrylic-tailored sizing significantly improved both the wettability and IFSS compared to the incompatible sizings, and the reactive latex was found to form a stronger interfacial bond than the non-reactive latex. An improvement in IFSS was also observed when comparing the acrylic-tailored sizing to a multi-compatible sizing, but this was with the nonreactive latex so may not be applicable to Elium® resins.

Studies by Charlier et al. [44, 78], in which the IFSS of GF/acrylic (Elium®) was measured via microbond testing, are more applicable. The IFSS was compared between acrylic-tailored and multi-compatible sizing agents, as well as with a GF/epoxy reference. No significant differences were observed between the sizing agents, but the GF/acrylic IFSS was around 40% lower than that of GF/epoxy (Table 2.4). The authors note that this may have been affected by the addition of a paraffin wax to the acrylic resin to prevent evaporation.

Table 2.4: *A summary of IFSS data from Charlier et al. [78]. The low IFSS using TP1 (acrylic resin without paraffin wax) is due to evaporation of the monomer and poor polymerisation. The sizing agent has no effect on IFSS with TP2 (acrylic resin with paraffin wax).*

		TP1-ASF	TP1-MSF	TP2-ASF	TP2-MSF	TS-ASF	TS-MSF
System	-	acrylic	acrylic	acrylic	acrylic	epoxy	epoxy
Paraffin wax	-	No	No	Yes	Yes	No	Yes
Cure 1	[h-°C]	-	-	1-80	1-80	1-80	1-80
Cure 2	[h-°C]	2 - 150	2 - 150	2 - 150	2 - 150	2 - 160	2 - 160
Sample size	-	21	23	18	20	12	12
IFSS	[MPa]	8.5 ± 2.4	7.8 ± 2.1	27.3 ± 4.2	27.2 ± 4.1	44.5 ± 5.1	48.8 ± 6.8

Work by Boufaida et al. [79], discussed further in Section 2.4.2, concluded that an acrylic-tailored sizing agent improved interfacial strength over a multi-compatible sizing. However, a chemical incompatibility between the multi-compatible sizing and the acrylic resin was observed. This highlights that sizing compatibility with a

resin requires more than simply the addition of an appropriate coupling agent, as incompatibilities with other components may reduce the interfacial strength [62, 79].

Davies et al. [80, 81] have carried out comparative studies on GF/acrylic composites immersed in water, and suggest that an acrylic-tailored sizing agent improves retention of properties over a multi-compatible sizing. Different layups were used with each reinforcement, however, as will be discussed in Section 2.3.3. Regardless of the sizing agent, reductions in mechanical properties were observed after water absorption, and so this is explored further in the following section.

2.3 Water Absorption

A key consideration for the application of acrylic resins in the marine and tidal energy sectors is their water absorption behaviour and retention of mechanical properties, even after a service life on the order of decades. In Section 2.1, the importance of choosing a resin which is resistant to water absorption was highlighted, and so in this section the mechanisms and effects of water absorption in composite materials are discussed.

2.3.1 Diffusion Theory

Diffusion of a fluid in a composite is often described using Fick's second law (Equation 2.1) [82]. In one dimension, this law states that the change in concentration c with respect to time t is related to the change in concentration gradient with respect to position x by a constant diffusion coefficient D. Upon immersion of a polymer in a fluid such as water, diffusion of this kind—i.e. *Fickian* diffusion—results in an initial linear relationship between concentration of the fluid and the square root of time ($\sqrt{t}$), eventually reaching an equilibrium content, M_m (see Figure 2.7a). This behaviour has been observed, though not consistently, in many materials including epoxy resins and composites of various chemistries [83–88], vinyl ester resin [89] and, as will be discussed further in Section 2.3.3, in acrylic resins and composites [80, 84, 90].

$$\frac{\partial c}{\partial t} = D\frac{\partial^2 c}{\partial x^2} \tag{2.1}$$

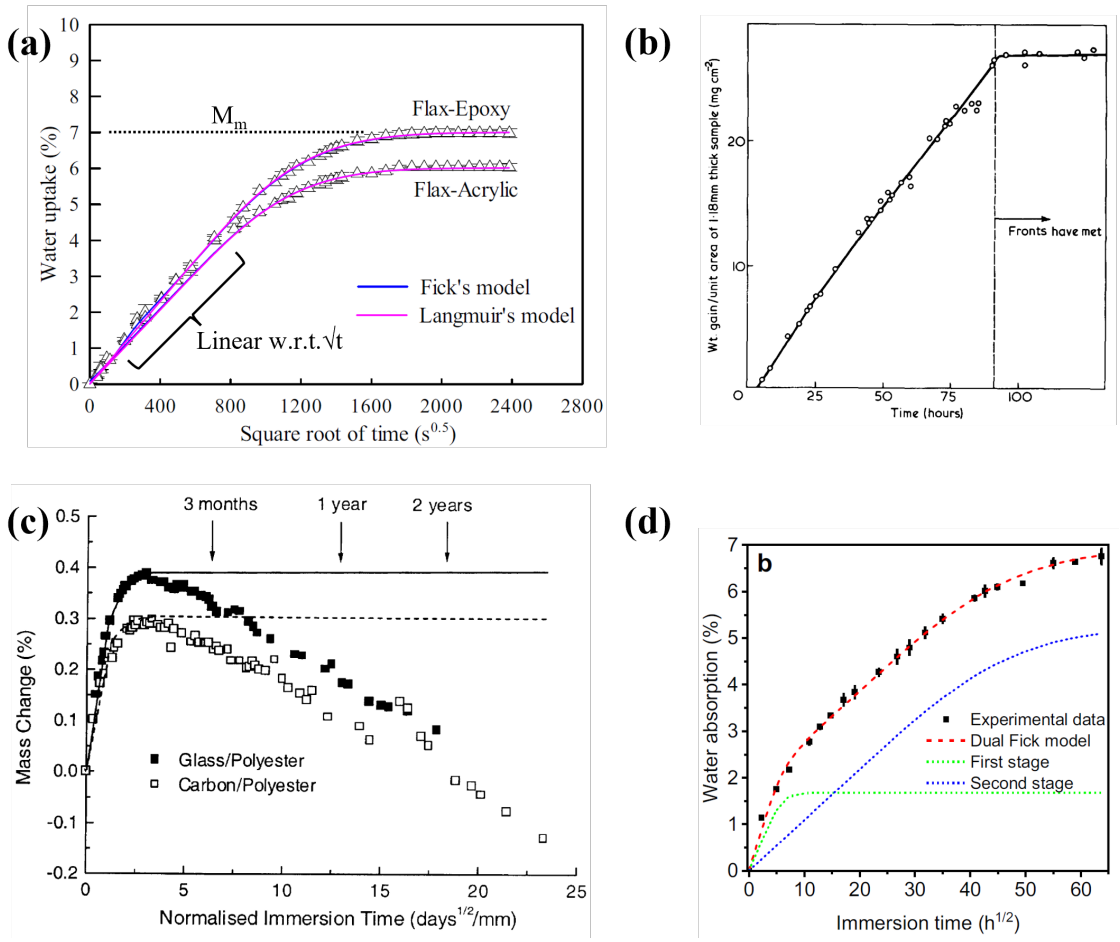

Figure 2.7: *Four types of diffusion curves that may be encountered in polymers and composites. (a) Fickian diffusion observed in flax-reinforced acrylic and epoxy, equally well described by a Langmuir model. The initial linear region and maximum water uptake are highlighted. Adapted from [84]. (b) Case II diffusion observed with PMMA and methanol. Note absorption is linear when plotted against time, and so it would be a parabola when plotted against* $\sqrt{t}$*. Reproduced from [91]. (c) Mass loss after saturation observed in polyester-matrix composites. Theoretical Fickian diffusion is shown by black lines for comparison. Reproduced from [92]. (d) Non-Fickian diffusion which can be described by a dual stage absorption model such as a dual Fick model (a sum of two Fickian diffusion curves). Reproduced from [93].*

Non-Fickian diffusion behaviour is often observed in polymers and composites, depending on a combination of material, fluid and temperature. In glassy polymers, non-Fickian *Case II* diffusion can often be observed. This occurs when there is a strong interaction between the fluid and polymer, leading to significant swelling [91, 94]. Case II diffusion is characterised by a sharp boundary between the swollen

and glassy polymer and a mass increase which is initially linear with time, resulting in a parabolic curve in a plot against $\sqrt{t}$ [94]. This behaviour was reported by Thomas et al. [91] when immersing PMMA in methanol (Figure 2.7b).

Apparent Fickian diffusion can be followed by a gradual decrease in mass, as shown in Figure 2.7c. This may occur when leaching of unreacted monomer or hydrolysis products occurs, as observed in several studies [92, 93, 95]. This is discussed further in Section 2.3.2.

Absorption can also continue to increase after starting to reach an apparent plateau, as in Figure 2.7d, and various absorption curves of this type have been described in the literature. For example, the absorption of water in CF/acrylic was described as the superposition of two Fickian diffusion curves by Placette et al. [96] to model non-Fickian diffusion of water in epoxy moulding compounds—i.e. a 'dual Fick' model. A dual Fick model was also employed by Bel Haj Frej et al. [93] to model water absorption in acrylic resin and composites, as shown in Figure 2.7d. The dual stage absorption was attributed to the presence of both free and bound water, as will be discussed below. In order to quantify the proportions of each state of water, a Langmuir-type Carter & Kibler model was employed by Bel Haj Frej et al. [97], in which bound water was found to diffuse more slowly than free water.

Similar results to Figure 2.7d may also be observed when a polymer is immersed in a mixture of solvents, leading to a mixture of fast Fickian and slower case II diffusion. For example, Alfrey et al. [94] report that when crosslinked polystyrene is immersed in a mixture of methanol and acetone, the methanol, which is a small molecule which does not interact strongly with the polymer, diffuses quickly and reaches a low equilibrium content, but the acetone, which is larger and diffuses more slowly, strongly interacts with and swells the polymer. Whitney and Browning [98] attribute similar behaviour in epoxy resin and composites to the development of matrix damage over time.

As mentioned above, the state of water in polymers can be described by two theories. In the *free-volume theory*, water molecules occupy voids caused by the imperfect packing of polymers, without interacting strongly with the polymer, whereas in the *polar interaction theory*, water molecules bind to polar sites in the polymer via dipole interactions or hydrogen bonds, resulting in 'bound' water [62, 99, 100].

These states of water can exist simultaneously, and have been investigated by several techniques.

Soles et al. [95, 100] used positron annihalation lifetime spectroscopy (PALS) to investigate the sizes of nanopores (free volume) in epoxy and their effect on the diffusion of water. Nanopores were found to have diameters of 2-20 Å, versus a diameter of 3 Å for water molecules. There was little correlation between the pore size and diffusion at low temperatures and no correlation above around 35 °C, possibly because the absorption of water causes changes in the topology, and the binding/unbinding of water from polar sites in the pores may be the rate determining step in the diffusion. Therefore, non-amine epoxies, which did not have polar groups in the pore structure, resulted in an order of magnitude increase in the diffusion coefficient. This effect is illustrated in Figure 2.8.

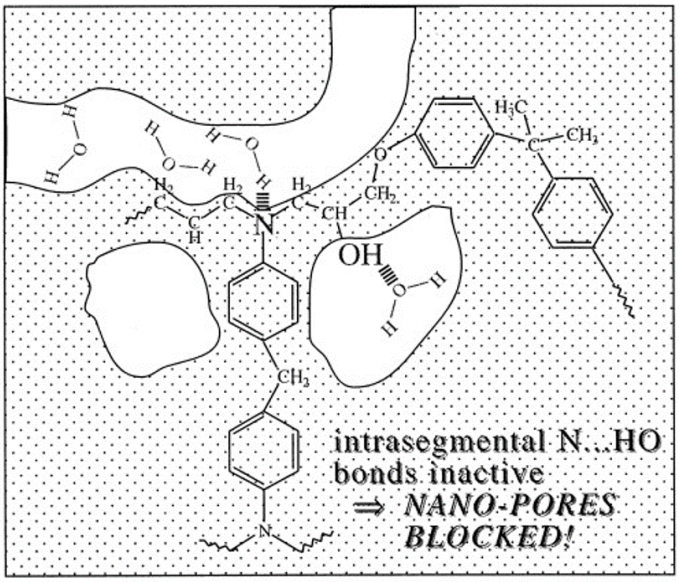

Figure 2.8: *Illustration of the diffusion mechanisms of water in epoxy proposed by Soles and Yee [100]. Diffusion is through free volume in the form of nanopores, but diffusion is slowed by water molecules binding to hydrophilic sites in the polymer. Reproduced from [100].*

DSC has been used to observe the different phases of water, with different binding energies of the polymer, and an example graph is shown in Figure 2.9. The exothermic peaks during cooling indicate the freezing temperatures of the various phases of water [101, 102]. Abdelmola et al. [101] used DSC to investigate absorbed water in epoxy of various void contents. In void-free water-saturated epoxy, the

water was found to be entirely non-freezing bound water which is tightly bound to the polymer. The presence of voids increased the water content, which exists as non-freezable bound water, free water and freezable bound water, the latter of which is loosely bound to the polymer. Similarly, after confirming the presence of free, loosely-bound and bound water in hydrated PMMA via quasi-elastic neutron scattering (QENS), Fujii et al. [102] determined that loosely-bound water made up 28% of the total water content using DSC.

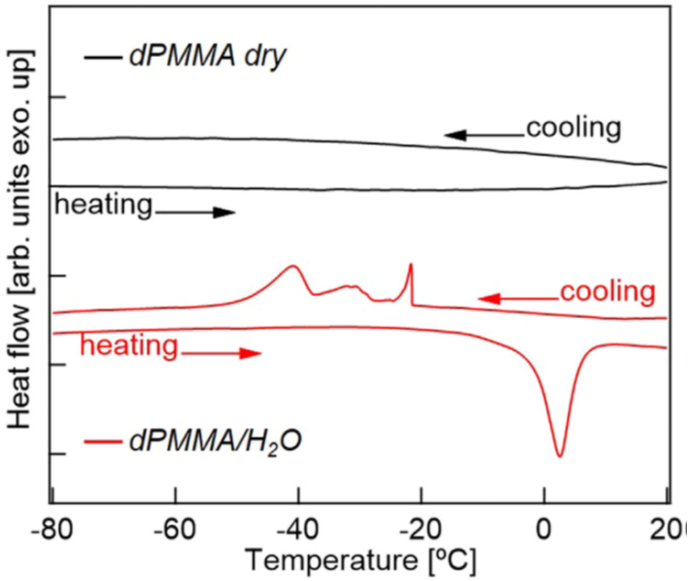

Figure 2.9: *DSC curves of deuterated PMMA (dPMMA), dry and water-saturated. Exothermic peaks in the cooling curve shows the presence of different phases of freezable water: free water and intermediate (loosely bound) water. Non-freezable, strongly bound water would not cause an exothermic peak and so cannot be directly detected using DSC. Reproduced from [102].*

Other methods may also be used to investigate the presence of free and bound water. Bel Haj Frej et al. [97] fit a Carter & Kibler diffusion model to water absorption data to determine the proportions of free and bound water in acrylic resin and CF/acrylic composites. Bound water diffused more slowly than free water, and the proportions of each phase varied depending on the ageing temperature and the presence of reinforcement. Zhou and Lucas [88] characterised hydrated epoxy resin through absorption/desorption studies and ^{1}H nuclear magnetic resonance (NMR). Their results suggest that water was bound to the epoxy via either one or two hydrogen bonds, causing different binding strengths to the polymer. The studies

summarised here show that the proportions of free and bound water in a polymer vary significantly depending on its chemistry and topology, with the free water content of PMMA being higher than in epoxy.

An additional consideration in fibre-reinforced composites is presence of voids and the fibre-matrix interface, which create additional diffusion pathways and can result in a diffusion coefficient 2 orders of magnitude greater along the direction of the fibres than in the resin, as measured by Humeau et al. [87]. This effect can be significant if the fibre sizing is incompatible with the matrix, creating interfacial voids [62]. For example, Gargano et al. [103] found that an incompatible sizing agent in CF/vinyl ester, i.e. a sizing which lacks the compatibility described in Section 2.2, caused the diffusion coefficient of water to triple.

Diffusion studies at ambient temperatures are often prohibitively time consuming, and so hydrothermal ageing—accelerated ageing via immersion in water at elevated temperatures—is often employed. The diffusion coefficient D may be related to temperature T via the Arrhenius equation (Equation 2.2), in which D_0 is a constant diffusion coefficient, E_a is the activation energy for the diffusion process and R is the molar gas constant [104, 105].

$$D(T) = D_0 \cdot e^{\frac{-E_a}{RT}} \tag{2.2}$$

To calculate D via Equation 2.2, it is assumed that D_0 and E_a are known constants. However, in practice, D is measured and E_a and D_0 are unknown. Therefore, by taking the ratio of the values of the diffusion coefficient (D_1 and D_2) at two different temperatures (T_1 and T_2) as shown in Equation 2.3, E_a can be determined and used to calculate D at any other temperature.

$$D_2 = D_1 \cdot exp\left[\frac{E_a}{R}\left(\frac{1}{T_1} - \frac{1}{T_2}\right)\right] \tag{2.3}$$

Therefore, so long as the assumption of Arrhenius behaviour is correct, hydrothermal ageing can be applied and the equivalent value of D at the temperature of real-world applications can then be calculated.

2.3.2 Effects of Water on Composites

2.3.2.1 The Matrix

The effects of water on matrices such as epoxy, polyester and vinylester have been studied extensively due to these polymers' long history of use in the marine environment, from leisure yachts to mine countermeasures vessels [20, 106, 107]. Once water is absorbed by the matrix, swelling and plasticisation occur and result in lower polymer strength, modulus and T_g [85, 105, 108, 109].

Chemical damage to the matrix can occur via hydrolysis, and subsequent leaching is evidenced by a decrease in the mass change vs. $\sqrt{t}$ curve similar to Figure 2.7c. This can be a particular problem in polyester resins, with Kootsookos and Mouritz [92] having demonstrated that GF/polyester and CF/polyester composites can lose around 0.5% of their mass after 3 years in seawater at 30°C, even at 100% cure rates. While in the study by Kootsookos and Mouritz [92] vinylester is shown to be more resistant to this chemical damage, in a study by Bel Haj Frej et al. [93], leaching from vinylester composites has been observed. Leaching has been observed by Soles et al. [95] in a flexible epoxy immersed in hot (90°C) distilled water, but not in rigid or semi-rigid epoxy resins. Degradation of epoxy resin during immersion in water at 90°C was also observed by Xiao et al. [110] and was attributed to chain scission due to hydrolysis of tertiary amines.

Absorption of water or other solvents can cause matrix cracking in composites, which can be exacerbated by subsequent drying. Whitney and Browning [98] noted the development of cracking in epoxy resin and composites after long-term exposure to humid environments. Vanlandingham et al. similarly noted non-Fickian absorption behaviour in epoxy resin which they attribute to the formation of microcracks [105]. After immersion of GF/vinylester microdroplets—small droplets of resin bonded to single reinforcement fibres for the testing of interfacial strength—in water by Thomason and Xypolias [89], gradually worsening matrix cracking was noted at the menisci of the droplets. In the same study [89], blistering of the matrix surface was attributed to stresses caused by swelling and the bi-phasic structure of the vinylester. Hydrothermal ageing can also cause matrix damage not seen at lower temperatures, as observed by Pogany [111] in water-saturated polyester and epoxy phenolic lacquer. In this study, cooling of the specimens resulted in a rapid change

in the equilibrium moisture content, causing crazing of the polymer as can be seen in Figure 2.10.

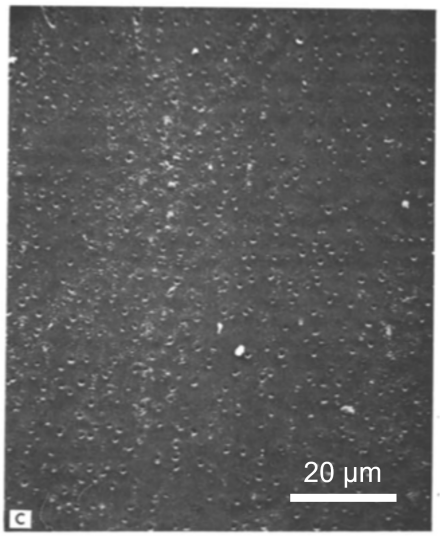

Figure 2.10: *Crazing in epoxy phenolic lacquer after immersion in hot water. SEM image from [111]. No scale is given in the original publication, but an approximate scale bar is provided based on the published image size and the stated* $\times 1000$ *magnification.*

Crosslinking in thermoset matrices restricts swelling [112], and moisture absorption in thermoplastics is hindered by increasing crystallinity [113, 114], but this does not mean that thermosetting and semi-crystalline polymers are more resistant to water absorption in general. Polymers with a high affinity for the solvent are often significantly affected by absorption. The semi-crystalline polymer nylon-6 (PA6), for example, is hydrophilic and absorbs around 10% by weight of water [115]. The amorphous thermoplastic PMMA, a more hydrophobic polymer than PA6 [102], has been shown to absorb around 2% water [102], which is similar to or lower than crosslinked epoxy resins [86, 101]. PEEK, another semi-crystalline thermoplastic, only absorbs around 0.5% water, even after immersion at 90°C [116].

2.3.2.2 The Fibres

Carbon and glass fibres tend to absorb very little water compared to the matrix [36], and are therefore of less importance in water absorption, but chemical damage to glass fibres can occur. Gu [117] found that E-glass fibres degrade in 2 wt.%

solutions of sodium chloride, losing approximately 11% of their strength over 4 weeks of immersion, with stronger salt solutions causing greater decreases. Hydrolysis of glass fibres, leading to slow mass loss and diameter reduction, has also been demonstrated after immersion in water [118].

Natural fibres, on the other hand, do tend to absorb water, and the effects of this in acrylic-matrix composites are discussed further in Section 2.3.3.2.

2.3.2.3 The Interface

Interfacial damage due to water absorption has been observed in several relevant composites, including glass and carbon fibre-reinforced epoxy [119], polyester [62], vinylester [103] and acrylic, as will be discussed in Section 2.3.3. Behera et al. [119] observed interfacial debonding after immersion of CF/epoxy composites in tap water at 70°C. Thomason and Xypolias [89] measured a complete loss of interfacial shear strength in GF/vinylester microdroplets after immersion in water for around 7 days at 23°C or 4 days at 50°C. Stresses due to swelling, along with a weakened interface, were determined to be the cause of interfacial debonding by Gibhardt et al. [120]. The authors attribute this weakening to plasticisation of the interphase region, although work by Ishida and Koenig [121] suggests that hydrolysis of the silane coupling agent can cause interfacial degradation.

The type of sizing agent used may have an effect on interfacial degradation due to water absorption. This was explored by Tsenoglou et al. [62], who studied the quality of an interfacial bond via repeated absorption-desorption cycles in GF/polyester short beam shear coupons. The reinforcement fibres were treated with one of: a silane coupling agent, an incompatible polymer (PDMS) or no coating. The short beam strength (SBS) was significantly affected by the fibre treatment, with the clean, PDMS-coated and silane-treated coupons having strengths of 14.1 MPa, 7.34 MPa and 29.6 MPa respectively. The composite coupons, along with neat resin coupons, were then immersed in distilled water at 25°C, 35°C and 45°C and their masses were monitored to allow diffusion coefficients to be calculated and compared. The silane surface treatment resulted in both slower diffusion and a lower maximum water content than clean or PDMS-coated fibres. The coupons were then dried for 30 hours under vacuum, and the absorption-desorption cycle was repeated a fur-

ther three times. By assuming that diffusion occurred via a free-volume mechanism, Tsenoglou et al. [62] compared the degree of interfacial loosening between the fibre treatments, as illustrated in Figure 2.11. For clean and silane-treated fibres, interfacial loosening increased with subsequent absorption-desorption cycles, although the silane treatment resulted in a lowered interfacial free volume fraction. In PDMS-coated fibres, interfacial loosening was not observed which was attributed to swelling of the coating. This study not only shows the importance of a silane coupling agent for interfacial strength, but also how the compatibility of other components of the sizing agent with the polymer may affect strength and absorption behaviour [64].

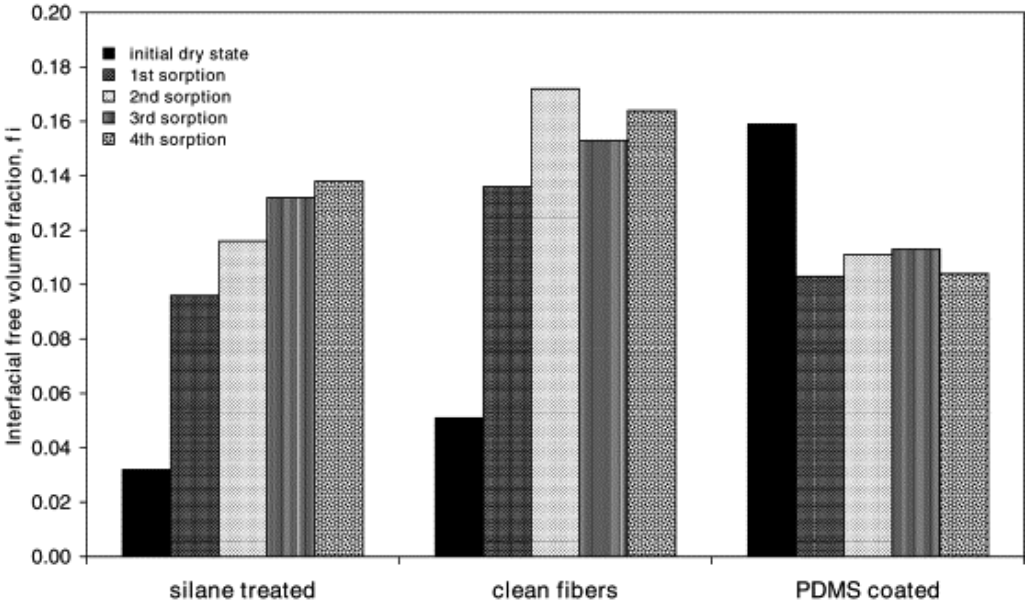

Figure 2.11: *The change in interfacial volume in GF/polyester composites with no sizing, a silane coupling agent and an incompatible PDMS coating after repeated water sorption-desorption cycles. Reproduced from [62].*

Thomason [61] conducted a study on the influence of fibre sizing, resin and void content on the absorption behaviour and SBS of GF/epoxy composites. The fibre surface coating was found to have a much smaller effect on absorption behaviour than the void content and matrix resin type, although it did affect the SBS. It is suggested by the author that this is due to most of the fibres tested being sold as 'epoxy-compatible'. Indeed, the only fibre which performed poorly in water absorption was the only one not marketed as 'epoxy-compatible'.

2.3.3 Water Absorption in Acrylic-Matrix Composites

The water ageing behaviour of acrylic-matrix composites has been reported in several studies, using a variety of reinforcements, layups and ageing conditions, as is detailed below.

2.3.3.1 Glass- and Carbon-Fibre Reinforced Acrylic

Davies et al. [80] performed an extensive study of water absorption in GF/acrylic, CF/acrylic and unreinforced acrylic resin. GF/acrylic laminates were manufactured using a $[0/90]_3$ layup of woven fabric with a non-specialised sizing agent. CF/acrylic coupons were manufactured using non-crimp biaxial fabric with either quadriaxial or ($\pm 45°$) layups. To investigate diffusion kinetics, unreinforced resin coupons were immersed in seawater at 25°C, 40°C and 60°C, and their weight gains were monitored. Non-Fickian diffusion was noted in the GF/acrylic coupons (Figure 2.12), with an initial plateau followed by further increases in mass, but Fickian curves were fit to the data for ease of comparison. The maximum water content of the resin was similar at each temperature, ranging between 1.85-1.90%, but the diffusion coefficients significantly increased with temperature at 0.55 $\times 10^{-12}$ $m^2\,s^{-1}$, 1.39 $\times 10^{-12}$ $m^2\,s^{-1}$ and 4.23 $\times 10^{-12}$ $m^2\,s^{-1}$ at 25°C, 40°C and 60°C respectively. By applying Equation 2.3, a consistent activation energy of approximately 48 $kJ\,mol^{-1}$ can be calculated between each increase in temperature, suggesting Arrhenius behaviour of the diffusion process. Diffusion was found to occur primarily in the matrix, with the composites reaching a maximum water content approximately half that of the unreinforced resin (Figure 2.12).

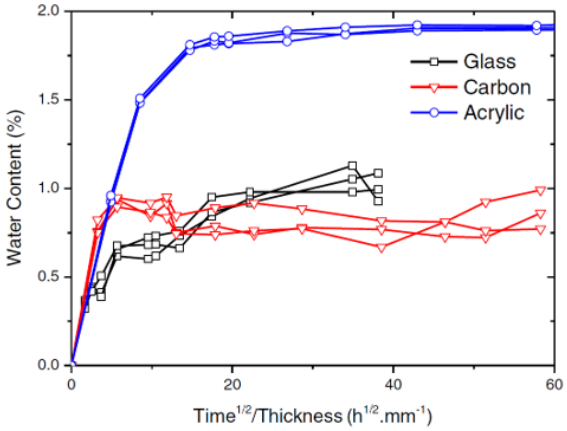

Figure 2.12: *Water absorption curves of GF/acrylic (black), CF/acrylic (red) and unreinforced acrylic resin (blue), after immersion in seawater at 60 °C. Greater absorption is visible in the neat resin, and non-Fickian diffusion was observed in GF/acrylic. Reproduced from [80].*

The study [80] also determined the mechanical properties of the coupons when dry, at various times during immersion, and dried after saturation. The 0/90° GF/acrylic coupons exhibited the largest decreases in tensile strength of 50% after 18 months of ageing in 60°C saltwater. The reported decreases in mechanical properties of the CF/acrylic coupons were generally smaller than those of GF/acrylic. Drying of the immersed resin resulted in almost complete recovery of its mechanical properties, suggesting reversible plasticisation as the main effect of water ingress. However, the composite coupons did not fully recover their original properties, with the worst performance being in the 0/90° GF/acrylic, which recovered only 62% of its strength after drying. Scanning electron microscopy (SEM) of the fracture surfaces (Figure 2.13) shows this is due to irreversible interfacial damage—absent in CF/acrylic—which the authors suggest could be prevented with a tailored sizing agent.

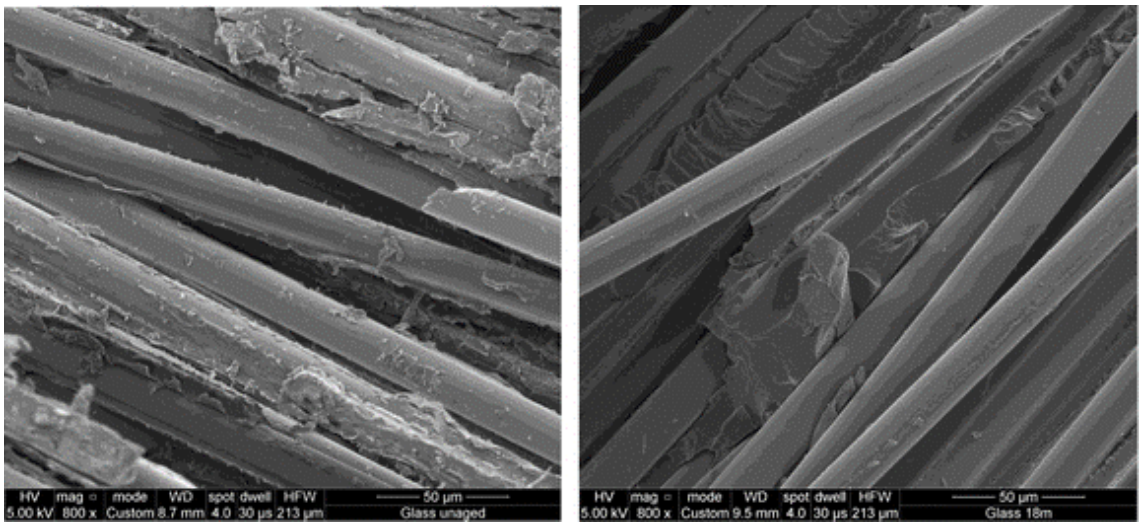

Figure 2.13: *SEM images of the fracture surfaces of ±45° GF/acrylic tensile coupons. The images are from before (left) and after (right) immersion in 60°C seawater for 18 months. Cleaner fibres in the aged coupons suggest interfacial degradation occurs. Reproduced from [80].*

Therefore, in a later study, Davies et al. [81] researched the effect of water absorption on the fatigue of GF/acrylic composites with an acrylic-tailored sizing agent. The fatigue aspects of this paper will be discussed in Section 2.4.2, but static testing was also performed and compared with the results using a non-specific sizing agent [80]. Greater property retention after immersion was observed with the acrylic-tailored sizing (65% vs. 50%), although differences in layup ($[0,(\pm45)_2,0]$ vs. $[0/90]_{3f}$) and the grade of Elium® resin between the studies make a direct comparison difficult.

Barbosa et al. [75] compared the performance of CF/acrylic and CF/epoxy composites after immersion in distilled water at 80°C for 8 weeks. The reinforcement was a woven 0/90° fabric treated with a multi-compatible sizing agent. The tensile properties of 0/90° coupons and the in-plane shear properties of ±45° coupons were measured, DMA was used to determine the T_g, and SEM was used for detailed fractographic analysis. As shown in Table 2.5, similar changes in the tensile and in-plane shear moduli were measured in both CF/acrylic and CF/epoxy. On the other hand, CF/epoxy had a higher retention of the tensile and in-plane shear strengths. In fact, both CF/acrylic and CF/epoxy experienced increases in their tensile strengths (+3% and +11% respectively).

Table 2.5: *Original strengths/moduli of CF/acrylic and CF/epoxy coupons and percentage changes due to 8 weeks of immersion in distilled water at 80 °C according to [75]. Tensile properties were tested with 0/90° coupons, and in-plane shear with ±45° coupons.*

	CF/acrylic		CF/epoxy	
Tensile Strength	783 MPa	+2.9%	624 MPa	+11.2%
Tensile Modulus	57.5 GPa	-3.9%	55.7 GPa	-4.2%
In-Plane Shear Strength	51.6 MPa	-18.1%	66.7 MPa	-9.8%
In-Plane Shear Modulus	2.9 GPa	-28.2%	5.7 GPa	-26.3%

SEM imaging suggested that interfacial weakening and matrix plasticisation caused the observed decreases in properties, but DMA unexpectedly showed that T_g increased after water absorption—the opposite of what would be expected for a plasticised matrix. The storage moduli of both composites did decrease after water absorption, indicating plasticisation, and the *tan* δ curve of wet CF/acrylic showed a split peak (Figure 2.14), which the authors attribute to phase separation of block copolymers [75].

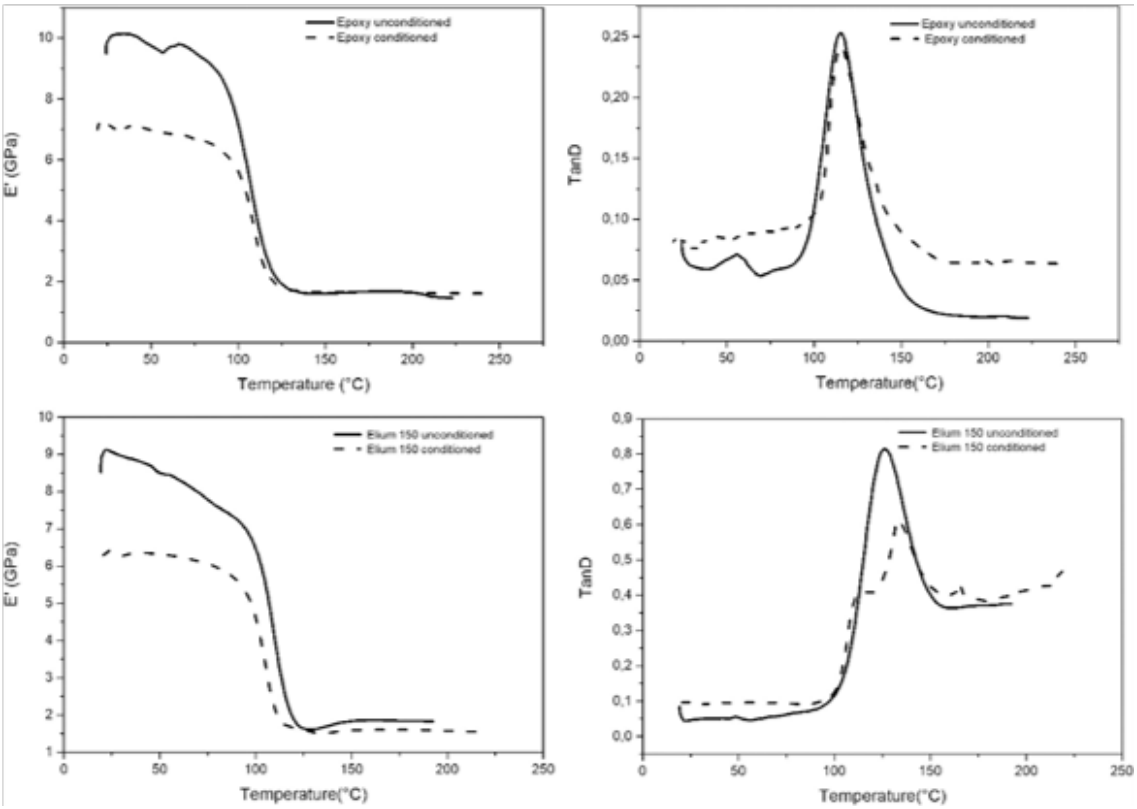

Figure 2.14: *Viscoelastic properties of CF/epoxy (top) and CF/acrylic (bottom) before and after immersion in 80* °C *distilled water for 8 weeks. Reproduced from [75].*

Nash et al. [76] immersed coupons of unidirectional GF/acrylic, GF/epoxy, GF/polyester and GF/vinylester in deionised water at 35°C for 28 days, and in diesel for 7 days. The reinforcement for GF/acrylic, GF/epoxy and GF/polyester was treated with a non-specific sizing agent, whereas the GF/vinylester reinforcement had a tailored sizing agent. The SBS of the composites and their T_g and onset temperatures were measured before and after immersion, and the fracture behaviour was characterised using SEM. The largest drop in the SBS was a 38% reduction for GF/acrylic coupons after immersion in water from an initial value of 57 MPa, although the SBS of GF/polyester and GF/epoxy also saw significant decreases of 21% and 16% from initial values of 38 MPa and 58 MPa respectively. GF/vinylester coupons saw little change (-1.6%) in SBS after immersion in water, which the authors attribute to the tailored sizing agent. Degradation was caused by a weakened interface, as revealed via SEM imaging, and plasticisation of the matrix, which resulted in a decrease in the T_g. Diesel was found to have little effect

on the composites, aside from GF/polyester which saw a -11% change in the onset temperature. It should be noted that the water/diesel content was measured at the 28 day mark, but mass increase vs. time data was not included, so the percentage saturation of the composites is unknown.

Bel Haj Frej et al. [93] characterised water absorption in CF/acrylic and CF/vinylester 0/90° coupons, as well as coupons of unreinforced resin. Coupons were immersed in deionised water at 70°C for 6 months and mass increases were tracked to allow calculation of the diffusion coefficient. Focusing on CF/acrylic, non-Fickian absorption behaviour was observed in both reinforced and unreinforced coupons. The mass of unreinforced acrylic resin increased continually over the 6 month period, reaching 6% water content without approaching equilibrium when the experiment was stopped. The CF/acrylic composite also showed non-Fickian behaviour, although the mass increase did approach an equilibrium water content of 6.8%. Dual Fick models—i.e. a sum of two Fickian diffusion models—were therefore fit to the data, which the authors attribute to parallel free-volume and molecular interaction diffusion mechanisms (shown previously in Figure 2.7d). Changes in tensile properties, in-plane shear and SBS due to water absorption were also characterised in CF/acrylic coupons after 6 months of ageing. The authors measured losses of 6% in tensile modulus and 10% in tensile strength, from initial values of 64 GPa and 1120 MPa respectively. The shear modulus and shear strength of dry coupons were 2 GPa and 66 MPa respectively when dry, but saw decreases of 9% and 17% upon ageing. The largest reduction of 43% was seen in the SBS, with an initial value of 14 MPa.

In another study by Bel Haj Frej et al. [97], the effect of temperature on diffusion behaviour in neat acrylic resin and CF/acrylic was explored. Coupons of neat Elium® 188 O, as well as 0°/90° and ±45° CF/acrylic coupons, were immersed in deionised water at 40°C or 70°C. Their water uptake was monitored, and tensile tests, modal analysis and DMA were applied to virgin, aged and dried coupons. Fickian diffusion was observed in neat resin at 40°C, reaching a plateau of 1.7% water content, but non-Fickian diffusion of the type previously shown in Figure 2.7d—which can be described as the superposition of two diffusion curves—was observed in neat resin at 70°C and composites at both temperatures (see Figure 2.15). The equilib-

rium water contents of the composites reached 2.95% at 40°C and 4.9% at 70°C, whereas in the neat resin at 70°C equilibrium was not reached even after 150 days of immersion and a water content of 6.7%. As discussed before, this was attributed to a combination of free and bound water, and so to quantify their proportions a Carter & Kibler diffusion model was fit to the data (Figure 2.15). Free water was found to diffuse quickly, whereas bound water diffused more slowly. The difference in behaviour between the temperatures was attributed to hydrolysis of the polymer side chains at 70°C, causing an increase in hydrophilicity.

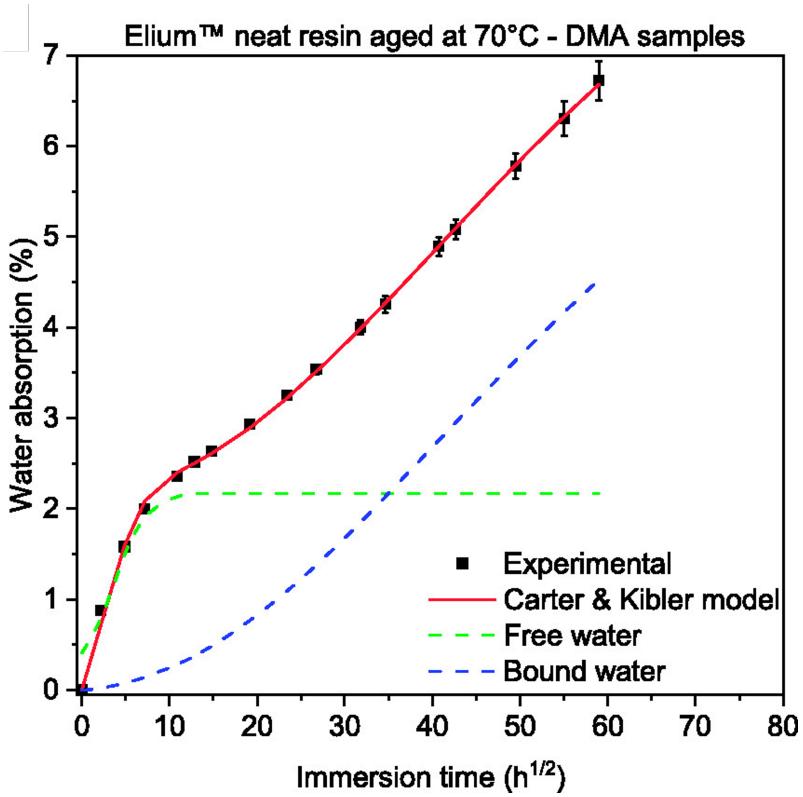

Figure 2.15: *Absorption of water in unreinforced acrylic, immersed at 70°C. Non-Fickian diffusion is visible, and a Carter & Kibler model is fit to the data. Free and bound water components are visible. Reproduced from [97].*

Comparing the equilibrium water contents from Bel Haj Frej et al. [93, 97] to the other studies discussed here, the values are unusually high. The ageing temperature of 70°C was given as a possible explanation, although Barbosa et al. [75] measured a mass increase of only 1.25% in CF/acrylic after immersion in distilled water at 80°C. The high void content (4.8%) and an incompatibility with the epoxy-sized reinforcement may contribute to the high water content of CF/acrylic, but not the

unreinforced resin.

Bandaru et al. [122] immersed quadriaxial GF/acrylic coupons in distilled water at 60°C for 6 months, measuring water uptake and performing tensile, flexural, short beam, double-cantilever beam, end-notch flexure and DMA tests. No mention is made of the sizing agent used. Water content was found to reach 0.78%, causing decreases in tensile strength (-30%), flexural strength (-59%), SBS (-46%) and mode II fracture toughness (-37%). Although plasticisation and weakening of the matrix was observed, the T_g of the composite *increased* by 6% after ageing, similar to the observations of Barbosa et al. [75]. The authors suggest this may be due to further polymerisation during hydrothermal ageing. An increase was also observed in the mode I fracture toughness due to increased fibre bridging in the aged coupons, caused by a weakening of the fibre-matrix interface.

2.3.3.2 Natural-Fibre Reinforced Acrylic

Chilali et al. [84] provide an in-depth study of water diffusion in flax-fibre reinforced acrylic (FF/acrylic) and FF/epoxy, determining the effects of coupon geometry, fibre orientation and the application of edge sealant on the absorption of both tap and salt water. The equilibrium water content and diffusion coefficient were strongly influenced by the coupon geometry and layup. The equilibrium water content, for example, had an approximate range of 6-11%, depending on the coupon characteristics. The reinforcement therefore played a significant role in water absorption.

These results may not be applicable to the glass-fibre reinforced composites which are the focus of this thesis, however, as the water absorption behaviour of natural fibres is significantly different. Unlike glass and carbon, natural fibres such as flax and jute absorb a significant amount of water. In most natural fibres—flax, for example—there is a hollow core called a *lumen* which allows for wicking of water along the centre of the fibre. Water can also diffuse into and swell the various biopolymers which make up the fibres [84, 123, 124]. These effects are illustrated in Figure 2.16.

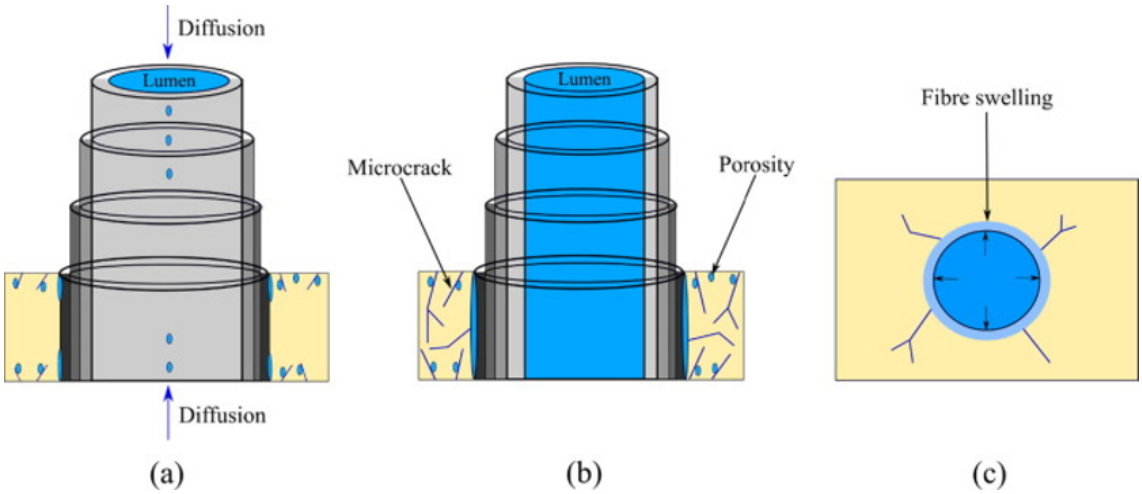

Figure 2.16: *An illustration of the diffusion of water into flax reinforced composites, along the direction of the fibres. Water can wick through the fibre lumen, and diffuse into the fibre itself, causing swelling. Reproduced from [84].*

To illustrate this difference, Das et al. [125] compared water absorption and mechanical properties of unidirectional flax- and glass-fibre (FF and GF respectively) reinforced acrylic and epoxy—both petrochemical and bio-based. Coupons were immersed in distilled water at temperatures between 23°C and 60°C, and their weight gain and mechanical properties were measured weekly between 0 and 8 weeks of immersion. The performance of GF/acrylic was in general similar to or better than GF/epoxy, but significant differences were observed between the glass- and flax-reinforced composites. As an example, GF/acrylic flexural coupons absorbed only 0.42% water over the course of 56 days at 23°C, and experienced respective decreases of 11% and 0.2% in flexural strength and modulus over the same period. FF/acrylic composites, however, increased by 12.67% in mass, and had much larger drops of 62% and 70% in flexural strength and modulus, respectively. Similar differences in behaviour were observed between FF/epoxy and GF/epoxy. Given these differences, which are summarised in Figure 2.17, the remaining literature on water absorption in natural-fibre reinforced acrylic [126–129] is not discussed here.

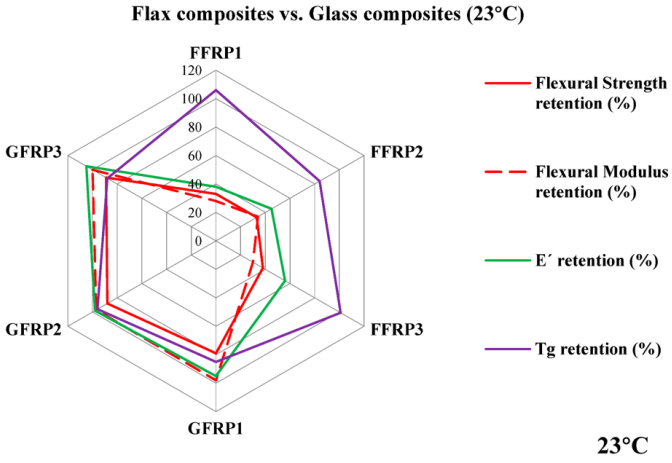

Figure 2.17: *Percentage retention of composite properties after saturation with water at 23°C, as reported by Das et al. [125]. Glass (GFR) and flax (GFR) fibres were used to reinforce three matrices: a petroleum based epoxy (P1), a bio-based recyclable epoxy with Recyclamine®(P2), and Elium®acrylic resin (P3). Reproduced from [125].*

2.3.3.3 Larger Scale Tests

Beyond coupon scale, a study on water absorption in 2.5 m long GF/acrylic and GF/epoxy tidal turbine blades has been performed by Murdy et al. [130]. The blades were immersed in water baths at ambient temperature and their masses were tracked. The GF/acrylic blade absorbed 0.14% over 6 months, and the GF/epoxy blade absorbed just 0.07% over 11 months. Osmotic blistering of the paint applied to the GF/acrylic blade (shown in Figure 2.18) was believed to have skewed the absorption measurements, as was the water absorption by the epoxy foam used to fill both blades.

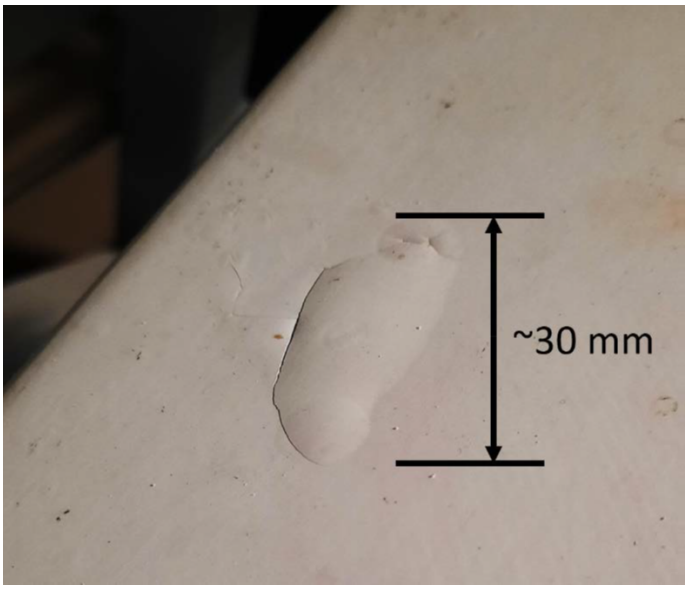

Figure 2.18: *Paint was applied to GF/epoxy and GF/acrylic tidal turbine blades, and osmotic blistering was observed in the GF/acrylic blade. Water is therefore pooling under the paint, increasing the measured water absorption.*

Coupons were also cut from GF/acrylic and GF/epoxy blades after 6 months of deployment [130]. The coupons were then immersed in water at 50°C for 4 months, and their water uptake was tracked. Fickian diffusion curves were fit to the data, which revealed that diffusion was faster in GF/acrylic than GF/epoxy (12.1×10^{-13} $m^2\,s^{-1}$ vs. 2.1×10^{-13} $m^2\,s^{-1}$ respectively), but that the maximum uptake of GF/epoxy was 1.7× that of GF/acrylic (0.78% vs. 0.47%). It should be noted, however, that the fibre volume fractions of the GF/acrylic and GF/epoxy were significantly different, at 60.9% and 48.8% respectively. This corresponds to matrix fractions of 39.1% and 51.2%. Considering that the matrix has been shown to dominate water absorption [80], it would make sense to normalise the maximum water content of each composite by its matrix fraction. This results in saturation water contents of the acrylic and epoxy resins of 1.2% and 1.5% respectively. Faster diffusion therefore occurs in GF/acrylic, although the epoxy resin appears to absorb 1.3× as much water as acrylic resin.

2.3.3.4 Summary

Overall, two main causes of degradation in mechanical properties of acrylic-matrix composites have been identified by several authors [75, 76, 80, 93] as swelling and

plasticisation of the matrix and degradation of the fibre-matrix interface. This results in water absorption causing large decreases in interface- and matrix-dominated properties, for example SBS is consistently shown to decrease by around 40%. Fibre-dominated properties such as 0° tensile modulus and strength are less strongly affected, and increases are even observed in some cases [75].

2.4 Fatigue of Composites

Wind and tidal turbine blades are subject to significant fatigue loading during their service life. Spatially and temporally varying flow speeds and turbulence, among other sources of cyclic loading, contribute to a blade withstanding large numbers of load cycles over its lifetime; for example, a wind turbine blade might be expected to undergo up to 10^9 fatigue cycles [131]. Fatigue damage is therefore a source of failure in wind and tidal turbine blades, requiring replacement and disposal of the affected blade.

2.4.1 An Introduction to Fatigue

Fatigue damage is caused by the progressive growth of cracks due to cyclic loading. In order to predict fatigue life, materials testing is usually employed to construct an *S-N curve* or *ε-N curve*—plot of the cyclic stress (σ) or strain (ε) amplitude respectively against the number of cycles before material failure, N. Talreja [132] proposed that the fatigue diagram for a unidirectional composite under 0° tension-tension fatigue can be split into three regions of strain/stress amplitude, as illustrated in Figure 2.19.

In Region I, damage occurs via the random breakage of reinforcement fibres rather than progressive damage. In Region II, progressive matrix cracking leads to fibre bridging and debonding. These matrix cracks initiate at stress concentrations cause by flaws. A detailed discussion of the various flaws which lead to progressive damage is given by Greenhalgh [133], but these flaws can be inherent in the constituent materials (e.g. fibre flaws which lead to breakage); they can be introduced during manufacture of the composite by e.g. introducing voids or inclusions; and they can be introduced during service, for example through impacts. The fibre-

matrix interface is highlighted as being particularly critical by Greenhalgh [133], and poor fibre-matrix bonding leads to poor fatigue performance. In Region III, the *fatigue limit* is reached as matrix cracks are arrested by reinforcement fibres, so progressive damage does not occur [132].

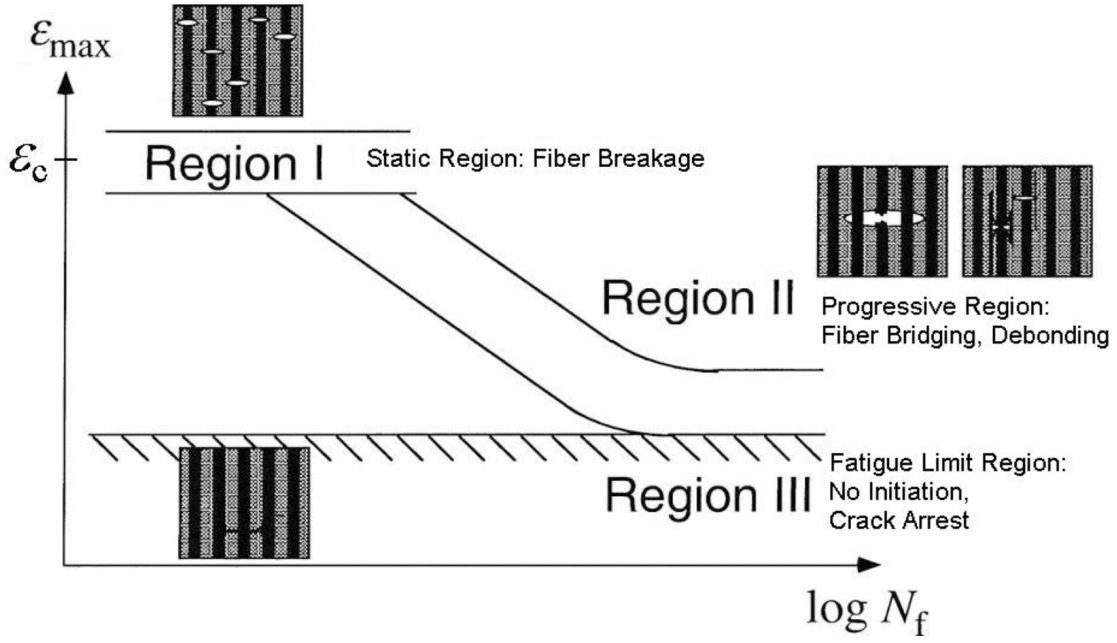

Figure 2.19: *The three regions of a strain (ε_c) vs. fatigue cycles (N_f) fatigue life diagram according to Talreja [132, 134]. Reproduced from [134].*

Region II shows a linear relationship between $\log N$ and $\log \varepsilon$ or $\log \sigma$. The simplest equation usually fit to data in this region is the Basquin equation [135, 136], shown in Equation 2.4, or equivalently in Equation 2.5. The factors A and b are constants, with b determining the slope of the curve.

$$S = A \cdot N^b \tag{2.4}$$

$$\log S = b \log N + \log A \tag{2.5}$$

Even small deviations from 0° loading can cause significant changes in the S-N curve [132]. According to Talreja [132], an angle of as little at 5° prevents the random, non-progressive fibre breakage that makes up region I, and so the S-N curve has only regions II and III. With increasing off-axis angle, the fracture strain and the strain at region III decrease until a minimum at 90° loading is reached. At this

point, fracture proceeds via transverse fibre debonding rather than the fibre fracture and interfacial debonding seen in 0° laminates [132].

The choices of matrix and reinforcement are both highly influential on the fatigue behaviour. The large variation in fatigue properties that can be caused by the matrix selection is illustrated in Figure 2.20. The importance of the fibres can be seen in the DNV standard DNV-ST-0164, which suggests values for b of -0.125 for GF/epoxy or GF/polyester, and -0.07 for CF/epoxy in the absence of experimental data, i.e. a lower S-N curve gradient is expected with carbon fibres.

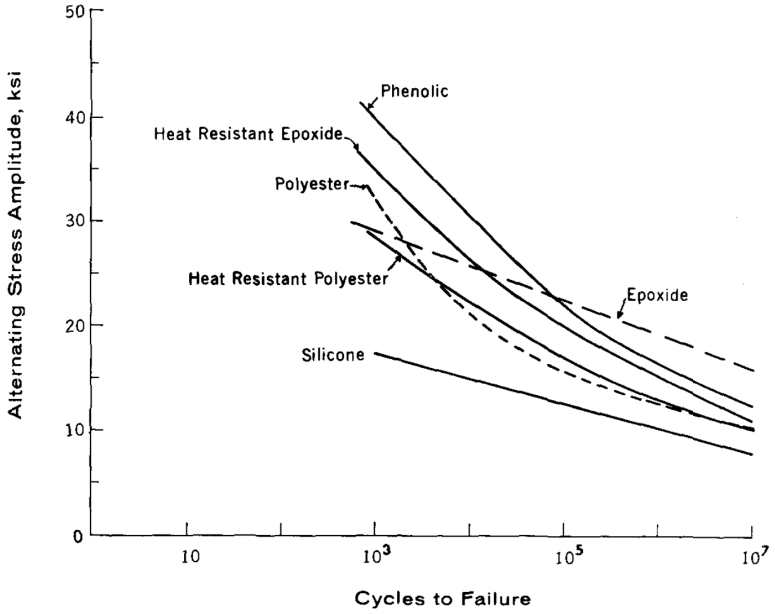

Figure 2.20: *An illustration of the effects of the matrix on the fatigue behaviour of GF-reinforced composites. Reproduced from [137].*

Region III is known as the 'fatigue limit'—the stress or strain amplitude at which the material has an indefinite fatigue life. The fatigue limit is a known feature of steel, but is known to be non-existent in aluminium [138]. The existence of a fatigue limit in composites is controversial, and D'Amore and Grassia [139] suggest that it has not been proven to exist. The fatigue of traditional composites has been characterised extensively, for example in the SNL/MSU/DOE fatigue database for wind turbine blade materials [140, 141], but many studies do not extend to Region III [132], possibly due to time constraints. However, a fatigue limit does appear to exist at around 360 MPa in the flexural fatigue data of CF/epoxy at 25 °C in Miyano et al. [142]. This corresponds to around 33% of the static flexural strength.

2.4.2 Fatigue of Acrylic-Matrix Composites

Given the large differences in fatigue behaviour that can exist between matrices, data from experimental testing must be used to ensure the fatigue performance of acrylic-matrix composites. The fatigue behaviour of glass- and carbon-reinforced acrylic has been characterised in several previous studies. Davies et al. [81] compared the tensile and flexural fatigue behaviour of GF/acrylic, GF/epoxy and CF/acrylic coupons before and after saturation with seawater. A $[0/(\pm 45)_2/0]$ layup was used for the GF-reinforced laminates, and a $[0/(\pm 45)_3/0]$ for the CF-reinforced laminates. The authors mention that the GF/acrylic reinforcement had an acrylic-tailored sizing, and the GF/epoxy and CF/acrylic reinforcements had non-specific sizings. In tensile fatigue, seawater ageing had little effect on CF/acrylic, but the fatigue lives of GF/acrylic and GF/epoxy were significantly reduced at high stresses. In flexural fatigue, the three materials' performance was similar and, in both tensile and flexural fatigue, GF/acrylic outperformed GF/epoxy. The dry tensile fatigue behaviour is included in Figure 2.21.

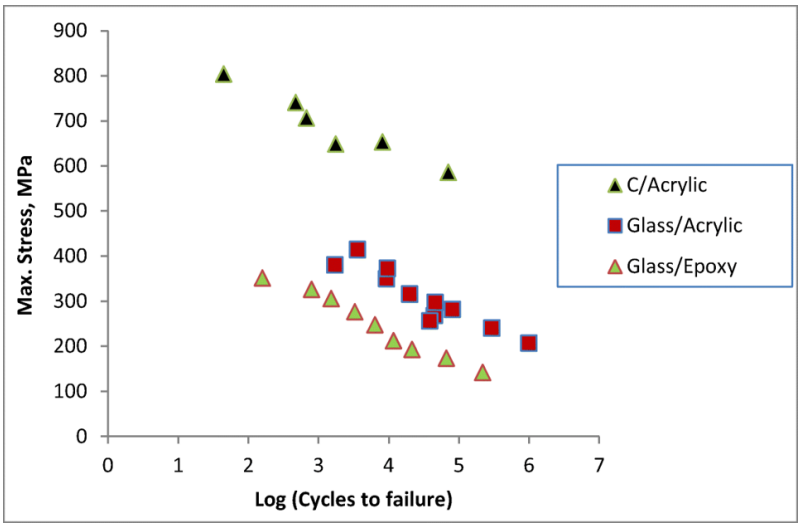

Figure 2.21: *Tension-tension S-N curves of dry GF/acrylic, GF/epoxy and CF/acrylic. Reproduced from [81].*

Cousins et al. [135] conducted extensive fatigue testing with GF/acrylic and GF/epoxy laminates as part of the IACMI Centre Project 4.2 [143]. Tensile fatigue tests were conducted on 0°, 90° and ±45° GF/acrylic laminates at room temperature and -30°C, on ±45° GF/epoxy and on ±45° GF/acrylic coupons with introduced de-

fects. Compressive fatigue tests were also conducted on 0°, 90° and ±45° GF/acrylic laminates. The fatigue life of GF/acrylic compared favourably to GF/epoxy in tension, and to GF/polyester in compression. The tensile and compressive S-N curves for 0° unidirectional coupons are included in Figure 2.22a and b respectively. The presence of voids in ±45° GF/acrylic laminates was found to reduce tension-tension fatigue life by an order of magnitude. The authors observed a stronger interface in GF/acrylic than in GF/epoxy as a coating of matrix remained after fracture of the former, but not the latter. This agrees with other studies [38, 81] and suggests good compatibility of acrylic resin with the multi-compatible sizing used in the study.

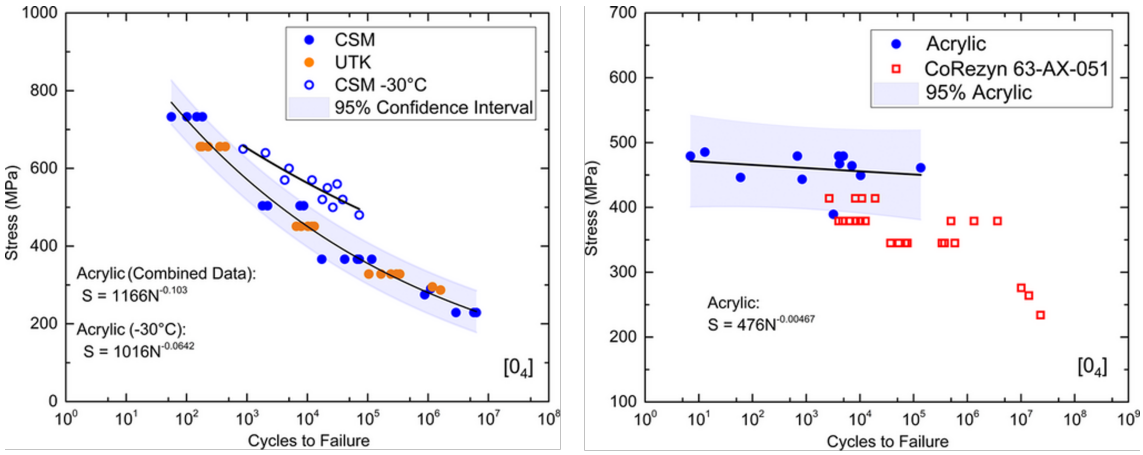

Figure 2.22: *S-N curves for 0° unidirectional GF/acrylic. (a) Tension-tension fatigue curves for testing at room temperature and -30°C. 'CSM' and 'UTK' refer to the two institutions which performed the tests. (b) Compression-compression fatigue data for GF/acrylic, with data included for GF/polyester from the MSU/DOE database [141]. Figures reproduced from [135].*

Data was also available on 0° GF/acrylic tension-tension fatigue in the SNL/MSU/DOE fatigue database [141], both before and after ageing in water. Limited data and details were included in the database, but the aged coupons absorbed 0.58% water and the data provided has been presented in Figure 2.23. Ageing decreased the tensile strength by 32%, but performance was similar, or even superior, in the aged coupons at low stress.

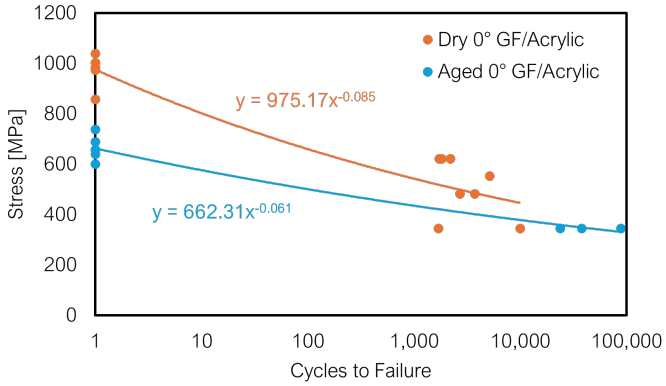

Figure 2.23: *Data from the SNL/MSU/DOE fatigue database [141] on 0° GF/acrylic composites under tension-tension fatigue. Both dry (orange) and water saturated (blue) coupons were tested. Curves of the form $S = AN^b$ have been fit to the data.*

Bakkal et al. [144] characterised the tensile fatigue behaviour of 0°/90°, 0°/90°/±45° and ±45° GF/acrylic composites with a multi-compatible sizing. The 0°/90° coupons had the best performance in low-cycle fatigue, followed by the 0°/90°/±45° and ±45° coupons respectively. As the applied stress decreased, the S-N curves of the 0°/90° and 0°/90°/±45° coupons converge. Stiffness degradation, as illustrated in Figure 2.24, was found to be greater in the 0°/90°/±45° coupons than the 0°/90° coupons. This indicates that there is greater damage accumulation in 0°/90°/±45° coupons. In addition, the authors calculate and measure increases in temperature during fatigue testing for multiple stress levels. Temperature increases were greater at higher stress levels, and generally calculated to be higher in the more resin-dominated 0°/90°/±45° laminates than the 0°/90° laminates but did not exceed the glass transition temperature of the matrix.

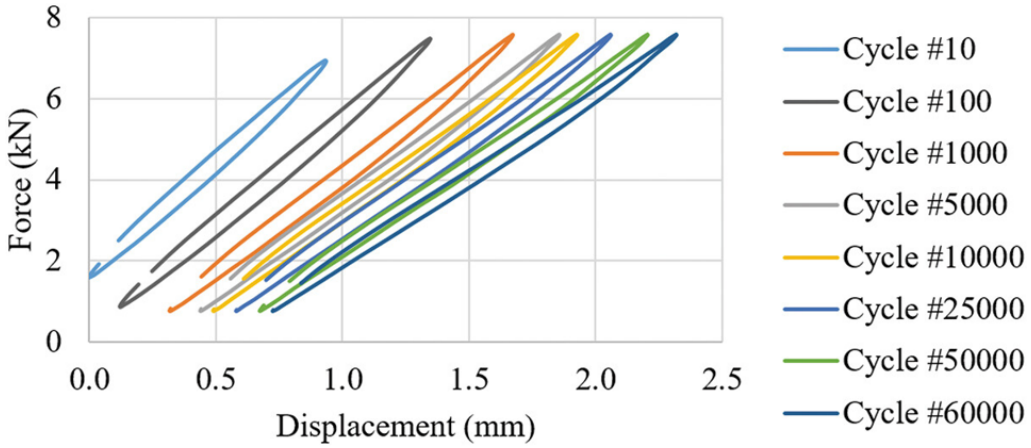

Figure 2.24: *The stiffness of a coupon tested under tension-tension fatigue decreases with increasing cycle number, as determined by the slope of the force-displacement curve. This is attributed to the accumulation of damage. Reproduced from [144].*

Boufaida et al. [79] applied static and cyclic in-plane shear testing to woven E-glass reinforced acrylic with either a multi-compatible or acrylic-tailored sizing agent. During static testing, coupons with the acrylic-tailored sizing had a 4% higher shear strength at a shear strain of 0.05 than coupons with a multi-compatible sizing agent. Rather than typical testing to failure to determine the S-N curves of the coupons, temperature increases during cyclic testing were monitored and used to determine the onset of damage in the coupons, and thereby predict how they would behave during fatigue. A higher damage onset threshold in the acrylic-sized coupons suggested that the tailored sizing increased fatigue life (Figure 2.25). The authors do note an incompatibility between the multi-compatible sizing and acrylic resin, however, as the sizing prevented resin polymerisation at room temperature. Elevated temperatures were therefore required to manufacture coupons with the multi-compatible sizing, which has not been observed in other studies and may have affected the results.

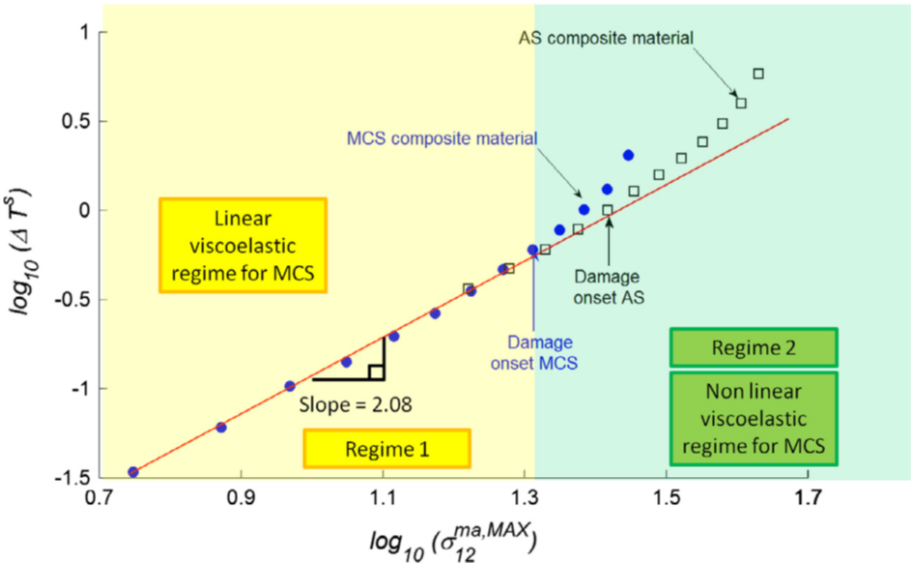

Figure 2.25: *The threshold stress ($\sigma_{12}^{ma,MAX}$) for damage accumulation in acrylic-sized (AS) and multi-compatible sized (MCS) ±45° GF/acrylic composites, as determined via thermal imaging. A departure from linear viscoelastic behaviour causes a sharp rise in the coupon's temperature (ΔT^s), and indicates the onset of damage progression.*

Flax-reinforced acrylic composites have also been tested in fatigue. Most relevant to the current work is a study by Davies et al. [145] in which flax/acrylic composites were tested before and after seawater ageing. Water absorption kinetics were studied for immersed and one-sided exposure, and a variety of tests (tensile, short beam shear and four-point flexure) and layups (0°, 0°/90° and ±45°) were used for static testing. Four-point flexural fatigue testing was conducted on dry 0° and 0°/90° coupons, and aged 0° coupons. Flax-fibre composites are shown to be much more susceptible to water absorption than glass composites, with the fatigue strength of 0° four-point bend coupons reducing by approximately 45% at 10^5 cycles after saturation.

Work on the effect of fibre moisture content in flax/acrylic composites has been undertaken by Javanshour et al. [146]. Fatigue testing of composites with woven 0°/90° flax reinforcement showed that storage of flax fibres in humid conditions (before the manufacture of the composite) decreases low-cycle fatigue life, but reduces the slope of the composite S-N curve and increases ductile failure modes. Static testing was conducted on 90°, ±45° and 0°/90° coupons, which revealed strong interfacial bonding and good compatibility with the acrylic resin with no need for a

sizing agent.

The studies discussed so far used coupon-scale testing to characterise acrylic-matrix composites, but full-scale fatigue testing of acrylic-matrix wind [4] and tidal turbine [7] blades has also been carried out by NREL. A 13 m long GF/acrylic wind turbine blade was compared to a GF/epoxy blade by Murray et al. [4], using reinforcements treated with a multi-compatible sizing agent. Static and fatigue loading were applied, and the overall performance was similar with less than a 0.5% variation in compliance over 1×10^6 cycles. Greater material damping in the acrylic-matrix blade resulted in faster free-decay of vibrations, which could have positive effects in the fatigue performance of the turbine [7].

Murray et al. [7] also compared 2.5 m long GF/acrylic and GF/epoxy tidal turbine blades in static and fatigue testing, before and after 6 months of deployment. The epoxy-matrix blade survived 2 million cycles of fatigue testing, whereas the acrylic-matrix blades failed by 1.2 million cycles, with stiffness degradation observed after only 400,000 cycles. A combination of incompatibility between the acrylic and the foaming epoxy used to fill the blade cavity, incompatibility with the epoxy-based paint used to coat the blades, and poor performance of the leading-edge overlay, led to failure of the adhesive bonds in the blade, and so failure was not caused by poor fatigue performance of the GF/acrylic blade skins.

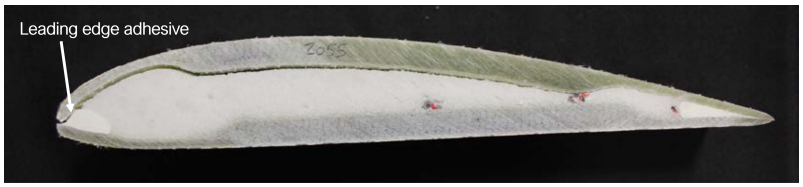

Figure 2.26: *Image from Murray et al. [7] of leading edge adhesive failure in a GF/acrylic tidal turbine blade. Failure initiated between the composite skin and the epoxy foam in the cavity.*

2.5 Joining of Acrylic-Matrix Composites

As discussed in Section 2.1, wind and tidal turbine blades are often manufactured in multiple sections which then require joining together. The current method of joining these parts is to use adhesives. However, as the results from Murray et

al. [7] show, adhesive bonds can be a source of failure (Figure 2.26). The use of thermoplastic matrices such as acrylic provides the opportunity to use welded joints instead, and it has been suggested that higher joint strengths, greater fatigue life and faster processing times could be achieved through welding [147].

There are several types of welding which can be used for thermoplastic polymer matrix composites. Literature on the welding of acrylic-matrix composites has concentrated on fusion welding, in which heat is applied to the adherends and the polymer matrix melts and interdiffuses when pressure is applied to the joint. Heat can be applied in several ways: for example, via a heating element in the joint (resistive and inductive welding), through frictional heating (ultrasonic, vibrational or spin welding), or via the direct heating of the adherends (e.g. with infrared or other radiation, a hot-plate, or hot gas) [148].

Four methods of welding acrylic-matrix composites are discussed in the literature: resistance, induction, ultrasonic and infra-red welding [147, 149–152]. Each of these is detailed in Figure 2.27, and all require the application of pressure across the bond. In resistance and induction welding, a heating element is pressed between the adherends, heat is applied, and the adherend polymer melts. Heating elements are conductive meshes, for example steel or carbon fibre, and can be impregnated with polymer before welding. In resistance welding, the element is heated by the direct application of a current, whereas in induction welding an electromagnetic field induces currents in the mesh [147, 148, 153, 154]. In ultrasonic welding, ultrasonic vibrations are generated and applied to the adherends via a sonotrode. These vibrations cause frictional heating and melting of the polymer at the bondline. The weld quality can be improved by including an energy director—a protrusion of extra polymer which melts first and fills the bondline [147, 155, 156]. Finally, in infrared welding the adherend surfaces are heated via an infrared lamp or proximity to a hot metal plate. This melts the polymer surface before the adherends are pressed together [152, 157].

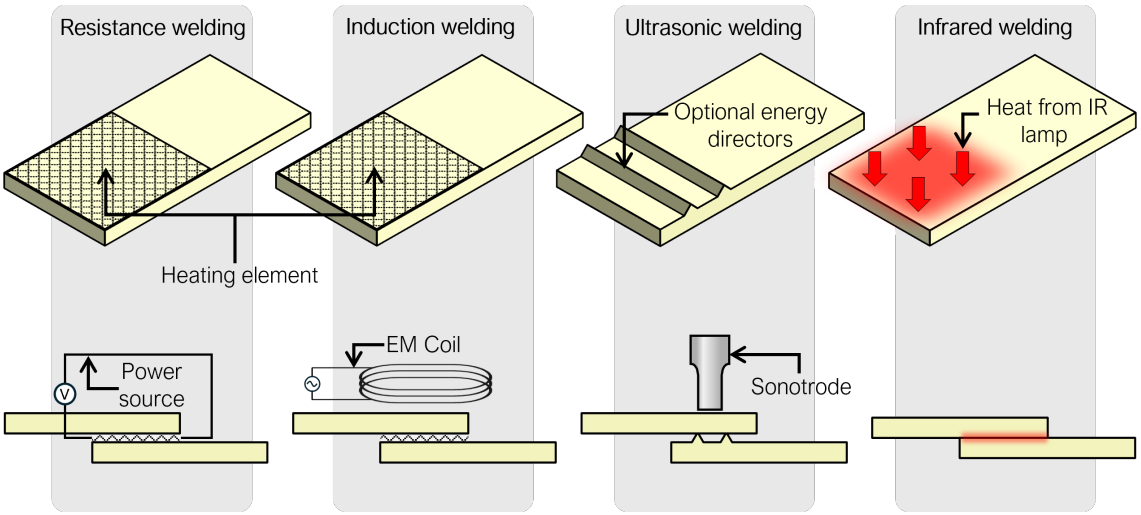

Figure 2.27: *Illustrations of resistance, induction, ultrasonic and infrared welding [147, 148]—the four welding methods demonstrated in acrylic-matrix composites.*

Resistance and induction welding in glass fibre reinforced acrylic composites have been explored by Murray et al. [147] using single lap shear testing. In this study, single lap resistance welds had average single lap strengths ranging between 19.1 MPa and 22.4 MPa depending on the heating element used (see Figure 2.28). The fatigue limit, defined by the authors as the stress at which a coupon survived 10 million cycles at a stress ratio of R=0.1 and a frequency of 10 Hz, was reported to be 5 MPa for resistance welds joined using a carbon fibre heating element [147]. Coupons joined via induction welding with a carbon fibre heating element reached a lower average single lap shear strength of 20.4 MPa.

For comparison, several adhesive joints were also tested, although the highest adhesive single lap strength and fatigue limit—achieved using Plexus MA310 methacrylate adhesive—were only 17.4 MPa and 3 MPa respectively. Two other adhesives were also tested, epoxy-based Acralock SA10-60 and another methacrylate adhesive Plexus MA590, both of which are suitable for thicker bondlines. Both formed significantly weaker bonds than Plexus MA310, at only 10 MPa and 8.5 MPa respectively [147], and testing by Murray et al. (2021) with a different epoxy adhesive (Hexion BPR 135) also showed an incompatibility with acrylic resin [4]. As discussed in [7], ensuring chemical compatibility between blade materials is therefore of paramount importance with novel resins such as acrylic.

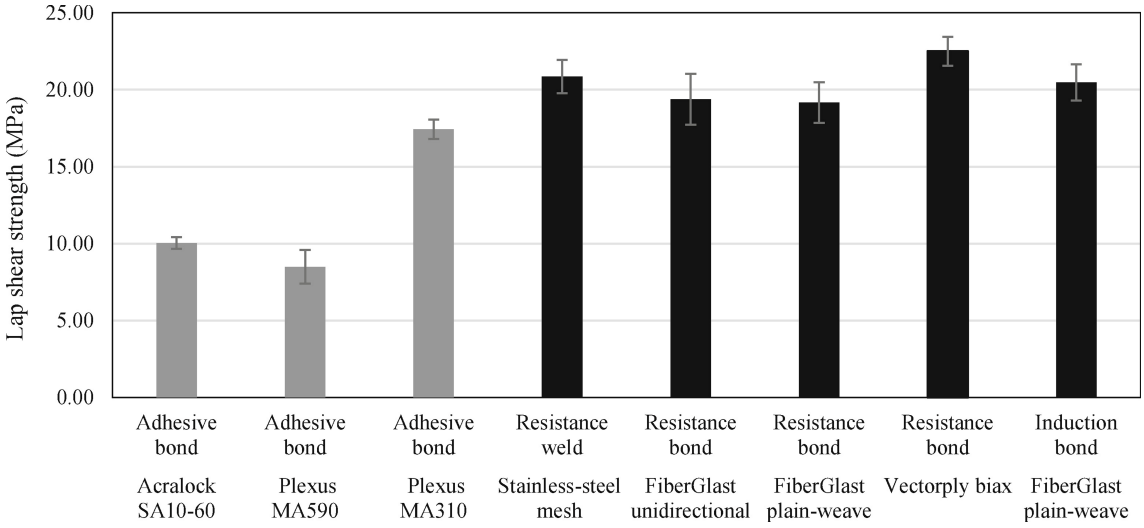

Figure 2.28: *The single lap shear strengths of GF/acrylic joined with adhesives, and resistance/induction welding with various heating elements. Reproduced from [147].*

In other studies, ultrasonic welding of carbon fibre reinforced acrylic was investigated by Bhudolia et al [149, 150]. Similar results were achieved to [147], with welded single lap joints reaching a strength of 18.9 MPa with proper optimisation, which was 33% higher than the strength of adhesive bonds (14.2 MPa) made with Bostik SAF 30-5 methacrylate adhesive. The fatigue strength of ultrasonically welded single lap coupons at 10^5 cycles (R = 0.1, frequency = 5Hz) was also 12% higher than that of adhesive bonds (7.26 MPa and 6.48 MPa respectively), although this reduced to a 7% difference at 10^7 cycles, as shown in Figure 2.29.

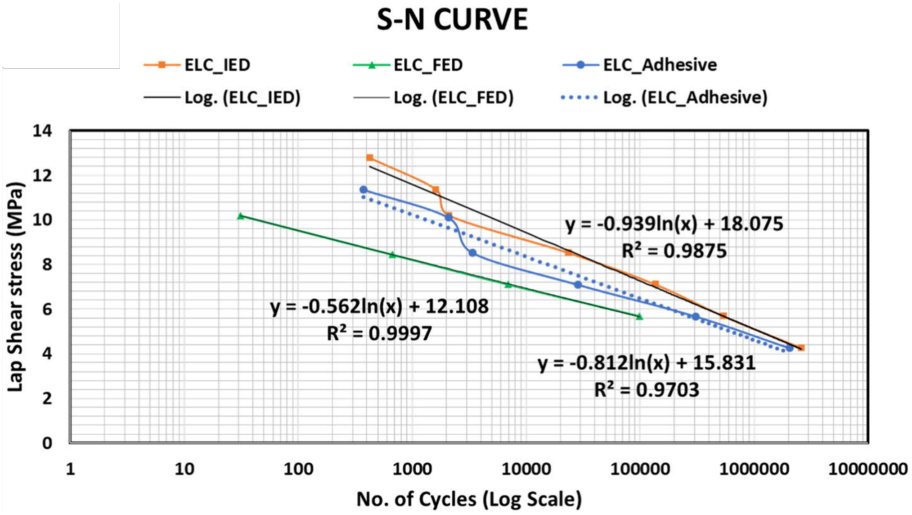

Figure 2.29: *S-N curves of single lap shear coupons bonded with an adhesive, or via ultrasonic welding with (IED) or without (FED) energy directors. Reproduced from [150].*

The fourth welding method demonstrated for acrylic-matrix composites in the literature is infrared welding. Perrin et al. [152] obtained single lap shear strengths of 12.3 MPa using this method, although this was improved up to 19.1 MPa by the addition of a small amount of crosslinker to the acrylic matrix of the adherends.

Although each welding method has its advantages and disadvantages, a common requirement for all three is intimate contact between the adherends while pressure is applied, which may not be possible when manufacturing large and complex parts. In wind turbine blades, for example, adhesive bondline thicknesses of up to 30 mm may be required due to large manufacturing tolerances [5, 158]. In addition, ultrasonic welding may not be suitable for joining thick sections as vibrations are attenuated through the adherend thickness [156, 159]. There is therefore uncertainty about the commercial application of polymer welding in the wind power industry, and there has not been a published demonstration of welding applied to wind turbine blades. The closest was a study by Murray et al. (2021) [160] which aimed to test a lightning protection for resistance-welded wind turbine blades, which may be vulnerable to lightning strike due to the heating element which remains in the bondline. However, equipment with the required power output was not available, and so the blade was adhesively bonded with the heating element inside to create a 'mock weld'.

2.6 Chapter Summary

Several recyclable resins are commercially available as composite matrices for use in the marine and renewable energy sectors. These resins belong to three families of polymer: thermosets with cleavable crosslinks, covalent adaptive networks, and infusible thermoplastics. Cleavable thermosets appear to be the most popular option among wind turbine manufacturers. However, liquid acrylic resins (Elium®) are the most promising thermoplastic resins for large structures, and are the only thermoplastic resin demonstrated in the large wind turbine blades that are common today.

For acrylic-matrix composites to be used in the marine environment, they must demonstrate low water absorption and good long-term durability. This is often tested by immersing composite coupons in heated water to accelerate absorption, and characterising the mass uptake and the mechanical properties after saturation. In general, acrylic resin was found to absorb in the region of 2% water, and glass- and carbon- reinforced acrylic absorbed around 1% water. Water absorption can cause several degradation mechanisms in polymers and composites, but the most significant in glass fibre reinforced acrylic composites were found to be interfacial degradation and matrix plasticisation. Carbon fibre composites seemed to experience less permanent damage, and flax-reinforced absorbed significantly more water with greater decreases in mechanical properties. Beyond the coupon scale, the immersion of 2.3 m long tidal turbine blades in water suggested that acrylic-matrix composites absorb water more quickly than epoxy-matrix composites, but that saturation is unlikely to be reached in either composite over the lifetime of a turbine.

The long-term durability of composites can be demonstrated via fatigue testing. The fatigue of acrylic-matrix composites has been studied be several authors, with both the tensile and compressive fatigue properties comparing favourably with traditional thermosets. Fatigue testing after saturation with water has also been studied, and has suggested that glass-fibre reinforced composites experience greater decreases in fatigue life than their carbon-fibre reinforced equivalents. Testing of full-scale acrylic-matrix wind and tidal turbine blades suggested good fatigue performance of the composite blade skins compared to equivalent epoxy-matrix blades, but that chemical incompatibility between the acrylic matrix and other blade com-

ponents may cause premature failure.

A correctly selected fibre sizing agent may improve the water absorption and fatigue properties of a composite by increasing interfacial strength, but it is less clear whether a tailored sizing agent provides benefits over a multi-compatible sizing. The effects of the sizing agent in acrylic-matrix composites have been studied to a limited extent, and conclusions are mixed, with some studies suggesting acrylic-tailored sizing agents improve performance over multi-compatible sizings, and others seeing little difference. Indeed, many of the studies discussed in this review used multi-compatible sizings successfully. However, the interfacial degradation observed in composites after saturation with water highlights the critical role of the fibre-matrix interface in seawater durability, and shows that further research into the topic is warranted.

While adhesives are commonly used to join thermoset composites, acrylic-matrix composites are thermoplastic and can therefore additionally be welded. Four types of welding have been demonstrated in the literature: ultrasonic, resistance, induction and infrared. The strengths of these welded bonds have been compared to adhesives using single lap shear testing, with welded bond strengths ($\sim$19–22 MPa) exceeding adhesive bond strengths ($\sim$8–17 MPa), and resulting in enhanced fatigue life. These demonstrations at the coupon scale show that the weldability of acrylic-matrix composites could be a benefit over its thermoset competitors, but welding of thermoplastic wind and tidal turbine blades still neesd to be demonstrated in practice.

In conclusion, acrylic-matrix composites may be the solution to achieve circularity in the marine and renewable energy industries. They are easily processed, their mechanical and fatigue properties compare favourably to thermoset resins, and they can be welded which could result in stronger bonds. However, their adoption in these industries will require continued research into their environmental durability, and questions remain about the optimisation of their fibre sizing agents.

2.7 Chapter References

[1] L. Mishnaevsky, K. Branner, H. N. Petersen, J. Beauson, M. McGugan, and B. F. Sorensen. Materials for wind turbine blades: An overview. *Materials (Basel)*, 10(11), 2017. ISSN 1996-1944 (Print) 1996-1944 (Linking). doi: 10.3390/ma10111285.

[2] Oliver Nixon-Pearson, Peter Greaves, Dimitrios Mamalis, and Lewis Stevenson. Wind turbine blades design and manufacturing, current state-of-the art literature review. Report, 2022.

[3] Anaële Lefeuvre, Sébastien Garnier, Leslie Jacquemin, Baptiste Pillain, and Guido Sonnemann. Anticipating in-use stocks of carbon fibre reinforced polymers and related waste generated by the wind power sector until 2050. *Resources, Conservation and Recycling*, 141:30–39, 2019. ISSN 0921-3449. doi: https://doi.org/10.1016/j.resconrec.2018.10.008.

[4] Robynne E. Murray, Ryan Beach, David Barnes, David Snowberg, Derek Berry, Samantha Rooney, Mike Jenks, Bill Gage, Troy Boro, Sara Wallen, and Scott Hughes. Structural validation of a thermoplastic composite wind turbine blade with comparison to a thermoset composite blade. *Renewable Energy*, 164:1100–1107, 2021. doi: 10.1016/j.renene.2020.10.040.

[5] K. P. Subrahmanian and Fabrice Dubouloz. Adhesives for bonding wind turbine blades. *Reinforced Plastics*, 53(1):26–29, 2009. ISSN 0034-3617. doi: https://doi.org/10.1016/S0034-3617(09)70044-X.

[6] Hexcel Corporation. Hexcel and vestas expand composite materials supply agreement for wind blades, 2017. URL `https://www.hexcel.com/News/News-Releases/2573/hexcel-and-vestas-expand-composite-materials-supply-agreement-for-wind-blades`.

[7] Robynne E. Murray, Ryan Beach, Paul Murdy, Scott Dana, and Scott Hughes. Structural characterization of deployed thermoplastic and thermoset composite tidal turbine blades. Report, 2024-04-08 2024.

[8] Tim Clark. New turbine blade design aims to reduce cost of tidal power, 2023. URL https://www.newcivilengineer.com/latest/new-turbine-blade-design-aims-to-reduce-cost-of-tidal-power-25-10-2023/.

[9] Siemens Wind Power. Siemens unveils 75 m wind turbine blade. *Reinforced Plastics*, 56(4):30–31, 2012. ISSN 0034-3617. doi: https://doi.org/10.1016/S0034-3617(12)70078-4.

[10] Tido Eger, Claudia M Eckert, and P John Clarkson. Engineering change analysis during ongoing product development. In *ICED 2007, the 16th International Conference on Engineering Design*, pages 629–630 (exec. Summ.), full paper no. DS42–P–27, 2007.

[11] P. Liu and C. Y. Barlow. Wind turbine blade waste in 2050. *Waste Management*, 62:229–240, 2017. ISSN 1879-2456 (Electronic) 0956-053X (Linking). doi: 10.1016/j.wasman.2017.02.007.

[12] Department for Energy Security and Net Zero. Energy trends uk, october to december 2023 and 2023, 2024. URL https://www.gov.uk/government/statistics/energy-trends-march-2024.

[13] Wind Europe. Accelerating wind turbine blade circularity. Report, 2020. URL https://windeurope.org/intelligence-platform/product/accelerating-wind-turbine-blade-circularity/.

[14] Jr. Mishnaevsky, L. Sustainable end-of-life management of wind turbine blades: Overview of current and coming solutions. *Materials (Basel)*, 14(5), 2021. ISSN 1996-1944 (Print) 1996-1944 (Linking). doi: 10.3390/ma14051124.

[15] Aubryn Cooperman, Annika Eberle, and Eric Lantz. Wind turbine blade material in the united states: Quantities, costs, and end-of-life options. *Resources, Conservation and Recycling*, 168, 2021. ISSN 09213449. doi: 10.1016/j.resconrec.2021.105439.

[16] Wind Europe. How to build a circular economy for wind turbine blades through policy and partnerships. Report, 2020. URL https://

windeurope.org/wp-content/uploads/files/policy/position-papers/WindEurope-position-paper-how-to-build-a-circular-economy.pdf.

[17] BladeBridge. Midleton to youghal greenway bridge, 2024. URL https://www.bladebridge.ie/products/midleton-to-youghal-greenway-bridge/.

[18] Dylan S. Cousins, Yasuhito Suzuki, Robynne E. Murray, Joseph R. Samaniuk, and Aaron P. Stebner. Recycling glass fiber thermoplastic composites from wind turbine blades. *Journal of Cleaner Production*, 209:1252–1263, 2019. doi: 10.1016/j.jclepro.2018.10.286.

[19] Winifred Obande, Danijela Stankovic, Ankur Bajpai, Machar Devine, Christian Wurzer, Anna Lykkeberg, Jennifer A. Garden, Conchúr M. Ó Brádaigh, and Dipa Ray. Thermal reshaping as a route for reuse of end-of-life glass fibre-reinforced acrylic composites. *Composites Part B: Engineering*, 257, 2023. ISSN 13598368. doi: 10.1016/j.compositesb.2023.110662.

[20] John Summerscales, Jasper Graham-Jones, and Richard Pemberton. *Marine Composites : Design and Performance*. Woodhead Publishing series in composites science and engineering. Woodhead Publishing, Cambridge, MA, 2018. ISBN 9780081019139.

[21] K. van Rijswijk and H. E. N. Bersee. Reactive processing of textile fiber-reinforced thermoplastic composites – an overview. *Composites Part A: Applied Science and Manufacturing*, 38(3):666–681, 2007. ISSN 1359835X. doi: 10.1016/j.compositesa.2006.05.007.

[22] Yang Qin, John Summerscales, Jasper Graham-Jones, Maozhou Meng, and Richard Pemberton. Monomer selection for in situ polymerization infusion manufacture of natural-fiber reinforced thermoplastic-matrix marine composites. *Polymers*, 12(12), 2020. ISSN 2073-4360. doi: 10.3390/polym12122928.

[23] Marlec Engineering. Rutland 1200 marine windcharger. URL https://www.marlec.co.uk/product/rutland-1200-windcharger/.

[24] Ryse Energy. Air 40 turbine, 2024. URL https://www.ryse.energy/air-40-turbine/.

[25] ÉireComposites. Renewable energy. URL https://www.eirecomposites.com/renewables/.

[26] SD Wind Energy. Sd6 and sd6+ wind turbine. URL https://sd-windenergy.com/small-wind-turbines/sd6-6kw-wind-turbine/.

[27] P. Mallon, Mahmoud Dweib, Saeed Ziaee, Amit Chatterjee, and John Gillespie Jr. Vartm and rtm processing of pbt and pa thermoplastic composites. Report, 10/30 2002.

[28] Zsófia Osváth, Anita Szőke, Szabolcs Pásztor, Györgyi Szarka, László Balázs Závoczki, and Béla Iván. Post-polymerization heat effect in the production of polyamide 6 by bulk quasiliving anionic ring-opening polymerization of ε-caprolactam with industrial components: A green processing technique. *Processes*, 8(7):856, 2020. ISSN 2227-9717. URL https://www.mdpi.com/2227-9717/8/7/856.

[29] James Murray, Colin Robert, Klaus Gleich, Edward McCarthy, and Conchur O'Bradaigh. Manufacturing of unidirectional stitched glass fabric reinforced polyamide 6 by thermoplastic resin transfer moulding. *Materials and Design*, 189:108512, 2020. doi: 10.1016/j.matdes.2020.108512.

[30] James Murray, Edward McCarthy, Conchur O'Bradaigh, Klaus Gleich, Tom Allen, and Simon Bickerton. Impact performance of thermoplastic resin transfer moulded carbon fibre composites. In *SAMPE Europe Conference 2020, Amsterdam*, 2020.

[31] Tobias Abt and Miguel Sánchez-Soto. A review of the recent advances in cyclic butylene terephthalate technology and its composites. *Critical Reviews in Solid State and Materials Sciences*, 42(3):173–217, 2017. ISSN 1040-8436. doi: 10.1080/10408436.2016.1160820.

[32] Conchúr M. Ó Brádaigh, Adrian Doyle, Derrick Doyle, and PJ Feerick. Electrically-heated ceramic composite tooling for out-of-autoclave manufacturing of large composite structures. *SAMPE Journal*, 47(4):6–14, 2011. ISSN 0091-1062.

[33] Larry Rulison. Boom cycle ends for cyclics corp., 2010. URL https://www.sfgate.com/default/article/Boom-cycle-ends-for-Cyclics-Corp-892623.php.

[34] Common Register Portal of the German Federal States. Ausdruck handelsregister hrb 6741 cb, 2010. URL https://www.handelsregister.de/.

[35] Adrian Doyle, James Lee, Edward Archer, Keith Doyle, Patrick Feerick, Siora Coll, Conchur O'Bradaigh, Adrian Murtaugh, Patrick Mallon, and Walter Stanley. Composite articles comprising in-situ-polymerisable thermoplastic material and processes for their construction, 2007/07/18 2010. URL https://lens.org/116-432-490-299-16X.

[36] Janek Herzog, Rainer Wendel, Peter G. Weidler, Michael Wilhelm, Philipp Rosenberg, and Frank Henning. Moisture adsorption and desorption behavior of raw materials for the t-rtm process. *Journal of Composites Science*, 5(1): 12, 2021. ISSN 2504-477X. URL https://www.mdpi.com/2504-477X/5/1/12.

[37] Kazue Ueda, Kazunobu Yamada, Makoto Nakai, Tsunetoshi Matsuda, Masahiro Hosoda, and Kazuo Tai. Synthesis of high molecular weight nylon 6 by anionic polymerization of ε-caprolactam. *Polymer Journal*, 28(5): 446–451, 1996. ISSN 1349-0540. doi: 10.1295/polymj.28.446.

[38] Winifred Obande, Dimitrios Mamalis, Dipa Ray, Liu Yang, and Conchúr M. Ó Brádaigh. Mechanical and thermomechanical characterisation of vacuum-infused thermoplastic- and thermoset-based composites. *Materials and Design*, 175, 2019. ISSN 02641275. doi: 10.1016/j.matdes.2019.107828.

[39] Winifred Obande, Conchúr M. Ó Brádaigh, and Dipa Ray. Continuous fibre-reinforced thermoplastic acrylic-matrix composites prepared by liquid resin infusion – a review. *Composites Part B: Engineering*, 215, 2021. ISSN 13598368. doi: 10.1016/j.compositesb.2021.108771.

[40] IRT Jules Verne. Zebra project achieves key milestone with production of the first prototype of its recyclable wind turbine blade, 2022. URL https://www.irt-jules-verne.fr/wp-content/uploads/zebra-pr-en-vdef.pdf.

[41] Robynne E. Murray, Scott Jenne, David Snowberg, Derek Berry, and Dylan Cousins. Techno-economic analysis of a megawatt-scale thermoplastic resin wind turbine blade. *Renewable Energy*, 131:111–119, 2019. ISSN 0960-1481. doi: https://doi.org/10.1016/j.renene.2018.07.032.

[42] Pierre Gerard, Michel Glotin, and Bernay Hochstetter. Composite material via in-situ polymerization of thermoplastic (meth) acrylic resins and its use, US Patent 9,777,140 B2, 2017.

[43] Pierre Gerard. Liquid (meth) acrylic syrup for impregnating a fibrous substrate, method for impregnating a fibrous substrate, and composite material produced after polymerisation of said pre-impregnated substrate, US Patent 10,280,271 B2, 2019.

[44] Q. Charlier, F. Lortie, and J. F. Gérard. Interfacial adhesion in glass-fiber thermoplastic composites processed from acrylic reactive systems, a multi-scale experimental analysis. *International Journal of Adhesion and Adhesives*, 98, 2020. ISSN 01437496. doi: 10.1016/j.ijadhadh.2019.102536.

[45] Haithem Bel Haj Frej, Romain Léger, Didier Perrin, Patrick Ienny, Pierre Gérard, and Jean-François Devaux. Recovery and reuse of carbon fibre and acrylic resin from thermoplastic composites used in marine application. *Resources, Conservation and Recycling*, 173, 2021. ISSN 09213449. doi: 10.1016/j.resconrec.2021.105705.

[46] Winifred Obande, Conchúr M. Ó Brádaigh, and Dipa Ray. Thermoplastic hybrid-matrix composite prepared by a room-temperature vacuum infusion and in-situ polymerisation process. *Composites Communications*, 22(August): 22–27, 2020. doi: 10.1016/j.coco.2020.100439.

[47] Winifred Obande, Weronika Gruszka, Jennifer A. Garden, Christian Wurzer, Conchúr M. Ó Brádaigh, and Dipa Ray. Enhancing the solvent resistance and thermomechanical properties of thermoplastic acrylic polymers and composites via reactive hybridisation. *Materials and Design*, 206, 2021. ISSN 02641275. doi: 10.1016/j.matdes.2021.109804.

[48] Raymond Hajj, Antoine Duval, Sébastien Dhers, and Luc Avérous. Network design to control polyimine vitrimer properties: Physical versus chemical approach. *Macromolecules*, 53(10):3796–3805, 2020. ISSN 0024-9297. doi: 10.1021/acs.macromol.0c00453.

[49] Mallinda. Vitrimax t130 tds, 2021. URL `https://mallinda.com/wp-content/uploads/2021/10/Mallinda-TDS-T130_10.12.21.pdf`.

[50] Philip Taynton, Huagang Ni, Chengpu Zhu, Kai Yu, Samuel Loob, Yinghua Jin, H. Jerry Qi, and Wei Zhang. Repairable woven carbon fiber composites with full recyclability enabled by malleable polyimine networks. *Advanced Materials*, 28(15):2904–2909, 2016. ISSN 0935-9648. doi: https://doi.org/10.1002/adma.201505245.

[51] Philip Taynton, Kai Yu, Richard K. Shoemaker, Yinghua Jin, H. Jerry Qi, and Wei Zhang. Heat- or water-driven malleability in a highly recyclable covalent network polymer. *Advanced Materials*, 26(23):3938–3942, 2014. ISSN 0935-9648. doi: https://doi.org/10.1002/adma.201400317.

[52] Pradip Kumar Dubey, Satish Kumar Mahanth, and Amit Dixit. Recyclamine® - novel amine building blocks for a sustainable world. In *SAMPE NEXUS 2021*, 2021. doi: 10.33599/nasampe/s.21.0632.

[53] Swancor. Swancor launched recyclable thermosetting epoxy resin "EzCiclo", leading to zero-carbon era, 2022. URL `http://www.swancor.com.cn/en/news_detail.aspx?id=226`.

[54] Chen Wang, Avantika Singh, Erik G. Rognerud, Robynne Murray, Grant M. Musgrave, Morgan Skala, Paul Murdy, Jason S. DesVeaux, Scott R. Nicholson, Kylee Harris, Richard Canty, Fabian Mohr, Alison J. Shapiro, David Barnes, Ryan Beach, Robert D. Allen, Gregg T. Beckham, and Nicholas A. Rorrer. Synthesis, characterization, and recycling of bio-derivable polyester covalently adaptable networks for industrial composite applications. *Matter*, 7(2):550–568, 2024. ISSN 2590-2393. doi: 10.1016/j.matt.2023.10.033.

[55] Ryan W. Clarke, Erik G. Rognerud, Allen Puente-Urbina, David Barnes, Paul Murdy, Michael L. McGraw, Jimmy M. Newkirk, Ryan Beach, Jacob A.

Wrubel, Levi J. Hamernik, Katherine A. Chism, Andrea L. Baer, Gregg T. Beckham, Robynne E. Murray, and Nicholas A. Rorrer. Manufacture and testing of biomass-derivable thermosets for wind blade recycling. *Science*, 385 (6711):854–860, 2024. doi: 10.1126/science.adp5395.

[56] Alexander Ahrens, Andreas Bonde, Hongwei Sun, Nina Kølln Wittig, Hans Christian D. Hammershøj, Gabriel Martins Ferreira Batista, Andreas Sommerfeldt, Simon Frølich, Henrik Birkedal, and Troels Skrydstrup. Catalytic disconnection of c–o bonds in epoxy resins and composites. *Nature*, 617(7962): 730–737, 2023. ISSN 1476-4687. doi: 10.1038/s41586-023-05944-6.

[57] Vestas. Vestas unveils circularity solution to end landfill for turbine blades, 2023. URL https://www.vestas.com/en/media/company-news/2023/vestas-unveils-circularity-solution-to-end-landfill-for-c3710818.

[58] Swancor. Swancor and siemens gamesa announced a strategic collaboration on recyclable blades with intention to utilize swancor's revolutionary recyclable thermosetting epoxy resin, 2022/07/08 2022. URL https://www.swancor.com/en/news/detail/Swancor-and-Siemens-Gamesa-announced-a-strategic-collaboration-on-recyclable-blades-with-intention-to-utilize-Swancors-revolutionary-recyclable-thermosetting-epoxy-resin-EzCiclo.

[59] Siemens Gamesa. A winning collaboration behind the recyclableblade, 2021/11/22 2021. URL https://www.siemensgamesa.com/en-int/explore/journal/2021/11/recyclable-blade.

[60] Swancor. Swancor cooperated with ming yang smart energy to build wind blade with swancor ezciclo recyclable thermosetting resin, 2023. URL http://www.swancor.com.cn/en/news_detail.aspx?id=249.

[61] J. L. Thomason. The interface region in glass fibre-reinforced epoxy resin composites: 2. water absorption, voids and the interface. *Composites*, 26(7):477–485, 1995. ISSN 0010-4361. doi: https://doi.org/10.1016/0010-4361(95)96805-G.

[62] Christos J. Tsenoglou, Sylvia Pavlidou, and Constantine D. Papaspyrides. Evaluation of interfacial relaxation due to water absorption in fiber–polymer composites. *Composites Science and Technology*, 66(15):2855–2864, 2006. ISSN 02663538. doi: 10.1016/j.compscitech.2006.02.022.

[63] James J. Murray, Ankur Bajpai, James Quinn, Jake McClements, Klaus Gleich, Edward D. McCarthy, and Conchúr M. Ó Brádaigh. Effect of glass fibre sizing on the interfacial properties of composites produced using in-situ polymerised polyamide-6 transfer moulding. *Composites Part B: Engineering*, 235:109743, 2022. ISSN 1359-8368. doi: https://doi.org/10.1016/j.compositesb.2022.109743.

[64] J. L. Thomason. Glass fibre sizing: A review. *Composites Part A: Applied Science and Manufacturing*, 127, 2019. ISSN 1359835X. doi: 10.1016/j.compositesa.2019.105619.

[65] David R. Hartman, L. U. C. Peters, and Jeffrey L. Antle. Sizing for high performance glass fibers and composite materials incorporating same, 2007/02/26 2012. URL `https://lens.org/022-846-758-187-655`.

[66] Edwin P. Plueddemann. *Chemistry of Silane Coupling Agents*, pages 31–54. Springer US, Boston, MA, 1991. ISBN 978-1-4899-2070-6. doi: 10.1007/978-1-4899-2070-6_2.

[67] Felipe M. de Souza, Pawan K. Kahol, and Ram K. Gupta. *Introduction to Polyurethane Chemistry*, volume 1380 of *ACS Symposium Series*, book section 1, pages 1–24. American Chemical Society, 2021. ISBN 9780841298408. doi: doi:10.1021/bk-2021-1380.ch00110.1021/bk-2021-1380.ch001.

[68] Paschalis Alexandridis and T. Alan Hatton. Poly(ethylene oxide) poly(propylene oxide) poly(ethylene oxide) block copolymer surfactants in aqueous solutions and at interfaces: thermodynamics, structure, dynamics, and modeling. *Colloids and Surfaces A: Physicochemical and Engineering Aspects*, 96(1):1–46, 1995. ISSN 0927-7757. doi: https://doi.org/10.1016/0927-7757(94)03028-X.

[69] Gregory S. Helwig and Jerry H. C. Lee. Method for producing a wet-laid fiber mat, 2005/07/07 2007. URL https://lens.org/072-861-464-278-681.

[70] National Center for Biotechnology Information. Pubchem, 2024. URL https://pubchem.ncbi.nlm.nih.gov/.

[71] Easy Composites. Glass fibre reinforcements. URL https://www.easycomposites.co.uk/glass-fibre-reinforcements.

[72] East Coast Fibreglass Supplies. Cloth, fabric and tapes. URL https://www.ecfibreglasssupplies.co.uk/cloth-fabric-and-tapes.

[73] Arkema. Elium product selector, 2024. URL https://www.arkema.com/files/live/sites/shared_arkema/files/downloads/products-documentations/Incubator/ProductSelector_ELIUM_2024.pdf.

[74] Willy Piret, Nadia Masson, and L. U. C. Peters. Glass fibre sizing composition, 2011/06/28 2013. URL https://lens.org/130-530-585-052-879.

[75] Lorena Cristina Miranda Barbosa, Monique Santos, Thiago Luiz Lara Oliveira, Guilherme Ferreira Gomes, and Antonio Carlos Ancelotti Junior. Effects of moisture absorption on mechanical and viscoelastic properties in liquid thermoplastic resin/carbon fiber composites. *Polymer Engineering and Science*, 59(11):2185–2194, 2019. ISSN 0032-3888 1548-2634. doi: 10.1002/pen.25221.

[76] N. H. Nash, A. Portela, C. I. Bachour-Sirerol, I. Manolakis, and A. J. Comer. Effect of environmental conditioning on the properties of thermosetting- and thermoplastic-matrix composite materials by resin infusion for marine applications. *Composites Part B: Engineering*, 177, 2019. ISSN 13598368. doi: 10.1016/j.compositesb.2019.107271.

[77] Johanna Beguinel, Gérard Jean-François, Lortie Frédéric, Gérard Pierre, and Jérôme Maupetit. New continuous fiber reinforced thermoplastic composites: An analysis of interfacial adhesion from the micro scale to the macro scale. In *20th International Conference on Composite Materials, Copenhagen*, 19-24th July 2015.

[78] Quentin Charlier, Frédéric Lortie, Pierre Gerard, and Jean-François Gerard. Interfacial adhesion between glass fibers and acrylic-based matrices as studied by micromechanical testing. In *20th International Conference on Composite Materials, Copenhagen*, 2015.

[79] Z. Boufaida, L. Farge, S. André, and Y. Meshaka. Influence of the fiber/matrix strength on the mechanical properties of a glass fiber/thermoplastic-matrix plain weave fabric composite. *Composites Part A: Applied Science and Manufacturing*, 75:28–38, 2015. ISSN 1359835X. doi: 10.1016/j.compositesa.2015.04.012.

[80] P. Davies, P. Y. Le Gac, and M. Le Gall. Influence of sea water aging on the mechanical behaviour of acrylic matrix composites. *Applied Composite Materials*, 24(1):97–111, 2016. ISSN 0929-189X 1573-4897. doi: 10.1007/s10443-016-9516-1.

[81] Peter Davies and Mael Arhant. Fatigue behaviour of acrylic matrix composites: Influence of seawater. *Applied Composite Materials*, 26(2):507–518, 2018. ISSN 0929-189X 1573-4897. doi: 10.1007/s10443-018-9713-1.

[82] Adolf Fick. Ueber diffusion. *Annalen der Physik*, 170(1):59–86, 1855. doi: https://doi.org/10.1002/andp.18551700105.

[83] V. Bellenger, J. Verdu, and E. Morel. Structure-properties relationships for densely cross-linked epoxide-amine systems based on epoxide or amine mixtures. *Journal of Materials Science*, 24(1):63–68, 1989. ISSN 1573-4803. doi: 10.1007/BF00660933.

[84] Abderrazak Chilali, Mustapha Assarar, Wajdi Zouari, Hocine Kebir, and Rezak Ayad. Effect of geometric dimensions and fibre orientation on 3d moisture diffusion in flax fibre reinforced thermoplastic and thermosetting composites. *Composites Part A: Applied Science and Manufacturing*, 95:75–86, 2017. ISSN 1359835X. doi: 10.1016/j.compositesa.2016.12.020.

[85] Andrea Toscano, Giuseppe Pitarresi, Michele Scafidi, Maria Di Filippo, Giuseppe Spadaro, and Sabina Alessi. Water diffusion and swelling stresses

in highly crosslinked epoxy matrices. *Polymer Degradation and Stability*, 133:255–263, 2016. ISSN 0141-3910. doi: https://doi.org/10.1016/j.polymdegradstab.2016.09.004.

[86] Matthew Jackson, Mukul Kaushik, Sergei Nazarenko, Steve Ward, Rob Maskell, and Jeffrey Wiggins. Effect of free volume hole-size on fluid ingress of glassy epoxy networks. *Polymer*, 52(20):4528–4535, 2011. ISSN 00323861. doi: 10.1016/j.polymer.2011.07.042.

[87] Corentin Humeau, Peter Davies, and Frédéric Jacquemin. Moisture diffusion under hydrostatic pressure in composites. *Materials and Design*, 96:90–98, 2016. ISSN 0264-1275. doi: https://doi.org/10.1016/j.matdes.2016.02.012.

[88] Jiming Zhou and James P. Lucas. Hygrothermal effects of epoxy resin. part i: the nature of water in epoxy. *Polymer*, 40(20):5505–5512, 1999. ISSN 0032-3861. doi: https://doi.org/10.1016/S0032-3861(98)00790-3.

[89] James L. Thomason and Georgios Xypolias. The effect of environmental ageing on the interphase in glass fibre – vinyl ester composites. *Composite Interfaces*, 30(4):377–391, 2023. ISSN 0927-6440. doi: 10.1080/09276440.2022.2116842.

[90] Masako Unemori, Yoko Matsuya, Shigeki Matsuya, Akane Akashi, and Akifumi Akamine. Water absorption of poly(methyl methacrylate) containing 4-methacryloxyethyl trimellitic anhydride. *Biomaterials*, 24(8):1381–1387, 2003. ISSN 0142-9612. doi: https://doi.org/10.1016/S0142-9612(02)00521-5.

[91] N. L. Thomas and A. H. Windle. A theory of case ii diffusion. *Polymer*, 23(4):529–542, 1982. ISSN 0032-3861. doi: https://doi.org/10.1016/0032-3861(82)90093-3.

[92] A. Kootsookos and A. P. Mouritz. Seawater durability of glass- and carbon-polymer composites. *Composites Science and Technology*, 64 (10):1503–1511, 2004. ISSN 0266-3538. doi: https://doi.org/10.1016/j.compscitech.2003.10.019.

[93] Haithem Bel Haj Frej, Romain Léger, Didier Perrin, and Patrick Ienny. A novel thermoplastic composite for marine applications: Comparison of the

effects of aging on mechanical properties and diffusion mechanisms. *Applied Composite Materials*, 2021. ISSN 0929-189X 1573-4897. doi: 10.1007/s10443-021-09903-0.

[94] Turner Alfrey, E. F. Gurnee, and W. G. Lloyd. Diffusion in glassy polymers. *Journal of Polymer Science Part C: Polymer Symposia*, 12(1):249–261, 2007. ISSN 0449-2994 1935-3065. doi: 10.1002/polc.5070120119.

[95] Christopher L. Soles, Fernando T. Chang, David W. Gidley, and Albert F. Yee. Contributions of the nanovoid structure to the kinetics of moisture transport in epoxy resins. *Journal of Polymer Science Part B: Polymer Physics*, 38(5):776–791, 2000. ISSN 0887-6266 1099-0488. doi: 10.1002/(sici)1099-0488(20000301)38:5⟨776::Aid-polb15⟩3.0.Co;2-a.

[96] Mark D. Placette, Xuejun Fan, Jie-Hua Zhao, and Darvin Edwards. Dual stage modeling of moisture absorption and desorption in epoxy mold compounds. *Microelectronics Reliability*, 52(7):1401–1408, 2012. ISSN 0026-2714. doi: https://doi.org/10.1016/j.microrel.2012.03.008.

[97] Haithem Bel Haj Frej, Romain Léger, Didier Perrin, and Patrick Ienny. Effect of aging temperature on a thermoset-like novel acrylic thermoplastic composite for marine vessels. *Journal of Composite Materials*, 55(19):2673–2691, 2021. ISSN 0021-9983 1530-793X. doi: 10.1177/0021998321996780.

[98] JM Whitney, CE Browning, and JR Vinson. *Some Anomalies Associated with Moisture Diffusion in Epoxy Matrix Composite Materials*, volume STP658-EB, page 0. ASTM International, 1978. ISBN 978-0-8031-0274-3. doi: 10.1520/stp34857s.

[99] Ehsan Moghbelli, Reid Banyay, and Hung-Jue Sue. Effect of moisture exposure on scratch resistance of pmma. *Tribology International*, 69:46–51, 2014. ISSN 0301-679X. doi: https://doi.org/10.1016/j.triboint.2013.08.012.

[100] Christopher L. Soles and Albert F. Yee. A discussion of the molecular mechanisms of moisture transport in epoxy resins. *Journal of Polymer Science Part B: Polymer Physics*, 38(5):792–802, 2000. ISSN 0887-6266 1099-0488. doi: 10.1002/(sici)1099-0488(20000301)38:5⟨792::Aid-polb16⟩3.0.Co;2-h.

[101] Fatmaelzahraa Abdelmola and Leif A Carlsson. State of water in void-free and void-containing epoxy specimens. *Journal of Reinforced Plastics and Composites*, 38(12):556–566, 2019. doi: 10.1177/0731684419833469.

[102] Y. Fujii, T. Tominaga, D. Murakami, M. Tanaka, and H. Seto. Local dynamics of the hydration water and poly(methyl methacrylate) chains in pmma networks. *Front Chem*, 9:728738, 2021. ISSN 2296-2646 (Print) 2296-2646 (Linking). doi: 10.3389/fchem.2021.728738.

[103] A. Gargano, J. Galos, and A. P. Mouritz. Importance of fibre sizing on the seawater durability of carbon fibre laminates. *Composites Communications*, 19:11–15, 2020. ISSN 24522139. doi: 10.1016/j.coco.2020.02.002.

[104] C. Yang, X. Xing, Z. Li, and S. Zhang. A comprehensive review on water diffusion in polymers focusing on the polymer-metal interface combination. *Polymers (Basel)*, 12(1), 2020. ISSN 2073-4360 (Electronic) 2073-4360 (Linking). doi: 10.3390/polym12010138.

[105] M. R. Vanlandingham, R. F. Eduljee, and J. W. Gillespie. Moisture diffusion in epoxy systems. *Journal of Applied Polymer Science*, 71(5):787–798, 1999. ISSN 0021-8995 1097-4628. doi: 10.1002/(sici)1097-4628(19990131)71:5⟨787::Aid-app12⟩3.0.Co;2-a.

[106] A. P. Mouritz, E. Gellert, P. Burchill, and K. Challis. Review of advanced composite structures for naval ships and submarines. *Composite Structures*, 53(1):21–42, 2001. ISSN 0263-8223. doi: https://doi.org/10.1016/S0263-8223(00)00175-6.

[107] Tim J. Searle and John Summerscales. *7 - Review of the durability of marine laminates*, pages 219–266. Woodhead Publishing, 1999. ISBN 978-1-85573-320-6. doi: https://doi.org/10.1533/9781845694876.219.

[108] A. Chateauminois, B. Chabert, J. P. Soulier, and L. Vincent. Dynamic mechanical analysis of epoxy composites plasticized by water: Artifact and reality. *Polymer Composites*, 16(4):288–296, 1995. ISSN 0272-8397 1548-0569. doi: 10.1002/pc.750160405.

[109] P. Nogueira, C. Ramírez, A. Torres, M. J. Abad, J. Cano, J. López, I. López-Bueno, and L. Barral. Effect of water sorption on the structure and mechanical properties of an epoxy resin system. *Journal of Applied Polymer Science*, 80(1):71–80, 2001. ISSN 0021-8995. doi: https://doi.org/10.1002/1097-4628(20010404)80:1⟨71::AID-APP1077⟩3.0.CO;2-H.

[110] G. Z. Xiao and M. E. R. Shanahan. Irreversible effects of hygrothermal aging on dgeba/dda epoxy resin. *Journal of Applied Polymer Science*, 69(2): 363–369, 1998. ISSN 0021-8995. doi: https://doi.org/10.1002/(SICI)1097-4628(19980711)69:2⟨363::AID-APP18⟩3.0.CO;2-X.

[111] G. A. Pogany. Anomalous diffusion of water in glassy polymers. *Polymer*, 17(8):690–694, 1976. ISSN 0032-3861. doi: https://doi.org/10.1016/0032-3861(76)90209-3.

[112] S. G. Croll. Application of the flory–rehner equation and the griffith fracture criterion to paint stripping. *Journal of Coatings Technology and Research*, 7 (1):49–55, 2009. ISSN 1547-0091 1935-3804. doi: 10.1007/s11998-009-9166-4.

[113] J. Trifol, D. Plackett, P. Szabo, A. E. Daugaard, and M. Giacinti Baschetti. Effect of crystallinity on water vapor sorption, diffusion, and permeation of pla-based nanocomposites. *ACS Omega*, 5(25):15362–15369, 2020. ISSN 2470-1343 (Electronic) 2470-1343 (Linking). doi: 10.1021/acsomega.0c01468.

[114] Takanori Negoro, Wiranphat Thodsaratpreeyakul, Yoko Takada, Supaphorn Thumsorn, Hiroyuki Inoya, and Hiroyuki Hamada. Role of crystallinity on moisture absorption and mechanical performance of recycled pet compounds. *Energy Procedia*, 89:323–327, 2016. ISSN 18766102. doi: 10.1016/j.egypro.2016.05.042.

[115] Yongpeng Lei, Tao Zhang, Jifeng Zhang, and Boming Zhang. Dimensional stability and mechanical performance evolution of continuous carbon fiber reinforced polyamide 6 composites under hygrothermal environment. *Journal of Materials Research and Technology*, 13:2126–2137, 2021. ISSN 2238-7854. doi: https://doi.org/10.1016/j.jmrt.2021.06.012.

[116] Li Zhang and M. R. Piggott. Water absorption and fiber-matrix interface durability in carbon-peek. *Journal of Thermoplastic Composite Materials*, 13 (2):162–172, 2000. doi: 10.1177/089270570001300205.

[117] Huang Gu. Tensile behaviours of quartz, aramid and glass filaments after nacl treatment. *Materials and Design*, 30(3):867–870, 2009. ISSN 02613069. doi: 10.1016/j.matdes.2008.05.055.

[118] Andrey E. Krauklis and Andreas T. Echtermeyer. Long-term dissolution of glass fibers in water described by dissolving cylinder zero-order kinetic model: Mass loss and radius reduction. 16(1):1189–1199, 2018. doi: doi:10.1515/chem-2018-0133.

[119] Alok Behera, Neeraj Kumar Bhoi, Manjusha M. Thawre, Atul Ballal, and Debashish Das. Quantification of hygrothermal aging-induced interfacial debonding of carbon fiber/epoxy composites at nano-to-micrometer length scales. *Journal of Composite Materials*, 57(30):4637–4647, 2023. doi: 10.1177/00219983231213912.

[120] Dennis Gibhardt, Audrius Doblies, Lars Meyer, and Bodo Fiedler. Effects of hygrothermal ageing on the interphase, fatigue, and mechanical properties of glass fibre reinforced epoxy. *Fibers*, 7(6), 2019. doi: 10.3390/fib7060055.

[121] Hatsuo Ishida and Jack L. Koenig. A fourier-transform infrared spectroscopic study of the hydrolytic stability of silane coupling agents on e-glass fibers. *Journal of Polymer Science: Polymer Physics Edition*, 18(9):1931–1943, 1980. ISSN 0098-1273. doi: https://doi.org/10.1002/pol.1980.180180906.

[122] Aswani Kumar Bandaru, Seaghan Hickey, Dilpreet Singh, Raghavendra Gujjala, and Subramani Pichandi. Influence of hygrothermal ageing on the novel infusible thermoplastic resin reinforced with quadriaxial non-crimp glass fabrics. *Journal of Thermoplastic Composite Materials*, 36(10):3813–3836, 2022. ISSN 0892-7057 1530-7980. doi: 10.1177/08927057221137805.

[123] S. Thomas, S. A. Paul, L. A. Pothan, and B. Deepa. *Natural Fibres: Structure, Properties and Applications*, pages 3–42. Springer Berlin Heidelberg, Berlin, Heidelberg, 2011. ISBN 978-3-642-17370-7. doi: 10.1007/978-3-642-17370-7_1.

[124] Abdul Moudood, Anisur Rahman, Andreas Öchsner, Mainul Islam, and Gaston Francucci. Flax fiber and its composites: An overview of water and moisture absorption impact on their performance. *Journal of Reinforced Plastics and Composites*, 38(7):323–339, 2018. ISSN 0731-6844 1530-7964. doi: 10.1177/0731684418818893.

[125] S. C. Das, C. Srivastava, S. Goutianos, A. D. La Rosa, and S. Grammatikos. On the response to hygrothermal ageing of fully recyclable flax and glass fibre reinforced polymer composites. *Materials (Basel)*, 16(17), 2023. ISSN 1996-1944 (Print) 1996-1944. doi: 10.3390/ma16175848.

[126] D. Koumba Mendoue, A. Benelfellah, R. Matadi Boumbimba, I. Royaud, M. Ponçot, M. Wary, and C. Noirel. Study of the thermomechanical behavior of composite based on elium acrylic resin, carbon nanotubes, and flax fibers: Experimental approach. *Polymer Composites*, n/a(n/a), 2024. ISSN 0272-8397. doi: https://doi.org/10.1002/pc.28597.

[127] Quentin Drouhet, Fabienne Touchard, and Laurence Chocinski-Arnault. Influence of hygrothermal aging on mechanical properties and damage mechanisms of hemp-reinforced biocomposites. *Journal of Natural Fibers*, 19(17):15404–15421, 2022. ISSN 1544-0478. doi: 10.1080/15440478.2022.2126424.

[128] Quentin Drouhet, Fabienne Touchard, and Laurence Chocinski-Arnault. Tensile behavior of [0/90]7 hemp/elium biocomposites after water aging: In-situ micro-ct testing and numerical analysis. *Micro*, 3(2):496–509, 2023. ISSN 2673-8023. URL `https://www.mdpi.com/2673-8023/3/2/33`.

[129] Quentin Drouhet, Fabienne Touchard, and Chocinski-Arnault Laurence. Influence of wet/dry cycling on mechanical properties of hemp-reinforced biocomposites. In *20th European Conference on Composite Materials, ECCM20*, 2022. URL `https://hal.science/hal-03822558/file/ECCM20-Drouhet.pdf`.

[130] Paul Murdy, Ariel Lusty, Robynne Murray, Scott Hughes, and Ryan Beach. Post-deployment characterization of glass fiber-reinforced thermoset and thermoplastic composite tidal turbine blades: Preprint. 4 2024. URL `https://www.osti.gov/biblio/2340123`.

[131] Robert Gasch and Jochen Twele. *Structural dynamics*, pages 272–306. Springer Berlin Heidelberg, Berlin, Heidelberg, 2012. ISBN 978-3-642-22938-1. doi: 10.1007/978-3-642-22938-1_8.

[132] R. Talreja. Fatigue of composite materials: Damage mechanisms and fatigue-life diagrams. *Proceedings of The Royal Society of London, Series A: Mathematical and Physical Sciences*, 378(1775):461–475, 1981. doi: 10.1098/rspa.1981.0163.

[133] Emile S. Greenhalgh, editor. *Defects and damage and their role in the failure of polymer composites*, pages 356–440. 2009. ISBN 9781845692179. doi: 10.1533/9781845696818.356.

[134] Ramesh Talreja. *Fatigue of Composite Materials*, pages 281–294. Springer, Vienna, 2003. ISBN 978-3-7091-2544-1. doi: 10.1007/978-3-7091-2544-1-6.

[135] Dylan S. Cousins, Zach Arwood, Stephen Young, Brandon Hinkle, David Snowberg, Dayakar Penumadu, and Aaron P. Stebner. Infusible thermoplastic composites for wind turbine blade manufacturing: Fatigue life of thermoplastic laminates under ambient and low-temperature conditions. *Advanced Engineering Materials*, 25(11), 2023. ISSN 1438-1656 1527-2648. doi: 10.1002/adem.202201941.

[136] Yukitaka Murakami, Toshio Takagi, Kentaro Wada, and Hisao Matsunaga. Essential structure of s-n curve: Prediction of fatigue life and fatigue limit of defective materials and nature of scatter. *International Journal of Fatigue*, 146:106138, 2021. ISSN 0142-1123. doi: https://doi.org/10.1016/j.ijfatigue.2020.106138.

[137] K. H. Boller. Fatigue fundamentals for composite materials, 1969.

[138] J. Wulff, H.W. Hayden, and L.G. Moffatt. *Structure and Properties of Materials: Mechanical Behavior*. Wiley, 1964. ISBN 9780471364696. URL `https://books.google.co.uk/books?id=pdLPBH9YbW4C`.

[139] A. D'Amore and L. Grassia. Principal features of fatigue and residual strength of composite materials subjected to constant amplitude (ca) loading. *Materi-*

als (Basel), 12(16), 2019. ISSN 1996-1944 (Print) 1996-1944 (Linking). doi: 10.3390/ma12162586.

[140] Daniel D. Samborsky, John F. Mandell, and David A. Miller. The SNL/MSU/DOE fatigue of composite materials database: Recent trends. In *53rd AIAA/ASME/ASCE/AHS/ASC Structures, Structural Dynamics and Materials Conference, Honolulu*, 2012. doi: https://doi.org/10.2514/6.2012-1573.

[141] SNL/MSU/DOE composite material fatigue database, 2019. URL `https://energy.sandia.gov/programs/renewable-energy/wind-power/rotor-innovation/rotor-reliability/mhk-materials-database/`.

[142] Yasushi Miyano, Masayuki Nakada, and Rokuro Muki. Applicability of fatigue life prediction method to polymer composites. *Mechanics of Time-Dependent Materials*, 3(2):141–157, 1999. ISSN 1573-2738. doi: 10.1023/A:1009873124095.

[143] David Snowberg, Derek Berry, Dana Swan, Zhang Mingfu, Steve Nolet, Douglas Adams, Johnathan Goodsell, Dayakar Penumadu, and Aaron Stebner. Iacmi project 4.2: Thermoplastic composite development for wind turbine blades. Report, Institute for Advanced Composites Manufacturing Innovation, 2021-12-07 2021.

[144] Mustafa Bakkal, Mete Kayihan, Azmi Timur, Zeynep Parlar, Canan Gamze Güleryüz Parasiz, Aysu Hande Yücel, İbrahim Mehmet Palabiyik, and Turgut Gülmez. Fatigue behavior and self-heating mechanism of novel glass fiber reinforced thermoplastic composite. *Advanced Composite Materials*, 32(6):899–915, 2023. ISSN 0924-3046 1568-5519. doi: 10.1080/09243046.2023.2175764.

[145] Peter Davies, Mael Arhant, and Erwan Grossmann. Seawater ageing of infused flax fibre reinforced acrylic composites. *Composites Part C: Open Access*, 8, 2022. ISSN 26666820. doi: 10.1016/j.jcomc.2022.100246.

[146] F. Javanshour, A. Prapavesis, N. Pournoori, G. C. Soares, O. Orell, T. Pärnänen, M. Kanerva, A. W. Van Vuure, and E. Sarlin. Impact and

fatigue tolerant natural fibre reinforced thermoplastic composites by using non-dry fibres. *Composites Part A: Applied Science and Manufacturing*, 161, 2022. ISSN 1359835X. doi: 10.1016/j.compositesa.2022.107110.

[147] Robynne E. Murray, Jason Roadman, and Ryan Beach. Fusion joining of thermoplastic composite wind turbine blades: Lap-shear bond characterization. *Renewable Energy*, 140:501–512, 2019. doi: 10.1016/j.renene.2019.03.085.

[148] C. Ageorges, L. Ye, and M. Hou. Advances in fusion bonding techniques for joining thermoplastic matrix composites: a review. *Composites Part A: Applied Science and Manufacturing*, 32(6):839–857, 2001. ISSN 1359-835X. doi: https://doi.org/10.1016/S1359-835X(00)00166-4.

[149] Somen K. Bhudolia, Goram Gohel, Leong Kah Fai, and Robert J. Barsotti. Investigation on ultrasonic welding attributes of novel carbon/elium® composites. *Materials*, 13(5):10–15, 2020. doi: 10.3390/ma13051117.

[150] Somen K. Bhudolia, Goram Gohel, Leong Kah Fai, and Robert J. Barsotti. Fatigue response of ultrasonically welded carbon/elium® thermoplastic composites. *Materials Letters*, 264:127362–127362, 2020. doi: 10.1016/j.matlet.2020.127362.

[151] S. K. Bhudolia, G. Gohel, J. Kantipudi, K. F. Leong, and Jr. Barsotti, R. J. Ultrasonic welding of novel carbon/ elium((r)) thermoplastic composites with flat and integrated energy directors: Lap shear characterisation and fractographic investigation. *Materials (Basel)*, 13(7), 2020. ISSN 1996-1944 (Print) 1996-1944 (Electronic) 1996-1944 (Linking). doi: 10.3390/ma13071634.

[152] H. Perrin, M. Bodaghi, V. Berthe, and R. Vaudemont. On the addition of multifunctional methacrylate monomers to an acrylic-based infusible resin for the weldability of acrylic-based glass fibre composites. *Polymers (Basel)*, 15 (5), 2023. ISSN 2073-4360 (Electronic) 2073-4360 (Linking). doi: 10.3390/polym15051250.

[153] Michael J. Troughton, editor. *Chapter 10 - Resistive Implant Welding*, pages 105–111. William Andrew Publishing, Boston, 2009. ISBN 978-0-8155-1581-4. doi: https://doi.org/10.1016/B978-0-8155-1581-4.50012-3.

[154] Michael J. Troughton, editor. *Chapter 11 - Induction Welding*, pages 113–120. William Andrew Publishing, Boston, 2009. ISBN 978-0-8155-1581-4. doi: https://doi.org/10.1016/B978-0-8155-1581-4.50013-5.

[155] Michael J. Troughton, editor. *Chapter 2 - Ultrasonic Welding*, pages 15–35. William Andrew Publishing, Boston, 2009. ISBN 978-0-8155-1581-4. doi: https://doi.org/10.1016/B978-0-8155-1581-4.50004-4.

[156] Somen K. Bhudolia, Goram Gohel, and Kah Fai Leong. Advances in ultrasonic welding of thermoplastic composites: A review. *Materials*, 13(6), 2020. ISSN 1996-1944. doi: 10.3390/ma13061284.

[157] Michael J. Troughton, editor. *Chapter 9 - Infrared Welding*, pages 97–103. William Andrew Publishing, Boston, 2009. ISBN 978-0-8155-1581-4. doi: https://doi.org/10.1016/B978-0-8155-1581-4.50011-1.

[158] Dimitrios Zarouchas and Rogier Nijssen. Mechanical behaviour of thick structural adhesives in wind turbine blades under multi-axial loading. *Journal of Adhesion Science and Technology*, 30(13):1413–1429, 2016. ISSN 0169-4243 1568-5616. doi: 10.1080/01694243.2016.1146392.

[159] Avraham Benatar and Zhang Cheng. Ultrasonic welding of thermoplastics in the far-field. *Polymer Engineering and Science*, 29(23):1699–1704, 1989. ISSN 0032-3888 1548-2634. doi: 10.1002/pen.760292312.

[160] Robynne E. Murray, Andy Plumer, Ryan Beach, and Peter Broome. Validation of a lightning protection system for a fusion-welded thermoplastic composite wind turbine blade tip. *Wind Engineering*, 2021. ISSN 0309-524X 2048-402X. doi: 10.1177/0309524x211024642.

Chapter 3

Research Motivation

3.1 Gaps in the Existing Literature

There is a need for recyclable composites in the renewable energy and marine industries, and of the various recyclable resins that are available, liquid acrylic resins are one of the few that are currently of commercial interest to manufacturers. From Chapter 2, while much research has been conducted on acrylic-matrix composites in recent years, they are still poorly understood compared to traditional thermosets such as epoxy, and so several knowledge gaps exist.

For example, glass fibre reinforcements are commonly used in wind/tidal turbine blades and composites. However, at the start of this project, only very limited data on fatigue and water absorption in unidirectional GF/acrylic composites was available, as presented in Figure 2.23. This data did not include diffusion kinetics data, and contained a limited number of datapoints for only 0° tensile coupons. Cousins et al. [1] have since published dry 0° GF/acrylic fatigue data, but to our knowledge no other mechanical, fatigue or water absorption data on unidirectional GF/acrylic has been published. Material properties after saturation, such as longitudinal and transverse moduli and strengths, are essential when deciding if GF/acrylic composites are suitable for use in the marine environment.

In Chapter 2.1.3, a hybrid acrylic-PPE matrix described by Obande et al. [2, 3] was discussed. The localised crosslinking in this modified polymer caused several mechanical and thermomechanical benefits, such as an increase in T_g, while the polymer remains recyclable via thermoforming. Additionally, PPE is known as

an additive to epoxy to reduce moisture absorption [4, 5]. It is therefore possible that similarly reduced moisture ingress could be seen in the acrylic-PPE hybrid matrix, compared to unmodified acrylic. This would be beneficial in the marine environment, in which water absorption should be minimised. Depending on the outcome, the benefits of acrylic-PPE described by Obande et al.[2, 3] combined with water absorption data could allow for its use in hot wet environments.

As discussed in Chapter 2.2, an appropriate sizing agent is essential for good interfacial strength. However, conflicting information is available in the literature on the effects of acrylic-tailored vs. multi-compatible sizings in glass fibre reinforced acrylic (GF/acrylic). On the one hand some researchers suggest that acrylic-tailored sizing agents improve interfacial strength, fatigue life and water absorption over multi-compatible sizing agents [6–9], but on the other hand microbond testing has found no difference in performance [10]. These publications have various complications in their comparisons, including chemical incompatibilities with the multi-compatible sizing agent [8], comparing coupons with different layups [6, 7], the use of acrylic latexes instead of Elium® resin [9], and the addition of paraffin wax to the resin [10]. Conclusions about GF/acrylic composites are therefore difficult to draw from these studies. Additionally, multi-compatible reinforcements have been successfully used with acrylic resin in the literature [11, 12], and Arkema itself recommends multi-compatible or vinylester sizing agents [13]. Acrylic-tailored reinforcements are under development, but further studies would be useful to better understand if these specialised reinforcements provide any benefits over their multi-compatible counterparts.

Finally, in Chapter 2.5, several welding methods as applied to acrylic-matrix composites were discussed. Each of these welding methods—resistance, induction, ultrasound and infrared—was shown to create strong bonds, but they also require intimate contact between the welded parts. This may not be possible in large structures such as wind turbine blades, where manufacturing tolerances can necessitate bondlines of up to 30 mm thickness [14]. It is therefore unclear how these welding methods could be practically applied in large structures, without the development of novel joint geometries [15]. Indeed, there does not appear to be an example of a welded thermoplastic wind or tidal turbine blade available in the literature. The

development of a joining method which combines the strength of traditional welding with the tolerance of adhesives would therefore be beneficial.

3.2 Thesis Objectives

The aim of this thesis is to improve understanding of the application of acrylic-matrix composites in wind turbine blades, tidal turbine blades, and in marine vessels. The knowledge gaps described in the previous section are therefore investigated with a focus on these applications. The following research topics are explored in each of the subsequent chapters:

1. **Investigate water absorption in unidirectional GF/acrylic and GF/acrylic-PPE composites.** Water absorption is a key consideration for a composite's use in the marine environment—for example, in tidal turbine blades and ships. A chapter is therefore dedicated to the hydrothermal ageing of GF/acrylic and GF/acrylic-PPE composites, in comparison with GF/epoxy as a baseline. Diffusion kinetics and the effect of water on mechanical properties will be used to assess the suitability of each material for the marine environment.

2. **Conduct fatigue studies of 0° GF/acrylic coupons with a specialised sizing agent.** Unidirectional GF/acrylic are subject to tension-tension fatigue, before and after hydrothermal ageing. This allows for comparisons with published data on epoxy-matrix composites, to determine if acrylic is a suitable replacement. The data can also be compared with GF/acrylic with a multi-compatible sizing agent to better understand the role of tailored sizing agents in the fatigue performance of GF/acrylic.

3. **Explore novel bonding methodologies for acrylic-matrix composites.** A novel bonding method termed *resin welding* is developed, with the aim of realising the benefits of welding while allowing for large manufacturing tolerances. In this study, the bonding strength is assessed via single lap shear testing to determine if the resin welding method compares favourably to traditional joining methods. The applicability to more complex bondlines is then

explored through the manufacture of a T-section demonstrator.

3.3 Chapter References

[1] Dylan S. Cousins, Zach Arwood, Stephen Young, Brandon Hinkle, David Snowberg, Dayakar Penumadu, and Aaron P. Stebner. Infusible thermoplastic composites for wind turbine blade manufacturing: Fatigue life of thermoplastic laminates under ambient and low-temperature conditions. *Advanced Engineering Materials*, 25(11), 2023. ISSN 1438-1656 1527-2648. doi: 10.1002/adem.202201941.

[2] Winifred Obande, Conchúr M. Ó Brádaigh, and Dipa Ray. Thermoplastic hybrid-matrix composite prepared by a room-temperature vacuum infusion and in-situ polymerisation process. *Composites Communications*, 22(August):22–27, 2020. doi: 10.1016/j.coco.2020.100439.

[3] Winifred Obande, Weronika Gruszka, Jennifer A. Garden, Christian Wurzer, Conchúr M. Ó Brádaigh, and Dipa Ray. Enhancing the solvent resistance and thermomechanical properties of thermoplastic acrylic polymers and composites via reactive hybridisation. *Materials and Design*, 206, 2021. ISSN 02641275. doi: 10.1016/j.matdes.2021.109804.

[4] Edward N Peters, Scott M Fisher, and Hua Guo. Polyphenylene ether macromonomers. iii. enhancement of dielectric materials. *Proceedings of the IPC Printed Circuits EXPO and APEX, Las Vegas, NV, USA*, 31, 2009.

[5] Edward N. Peters. Poly(phenylene ether) based amphiphilic block copolymers. *Polymers*, 9(9), 2017. ISSN 2073-4360. doi: 10.3390/polym9090433.

[6] P. Davies, P. Y. Le Gac, and M. Le Gall. Influence of sea water aging on the mechanical behaviour of acrylic matrix composites. *Applied Composite Materials*, 24(1):97–111, 2016. ISSN 0929-189X 1573-4897. doi: 10.1007/s10443-016-9516-1.

[7] Peter Davies and Mael Arhant. Fatigue behaviour of acrylic matrix composites:

Influence of seawater. *Applied Composite Materials*, 26(2):507–518, 2018. ISSN 0929-189X 1573-4897. doi: 10.1007/s10443-018-9713-1.

[8] Z. Boufaida, L. Farge, S. André, and Y. Meshaka. Influence of the fiber/matrix strength on the mechanical properties of a glass fiber/thermoplastic-matrix plain weave fabric composite. *Composites Part A: Applied Science and Manufacturing*, 75:28–38, 2015. ISSN 1359835X. doi: 10.1016/j.compositesa.2015.04.012.

[9] Johanna Beguinel, Gérard Jean-François, Lortie Frédéric, Gérard Pierre, and Jérôme Maupetit. New continuous fiber reinforced thermoplastic composites: An analysis of interfacial adhesion from the micro scale to the macro scale. In *20th International Conference on Composite Materials, Copenhagen*, 19-24th July 2015.

[10] Quentin Charlier, Frédéric Lortie, Pierre Gerard, and Jean-François Gerard. Interfacial adhesion between glass fibers and acrylic-based matrices as studied by micromechanical testing. In *20th International Conference on Composite Materials, Copenhagen*, 2015.

[11] Winifred Obande, Dimitrios Mamalis, Dipa Ray, Liu Yang, and Conchúr M. Ó Brádaigh. Mechanical and thermomechanical characterisation of vacuum-infused thermoplastic- and thermoset-based composites. *Materials and Design*, 175, 2019. ISSN 02641275. doi: 10.1016/j.matdes.2019.107828.

[12] Robynne E. Murray, Ryan Beach, David Barnes, David Snowberg, Derek Berry, Samantha Rooney, Mike Jenks, Bill Gage, Troy Boro, Sara Wallen, and Scott Hughes. Structural validation of a thermoplastic composite wind turbine blade with comparison to a thermoset composite blade. *Renewable Energy*, 164:1100–1107, 2021. doi: 10.1016/j.renene.2020.10.040.

[13] Arkema. Elium product selector, 2024. URL `https://www.arkema.com/files/live/sites/shared_arkema/files/downloads/products-documentations/Incubator/ProductSelector_ELIUM_2024.pdf`.

[14] K. P. Subrahmanian and Fabrice Dubouloz. Adhesives for bonding wind turbine

blades. *Reinforced Plastics*, 53(1):26–29, 2009. ISSN 0034-3617. doi: https://doi.org/10.1016/S0034-3617(09)70044-X.

[15] Robynne E. Murray, Jason Roadman, and Ryan Beach. Fusion joining of thermoplastic composite wind turbine blades: Lap-shear bond characterization. *Renewable Energy*, 140:501–512, 2019. doi: 10.1016/j.renene.2019.03.085.

Chapter 4

Seawater Ageing of Thermoplastic Hybrid Matrix Composites

As discussed in Chapter 2, water absorption can reduce the mechanical performance of polymer-matrix composites. Therefore, if relatively new materials such as acrylic-matrix composites are to be used in the marine environment, water absorption and its effects on the composite should be characterised. Indeed, measuring the properties of seawater-saturated coupons is a mandatory part of some standards for determining the suitability of a resin for tidal turbine blades (DNV-ST-0164) and ships (Lloyd's Register MQPS Book K).

Liquid acrylic resins have been modified by Obande et al. [1, 2] via the addition of a PPE oligomer. Improvements were made to the solvent resistance, ductility, transverse flexural strength and modulus and initiation fracture toughness. PPE is marketed as an additive for resins such as epoxy to improve moisture resistance, for example in the manufacture of printed circuit boards [3, 4]. It was therefore of interest to determine the effect of reactive hybridisation with PPE on water diffusion in acrylic-matrix composites. Therefore, in the following sections, water absorption in GF1-MCS/acrylic-PPE is compared to GF1-MCS/acrylic, with GF1-MCS/epoxy as a reference for traditional thermoset composites. The diffusion of water and the resulting changes in mechanical properties after ageing are compared between the composites. The dry and aged samples are examined via scanning electron microscopy (SEM) to study the behaviour of the interface due to water ingress. Finally, the change in glass transition temperature due to seawater ageing

is studied via dynamic mechanical analysis (DMA).

4.1 Materials and Methods

4.1.1 Manufacturing and sample preparation

Three types of unidirectional (UD) glass fibre (GF) reinforced laminates were manufactured using the same multi-compatible reinforcement (GF1-MCS) from Ahlstrom-Munksjö, containing 600 $g\,m^{-2}$ of 0° fibres, 36 $g\,m^{-2}$ of 90° fibres and 10 $g\,m^{-2}$ of polyester stitching. These laminates are termed GF1-MCS/acrylic, GF1-MCS/acrylic-PPE and GF1-MCS/epoxy. GF1-MCS/acrylic laminates were made with an acrylic resin (Elium® 188 O, Arkema) and peroxide initiator (BP-50-FT, United Initiators) in a 100:3 ratio by weight. GF1-MCS/acrylic-PPE laminates were made by mixing 5 wt% of PPE oligomer with methacrylate end functionality (NORYL™ SA9000 Resin, SABIC) in the same acrylic resin, again with the BP-50-FT peroxide initiator in a 100:3 ratio. GF1-MCS/epoxy laminates were prepared using SR 1710 Injection epoxy resin and SD 7820 hardener (Sicomin) in a 100:36 ratio by weight.

All laminates were prepared via a standard vacuum resin infusion route on a glass plate coated with release agent (Marbocote 227 CEE) as detailed in Figure 4.1. Laminate thicknesses were 1.5 mm for tensile testing, 4 mm for flexural testing and SBS and 2 mm for diffusion coefficient measurement, and the coupon dimensions are summarised in Table 4.1.

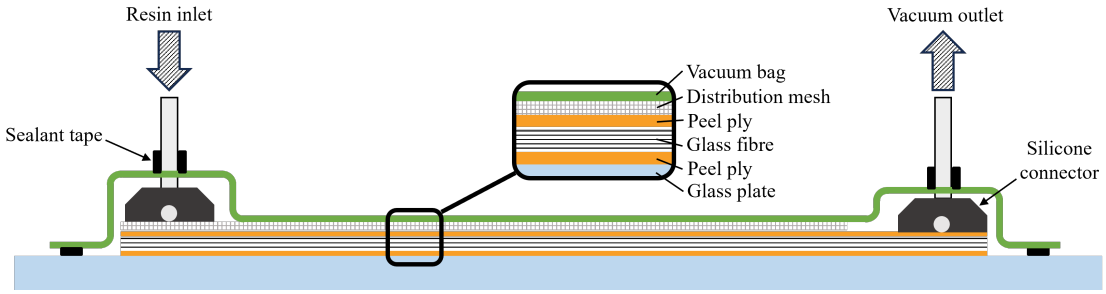

Figure 4.1: *The infusion setup used to manufacture the composites.*

Table 4.1: *Tests and specimen dimensions used in the study.*

Test	Nominal Coupon Dimensions (mm)
0° Tension	250 × 15 × 1.5
90° Tension	200 × 25 × 1.5
0° Flexure	154 × 13 × 4
90° Flexure	154 × 13 × 4
Short Beam Strength	24 × 8 × 4
Water Absorption	160 × 160 × 2
DMA	60 × 13 × 1.5

After infusion, the laminates were left to polymerise at room temperature for 24 h. The GF1-MCS/epoxy laminates were then subject to a freestanding post-cure at 60 °C for 8 h followed by 100 °C for 4 h according to the manufacturer's recommendations. The GF1-MCS/acrylic and GF1-MCS/acrylic-PPE laminates did not require any post-cure.

4.1.2 Seawater ageing

Composite specimens were subject to seawater ageing. Filtered natural seawater, collected from Gullane Beach in the Firth of Forth, Scotland, was maintained at 50 °C, and samples for mechanical testing were immersed for 3 months. Evaporated water was replaced with distilled water to maintain a constant level in the tank. Aged specimens were kept immersed in seawater at room temperature until testing to prevent them from drying. Each of the mechanical tests detailed in the following sections was conducted on dry specimens as well as on aged specimens. In addition to specimens for mechanical testing, three specimens each of GF1-MCS/acrylic, GF1-MCS/acrylic-PPE and GF1-MCS/ epoxy were used to determine the diffusion coefficient and maximum water uptake. They were first oven-dried at 50°C for 5 days and then immersed in seawater at 50°C for 5 months. The specimens were removed from the water bath at 24-h intervals, their surfaces were wiped with a cloth and their weights were measured.

At each measurement interval, the percentage mass increase was calculated ac-

cording to Equation 4.1 (ASTM D5229M) in which $M(t)$ is the percentage increase in mass caused by water uptake at time t, W_i is the measured specimen mass at time t and W_o is the oven-dry specimen mass.

$$M(t) = \frac{W_i - W_o}{W_o} \times 100 \tag{4.1}$$

A Fickian diffusion curve of the form in Equation 4.2 (ASTM D5229M) where h is the specimen thickness, was then fitted, and values for the diffusion coefficient (D_z) and equilibrium water content (M_m) at 50 °C were taken from the fitted curve.

$$M(t) = M_m \left\{ 1 - exp \left[-7.3 \left(\frac{D_z t}{h^2} \right)^{0.75} \right] \right\} \tag{4.2}$$

4.1.3 Testing

4.1.3.1 Mechanical tests

Tensile testing (0° and 90°) was carried out according to ASTM D3039, using an MTS Criterion Model 45 test machine (serial number 10523451A) with a 300 kN load cell (serial number 578061). Specimens were spray-painted with a black and white speckle pattern to allow strain measurements to be taken with an Imetrum UVX video extensometer system with a Manta G-146B camera. The 0° tensile specimens were tabbed with GF/epoxy PCB board. All tensile tests were conducted with a crosshead extension rate of 2 mm/min.

Flexural testing (0° and 90°) was carried out according to ASTM D7264 on an Instron 3369 test system (system ID 3369J5245) using a span-to-thickness ratio of 32:1. A 10 kN load cell (serial number 168483) was used. The crosshead extension rate was set at 7 mm/min, and mid-span deflection was taken to be the crosshead extension. SBS tests were performed in accordance with ASTM D2344, using a span-to-thickness ratio of 4:1. The crosshead extension rate was set at 1 mm/min.

4.1.3.2 Fibre volume fraction

The fibre volume fraction (FVF) and void fraction of the composites were measured using a matrix burn-off method according to ASTM D3171. The densities of the

composite coupons, matrices and glass fibres were measured using a displacement method (ASTM D792). The specimens were cut to 30 mm squares.

4.1.3.3 Scanning electron microscopy

Scanning electron microscopy (SEM) was carried out using a JEOL JSM series microscope on fragments of 0 ° tensile specimens after fracture (Figure 4.2). Samples were sputter-coated with 30 nm of gold before imaging at 15 kV.

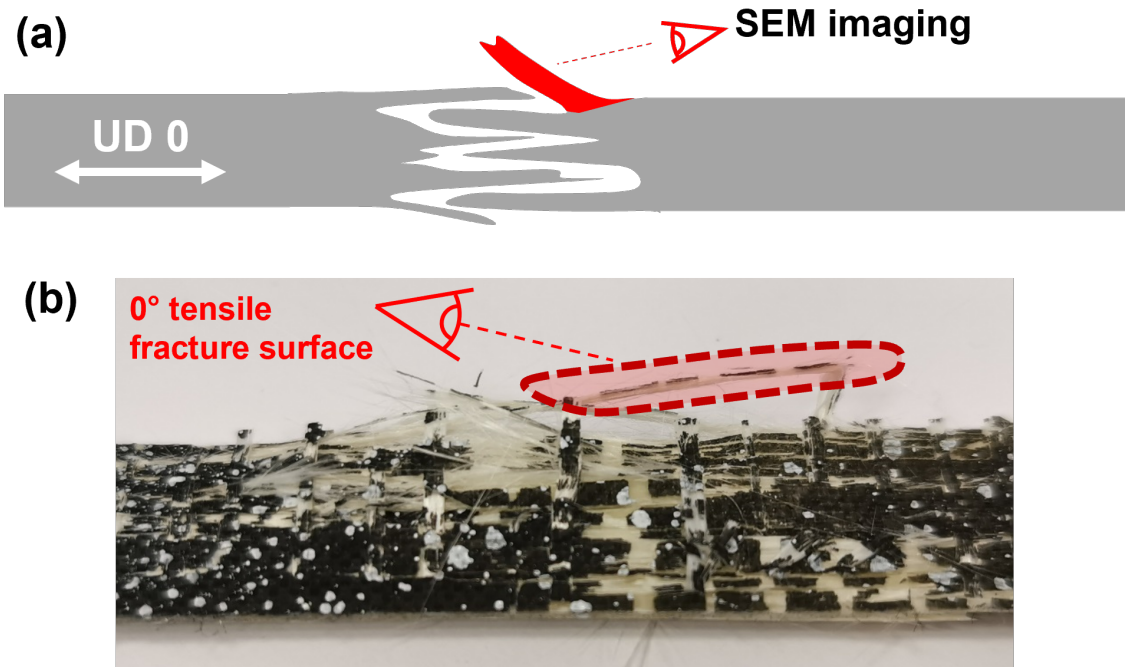

Figure 4.2: *SEM images were taken of 0° tensile specimens which failed via longitudinal splitting. Fragments were cut for gold coating and imaging. (a) A diagram of a failed coupon with the fibre direction and longitudinal splitting shown. (b) A representative failed coupon with an example of an imaged fragment highlighted in red.*

4.1.3.4 Dynamic mechanical analysis

The glass transition temperatures of both dry and aged specimens were measured using dynamic mechanical analysis (DMA). A TA Instruments Discovery DMA 850 was used in 3-point bend mode at a frequency of 1 Hz and an amplitude of 20 µm. Specimens were 50 × 13 × 1.5 mm with 0° fibres in the span direction. A ramp rate of 1°C/min between ambient temperature and 180°C was selected and 1 specimen

was tested for each composite type, both dry and saturated with water. Aged specimens were removed from the water bath, wiped to remove surface water and then immediately tested.

4.2 Results and discussion

4.2.1 Fibre and void volume fractions

The densities of the unreinforced acrylic, acrylic-PPE and epoxy matrices—as measured according to Section 4.1.3—used to calculate the fibre and void volume fractions were 1.18 $\mathrm{g\,cm^{-3}}$, 1.15 $\mathrm{g\,cm^{-3}}$, and 1.14 $\mathrm{g\,cm^{-3}}$ respectively. The density of the glass fibres was similarly measured to be 2.6 $\mathrm{g\,cm^{-3}}$. The fibre and void volume fractions of the laminates manufactured for each test are given in Table 4.2.

Table 4.2: *Fibre and void volume fractions of composites used for mechanical and diffusion testing. Values are the average of 5 measurements, ± one standard deviation.*

	Matrix	Fibre fraction (vol.%)	Void fraction (vol.%)
Diffusion Specimens	Acrylic	56.8 ± 0.4	1.4 ± 0.1
	Acrylic-PPE	55.8 ± 0.3	1.0 ± 0.3
	Epoxy	52.8 ± 0.2	0.5 ± 0.1
90° Tension Specimens	Acrylic	53.5 ± 0.5	2.1 ± 0.3
	Acrylic-PPE	53.5 ± 0.3	0.8 ± 0.4
	Epoxy	50.9 ± 0.7	1.7 ± 0.5
0° Tension Specimens	Acrylic	53.5 ± 0.8	1.9 ± 0.8
(Average of 2 Laminates)	Acrylic-PPE	54.7 ± 0.8	1.9 ± 0.7
	Epoxy	49.0 ± 1.2	0.4 ± 0.3
0/90° Flexure & Short Beam	Acrylic	56.4 ± 0.3	1.9 ± 0.4
Strength Specimens	Acrylic-PPE	52.7 ± 0.2	1.9 ± 0.3
	Epoxy	54.6 ± 0.3	1.1 ± 0.1

4.2.2 Water absorption

A graph of percentage mass increase against the square root of time is presented in Figure 4.3. The experimental data as well as the fitted diffusion curves are shown

in Figure 4.3 and the resulting M_m and D_z are given in Table 4.3. Each data point is the average increase of 3 specimens.

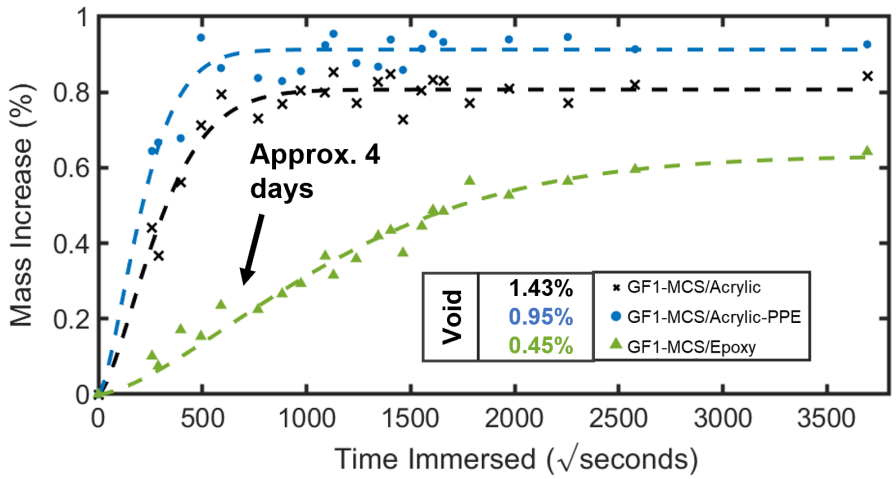

Figure 4.3: *The water absorption curves of the three composites with their corresponding void volume fractions. The experimental data are presented as points and the fitted Fickian diffusion curves as dotted lines. A decrease in the diffusion coefficient is visible in the GF1-MCS/epoxy after approximately 4 days.*

Table 4.3: *The diffusion coefficients measured in this study along with values from literature for comparison.*

Material	Ageing Conditions	D_z ($\times 10^{-12}$ m^2 s^{-1})	M_m (%)	Source
GF1-MCS/acrylic [0°]4	50°C seawater 5 months	1.81	0.81	Current work
GF1-MCS/acrylic-PPE [0°]4	50°C seawater 5 months	3.4	0.91	Current work
GF1-MCS/epoxy [0°]4	50°C seawater 5 months	0.15	0.63	Current work
GF/acrylic	50°C water 4 months	1.21	0.47	[5]
GF/epoxy	50°C water 4 months	0.21	0.78	[5]
PMMA Cast Resin	60°C deionised water	4.54	-	[6]
Elium 190 Cast Resin	60°C seawater 365 days	4.23	1.9	[7]

*A dual Fickian model was fitted. Both diffusion coefficients and values for Mm are presented.

The GF1-MCS/acrylic and GF1-MCS/acrylic-PPE both exhibited Fickian behaviour—a linear increase in absorbed water when plotted against $\sqrt{t}$ which plateaus after reaching saturation (Figure 4.3). Although a Fickian diffusion curve is also fitted to the GF1-MCS/epoxy data, there is a slight deviation from purely Fickian

behaviour as there was an initial period of more rapid absorption followed by a more gradual mass increase after approximately 4 days (600 $\sqrt{s}$). The diffusion coefficients of GF1-MCS/acrylic, GF1-MCS/acrylic-PPE and GF1-MCS/epoxy composites are given in Table 4.3 along with diffusion coefficient values of acrylic-matrix composites and unreinforced acrylic resin reported in published literature. The diffusion in GF1-MCS/epoxy was an order of magnitude slower than in GF1-MCS/acrylic and GF1-MCS/ acrylic-PPE. This is supported by a study by Murdy et al. [5], in which faster diffusion was observed in GF/acrylic coupons than GF/epoxy coupons immersed in 50°C water for 4 months (see Table 4.3). Unlike in the current study, Murdy et al. [5] observed a lower saturation water content in GF/acrylic than GF/epoxy, but this difference narrows when the values are normalised by the matrix fraction, as discussed in Chapter 2.

These differences may be explained by considering the differences in structure and chemistry between the polymers and relating these to theories of diffusion. The structure of the acrylic matrix is typical of an amorphous thermoplastic and the epoxy has the typical structure of a thermoset. The structure of acrylic-PPE (5 wt% PPE), depicted in Figure 4.4 and Figure 4.5b, has been previously investigated by Obande et al. [1] and is believed to consist of PPE-rich cross-linked zones surrounded by acrylic-rich regions. The PPE with methacrylate end functionality reacts with the acrylic monomers during in-situ polymerisation to form crosslinks between acrylic chains

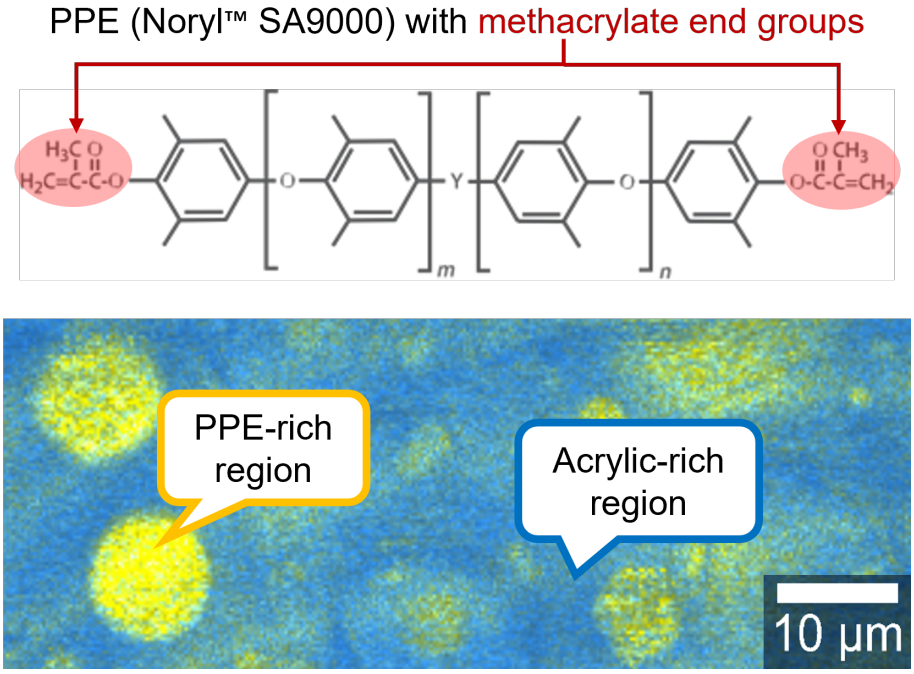

Figure 4.4: *(Top) The chemical structure of the PPE grade used in this study with methacrylate end groups highlighted and (Bottom) the polymer structure of the acrylic-PPE hybrid as determined by confocal Raman spectroscopy in [1]. Yellow regions are rich in PPE and blue regions are rich in acrylic.*

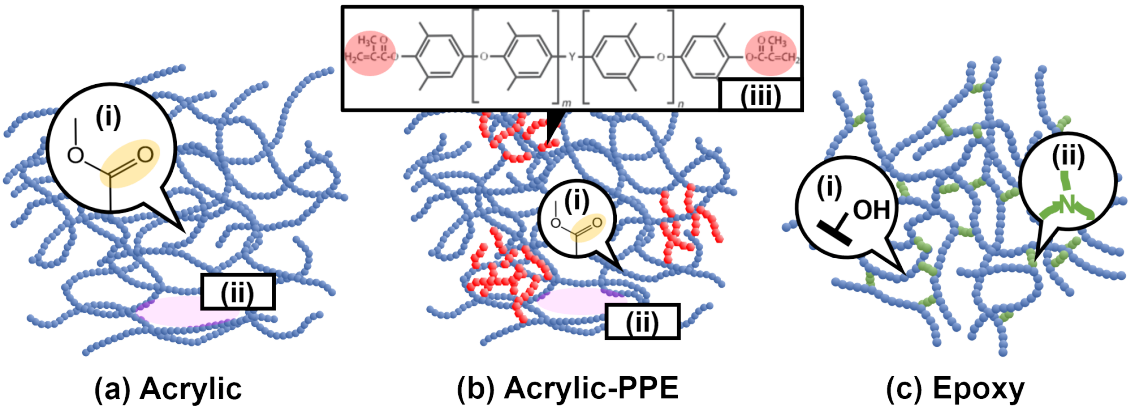

Figure 4.5: *A comparison of the polymer and composite structures as relevant to the diffusion of water. (a) Acrylic polymer with (i) polar carbonyl groups in the side chain of the acrylic polymer and (ii) free volume in purple. (b) Acrylic-PPE with (i) carbonyl groups in the side chain of the acrylic polymer, (ii) free volume in purple and (iii) PPE oligomers with methacrylate end groups highlighted in red. (c) Epoxy has (i) hydroxyl groups and (ii) amine groups from the hardener.*

As discussed in Chapter 2, diffusion can be modelled using the free volume of the material, or by modelling the interaction between the polymer and the diffusant. In the free volume theory, the diffusant is assumed not to interact strongly with the material and instead diffuses through voids in the composite and the free volume in the matrix, to which the diffusion rate is highly sensitive [8, 9]. In the polar interaction theory, the diffusant forms bonds with polar sites in the polymer and water diffuses by hopping between these sites [8].

Free-volume diffusion is expected to occur in all three composites in this study, but the extent of free volume is likely to be less in GF/epoxy due to its 3D crosslinked network. Fujii et al. [10] demonstrated via quasi-elastic neutron scattering studies that the majority of water in PMMA is free-water, which occupies matrix free-volume and interacts little with the PMMA polymer. We expect similar behaviour in acrylic and acrylic-PPE matrix composites, shown schematically in Figure 4.5a(ii) and b(ii). Even if free-volume diffusion does not occur through the polymer, voids introduced by resin infusion and the presence of fibres also provide a route for water ingress. For example, in void-free epoxy, free-volume diffusion is not expected to be significant, but free water content increases as more voids are introduced [11].

Additionally, polar interactions occur in all three matrices. In PMMA around 28% of water molecules exist as intermediate water [10] which interacts through hydrogen bonding with carbonyl groups on the PMMA side chains (Figure 4.5a(i) and b(i)). This interaction results in a slower motion of water molecules than in free water. In epoxy, water interacts with the hydroxyl groups attached to the polymer backbone and amine groups of the curing agents (Figure 4.5c) [12]. Epoxy/amine resins such as the Sicomin SR1710/SD7820 system used in this study are regarded as hydrophilic due to these groups, and hence the interaction with water is stronger than in PMMA [13].

In this study, GF1-MCS/acrylic and GF1-MCS/acrylic-PPE diffusion coupons both had higher void contents than the GF1-MCS/epoxy, as displayed in Figure 4.3 and Table 4.2, which could explain the higher D_z values of the thermoplastic composites. In addition to a higher void content, the acrylic matrices are thermoplastic amorphous polymers and are therefore likely to have more free volume than the crosslinked epoxy matrix [6, 12]. The GF1-MCS/acrylic-PPE, however, shows a

higher diffusion rate and final water content than the GF1-MCS/acrylic, whereas the lower void fraction measured in the GF1-MCS/acrylic-PPE would correspond to a lower diffusion rate under the free-volume theory. The differences in the polymer structure induced by the addition of PPE oligomers (Figure 4.5b) could increase the free volume and explain this observation. Considering the polar interaction theory, an increase in hydrophilicity is associated with slower diffusion [12, 14] and non-Fickian absorption behaviour, as noted in the GF/epoxy specimens in this study due to a combination of free-volume and polar interaction diffusion [15, 16]. The stronger interaction between the water and epoxy compared with the acrylic could therefore also contribute to the slower diffusion in GF/epoxy.

4.2.3 Dynamic mechanical analysis

DMA was used to determine the T_g of each composite specimen before and after ageing. Figure 4.6 presents the T_g of each composite and the damping parameter ($tan\ \delta$) vs temperature curves of each composite type from which the T_g is derived. The reductions in T_g in the aged composites indicate plasticisation of the matrices caused by the ingress of water [17, 18], which is associated with a decrease in matrix modulus and strength. Secondary peaks or shoulders in the $tan\ \delta$ curves of the aged specimens are observed in Figure 4.6 with the most prominent being in the case of GF/epoxy. This is attributed to drying of the specimens during DMA as observed in other studies [19]. After the drying peak, the $tan\ \delta$ curves closely follow the curves of the dry specimens.

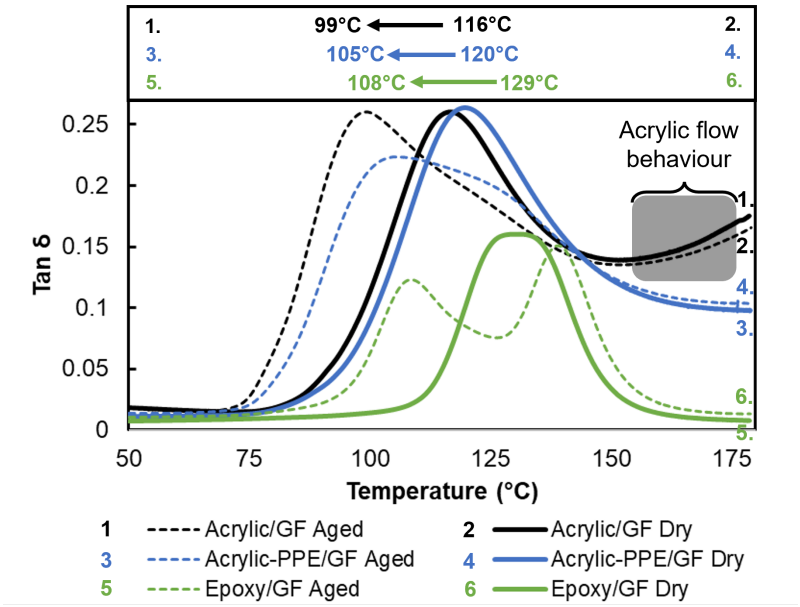

Figure 4.6: *(Top) The T_g of GF1-MCS/acrylic, GF1-MCS/acrylic-PPE and GF1-MCS/epoxy before and after ageing as determined via DMA. (Bottom) Tan δ vs. temperature for the dry (solid lines) and aged (dotted lines) coupons. In the aged specimens, a shoulder or secondary peak is present due to drying. Flow behaviour of the acrylic matrix in the dry and aged GF1-MCS/acrylic is highlighted (curves 1 and 2).*

The addition of PPE resulted in enhanced thermomechanical properties. Firstly, the T_g of GF1-MCS/acrylic-PPE was 4°C higher than that of GF1-MCS/acrylic when dry (120°C vs. 116°C), and 6°C higher when aged (105°C vs. 99°C). The GF1-MCS/epoxy had a higher T_g of 129°C when dry and 108°C when aged, as was expected due to its highly crosslinked structure. Secondly, there is a clear difference in behaviour between the acrylic and the acrylic-PPE composites at temperatures above the T_g in Figure 4.6. A rise in *tan* δ after the T_g peak is observed in GF1-MCS/acrylic which is indicative of the beginning of flow behaviour, but this behaviour is absent in the GF1-MCS/acrylic-PPE and the GF1-MCS/epoxy. This difference in the behaviour of GF1-MCS/acrylic-PPE is due to the presence of intermittent crosslinked regions as depicted in Figure 4.4 and Figure 4.5. The suppression of flow behaviour through the addition of PPE may have positive im-

plications in its use at high temperatures and in the fire safety of acrylic-PPE over acrylic, as melting and dripping of thermoplastics during a fire is a known safety hazard [20].

4.2.4 Mechanical testing

Dry and aged specimens were tested in 0° and 90° tension, 0° and 90° flexure and for SBS. All 0° tensile and 0° flexural properties are normalised to 50% FVF.

4.2.4.1 Tension

As shown in Figure 4.7a, the 0° tensile moduli were not decreased by water ageing, and the marginal increases after ageing are considered within experimental error. The 0° modulus is dominated by the fibres which are not significantly affected by ageing; therefore, the moduli remain approximately constant. In the dry specimens, the GF1-MCS/epoxy had a 9% and 4% higher strength than GF1-MCS/acrylic and GF1-MCS/acrylic-PPE respectively. The decrease due to ageing is highest in GF1-MCS/epoxy, however, with 21% versus 11% and 13% drops in GF1-MCS/acrylic and GF1-MCS/acrylic-PPE respectively (Figure 4.7b), therefore the GF1-MCS/epoxy has the lowest 0° tensile strength after ageing.

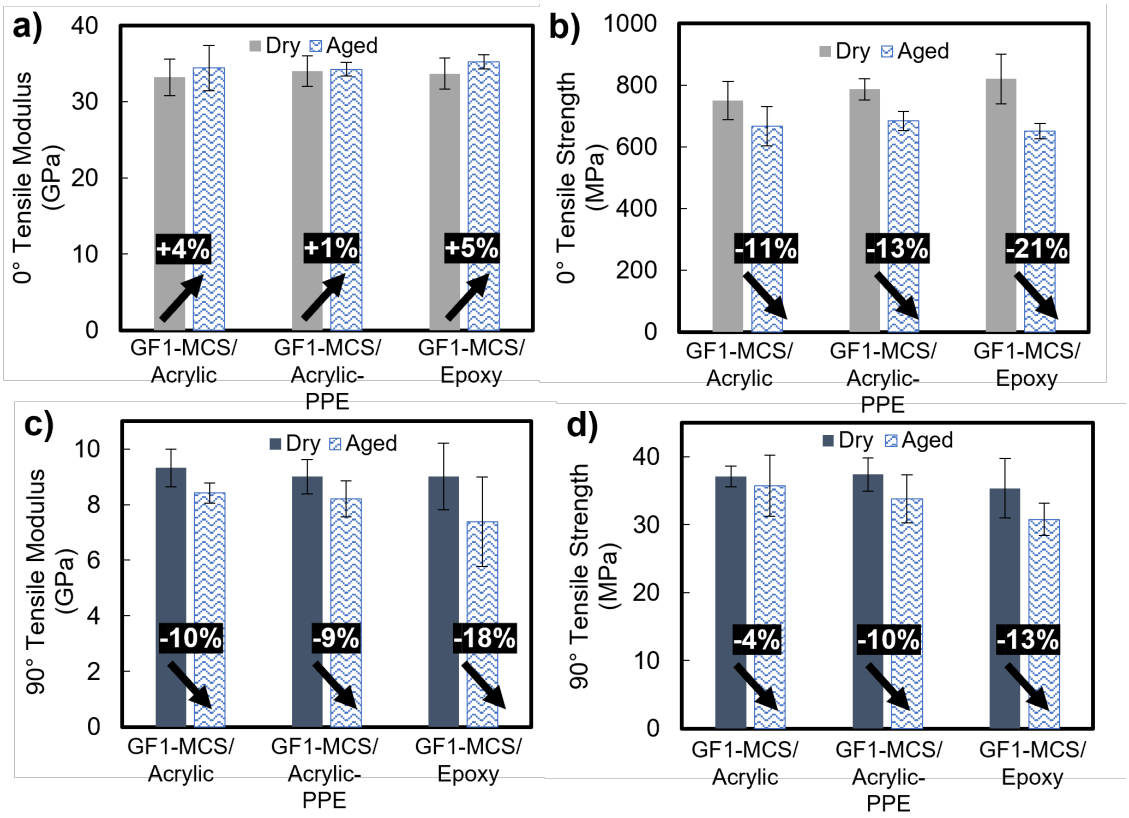

Figure 4.7: *The tensile properties of the composites are displayed before and after ageing with percentage changes. The 0° tensile properties are normalised to 50% FVF and found in (a) and (b). The 90° tensile properties are in (c) and (d). All error bars are ±1 standard deviation.*

Representative stress-strain curves of 0° tensile coupons are included in Figure 4.8, and stress-strain curves for all coupons are available in Appendix B.

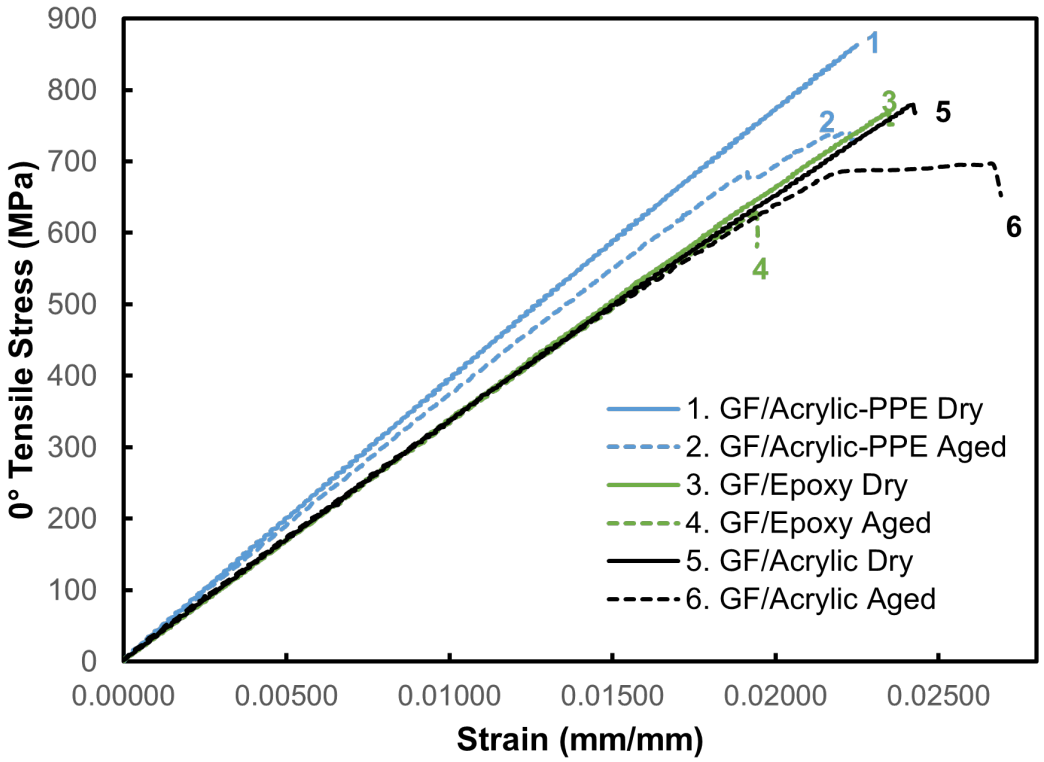

Figure 4.8: *Representative stress-strain curves of 0° tensile coupons.*

In contrast to tests in 0° tension, there were drops in the 90° tensile modulus attributed to matrix plasticisation. The decrease in modulus was largest for GF1-MCS/epoxy at 18%, nearly double the drop observed in the GF1-MCS/acrylic and GF1-MCS/acrylic-PPE (Figure 4.7c). Before ageing, the moduli of the three composites were approximately equal, but the larger decrease in GF1-MCS/epoxy modulus meant that after ageing the GF1-MCS/acrylic and GF1-MCS/acrylic-PPE had 14% and 11% higher moduli respectively.

The 90° tensile strengths of the GF1-MCS/acrylic and GF1-MCS/acrylic-PPE were higher than GF1-MCS/epoxy when both dry and aged. Water ageing caused only a small decrease in GF1-MCS/acrylic strength of 4%, but the decreases in GF1-MCS/acrylic-PPE and GF1-MCS/epoxy were larger at 10% and 13% respectively (Figure 4.7d). After ageing, therefore, the GF1-MCS/acrylic's strength was 16% higher than GF1-MCS/epoxy and 10% higher than GF1-MCS/acrylic-PPE.

Representative stress-strain curves for the 90° tensile coupons are shown in Figure 4.9. The GF1-MCS/acrylic and GF1-MCS/acrylic-PPE coupons has a smooth transition from elastic to plastic behaviour at a stress of approximately 30–35 MPa, but in the GF1-MCS/epoxy coupon a sharper 'knee' is visible at lower stresses

between approximately 15–20 MPa. This was attributed to the accumulation of transverse cracks in the epoxy matrix by Obande et al. [21].

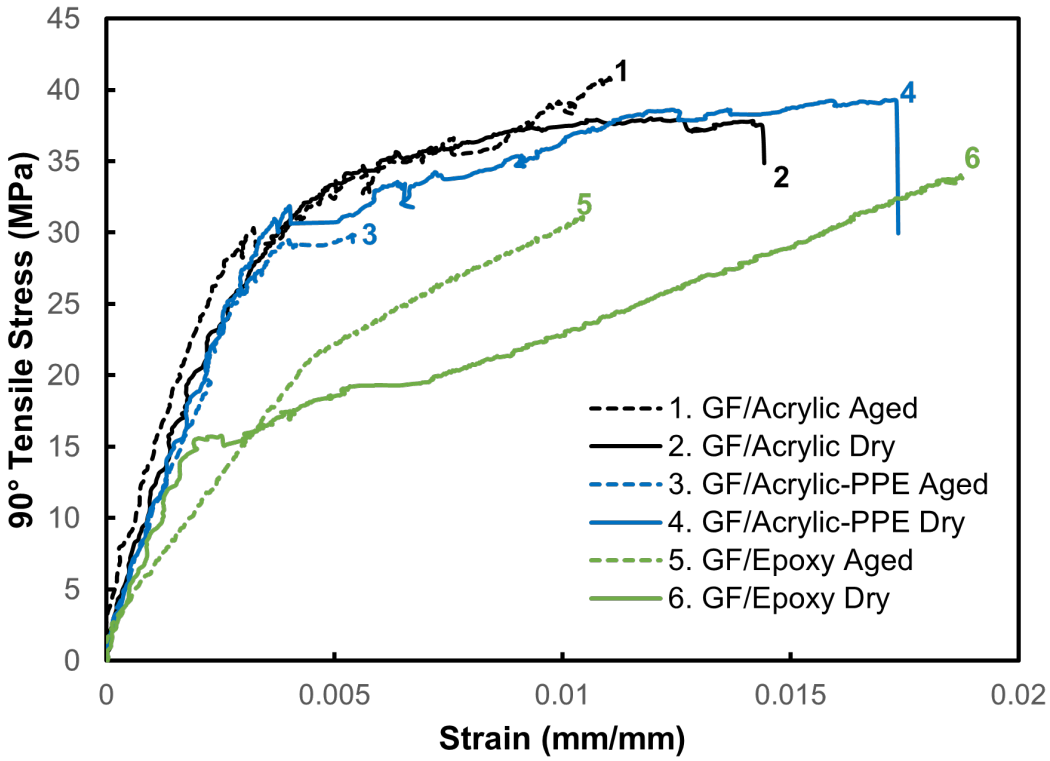

Figure 4.9: *Representative stress-strain curves of 90° tensile coupons.*

For comparison, as noted in Chapter 2, a larger decrease in tensile strength (-50%) was reported by Davies et al. [7] for 0/90° woven GF/acrylic composites. The differences in fabric weave, sizing agent, resin (Elium® RT300) and ageing conditions (18 months in 80°C seawater) used by the authors may account for this discrepancy from the current results.

4.2.4.2 Flexure

Data from flexural testing is presented in Figure 4.10. As was observed in the 0° tensile testing, there were no large decreases in 0° flexural modulus as this is a fibre-dominated property. Only GF1-MCS/epoxy saw an appreciable decrease of 6% (Figure 4.10a). The 0° flexural strengths saw larger decreases due to ageing, but there weren't significant differences in the percentage drops between materials, which ranged between 15% and 18%.

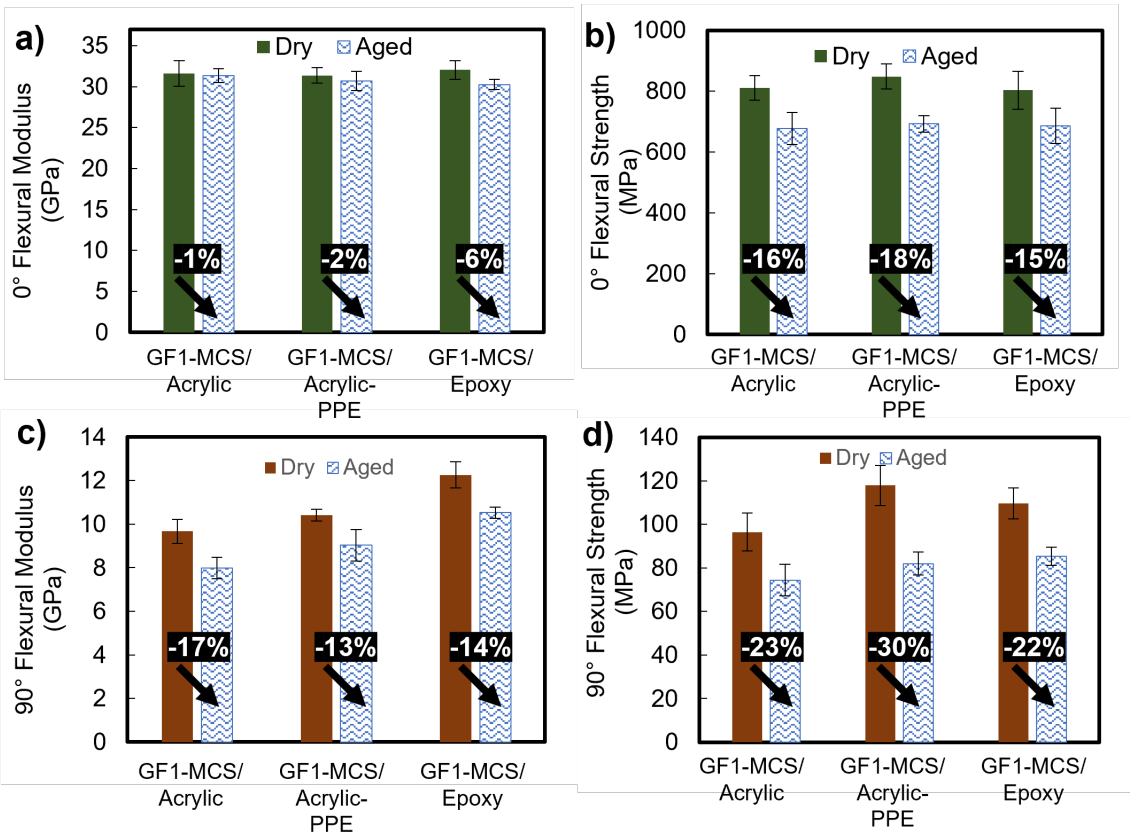

Figure 4.10: *The flexural properties of the composites are displayed before and after ageing with percentage changes. The 0° flexural properties are normalised to 50% FVF and are found in (a) and (b). The 90° flexural properties are in (c) and (d).*

Representative stress-strain curves for 0° flexural coupons are presented in Figure 4.11, and highlight the reduction in strength but similar modulus after ageing.

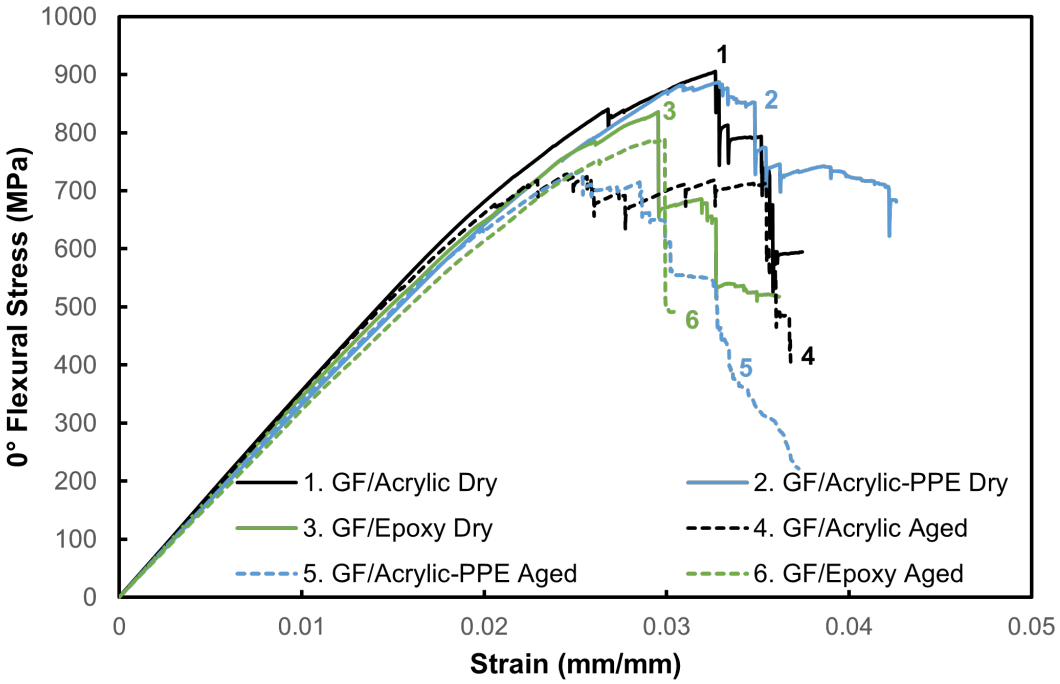

Figure 4.11: *Representative stress-strain curves of 0° flexure coupons, with GF1-MCS reinforcement.*

In 90° flexure, all three composites were affected by ageing. Reductions in 90° flexural modulus were 17% for GF1-MCS/acrylic, 13% for GF1-MCS/acrylic-PPE, and 14% for GF1-MCS/epoxy (Figure 4.10c). Even larger drops of 23%, 30% and 22% were observed in the 90° flexural strengths of GF1-MCS/acrylic, GF1-MCS/acrylic-PPE, and GF1-MCS/epoxy respectively (Figure 4.10d). The GF1-MCS/epoxy had the highest 90° flexural modulus when dry at 27% higher than GF1-MCS/acrylic and 18% higher than GF1-MCS/acrylic-PPE. Similar differences were seen after ageing when GF1-MCS/epoxy had a 32% higher modulus than GF1-MCS/acrylic and a 16% higher modulus than GF1-MCS/acrylic-PPE. This can be attributed to the high degree of crosslinking present in the epoxy matrix adding rigidity.

Comparing the GF1-MCS/acrylic and GF1-MCS/acrylic-PPE, the addition of PPE enhanced 90° flexural properties. GF1-MCS/acrylic-PPE had an 8% higher modulus when dry and a 13% higher modulus when aged (Figure 4.10c). Strength was increased by 22% when dry and 10% when aged (Figure 4.10d). The localised crosslinked regions in the acrylic-PPE matrix therefore have a similar effect to the crosslinking in epoxy, increasing both strength and modulus, but thermoplasticity

is retained as acrylic-PPE resin coupons can be reshaped upon heating [1].

Representative stress-strain curves for 90° flexural coupons are presented in Figure 4.12. Reductions in both strength and modulus are visible, as is the superior 90° flexural modulus of GF1-MCS/epoxy.

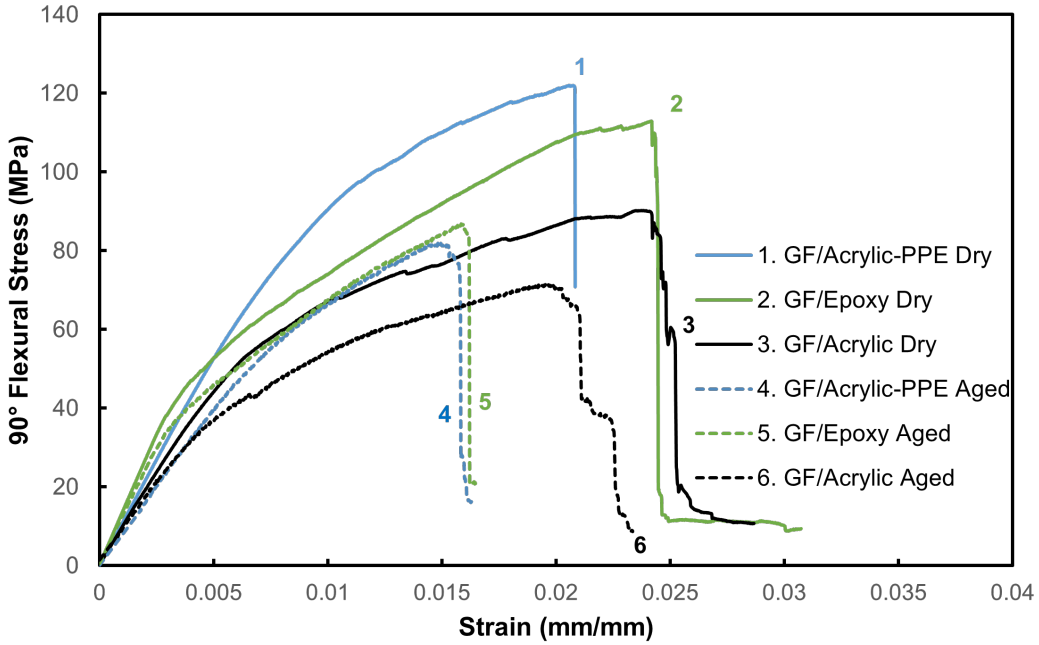

Figure 4.12: *Representative stress-strain curves of 90° flexure coupons with GF1-MCS reinforcement.*

4.2.4.3 Short beam strength

The short beam strength (Figure 4.13) of GF1-MCS/acrylic and GF1-MCS/acrylic-PPE were equivalent when dry and 28% higher than GF1-MCS/epoxy. During water ageing, however, GF1-MCS/acrylic and GF1-MCS/acrylic-PPE saw larger drops of approximately 30% vs. 13% for GF1-MCS/epoxy. The strengths after ageing were equivalent for the three materials. The higher drop in SBS in the GF1-MCS/acrylic and GF1-MCS/acrylic-PPE can be attributed to both the plasticisation of the matrix and weakening of the fibre/matrix interface [22]. As will be discussed in Section 4.2.5, however, interfacial degradation is dominant over matrix plasticisation.

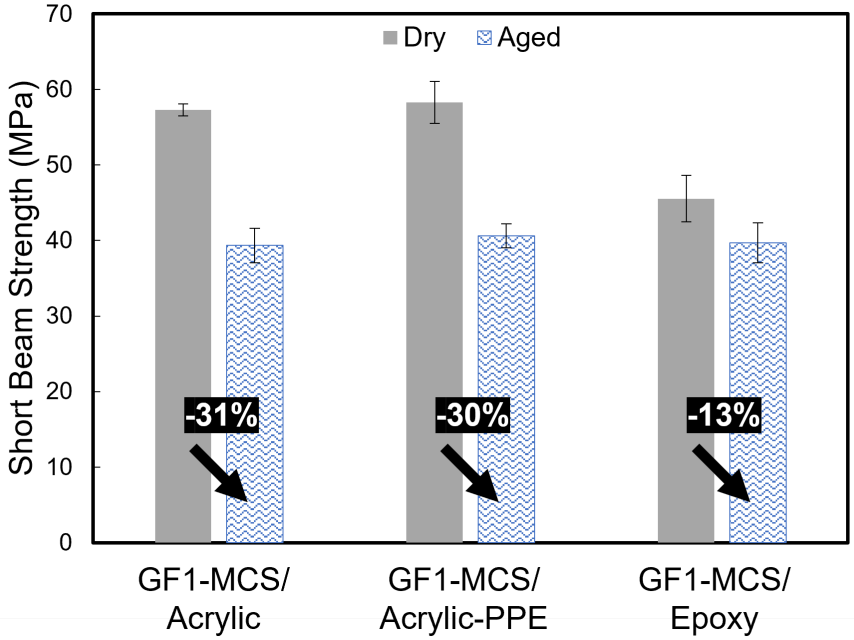

Figure 4.13: *The SBS of the composites when dry (grey) and aged (blue). The percentage drop in strength due to ageing is highlighted.*

Representative load-extension curves for the SBS coupons are shown in Figure 4.14. The graphs are truncated at 2 mm extension, as beyond this crushing was observed as an increase in load. The smoothness of GF1-MCS/acrylic curve indicates greater plastic deformation than in the GF1-MCS/epoxy and GF1-MCS/acrylic-PPE coupons, likely due to the lack of crosslinking in the former [21]. As with the previous mechanical tests, all stress-strain curves are available in Appendix B.

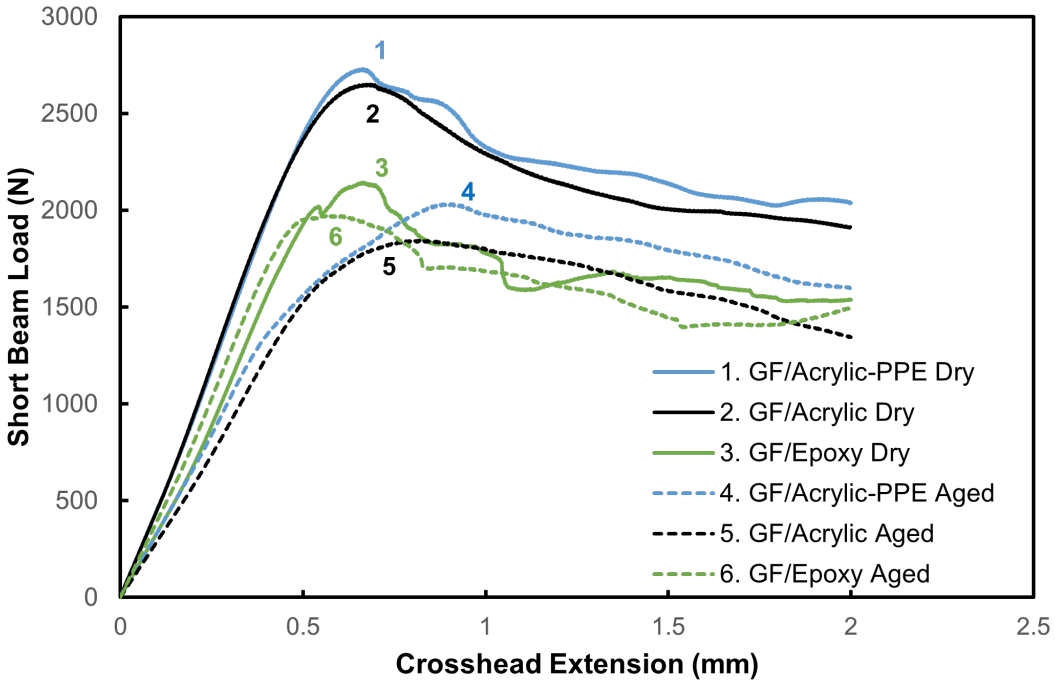

Figure 4.14: *Representative load-extension curves for SBS coupons.*

4.2.5 SEM and fracture

In this section, the reasons for the observed differences in mechanical properties caused by ageing are explored using SEM. The 0° tensile specimens of all matrices, both dry and aged, failed via longitudinal splitting or brooming. The differences in crack propagation between the composites were determined via SEM imaging of failed 0° tensile specimens as shown schematically in Figure 4.2. Representative images of 0° tensile fracture surfaces of dry and aged composites are compared in Figure 4.15.

4.2.5.1 GF1-MCS/acrylic and GF1-MCS/acrylic-PPE

The images of GF1-MCS/acrylic and GF1-MCS/acrylic-PPE show similar fracture behaviour. In the dry state, there is a matrix layer covering the fibres after fracture (Figures 4.15a and b). Evidence of the microductility of the thermoplastic matrices is also seen in Figures 4.15a and b, as are cusps, which are formed by shear failure during longitudinal splitting. After ageing, however, the fibres appear bare, devoid of any adhered matrix layer.

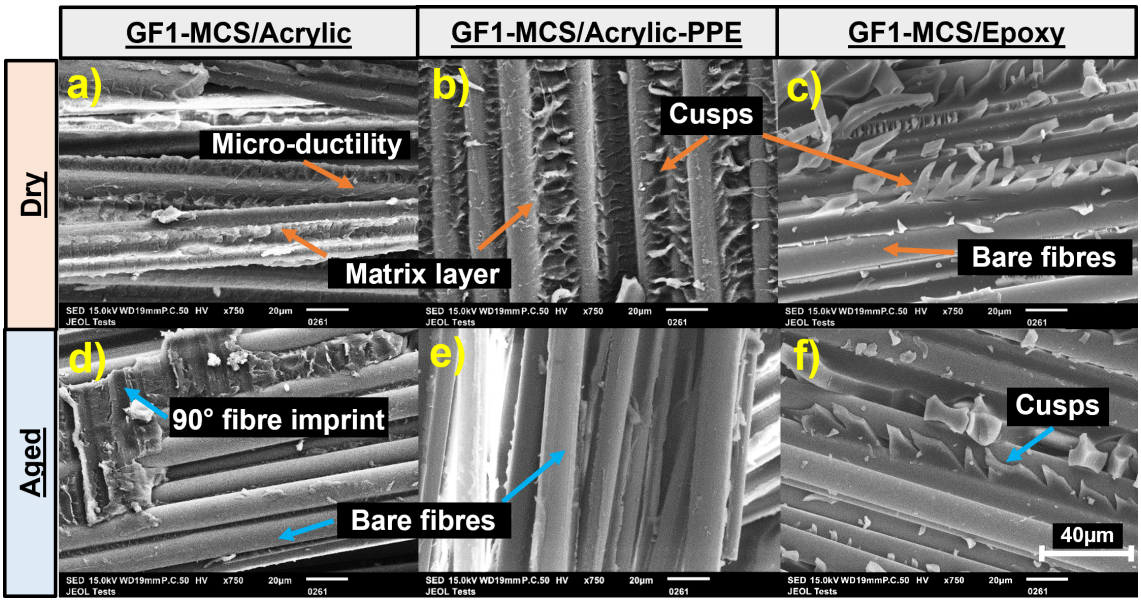

Figure 4.15: *SEM images of 0° tension specimen fracture surfaces with fractographic features annotated.*

This difference in behaviour can be explained through the Cook-Gordon mechanism [23–27], which describes the propagation of a crack through an anisotropic, inhomogeneous material as it reaches a weak plane—in this case, the fibre-matrix interface. Immediately at the crack tip in 0° tensile testing, the 0° tensile stress (σ_1) is at a maximum. In addition, shear (τ) and transverse tensile (σ_2) stresses are present, the latter of which reaches a maximum ahead of the crack tip. If the interface is weak relative to the matrix, σ_2 causes interfacial debonding ahead of the crack tip, and the crack propagates along the interface (adhesive failure in Figure 4.16c). If the interface is strong, shear forces cause longitudinal splitting through the matrix, parallel to the fibres, and the formation of shear cusps (cohesive failure in Figure 4.16b) [28].

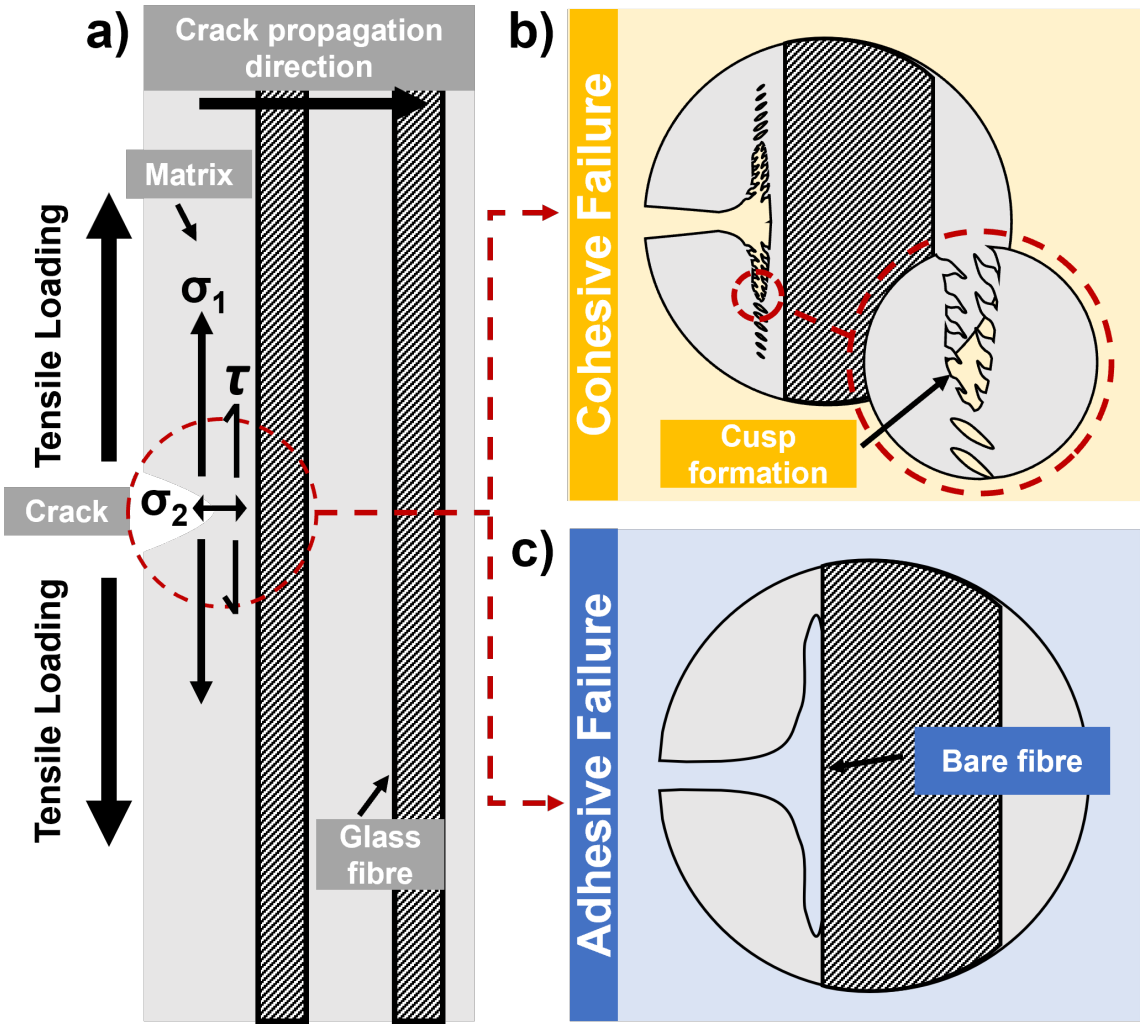

Figure 4.16: *Fracture propagation under 0° tension with 0° tensile stress (σ_1), 90° tensile stress (σ_2) and shear stress (τ) ahead of the crack tip [23]. Cohesive failure indicates a strong interface and adhesive failure indicates a weak interface relative to the matrix.*

Cohesive failure was detected in the dry GF1-MCS/acrylic and GF1-MCS/acrylic-PPE specimens (Figures 4.15a and b) whereas adhesive failure was detected in the aged GF1-MCS/acrylic, the aged GF1-MCS/acrylic-PPE and both dry and aged GF1-MCS/epoxy specimens (Figure 4.15c–f). The GF1-MCS/acrylic and GF1-MCS/acrylic-PPE therefore have a strong interface when dry and a weak interface after ageing. This switch from cohesive to adhesive failure in GF1-MCS/acrylic and GF1-MCS/acrylic-PPE suggests the weakening of the interface must be more significant than any weakening of the acrylic and acrylic-PPE matrices from plasticisation. This is confirmed by the large drops in SBS measured in these specimens

(Figure 4.13).

The reduction in interfacial strength can be attributed to the hydrolysis of the sizing agent which, although proprietary, can be assumed to contain a silane coupling agent which is typical for glass-fibre composites [29]. The bond formed between the coupling agent and the GF is reversible via hydrolysis; for example, silane sizings can be removed from GF by simply boiling in water [29, 30]. As depicted in Figure 4.17, sizing hydrolysis in combination with matrix swelling causes debonding of the matrix from the fibres and therefore leads to interfacial degradation as observed in this study.

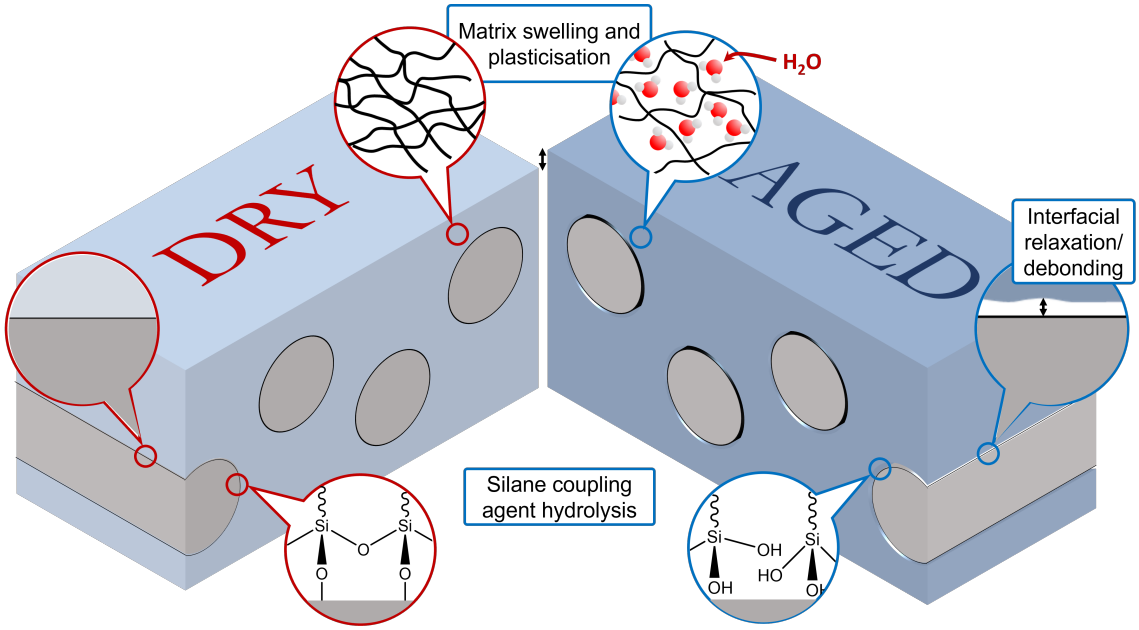

Figure 4.17: *A comparison of dry (left) and seawater aged (right) composites demonstrating relevant damage mechanisms of seawater ageing [15, 31].*

4.2.5.2 GF1-MCS/epoxy

The SEM images in Figure 4.15 show differing failure behaviour between the thermoplastic composites and the thermoset GF1-MCS/epoxy. In the former, crack propagation is through the matrix (cohesive failure) when dry but along the interface (adhesive failure) when aged. In contrast, crack propagation is along the interface in both dry and aged epoxy, suggesting that the epoxy matrix is stronger than the epoxy-GF interface both before and after ageing.

4.2.6 Practical Significance

Beyond lab-scale testing, these water absorption and (thermo)mechanical test results have implications for the commercial use of acrylic and acrylic-PPE resins in the marine environment. The DNV standard DNV-ST-0164 requires that a $50 \times 50 \times 2$ mm coupon of the unreinforced resin used to manufacture a tidal turbine blade absorb less than 50 mg of water after 7 days, and less than 100 mg of water after 28 days. Unreinforced resin was not tested in the current study, but Davies et al. [7] immersed $50 \times 50 \times 2.7$ mm coupons of unreinforced acrylic in seawater at 25 °C, and measured the diffusion coefficient as 0.55×10^{-12} $\mathrm{m^2\,s^{-1}}$, and the maximum water uptake as 1.87%.

Although this study [7] used seawater and a slightly thicker coupon than the standard requires, if we assume a resin density of 1.18 $\mathrm{g\,cm^{-3}}$ then these values can be used to create a hypothetical absorption curve for a $50 \times 50 \times 2$ mm unreinforced acrylic coupon using Equation 4.2. This is shown in Figure 4.18, in which it can be seen that the water content at 28 days (1.8%) only slightly exceeds the allowable 1.7%, but that the fast diffusion of water in acrylic resin means that 1.3% water is absorbed after 7 days, far exceeding the allowable 0.85%. Therefore, even though the mechanical effects of water on GF/acrylic is acceptable in comparison to GF/epoxy, alterations to the acrylic resin chemistry may be required if a tidal turbine blade manufacturer wishes to conform to current DNV specifications, although this should be confirmed experimentally. While it was theorised that reactive hybridisation with PPE could cause this reduction in moisture absorption, as it is one of its marketed use in epoxy resins [3, 4], the results from Section 4.2.2 suggest that this is not the case.

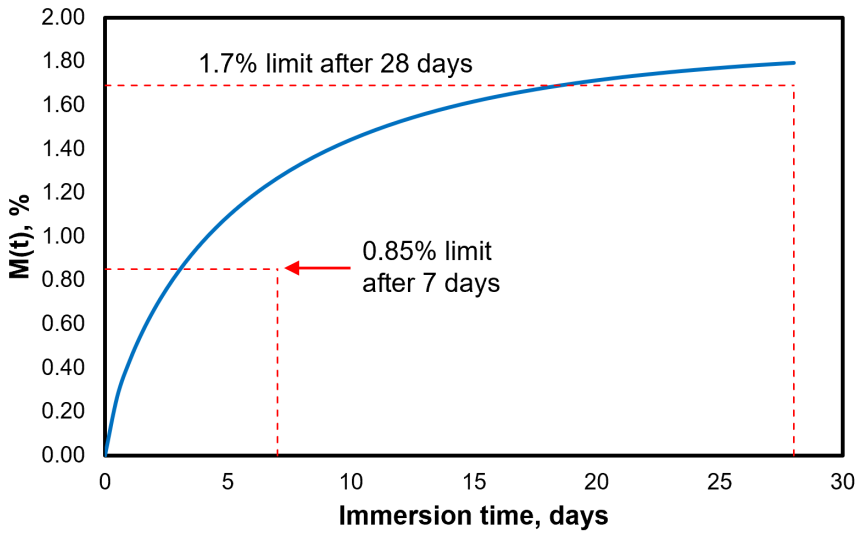

Figure 4.18: *Calculated absorption curve for a* $50 \times 50 \times 2$ *mm coupon of unreinforced acrylic resin. The maximum allowable water contents of the coupon at 7 and 28 days, according to DNV-ST-0164, are highlighted. The resin exceeds both limits. Absorption data from [7].*

Slower diffusion of water in the resin would therefore be an advantage for its use in tidal turbine blades, and is essential if it is to conform to DNV-ST-0164. The faster diffusion of water in GF1-MCS/acrylic could cause deeper penetration into a tidal turbine blade and cause greater reductions in the blade's properties, but on the other hand water penetration is limited in real tidal turbine blades due to the thickness of the composites [32]. For example, in a study by Murdy et al. [5], GF/acrylic and GF/epoxy tidal turbine blades were immersed in water at ambient temperature for 6 and 11 months respectively while their weight gain was tracked. Faster water absorption was observed in the GF/acrylic blade, reaching 0.14% after 6 months vs. 0.07% after 11 months for GF/epoxy. Extrapolation of the data by Murdy et al. [5] suggested that the GF/acrylic blade would absorb around 1% water after 20 years, and the GF/epoxy blade would absorb around 0.4% water. The authors [5] suggest this is an inflated value due to absorption of water into the foam cavity of the blades, and due to osmotic blistering in the GF/acrylic blade, and so they do not believe the composite skins would approach saturation in this time.

The limited extent of diffusion in a tidal turbine blade can be further illustrated using some approximate calculations. Consider two composite laminates,

50 mm thick to represent a tidal turbine blade shell, and wide enough to minimise edge diffusion, with one laminate made of GF1-MCS/acrylic and the other of GF1-MCS/epoxy as in the present study. If they were immersed in seawater at 10 °C (283 K), then the Arrhenius Equation (Equation 2.3) can be used to calculate the value of D_z at this temperature. Values for D_z at 50 °C (323 K) are found in Table 4.3, and the value for the activation energy, E_a, of 48 kJ mol^{-1} for GF/acrylic is calculated from data in [7] as described in Chapter 2. The value of E_a can vary significantly depending on resin chemistry—for example, Li et al. [33] found that E_a for the diffusion of water in a single epoxy resin could be varied between approximately 32–45 kJ/mol through esterification of the curing agent. The same value of $E_a = 48$ kJ mol^{-1} is therefore used for GF1-MCS/epoxy for simplicity. Therefore, starting from Equation 2.3:

$$D_2 = D_1 \cdot exp\left[\frac{E_a}{R}\left(\frac{1}{T_1} - \frac{1}{T_2}\right)\right]$$

$$\begin{aligned} D_{GF/acrylic,10°C} &= 1.8 \times 10^{-6}\ \text{mm}^2\,\text{s}^{-1} \cdot exp\left[\frac{48000\ \text{J mol}^{-1}}{8.314\ \text{J K}^{-1}\,\text{mol}^{-1}}\left(\frac{1}{323\ K} - \frac{1}{283\ K}\right)\right] \\ &= 1.4 \times 10^{-7}\ \text{mm}^2\,\text{s}^{-1} \end{aligned}$$

$$\begin{aligned} D_{GF/epoxy,10°C} &= 0.15 \times 10^{-6}\ \text{mm}^2\,\text{s}^{-1} \cdot exp\left[\frac{48000\ \text{J mol}^{-1}}{8.314\ \text{J K}^{-1}\,\text{mol}^{-1}}\left(\frac{1}{323\ K} - \frac{1}{283\ K}\right)\right] \\ &= 1.2 \times 10^{-8}\ \text{mm}^2\,\text{s}^{-1} \end{aligned}$$

Using the values of M_m of 0.63% for GF1-MCS/epoxy and 0.81% for GF1-MCS/acrylic (Table 4.3), as well as the values for D calculated above, the hypothetical absorption curves of the 50 mm thick GF1-MCS/acrylic and GF1-MCS/epoxy laminates in 10 °C seawater can be calculated, and are shown in Figure 4.19. While neither laminate is expected to saturate, the GF1-MCS/acrylic absorbs significantly more water than the GF1-MCS/epoxy.

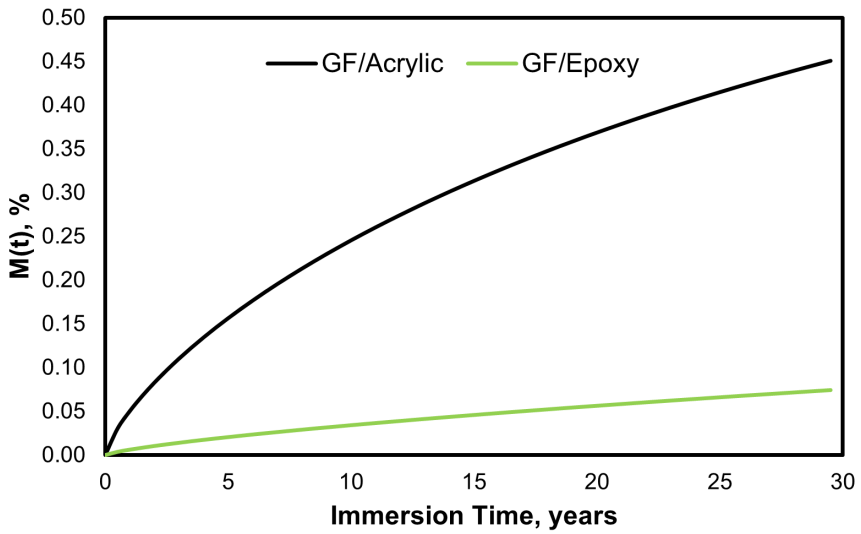

Figure 4.19: *Calculated water absorption curves over a 30 year time period for GF1-MCS/acrylic and GF1-MCS/epoxy laminates. Laminates are of 50 mm thickness and immersed in seawater at 10 °C. Diffusion coefficients and maximum water uptakes are calculated from the current study.*

The effects of thickness and immersion time on the water content of GF1-MCS/acrylic and GF1-MCS/epoxy laminates are shown as contour plots in Figure 4.20, as calculated using Equation 4.2. The figure illustrates that thin sections of a blade—below $\sim$ 20 *mm* for GF1-MCS/acrylic and $\sim$ 5 *mm* for epoxy—will approach saturation within its 20 year lifespan (perhaps at the blade tip, for example). Thicker sections will absorb significantly lower percentages of water, and water absorption is negligible ($< 0.1\%$) above 50 mm thickness in GF1-MCS/epoxy after 20 years.

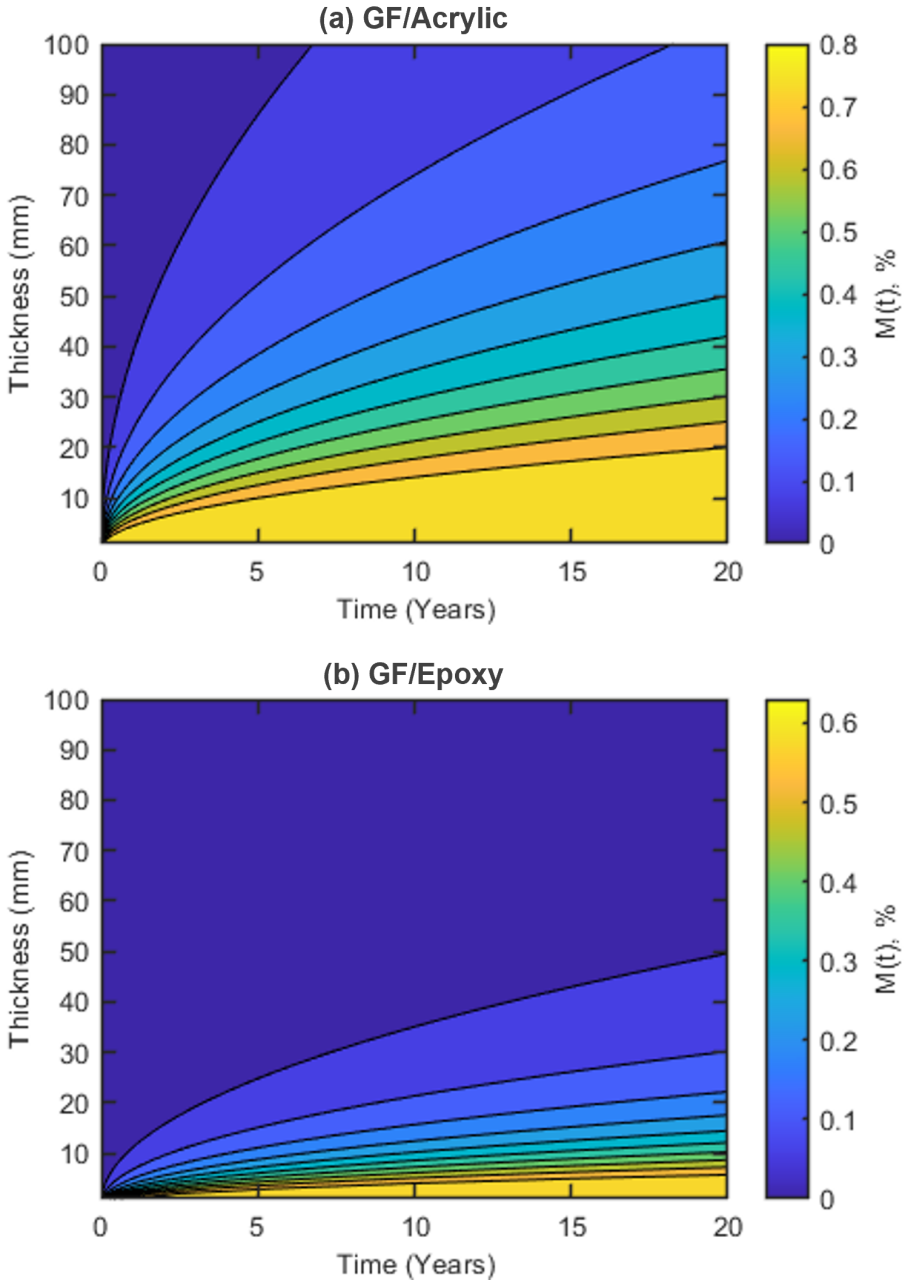

Figure 4.20: *Contour plots comparing the calculated moisture content of (a) GF1-MCS/acrylic and (b) GF1-MCS/epoxy laminates of varying thicknesses and immersion times. For example, after 15 years, 50 mm thick laminates of GF1-MCS/acrylic and GF1-MCS/epoxy would reach 0.31% and 0.05% water content respectively.*

These are just approximations, but they illustrate both that saturation would be reached much more quickly in GF/acrylic than in GF/epoxy, and that the long saturation times mean that full saturation may never be achieved over a turbine's typical lifespan. The effects on a real tidal turbine blade would be more complex, of course, due to the geometry of the blade; the possibility of single-sided exposure

of the composite to water; the inclusion of other materials, for example paints, adhesives and foam fillers; and the varying stress through the composite thickness due to flexural loading of the blade. A 2.5 m long GF/acrylic tidal turbine blade was immersed in seawater for 6 months by Murray et al. [34] without significant changes in stiffness, but further experimental testing and numerical simulations should be performed to understand long-term water absorption in acrylic-matrix tidal turbine blades.

4.3 Chapter Summary

The aim of this chapter was to determine the behaviour of thermoplastic GF/acrylic and GF/acrylic-PPE composites during and after ageing in seawater at 50°C, in comparison with an equivalent thermoset GF/epoxy composite.

The diffusion coefficients of the GF1-MCS/acrylic ($1.8 \times 10^{-12} m^2 s^{-1}$) and GF1-MCS/acrylic-PPE ($3.4 \times 10^{-12} m^2 s^{-1}$) were an order of magnitude larger than that of GF1-MCS/epoxy ($0.16 \times 10^{-12} m^2 s^{-1}$), and the final masses of absorbed water in GF1-MCS/acrylic and GF1-MCS/acrylic-PPE were also higher at 0.91% and 0.81% vs. 0.63% for GF1-MCS/epoxy, respectively. This difference is likely due to a combination of higher void contents in the thermoplastic composite coupons used for water diffusion studies and a stronger interaction of the epoxy matrix with water in GF1-MCS/epoxy that slows down the water diffusion. However, the faster water diffusion in the thermoplastic composites did not correspond to greater reductions in mechanical properties due to ageing. In general, the GF1-MCS/acrylic and GF1-MCS/acrylic-PPE compared favourably and had similar or smaller reductions in mechanical properties due to seawater ageing compared to the GF1-MCS/epoxy baseline. The effect of free water in voids and interstitial sites may therefore be less detrimental than bound water.

The 0° tensile and flexural moduli were approximately equal between matrices and not significantly affected by ageing. The strengths, however, saw larger decreases—up to 20% in the case of GF1-MCS/epoxy in 0° tension. SEM imaging of these specimens, along with DMA studies, revealed that interfacial degradation and matrix plasticisation are the causes of deterioration in mechanical properties

after seawater ageing. Future studies may therefore focus on determining the effects of acrylic-tailored sizings on the degradation of GF/acrylic composites in water.

An analysis of these results from the viewpoint of the resins' commercial use in tidal turbine blades suggested that, although the comparisons between GF1-MCS/acrylic and GF1-MCS/epoxy were generally positive, the faster diffusion in GF/acrylic may prove to be a barrier for its commercial adoption. Calculated water diffusion curves of thick GF1-MCS/acrylic composites showed that significantly more water would be absorbed over a tidal turbine blade's life than in GF1-MCS/epoxy. This was confirmed experimentally in the literature, although it was also shown that a blade is unlikely to saturate in its lifetime. Furthermore, using data from the literature, it was found that fast diffusion of water into acrylic resin means that it may not conform to DNV-ST-0164, which specifies a minimum standard for tidal turbine blade materials. This does not mean the resin cannot be used commercially in tidal turbine blades—there are other standards such as IEC TS 62600 which does not have such requirements for the resin, and manufacturers do not necessarily need to follow a standard at all—but it may make investment and insurance more challenging to obtain.

Reactive hybridisation with PPE did not reduce the diffusion coefficient of water in acrylic resin, nor did it reduce the maximum water uptake. However, there were several mechanical benefits of GF/acrylic-PPE over GF/acrylic, the most significant of which was in 90° flexural testing. GF1-MCS/acrylic-PPE had higher 90° flexural strength (+22%) and modulus (+8%) when dry, and also enhanced 90° flexural strength (+10%) and modulus (+13%) when aged, compared to GF/acrylic. In addition, the T_g of the GF1-MCS/acrylic-PPE was 4°C higher than the GF1-MCS/acrylic before ageing and 6°C after ageing. DMA revealed no evidence of melt-softening behaviour by 180°C in GF1-MCS/acrylic-PPE, whereas the onset of softening was observed in GF1-MCS/acrylic after the T_g.

These results add further evidence that thermoplastic acrylic composites are a promising recyclable alternative to thermosets in marine applications, given their favourable material properties when compared to an epoxy baseline. Further research into acrylic resin's use in tidal turbine blades is, however, required. In addition, acrylic-PPE allows for improved mechanical and thermomechanical properties

while retaining recyclability.

4.4 Chapter References

[1] Winifred Obande, Weronika Gruszka, Jennifer A. Garden, Christian Wurzer, Conchúr M. Ó Brádaigh, and Dipa Ray. Enhancing the solvent resistance and thermomechanical properties of thermoplastic acrylic polymers and composites via reactive hybridisation. *Materials and Design*, 206, 2021. ISSN 02641275. doi: 10.1016/j.matdes.2021.109804.

[2] Winifred Obande, Conchúr M. Ó Brádaigh, and Dipa Ray. Thermoplastic hybrid-matrix composite prepared by a room-temperature vacuum infusion and in-situ polymerisation process. *Composites Communications*, 22(August):22–27, 2020. doi: 10.1016/j.coco.2020.100439.

[3] Edward N Peters, Scott M Fisher, and Hua Guo. Polyphenylene ether macromonomers. iii. enhancement of dielectric materials. *Proceedings of the IPC Printed Circuits EXPO and APEX, Las Vegas, NV, USA*, 31, 2009.

[4] Edward N. Peters. Poly(phenylene ether) based amphiphilic block copolymers. *Polymers*, 9(9), 2017. ISSN 2073-4360. doi: 10.3390/polym9090433.

[5] Paul Murdy, Ariel Lusty, Robynne Murray, Scott Hughes, and Ryan Beach. Post-deployment characterization of glass fiber-reinforced thermoset and thermoplastic composite tidal turbine blades: Preprint. 4 2024. URL `https://www.osti.gov/biblio/2340123`.

[6] Masako Unemori, Yoko Matsuya, Shigeki Matsuya, Akane Akashi, and Akifumi Akamine. Water absorption of poly(methyl methacrylate) containing 4-methacryloxyethyl trimellitic anhydride. *Biomaterials*, 24(8):1381–1387, 2003. ISSN 0142-9612. doi: https://doi.org/10.1016/S0142-9612(02)00521-5.

[7] P. Davies, P. Y. Le Gac, and M. Le Gall. Influence of sea water aging on the mechanical behaviour of acrylic matrix composites. *Applied Composite Materials*, 24(1):97–111, 2016. ISSN 0929-189X 1573-4897. doi: 10.1007/s10443-016-9516-1.

[8] Ehsan Moghbelli, Reid Banyay, and Hung-Jue Sue. Effect of moisture exposure on scratch resistance of pmma. *Tribology International*, 69:46–51, 2014. ISSN 0301-679X. doi: https://doi.org/10.1016/j.triboint.2013.08.012.

[9] Christos J. Tsenoglou, Sylvia Pavlidou, and Constantine D. Papaspyrides. Evaluation of interfacial relaxation due to water absorption in fiber–polymer composites. *Composites Science and Technology*, 66(15):2855–2864, 2006. ISSN 02663538. doi: 10.1016/j.compscitech.2006.02.022.

[10] Y. Fujii, T. Tominaga, D. Murakami, M. Tanaka, and H. Seto. Local dynamics of the hydration water and poly(methyl methacrylate) chains in pmma networks. *Front Chem*, 9:728738, 2021. ISSN 2296-2646 (Print) 2296-2646 (Linking). doi: 10.3389/fchem.2021.728738.

[11] Fatmaelzahraa Abdelmola and Leif A Carlsson. State of water in void-free and void-containing epoxy specimens. *Journal of Reinforced Plastics and Composites*, 38(12):556–566, 2019. doi: 10.1177/0731684419833469.

[12] V. Bellenger, J. Verdu, and E. Morel. Structure-properties relationships for densely cross-linked epoxide-amine systems based on epoxide or amine mixtures. *Journal of Materials Science*, 24(1):63–68, 1989. ISSN 1573-4803. doi: 10.1007/BF00660933.

[13] Pierre Gilormini and Jacques Verdu. On the role of hydrogen bonding on water absorption in polymers. *Polymer*, 142:164–169, 2018. ISSN 00323861. doi: 10.1016/j.polymer.2018.03.033.

[14] Francette Thominette, Emmanuelle Gaudichet-Maurin, and Jacques Verdu. Effect of structure on water diffusion in hydrophilic polymers. *Defect and Diffusion Forum*, 258-260:442 – 446, 2006.

[15] David A. Bond and Paul A. Smith. Modeling the transport of low-molecular-weight penetrants within polymer matrix composites. *Applied Mechanics Reviews*, 59(5):249–268, 2006. ISSN 0003-6900. doi: 10.1115/1.2202873.

[16] Haithem Bel Haj Frej, Romain Léger, Didier Perrin, and Patrick Ienny. Effect of aging temperature on a thermoset-like novel acrylic thermoplastic composite

for marine vessels. *Journal of Composite Materials*, 55(19):2673–2691, 2021. ISSN 0021-9983 1530-793X. doi: 10.1177/0021998321996780.

[17] L. S. A. Smith and V. Schmitz. The effect of water on the glass transition temperature of poly(methyl methacrylate). *Polymer*, 29(10):1871–1878, 1988. ISSN 0032-3861. doi: https://doi.org/10.1016/0032-3861(88)90405-3.

[18] W. W. Wright. The effect of diffusion of water into epoxy resins and their carbon-fibre reinforced composites. *Composites*, 12(3):201–205, 1981. ISSN 0010-4361. doi: https://doi.org/10.1016/0010-4361(81)90505-X.

[19] A. Chateauminois, B. Chabert, J. P. Soulier, and L. Vincent. Dynamic mechanical analysis of epoxy composites plasticized by water: Artifact and reality. *Polymer Composites*, 16(4):288–296, 1995. ISSN 0272-8397 1548-0569. doi: 10.1002/pc.750160405.

[20] P. Joseph and S. Tretsiakova-McNally. Melt-flow behaviours of thermoplastic materials under fire conditions: Recent experimental studies and some theoretical approaches. *Materials (Basel)*, 8(12):8793–8803, 2015. ISSN 1996-1944 (Print) 1996-1944 (Linking). doi: 10.3390/ma8125492.

[21] Winifred Obande, Dimitrios Mamalis, Dipa Ray, Liu Yang, and Conchúr M. Ó Brádaigh. Mechanical and thermomechanical characterisation of vacuum-infused thermoplastic- and thermoset-based composites. *Materials and Design*, 175, 2019. ISSN 02641275. doi: 10.1016/j.matdes.2019.107828.

[22] Haithem Bel Haj Frej, Romain Léger, Didier Perrin, and Patrick Ienny. A novel thermoplastic composite for marine applications: Comparison of the effects of aging on mechanical properties and diffusion mechanisms. *Applied Composite Materials*, 2021. ISSN 0929-189X 1573-4897. doi: 10.1007/s10443-021-09903-0.

[23] J. Cook and J. E. Gordon. A mechanism for the control of crack propagation in all-brittle systems. *Proceedings of the Royal Society of London. Series A. Mathematical and Physical Sciences*, 282(1391):508–520, 1964. doi: doi:10.1098/rspa.1964.0248.

[24] Yan Ma, Yuqiu Yang, Toshi Sugahara, and Hiroyuki Hamada. A study on the failure behavior and mechanical properties of unidirectional fiber reinforced thermosetting and thermoplastic composites. *Composites Part B: Engineering*, 99:162–172, 2016. doi: 10.1016/j.compositesb.2016.06.005.

[25] M. Thouless and John Parmigiani. Mixed-mode cohesive-zone models for delamination and deflection in composites. *Proceedings of the 28th Risø International Symposium on Material Science: Interface Design of Polymer matrix Composites*, 2007.

[26] Miroslav Raab, Eckhard Schulz, and Miloš Sova. The cook-gordon mechanism in polymeric materials. *Polymer Engineering and Science*, 33(21):1438–1443, 1993. ISSN 0032-3888. doi: https://doi.org/10.1002/pen.760332110.

[27] Emile S. Greenhalgh, editor. *Fibre-dominated failures of polymer composites*, pages 107–163. Woodhead Publishing, 2009. ISBN 9781845692179. doi: 10.1533/9781845696818.107.

[28] Emile S. Greenhalgh, editor. *Delamination-dominated failures in polymer composites*, pages 164–237. Woodhead Publishing, 2009. ISBN 9781845692179. doi: 10.1533/9781845696818.164.

[29] J. L. Thomason. Glass fibre sizing: A review. *Composites Part A: Applied Science and Manufacturing*, 127, 2019. ISSN 1359835X. doi: 10.1016/j.compositesa.2019.105619.

[30] Ori Ishai. Environmental effects on deformation, strength, and degradation of unidirectional glass-fiber reinforced plastics. ii. experimental study. *Polymer Engineering and Science*, 15(7):491–499, 1975. ISSN 0032-3888. doi: https://doi.org/10.1002/pen.760150704.

[31] T. Nihei. Dental applications for silane coupling agents. *J Oral Sci*, 58(2):151–5, 2016. ISSN 1880-4926 (Electronic) 1343-4934 (Linking). doi: 10.2334/josnusd.16-0035.

[32] N. Tual, N. Carrere, and Peter Davies. Characterization of sea water ageing effects on mechanical properties of carbon/epoxy composites for tidal turbine

blades. In Aalborg Univ Press, editor, *ICCM20 Proceedings, 20th International Conference on Composite Materials, July 19-24, 2015. Ole Thybo Thomsen, Christian Berggreen and Bent F Sørensen (Eds). 4216-4, 12p.*, pages –, 2015. URL https://archimer.ifremer.fr/doc/00749/86101/.

[33] Liang Li, ShuYong Zhang, YueHui Chen, MoJun Liu, YiFu Ding, XiaoWen Luo, Zong Pu, WeiFang Zhou, and Shanjun Li. Water transportation in epoxy resin. *Chemistry of Materials*, 17(4):839–845, 2005. doi: 10.1021/cm048884z.

[34] Robynne E. Murray, Ryan Beach, Paul Murdy, Scott Dana, and Scott Hughes. Structural characterization of deployed thermoplastic and thermoset composite tidal turbine blades. Report, 2024-04-08 2024.

Chapter 5

The Fatigue of Glass-Fibre Reinforced Acrylic Composites

In Chapter 4, it was demonstrated that seawater ageing reduces the static mechanical properties of GF/acrylic via interfacial degradation and matrix plasticisation. In renewable energy applications, the fatigue properties of the materials used are of paramount importance, as wind and tidal turbine blades undergo millions to hundreds of millions of load cycles over their lifespan [1, 2]. As discussed in Chapter 2, the sizing agent applied to the reinforcement fibres can affect interfacial bonding strength and resistance to water absorption. This lead Davies et al. [3, 4] to suggest that an improved resistance to interfacial degradation may be achieved if a multi-compatible sizing agent, such as that used in Chapter 4, were replaced with an acrylic-tailored sizing agent. Therefore, in the following chapter, the tension-tension fatigue behaviour of GF/acrylic coupons with an acrylic-tailored sizing agent is characterised both before and after ageing in seawater. Comparisons are then made with a multi-compatible sizing agent, to explore whether there is a benefit to developing these specialised formulations.

5.1 Materials and Methods

In the current work, GF/acrylic with an acrylic-tailored sizing agent was manufactured. Comparisons are made with the multi-compatible GF/acrylic from Chapter 4. Static testing and seawater ageing of this multi-compatible GF/acrylic was

described in Chapter 4, but its fatigue properties were characterised in a parallel study [5] which is summarised in Appendix A.1. This is discussed again in the following sections, but is highlighted here for clarity.

5.1.1 Manufacture of Composites

Laminates were manufactured using a standard vacuum infusion process using a $[0°]_2$ layup of unidirectional non-crimp glass fibre with an acrylic-tailored sizing agent. The fibres were supplied by Johns Manville and stitched by SAERTEX to give a fabric with 1152 $\mathrm{g\,m^{-2}}$ of 0° fibres, 35 $\mathrm{g\,m^{-2}}$ of 90° fibres for stability, and 13 $\mathrm{g\,m^{-2}}$ of polyester stitching. The resin used was Elium® 188 O (Arkema), mixed in a 100:3 ratio with BP-50-FT benzoyl peroxide initiator (United Initiators) and polymerised at room temperature for 24 hours before demoulding and cutting. Coupons were cut to nominal 250×15×2 mm dimensions with a diamond-tipped water-cooled saw, although stresses were calculated based on their measured sizes.

Comparisons will be made between these laminates and the multi-compatible GF/acrylic material described in Chapter 4, although tested in fatigue as part of a parallel study [5]. See Appendix A.1 for more information. This fabric and sizing agent were previously shown to have excellent compatibility with acrylic resin [6], which is supported by the results in Chapter 4. Aside from the difference in sizing, the two glass fabrics also differed in fibre diameter and tow linear density, as detailed in Table 5.1. The fabrics will be referred to as GF1-MCS (multi-compatible sizing) and GF2-AS (acrylic sizing).

Table 5.1: *A summary of the differences between the reinforcements being compared*

	GF1-MCS	GF2-AS
Manufacturing/testing	Parallel study [5]	Current study
Fibre diameter (µm)	13	16
Tow linear density (tex)	1200	2400
Areal weight ($g\,m^{-2}$)	646	1200
Sizing agent	Multi-compatible	Acrylic specialised
Image	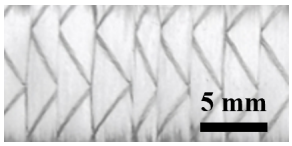	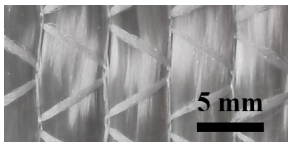

5.1.2 Fibre Volume Fraction

Fibre (FVF), matrix and void volume fractions were determined using a burn-off method (ASTM D3171, Procedure G). Values for the fibre, matrix and composite densities were measured via the displacement of water (ASTM D792). Five coupons, cut to 30 mm squares, were tested for each material.

5.1.3 Water Immersion

Half of the coupons were immersed in natural seawater from the Firth of Forth, Scotland, held at 50°C for 3 months to match the previous work with GF1-MCS/acrylic in Chapter 4. The immersed coupons were then stored in room temperature seawater until testing. These coupons are referred to as 'aged', and the remaining specimens which were not immersed in water are referred to as 'dry'. GF1-MCS/acrylic coupons of 1.5 mm thickness had a time to saturation of approximately 3 days in Chapter 4. Therefore, given the similarity in thickness and the 3 months of immersion, the aged GF2-AS/acrylic coupons in the present work are expected to be fully saturated before testing.

5.1.4 Quasi-Static Tensile Testing

The ultimate tensile strengths (UTS) of 5 dry and 5 aged 0° GF/acrylic coupons were tested according to ASTM D3039 using an MTS Criterion Model 45 test machine (serial number 10523451A) with a 300 kN load cell (serial number 578061). Coupons were tabbed with 1.6 mm thick GF/epoxy PCB board bonded with cyanoacrylate adhesive and then tested at a 2 mm/min extension rate.

5.1.5 Fatigue Testing

Coupons were tested in tension-tension fatigue using an Instron 8802 servohydraulic fatigue testing system (system ID 8802J5704) equipped with a 250 kN load cell (system ID 2742–501) and grip pressure of 60 bar, using a testing frequency of 5 Hz and an R-ratio of 0.1. Fatigue coupons were also tabbed with GF/epoxy PCB board bonded with cyanoacrylate adhesive.

Given the expected differences between the mechanical properties of the fabrics, the stress levels (the maximum stress applied during a load cycle) for GF2-AS/acrylic were set at 80%, 60% and 40% of the UTS of GF2-AS/acrylic, as well as 80%, 60% and 40% of the UTS of GF1-MCS/acrylic, i.e. 6 stress levels. A single additional test was performed at 30% of the UTS of dry and aged GF2-AS/acrylic to investigate higher-cycle fatigue and the existence of a fatigue limit. The applied stresses are summarised in Table 5.2, using the UTS values discussed later in Section 5.2.2. Coupons were randomly assigned to an ageing condition and stress level after cutting.

Table 5.2: *The stress levels used to test dry and aged GF2-AS/acrylic coupons.*

Dry		Aged	
Stress (MPa)	%UTS	Stress (MPa)	%UTS
710	100	578	100
639	90	520	90
568	80	462	80
481	68	428	74
426	60	347	60
321	45	286	49
284	40	231	40
213	30	173	30

To keep the aged coupons wet during testing, they were covered in a wet cloth and wrapped in plastic vacuum bag (Figure 5.1).

Figure 5.1: *Aged coupons were kept wet during testing by covering with a saturated cloth and plastic wrap.*

The Basquin relation (Equation 5.1) relates stress (S) to the number of cycles to failure (N) with two coefficients A and b. Although S may be defined in several ways, in the present work it refers to the maximum stress applied in a load cycle. This relationship applies to the portion of the S-N curve in which progressive damage occurs, and only above the fatigue limit of the material (Figure 5.2) [7, 8]. Therefore, Equation 5.1 was fit to the experimental data between 80% and 40% of the UTS, using the MATLAB Curve Fitting Toolbox v3.5.13.

$$S = A \cdot N^b \tag{5.1}$$

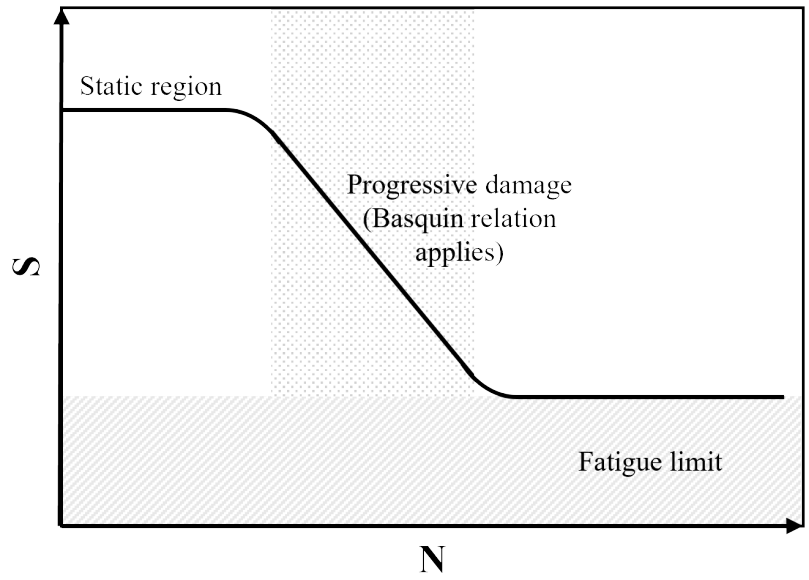

Figure 5.2: *The structure of an S-N curve, adapted from Talreja [8]. Equation 5.1 was fit to the data in the region of progressive damage*

Since comparisons will be made between different S-N curves, the effect of changing the values of the coefficients in Equation 5.1 is illustrated in Figure 5.3.

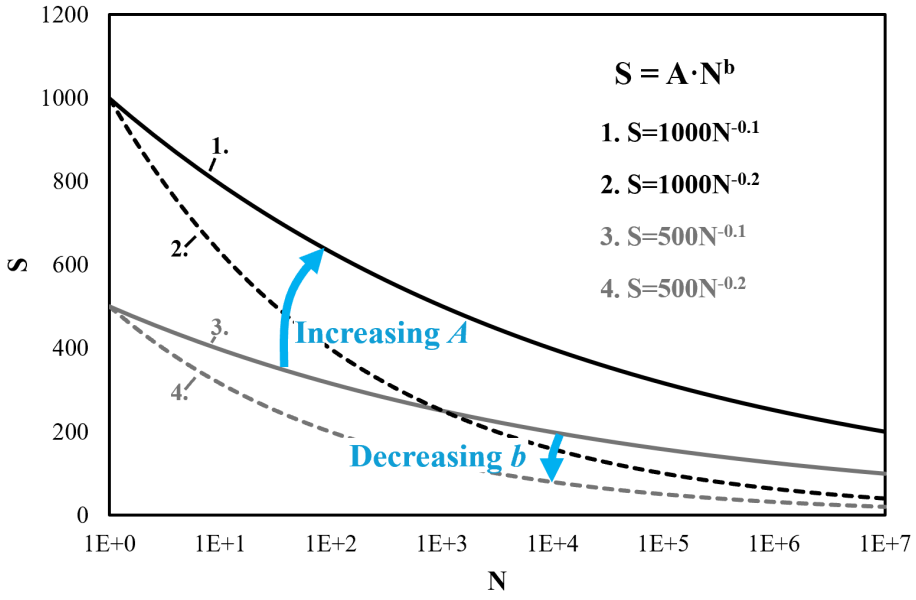

Figure 5.3: *The effects of changing the values of the coefficients A and b in Equation 5.1. An increased A, e.g. from a higher UTS, increases the intercept with the ordinate. A decrease in b (more negative) increases the slope of the curve i.e. increased sensitivity to changes in stress.*

5.2 Results and Discussion

5.2.1 Fibre Volume Fraction

The fibre and void volume fractions of the laminates are provided in Table 5.3. The values for GF1-MCS/acrylic are from Chapter 4 and those for GF2-AS/acrylic are from the current study. GF1-MCS/acrylic had a higher FVF than GF2-AS/acrylic, and the mean void content of GF1-MCS/acrylic was lower but had a larger standard deviation.

Table 5.3: *Average fibre and void volume fractions of the two composites, ± one standard deviation. FVF values for GF1-MCS/acrylic are from Chapter 4.*

	GF1-MCS/Acrylic	GF2-AS/Acrylic
FVF (%)	53.5 ± 0.8	49.9 ± 1.3
Void Fraction (%)	1.9 ± 0.8	2.4 ± 0.3

5.2.2 Static Testing

The results of the static tests are presented in Table 5.4, along with results for GF1-MCS/acrylic from Chapter 4. A more detailed comparison between the mechanical and water absorption properties of the composites, which were manufactured and tested separately as part of an MEng project, is available in Appendix A.2, and so only the UTS values and retention of strength after ageing were measured in the current work. The higher UTS of GF1-MCS/acrylic compared to GF2-AS/acrylic can be attributed to the lower fibre diameter of GF1-MCS, as well as to the higher FVF of GF1-MCS/acrylic (53.5% vs. 49.9%) and the larger tow size of GF2-AS/acrylic. A lower fibre diameter is linked to an increased fibre strength due to a lower probability of flaws causing premature failure [9, 10], or due to differences in the manufacturing (drawing speed, melt temperature and chemical composition) of the fibres [10, 11]. The larger tow size of GF2-AS/acrylic is similarly expected to decrease static performance due to the increased volume between tows, leading to larger resin-rich volumes (RRVs) in the composite [12].

Table 5.4: *Dry and aged UTS values of GF2-AS/acrylic (from the current study) and GF1-MCS/acrylic (from Chapter 4), as well as the percentage decreases in strength due to saturation with water.*

	UTS, Dry (MPa)	UTS, Aged (MPa)	% Change
GF1-MCS/acrylic	802 ± 66	714 ± 68	-11
GF2-AS/acrylic	710 ± 11	578 ± 19	-19

5.2.3 Fatigue

5.2.3.1 S-N Curves

S-N curves comparing dry and aged GF2-AS/acrylic are presented in Figure 5.4, and comparisons between GF2-AS/acrylic and GF1-MCS/acrylic (from [5]) are presented in Figure 5.5. The values for A and b (Equation 5.1) from the fitted curves are available in Table 5.5. All experimental data is provided as points in each graph, and the fitted curve is provided as a solid line between 40% and 80% of the UTS. The 95% confidence intervals of the fit are shown as dashed lines.

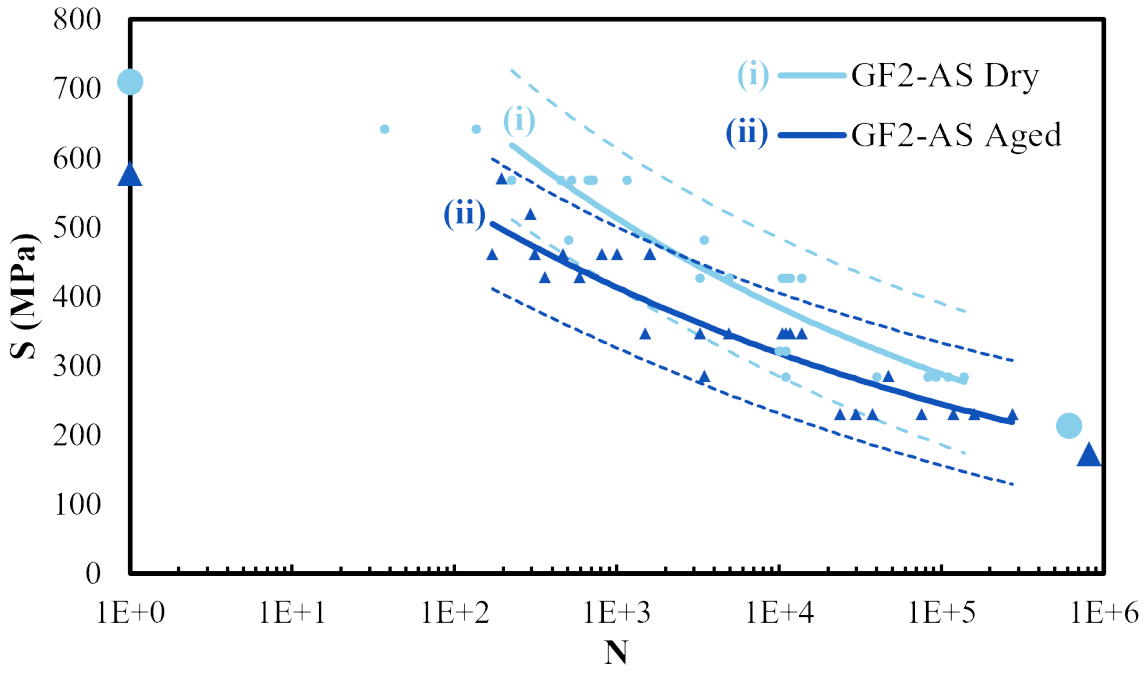

Figure 5.4: *A comparison of the S-N curves for dry (light blue circles) and aged (dark blue triangles) GF2-AS/acrylic. The solid lines are the Basquin relation fit to the experimental data between 80% and 40% of the UTS, and the dashed lines represent the 95% confidence intervals of the fit. The mean static UTS at $N = 1$ and the single datapoints at 30% of the UTS are included as larger data markers.*

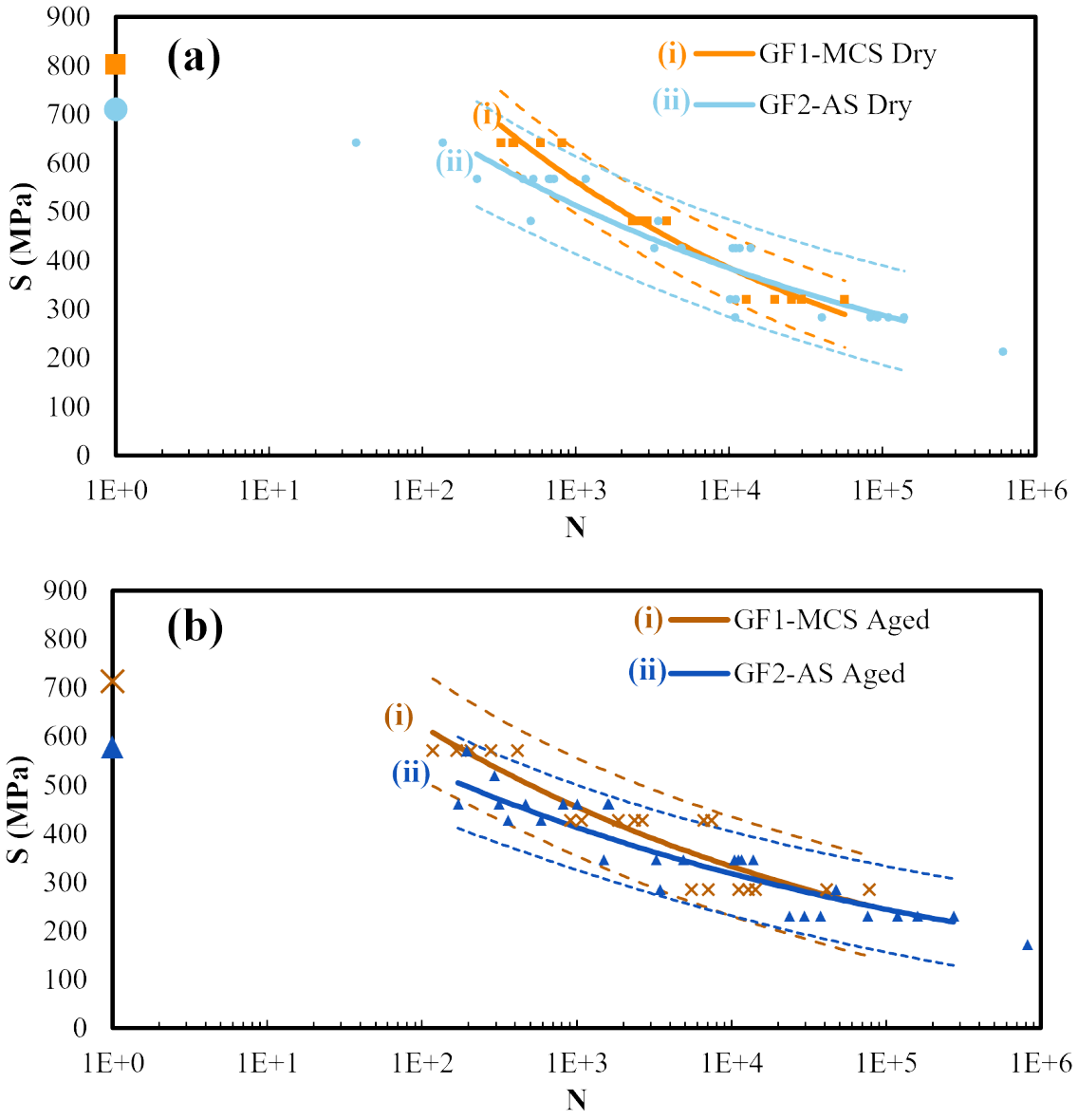

Figure 5.5: *Comparisons between the S-N curves of GF1-MCS/acrylic (from [5]) and GF2-AS/acrylic for (a) dry and (b) saturated coupons.*

Table 5.5: *Basquin coefficients for the curve $S = AN^b$ fit to the fatigue data of each material. Data for GF1-MCS/acrylic is taken from [5] and used to fit the Basquin model, rather than the linear combination of exponential functions in the original publication. The 95% confidence intervals are provided in square brackets.*

Reinforcement	Condition	A (MPa)	b
GF1-MCS [5]	Dry	1750 [1458, 2041]	-0.164 [-0.187, -0.142]
GF1-MCS [5]	Aged	1163 [912, 1413]	-0.136 [-0.166, -0.106]
GF2-AS	Dry	1221 [971, 1472]	-0.125 [-0.151, -0.100]
GF2-AS	Aged	906 [727, 1085]	-0.114 [-0.138, -0.089]

The fatigue strength in low-cycle fatigue (higher stress levels) of dry GF2-AS/acrylic is higher than that of the aged GF2-AS/acrylic coupons (Figure 5.4) due to the difference between their average UTS. This decrease in UTS due to ageing has been shown to be due to interfacial weakening, which allows for rapid debonding during failure as shown in Chapter 4. The fatigue strength of GF1-MCS/acrylic is also higher than GF2-AS/acrylic in low-cycle fatigue, in both dry (Figure 5.5a) and aged (Figure 5.5b) coupons, due to the lower fibre diameter of GF1-MCS and the resulting higher UTS [9–11].

5.2.3.2 Normalised S-N Curves

At lower stresses in Figure 5.5a and b, which is typically the region of interest for blade fatigue, the S-N curves converge, and each fabric performs similarly despite the difference in low-cycle performance. The S-N curves of dry and aged GF2-AS/acrylic (Figure 5.4) also converge at lower stresses, with a 21% decrease in fatigue strength between the dry and aged coupons at 2×10^2 cycles vs. a 14% decrease at 2×10^5 cycles. Convergence of the S-N curves was observed by Davies et al. [4, 13] in dry and aged acrylic-matrix composites, and by Shah et al. [14] in dry composites with different flax reinforcements. In each case, normalisation of the S-N curves to the ultimate strength was found to result in similar S-N curves. Therefore S-N curves are also plotted with stress normalised to each material's respective UTS value (Figure 5.6 and Figure 5.7) as provided in Table 5.4, to minimise the effect of

the differences in UTS.

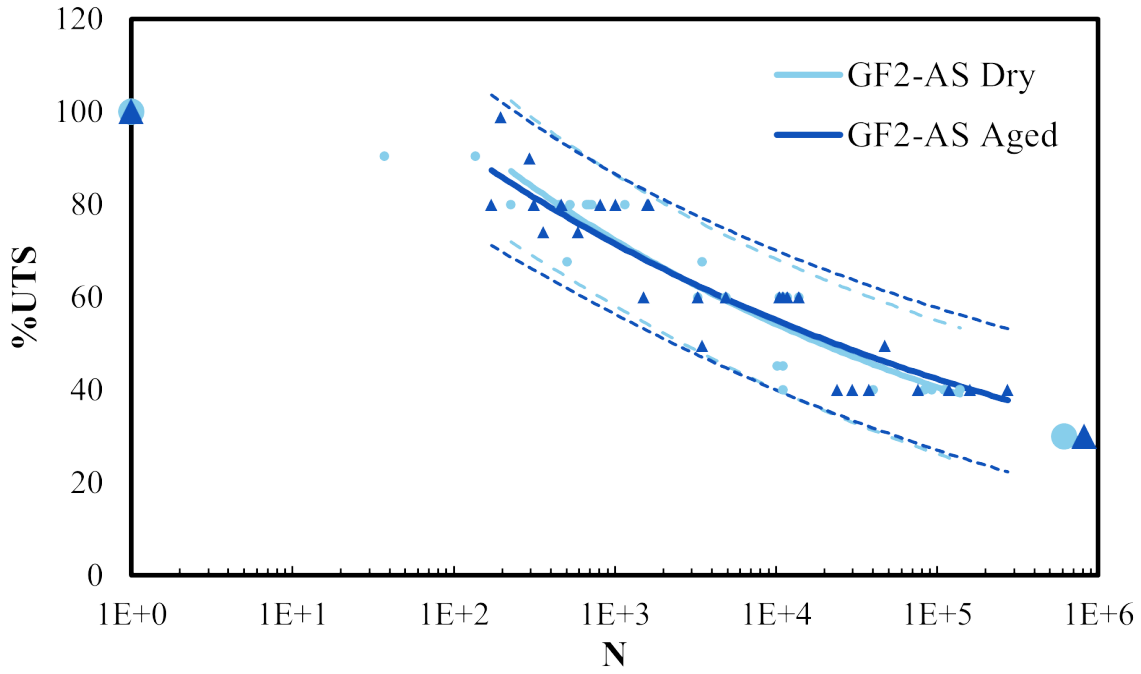

Figure 5.6: *The S-N curves of dry and aged GF2-AS/acrylic with stress expressed as a percentage of each material's UTS. The mean static UTS at N = 1 and the single datapoints at 30% of the UTS are included as larger data markers.*

After expressing the stress as a percentage of the UTS, the fatigue behaviour of each composite is more similar, and the S-N curves for dry and aged GF2-AS/acrylic become nearly identical (Figure 5.6) due to their similar values for the fatigue exponent, b (see Equation 5.1 and Table 5.5). However, as a percentage of UTS, GF2-AS/acrylic seems to perform better than GF1-MCS/acrylic, both dry and aged (Figure 5.7a and b). The value of b for GF1-MCS/acrylic is lower than that for GF2-AS/acrylic in both the dry and aged coupons (Table 5.5), and therefore GF1-MCS/acrylic appears more sensitive to changes in the stress level.

Given the significant overlap of the 95% confidence intervals of the fitted curves, differences between them should be interpreted with caution, however there are several factors which could contribute to a steeper slope in the S-N curves of GF1-MCS/acrylic (Figure 5.7a and b). The first possibility is the tailored sizing agent of GF2-AS, but its effect is unclear given the differences in tow size, FVF and fibre diameter between the fabrics. As discussed previously, the greater tow size of GF2-AS results in larger RRVs than in GF1-MCS, which may act as sites of crack

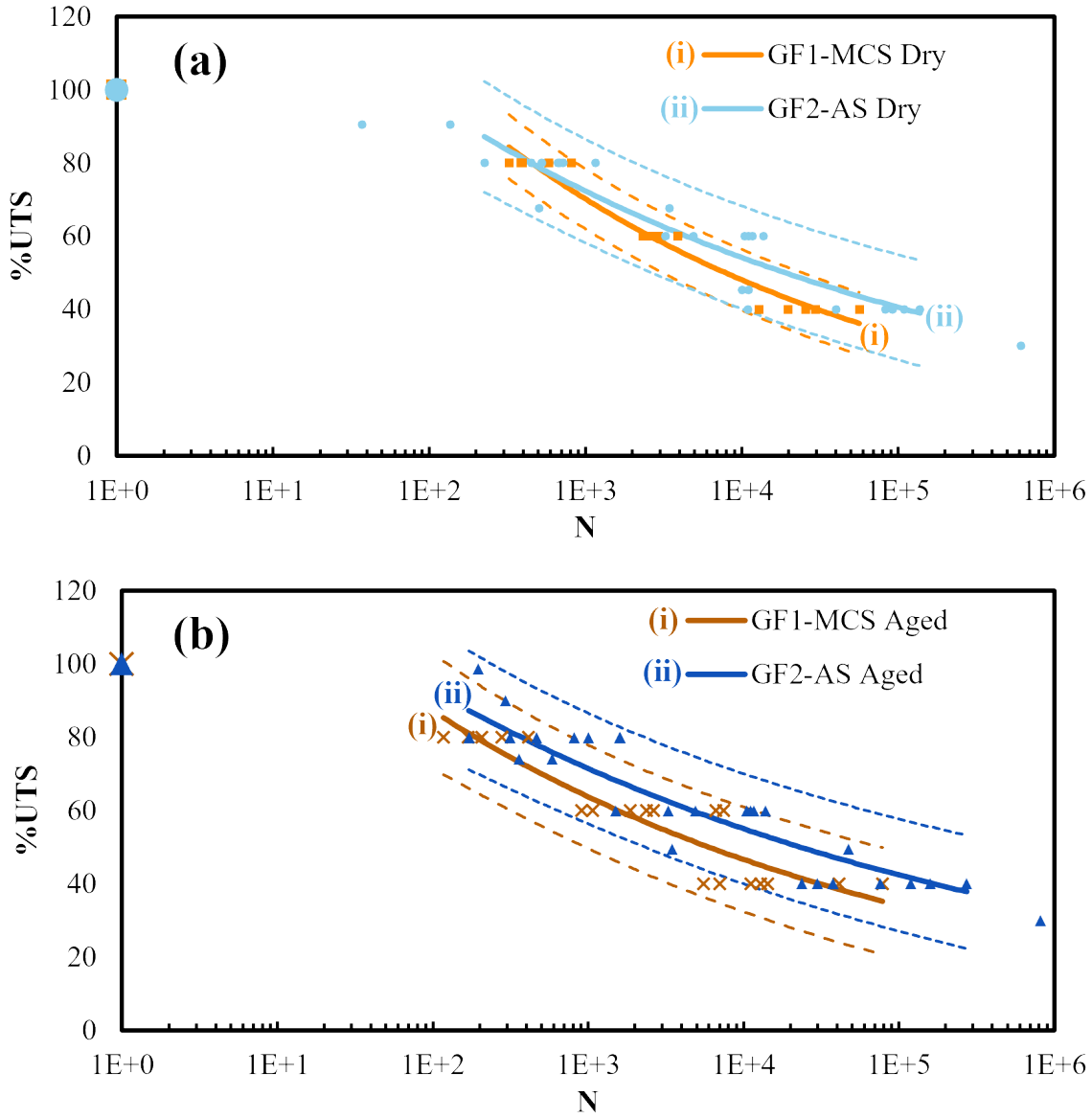

Figure 5.7: *S-N curves comparing (a) dry and (b) aged GF1-MCS/acrylic (from [5]) and GF2-AS/acrylic, with stress expressed as a percentage of each material's UTS.*

initiation and also hasten crack propagation, leading to poorer fatigue performance [12]. FVF values greater than approximately 40% have also been linked to poorer fatigue performance, which is seen as a decrease in the fatigue exponent b, and therefore a steeper slope [14–16]. This has been attributed to an increased likelihood of fibre-fibre contacts, greater shear stresses at the fibre-matrix interface due to closer fibre packing, and an increase in interfacial area increasing the likelihood of interfacial cracks developing [14, 15].

For a given FVF, a smaller fibre diameter also results in a larger number of fibres and a higher interfacial area—23% higher in GF1-MCS vs. GF2-AS given that the surface area to volume ratio ($SA : V$) of a long fibre with radius r is given by $SA : V = \frac{2}{r}$. This would increase the probability of fibre-fibre contacts, and result in a greater surface to volume ratio; a combination which may result in a sharper decline in the S-N curve, similar to the effects observed with a higher FVF.

On the other hand, a smaller fibre diameter is expected to increase fibre strength and composite UTS, as UTS is usually proportional to the FVF, as observed when comparing the static and low-cycle fatigue performance of GF1-MCS/acrylic and GF2-AS/acrylic (Table 5.4 and Figure 5.5). A higher FVF and smaller fibre diameter would therefore cause an improvement in low-cycle fatigue via an increase in the UTS, but the lower value of the fatigue exponent (b) would cause a more rapid decrease in fatigue life towards lower stresses. There is therefore a balance to be struck between static and fatigue performance. However, since tidal turbine blades are usually designed to maximise stiffness [1], a high FVF is a likely target for manufacturers.

5.2.3.3 Low- and High-Cycle Fatigue

The datapoints outside of the fitted curves (outside the 40-80% UTS range) also provide useful information. In low-cycle fatigue, above 80% of the UTS, the S-N curves begin to level off. As discussed by Talreja [8, 17, 18], this points to non-progressive fibre breakage being the dominant failure mechanism in this region. The additional single datapoints at 30% of the dry and aged UTS of GF2-AS/acrylic (Figure 5.6) show that the S-N curve continues to decrease beyond the fitted curves, and that the fatigue limit must be lower than 30% of the UTS, if it exists [16, 19].

5.2.3.4 Comparisons with Literature

A comparison with S-N curves of glass-fibre reinforced acrylic and epoxy from the literature, in which Equation 5.1 has been fit to the experimental data, is provided in Figure 5.8. Various 0° UD glass-reinforced epoxy composites have been tested as part of the SNL/MSU/DOE Composite Material Fatigue Database [20], which characterises the fatigue properties of materials designed for use in wind turbine blades. Only a few key GF/epoxy S-N curves are explicitly included and detailed in Table 5.6, but the approximate range of all comparable data for recently tested UD0 GF/epoxy (i.e. reinforced with unidirectional stitched 0° E-glass fabric) is shaded in yellow. The S-N curves of dry GF1-MCS/acrylic and GF2-AS/acrylic are included, and their performance is comparable with the lower range of GF/epoxy composites in high-cycle fatigue.

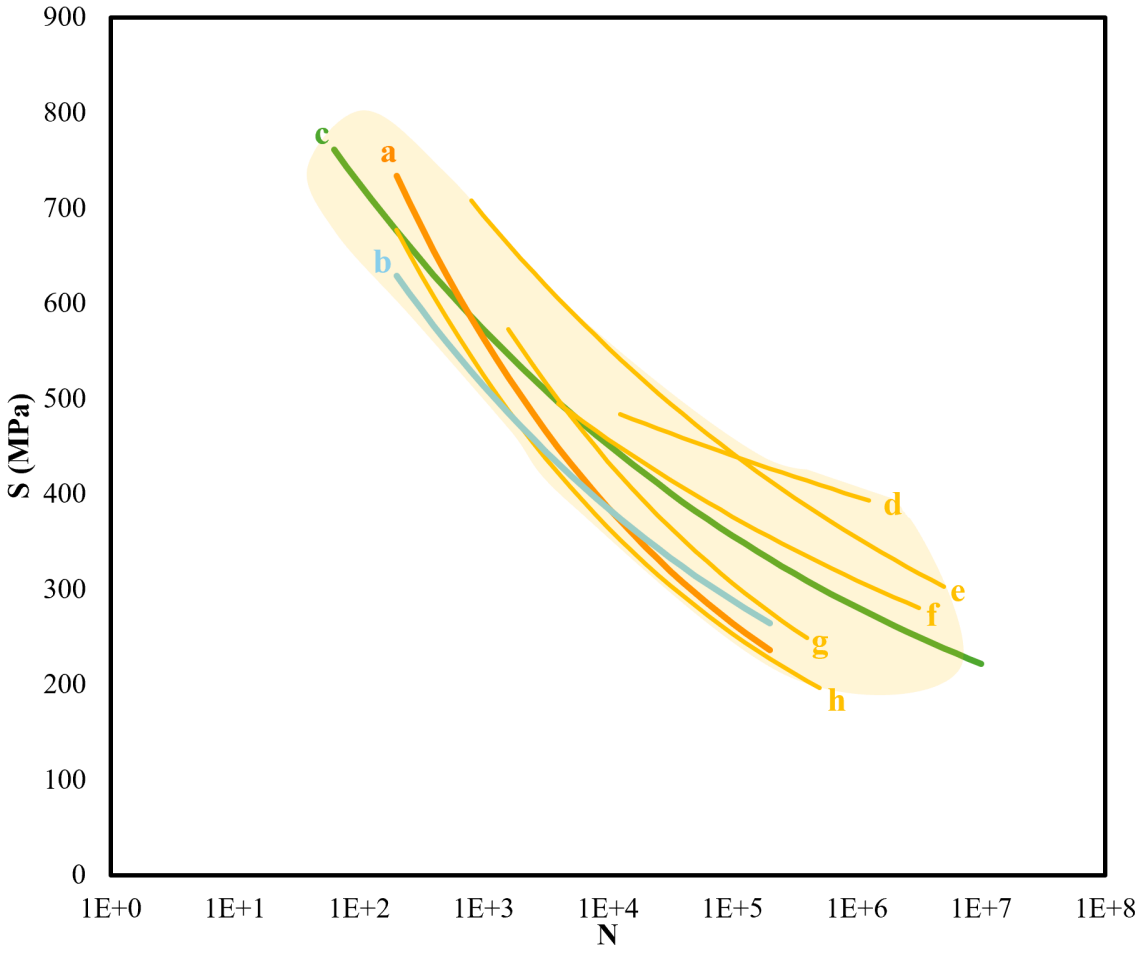

Figure 5.8: *S-N curves of various UD0 composites tested in tension-tension fatigue (R=0.1), with curves of the form of Equation 5.1 fitted to the data. Curve (a) is dry GF1-MCS/acrylic from [5], (b) is dry GF2-AS/acrylic from the current study, (c) is GF/acrylic from Cousins et al. [7] and curves (d)–(h) are select GF/epoxy data from the SNL/MSU/DOE database [20]. Other stitched UD0 GF/epoxy S-N curves from the database are approximately bounded by the region shaded in yellow.*

Table 5.6: *Details of the UD0 GF/epoxy composites from the SNL/MSU/DOE database [20] which are included as curves in Figure 5.8. The curves refer to those in Figure 5.8, and the other details are taken from the database. The naming convention is Reinforcement Type-Fabric-Matrix e.g. UNI-PPG1250-EP5 is a unidirectional fabric L1200/G50-E07, supplied by PPG Fiber Glass, using epoxy resin EP5. For further details the reader is directed to the database [20].*

Curve	Material Name in Database
(d)	UNI-PPG1250-EP5
(e)	UNI-PPG1200-EP1
(f)	UNI-OCV1000-EP1
(g)	UNI-PPG1250-EP1
(h)	UNI-PPG1250-EP9

Curve (c) in Figure 5.8 is GF/acrylic from Cousins et al. [7] which was reinforced with Johns Manville StarRov 086 (1200 TEX, 16 µm fibre diameter) with a multi-compatible sizing agent. Comparing this material with GF2-AS/acrylic (2400 TEX, 16 µm fibre diameter, acrylic-tailored sizing) in Figure 5.8, curve (b), therefore suggests that a tailored sizing agent does not necessarily result in a superior fatigue response. The superior performance in Cousins et al. [7] compared to GF2-AS/acrylic may be due to a lower void content, which X-ray CT scans suggest is 1.4% vs. the 2.4% measured in the current study for GF2-AS/acrylic (Table 5.3). This difference in void content is likely due to the difference in fabric tow linear densities—1200 tex in Cousins et al. [7] vs. 2400 tex in GF2-AS/acrylic.

The fatigue data highlights that a high UTS and good low-cycle performance does not necessarily mean superior performance in high-cycle fatigue; for example, comparing Figure 5.8 curves (d) and (e), the former has poorer performance at 10^4 cycles but improved performance at 10^6 cycles.

5.3 Chapter Summary

The tension-tension fatigue behaviour of dry and water-saturated (aged) GF/acrylic composites with an acrylic-tailored sizing agent (GF2-AS/acrylic) was characterised, and compared to the results from a previous study which used a multi-compatible sizing agent (GF1-MCS/acrylic). Ageing decreased the UTS of the composite, but also reduced the S-N curve slope. The dry coupons therefore outperformed the aged coupons in low-cycle fatigue, but the dry and aged S-N curves converged at lower stresses. The results indicate that the losses in UTS due to water absorption might not be so significant from a fatigue perspective, as the fatigue performance of the dry and aged coupons was similar at the lower stresses a turbine blade is likely to be subject to.

Similarly, the GF/acrylic with a multi-compatible sizing agent had a higher UTS than GF/acrylic with an acrylic-tailored sizing agent, but the former also had a steeper slope of the S-N curve, resulting in better performance of the acrylic-tailored fabric at low cycle fatigue. These increases in UTS and sensitivity to changes in fatigue stress can be attributed to a combination of a difference in fibre volume fraction and fibre diameter, rather than the difference in sizing agent. This would be consistent with the results of static testing, which showed excellent fibre-matrix compatibility with both sizing agents.

The larger fibre diameter and tow linear density of the reinforcement with an acrylic-tailored sizing agent mean that it is likely to be more cost-effective for large structures, and the similarity between the high-cycle fatigue behaviour of GF1-MCS/acrylic and GF2-AS/acrylic, along with comparisons with literature, suggest that the performance of the acrylic-tailored and multi-compatible sizing agents are similar. Although sizing formulations will vary between manufacturers, these results suggest that the fact that a sizing is marketed as 'acrylic-tailored' does not always mean that it is superior to a multi-compatible sizing. While an acrylic-tailored sizing agent guarantees compatibility with acrylic resin, equally good results can be obtained with a carefully selected multi-compatible sizing agent. Large diameter fabrics with readily available multi-compatible sizing agents may therefore be a cost-effective option for acrylic-matrix tidal turbine blades.

5.4 Chapter References

[1] Robynne E. Murray, Ryan Beach, Paul Murdy, Scott Dana, and Scott Hughes. Structural characterization of deployed thermoplastic and thermoset composite tidal turbine blades. Report, 2024-04-08 2024.

[2] Robert Gasch and Jochen Twele. *Structural dynamics*, pages 272–306. Springer Berlin Heidelberg, Berlin, Heidelberg, 2012. ISBN 978-3-642-22938-1. doi: 10.1007/978-3-642-22938-1_8.

[3] P. Davies, P. Y. Le Gac, and M. Le Gall. Influence of sea water aging on the mechanical behaviour of acrylic matrix composites. *Applied Composite Materials*, 24(1):97–111, 2016. ISSN 0929-189X 1573-4897. doi: 10.1007/s10443-016-9516-1.

[4] Peter Davies and Mael Arhant. Fatigue behaviour of acrylic matrix composites: Influence of seawater. *Applied Composite Materials*, 26(2):507–518, 2018. ISSN 0929-189X 1573-4897. doi: 10.1007/s10443-018-9713-1.

[5] Danijela Stankovic, Winifred Obande, Machar Devine, Ankur Bajpai, Conchúr M. Ó Brádaigh, and Dipa Ray. Accelerated seawater ageing and fatigue performance of glass fibre reinforced thermoplastic composites for marine and tidal energy applications. *Composites Part C: Open Access*, 14:100470, 2024. ISSN 2666-6820. doi: https://doi.org/10.1016/j.jcomc.2024.100470.

[6] Winifred Obande, Dimitrios Mamalis, Dipa Ray, Liu Yang, and Conchúr M. Ó Brádaigh. Mechanical and thermomechanical characterisation of vacuum-infused thermoplastic- and thermoset-based composites. *Materials and Design*, 175, 2019. ISSN 02641275. doi: 10.1016/j.matdes.2019.107828.

[7] Dylan S. Cousins, Zach Arwood, Stephen Young, Brandon Hinkle, David Snowberg, Dayakar Penumadu, and Aaron P. Stebner. Infusible thermoplastic composites for wind turbine blade manufacturing: Fatigue life of thermoplastic laminates under ambient and low-temperature conditions. *Advanced Engineering Materials*, 25(11), 2023. ISSN 1438-1656 1527-2648. doi: 10.1002/adem.202201941.

[8] R. Talreja. Fatigue of composite materials: Damage mechanisms and fatigue-life diagrams. *Proceedings of The Royal Society of London, Series A: Mathematical and Physical Sciences*, 378(1775):461–475, 1981. doi: 10.1098/rspa.1981.0163.

[9] Alan Arnold Griffith and Geoffrey Ingram Taylor. Vi. the phenomena of rupture and flow in solids. *Philosophical Transactions of the Royal Society of London. Series A, Containing Papers of a Mathematical or Physical Character*, 221(582-593):163–198, 1921. doi: doi:10.1098/rsta.1921.0006.

[10] Prabhat K. Gupta. *Strength of Glass Fibers*, pages 127–153. Elsevier Science Ltd, Oxford, 2002. ISBN 978-0-08-044104-7. doi: https://doi.org/10.1016/B978-008044104-7/50008-3.

[11] William H. Otto. Relationship of tensile strength of glass fibers to diameter. *Journal of the American Ceramic Society*, 38(3):122–125, 1955. ISSN 0002-7820. doi: https://doi.org/10.1111/j.1151-2916.1955.tb14588.x.

[12] Amjed Saleh Mahmood, John Summerscales, and Malcolm Neil James. Resin-rich volumes (rrv) and the performance of fibre-reinforced composites: A review. *Journal of Composites Science*, 6(2), 2022. ISSN 2504-477X. doi: 10.3390/jcs6020053.

[13] Peter Davies, Mael Arhant, and Erwan Grossmann. Seawater ageing of infused flax fibre reinforced acrylic composites. *Composites Part C: Open Access*, 8, 2022. ISSN 26666820. doi: 10.1016/j.jcomc.2022.100246.

[14] Darshil U. Shah, Peter J. Schubel, Mike J. Clifford, and Peter Licence. Fatigue life evaluation of aligned plant fibre composites through s–n curves and constant-life diagrams. *Composites Science and Technology*, 74:139–149, 2013. ISSN 0266-3538. doi: https://doi.org/10.1016/j.compscitech.2012.10.015.

[15] J. F. Mandell, D. D. Samborsky, and H. J. Sutherland. Effects of materials parameters and design details on the fatigue of composite materials for wind turbine blades. Research Org.: Sandia National Lab. (SNL-NM), Albuquerque, NM (United States); Sandia National Lab. (SNL-CA), Livermore, CA (United States), Sponsor Org.: US Department of Energy (US).

URL https://www.osti.gov/biblio/4194,https://www.osti.gov/servlets/purl/4194. Conference: European Wind Energy Conference and Exhibition, Nice (FR), 03/01/1999–03/05/1999; Other Information: PBD: 4 Mar 1999.

[16] Rogier Pieter Louis Nijssen. Fatigue life prediction and strength degradation of wind turbine rotor blade composites. *Contractor Report SAND2006-7810P, Sandia National Laboratories, Albuquerque, NM*, 2006.

[17] Ramesh Talreja. *Fatigue of Composite Materials*, pages 281–294. Springer, Vienna, 2003. ISBN 978-3-7091-2544-1. doi: 10.1007/978-3-7091-2544-1-6.

[18] E. K. Gamstedt and R. Talreja. Fatigue damage mechanisms in unidirectional carbon-fibre-reinforced plastics. *Journal of Materials Science*, 34(11): 2535–2546, 1999. ISSN 1573-4803. doi: 10.1023/A:1004684228765.

[19] A. D'Amore and L. Grassia. Principal features of fatigue and residual strength of composite materials subjected to constant amplitude (ca) loading. *Materials (Basel)*, 12(16), 2019. ISSN 1996-1944 (Print) 1996-1944 (Linking). doi: 10.3390/ma12162586.

[20] SNL/MSU/DOE composite material fatigue database, 2019. URL https://energy.sandia.gov/programs/renewable-energy/wind-power/rotor-innovation/rotor-reliability/mhk-materials-database/.

Chapter 6

Resin Welding: A Novel Technique for Joining Acrylic-Matrix Composites

6.1 Initial Development

The following work expands on a concept which was initially explored in an MEng project by O'Rourke [1], in which it was shown that multi-stage infusions with acrylic resin could create laminates with superior mechanical properties to those manufactured via a single-stage infusion (Figure 6.1). This was explored further by Obande et al. [2], in parallel with the current study, as a method of avoiding the large exotherms which can make thick-section infusions with acrylic resin challenging.

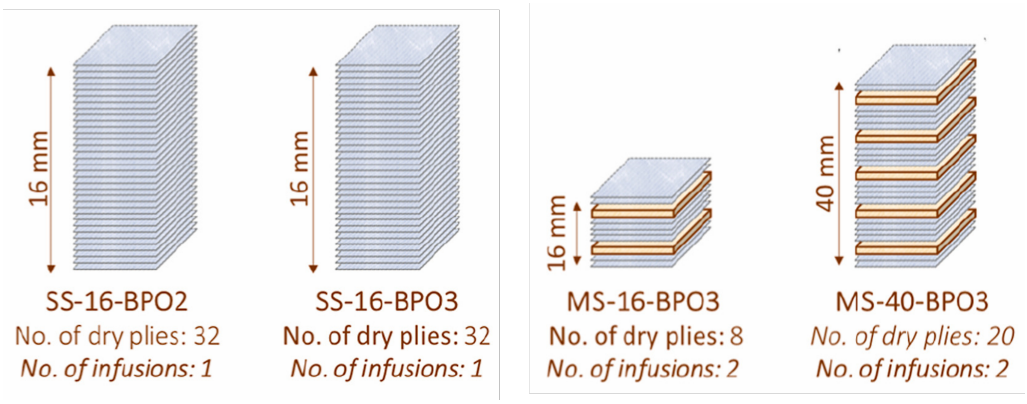

Figure 6.1: *An illustration of the single-stage and multi-stage infusion processes for GF/acrylic from [2]. Single-stage laminates are produced in one infusion using dry glass fibre (grey). Multi-stage laminates are produced from a mixture of dry glass fibre and pre-consolidated GF/acrylic laminates (orange). Reproduced from [2].*

The excellent mechanical properties of the multi-stage infusions showed that strong bonding occurred between the pre-consolidated laminates and the infused resin. It was, therefore, envisaged that the same process could be applied to the joining of acrylic-matrix composite parts, in a process we term *resin welding*, as will be explained in the following paragraphs.

Thermoplastic polymers and composites can be joined via various fusion welding techniques (ultrasonic, resistance, induction etc.) as they soften upon heating. The application of sufficient heat and pressure to the parts to be joined therefore allows the polymer chains to interdiffuse at the joining layer, creating a bond as illustrated in Figure 6.2a. Amorphous thermoplastics like acrylics not only soften when heated, but also dissolve in suitable solvents. This property has been used to join thermoplastics via solvent welding and solvent cementing, in which the application of a solvent, rather than heat, allows for polymer chain mobility and subsequent interdiffusion and bonding of the thermoplastic polymer (Figure 6.2b). However, residual solvent remains in the polymer and weakens the joint [3, 4].

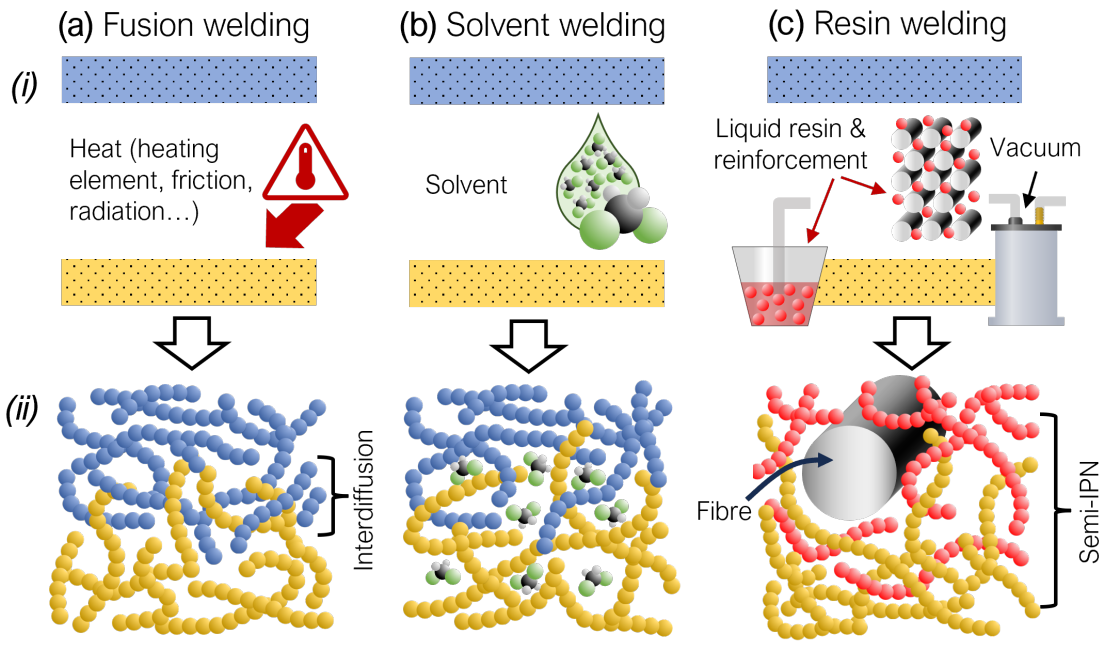

Figure 6.2: *Illustrations of the welding methods for thermoplastic polymers and composites. (a) Fusion bonding increases polymer mobility by heating. Applying pressure allows the polymer to interdiffuse. (b) Solvent welding increases polymer mobility by dissolution at room temperature, but solvent remains trapped in the polymer. (c) In the resin welding method, the acrylic monomer acts as a reactive solvent and polymerises around the adherend matrix. The same mechanism is applicable to reactive solvent cements.*

Interestingly, MMA monomer is also a solvent for acrylic polymer and is available in commercial formulations to solvent weld PMMA [5]. This provides an opportunity to avoid the weakening effects of solvent welding as, if the acrylic monomer is mixed with an initiator as in some commercial solvent cement formulations [6], the monomer will act as a reactive solvent and polymerise around the existing polymer network. This forms a semi-interpenetrating polymer network (semi-IPN), rather than the solvent remaining as a monomer and weakening the bond (Figure 6.2c).

Since Elium® resins are largely composed of MMA monomers [7], acrylic polymer matrix is soluble in liquid acrylic resin, as shown in Figure 6.3. The concept of solvent welding and reactive solvent cements can therefore be extended to the joining of acrylic-matrix composite parts by the vacuum infusion of acrylic monomer resin (Elium®) into a bondline packed with reinforcement fibres, as in Figure 6.2c. This is followed by room temperature polymerisation, allowing for bonds with large and

varying bondlines and no requirement for heat input. The method works via the entanglement of polymer chains to create a continuous material, but the process is significantly different from both fusion and solvent welding; hence, the term *resin welding*.

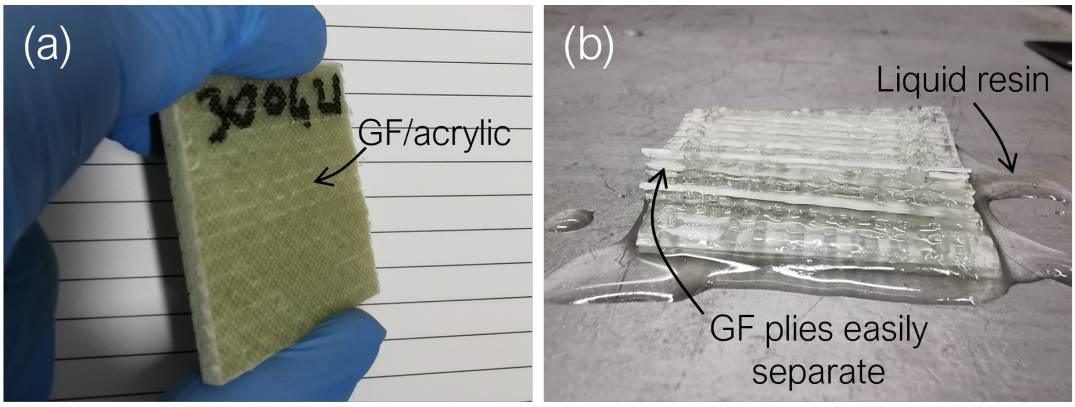

Figure 6.3: *A demonstration of the solubility of the acrylic matrix in Elium® acrylic resin. (a) A GF/acrylic coupon was immersed in Elium® resin. (b) After 48 hours, the matrix had dissolved and the reinforcement plies could be separated.*

The initial development of resin welding involved the creation of a method which would allow comparison with other published joining techniques, while being representative of its use in large structures such as wind turbine blades. As seen in Chapter 2, single-lap shear testing is the method which has been used to characterise weld and adhesive bond strengths of acrylic-matrix composites. Therefore, to simplify comparisons with other bonding methods, single lap shear geometry was decided upon for coupon-scale tests. The first resin welded specimens were made using clear cast PMMA to allow observation of the infusion quality in the bondline. Two sheets of PMMA were overlapped with a layer of glass fibre between them. Resin inlets and outlets were attached using epoxy adhesive, and sealant tape was used to seal the edges of the overlap before resin was infused (Figure 6.4).

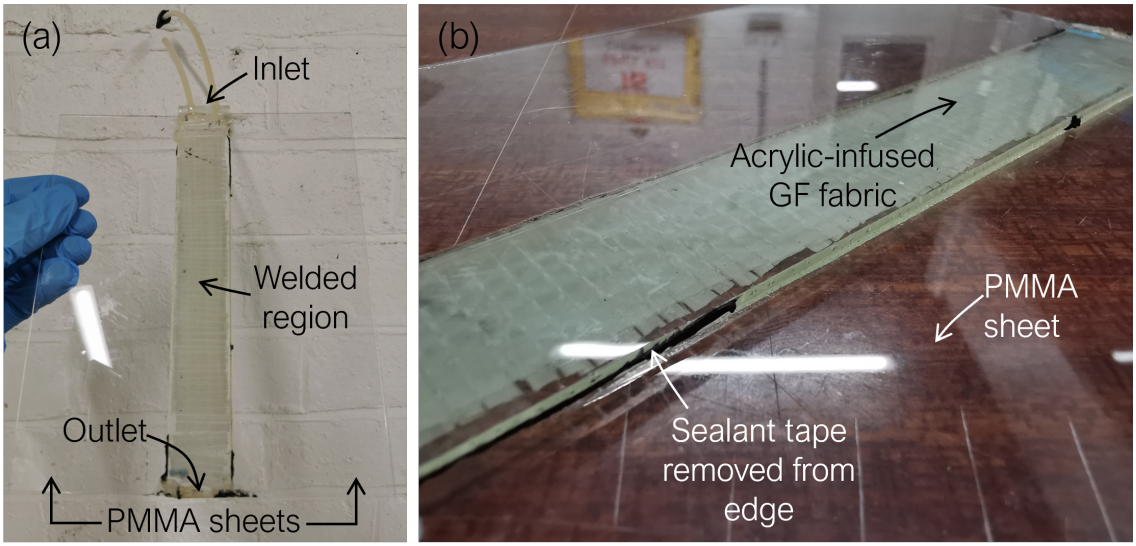

Figure 6.4: *An example of one of the initial resin welded single lap specimens. (a) The clear PMMA adherends allowed the infusion of the reinforcement in the bondline to be observed. (b) A close-up of the weld quality, with visible remnants of the sealant tape used to seal the weld region.*

Visual inspection of the weld in Figure 6.4 showed that this method was effective for the manufacture of high quality bonds with a low void content. A similar method was therefore used to manufacture the resin-welded GF/acrylic coupons. In the following sections, the manufacture and testing of these coupons are detailed, and the strengths of resin-welded single lap shear specimens are reported and compared with adhesively bonded coupons and welded coupons from the literature. The effect of including filler glass fibres between the adherends with 0° and 90° orientations is explored, as is the effect of changing the bondline thickness from 0.5 mm to 1 mm. The bonding mechanisms are then investigated, firstly through fractographic analysis of the single lap shear coupons' fracture surfaces, and then by examining the interface between dyed acrylic resin and clear cast acrylic polymer for signs of dissolution of the polymer and formation of a semi-IPN. The application of the method beyond the coupon scale is then discussed.

6.2 Materials and Methods

6.2.1 Single lap coupon manufacturing and testing

6.2.1.1 Laminate preparation

Glass fibre reinforced acrylic (GF/acrylic) laminates were prepared using a $[0°_4]$ layup of GF1-MCS—a 646 g/m^2 unidirectional non-crimp E-glass fibre fabric (TEST2594-125-50, Ahlstrom-Munksjö) with multi-compatible sizing—for a total thickness of 2 mm. Laminates were prepared through the vacuum infusion of Elium® 188 O acrylic monomer resin (Arkema) mixed in a 100:3 weight ratio with BP-50-FT peroxide initiator (United Initiators). The resin polymerised at room temperature for 24 hours before cutting with a water-cooled diamond-tipped saw.

6.2.1.2 Bonding Methodology

Single lap shear coupons are commonly used to characterise adhesive strengths, and previous work published on welding acrylic-matrix composites used single lap shear geometry [8–10]. The single lap geometry specified by ASTM D5868 was therefore chosen to allow for comparisons with published values. This was achieved by bonding two GF1-MCS/acrylic adherend laminates with a 25 mm overlap, from which 5 single lap coupons of 25 mm width (and therefore 25 × 25 mm joint area) were cut. The coupons were prepared so that the adherend reinforcement was parallel to the test direction.

Four types of bonds were prepared, as shown in Figure 6.5:

- Resin-welded joints with neat resin in the bondline
- Resin-welded joints with 0° fibres
- Resin-welded joints with 90° fibres
- Adhesive bonds

Two bondline thicknesses (0.5 mm and 1 mm) were manufactured for each bond type to match the thickness of 1 and 2 plies of GF fabric.

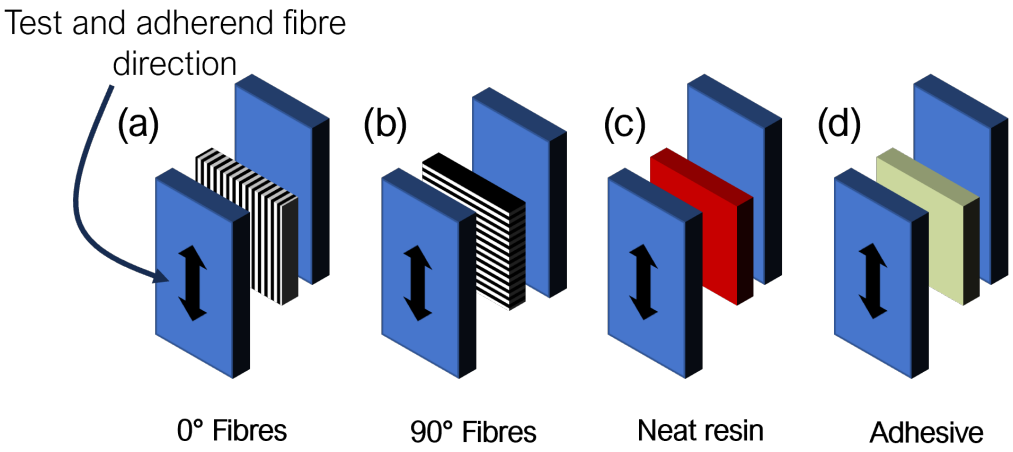

Figure 6.5: *The four types of single lap joint which were manufactured. Specimens were made with: (a) 0° fibres in the bondline, oriented in the same direction as testing and the fibre direction of the adherends; (b) 90° fibres which were placed perpendicular to the test direction; (c) neat acrylic resin with no fibres in the joint; and (d) an adhesive rather than acrylic resin.*

Adhesively joined specimens were prepared using Plexus MA310 two-part methacrylate adhesive, which has been previously shown to have good compatibility with acrylic-matrix composites [8]. The adhesive was applied between the adherends using a mixer nozzle and the bondline thickness was set using wire spacers of either 0.5 mm or 1 mm diameter. Pressure was applied using butterfly clips and the adhesive was left to cure at room temperature.

Resin-welded joints with reinforcement in the weld were prepared by placing glass fabric in the bondline between two adherend laminates (Figure 6.5 and Figure 6.6). Sealant tape was found to adhere poorly to the surface of the composite, therefore during vacuum bagging, a resin inlet and a vacuum outlet were attached using an epoxy adhesive to seal the weld region. Vacuum was applied and acrylic resin mixed with initiator was infused and left to polymerise for 24 hours to allow the adherends to bond. Joints with neat resin in the bondline were prepared in a similar manner but using wire spacers instead of fabric to set the thickness.

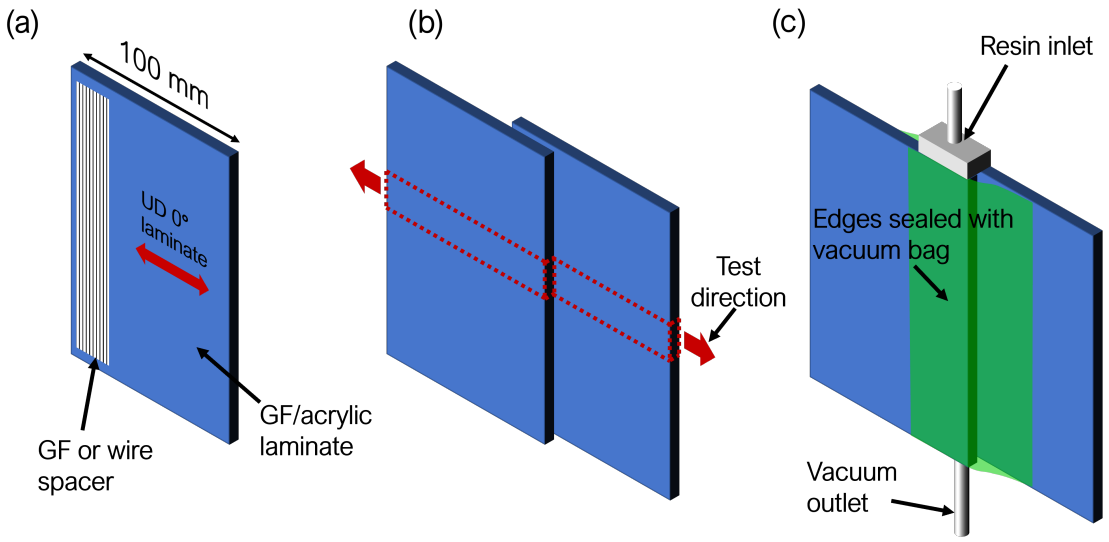

Figure 6.6: *Details of the resin-welding process. (a) Glass reinforcement, or a wire spacer for adhesive and neat-resin bonds, is placed on the adherend then (b) a second adherend is placed on top—the coupon outline and test direction are highlighted—and (c) the weld region is sealed with vacuum bagging and a resin inlet and outlet.*

The vacuum bagging, epoxy adhesive and tubing were then removed, and single lap coupons were cut with a diamond-tipped water-cooled saw (Figure 6.7a). Composite tabs were applied to reduce loading eccentricities during single lap shear testing (Figure 6.7b). Five coupons were cut for each weld type and thickness, and the 90° and neat resin welds at 1 mm thickness were repeated to give a total of ten coupons for each. Out of the samples cut, only 3 samples each were successfully tested from the 0° fibre welds. This was due to manufacturing difficulties creating voids in the coupon edges, particularly close to the resin inlet and outlet.

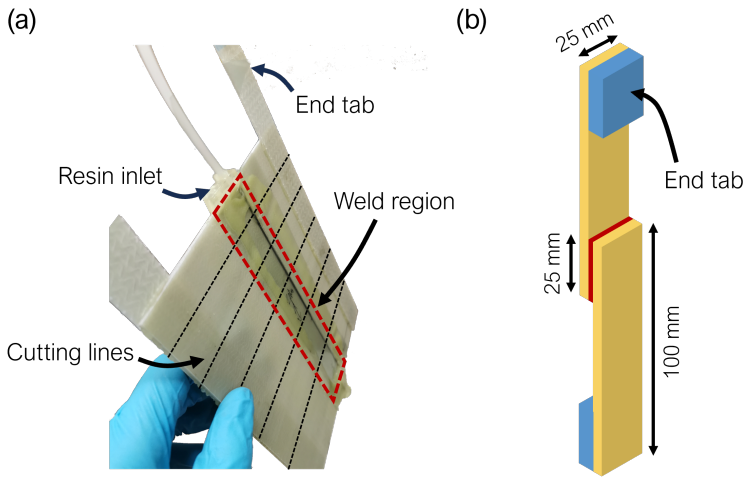

Figure 6.7: *(a) A prepared weld with lines depicting where coupons are cut in black, and the weld region highlighted in red. (b) The single lap coupon geometry with tabs applied.*

6.2.1.3 Mechanical testing

Single lap shear coupons were tested in tension according to ASTM D5868 using an Instron 3369 test machine (system ID 3369J5245) with a 50 kN load cell (serial number 33197). A crosshead extension rate of 1 mm/min was selected due to the lower ductility of acrylic resin compared to typical adhesives. The sides of the coupons were speckled with spray paint so that deformations could be tracked using an Imetrum UVX video extensometer system with a Manta G-146B camera and the GOM Correlate Digital Image Correlation (DIC) software.

6.2.1.4 Statistical analysis

Statistical analysis of the weld strengths was performed using Minitab® 20 statistical software. A Welch's ANOVA test (α=0.05) was employed, which selected due to its robustness to unequal variances between the tested populations, unlike a standard ANOVA. This was followed by a Games-Howell post-hoc test, again because it does not assume homogeneity of variances. A difference was deemed statistically significant if the P value obtained from the test was less than 0.05.

6.2.1.5 Fractography

Scanning electron microscopy (SEM) was used to observe the fracture surfaces of the single lap shear coupons after testing. The fracture surfaces were sputter-coated with 30 nm of gold and were imaged at 15 kV using a JEOL JSM series scanning electron microscope.

6.2.2 Investigation of the proposed bonding mechanism

The bonding mechanism that occurs during resin welding was investigated by comparing the diffusion of acrylic resin in PMMA and epoxy polymers using optical microscopy. Epoxy was included for comparison since thermosets do not dissolve in solvents and should therefore not bond via extensive semi-IPN formation, resulting in a difference between the acrylic–acrylic and acrylic–epoxy interfaces.

Cuboids of clear cast PMMA and epoxy were cut and placed into a sample cup of 40 mm diameter which was coated in release agent. Elium® 188 O acrylic resin was dyed with Bestoil Blue 2N (FastColours Ltd.)—a solvent/oil soluble dye—then mixed in a 100:3 ratio with BP-50-FT peroxide initiator. The resin was then poured into the sample cup to immerse the polymer cuboids (Figure 6.8a). The dye allowed diffusion of the resin to be observed visually, and Bestoil Blue 2N was chosen for its resistance to bleaching during the free-radical polymerisation of the acrylic. The resin was left to polymerise for 24 hours, and the resulting cylinder was demoulded then ground and polished (Figure 6.8b) to a thin disc to reveal the immersed polymers for optical microscopy (Figure 6.8c).

Grinding and polishing were performed using a water-cooled ATA Saphir 520 polisher. The coupon was first ground to a thin disc using a P180 grinding disc, and was then polished using a force of 30 N with increasingly fine polishing discs (P400, P800, P1200, P2500, 3 µm and 1 µm) for approximately 3 minutes on each side.

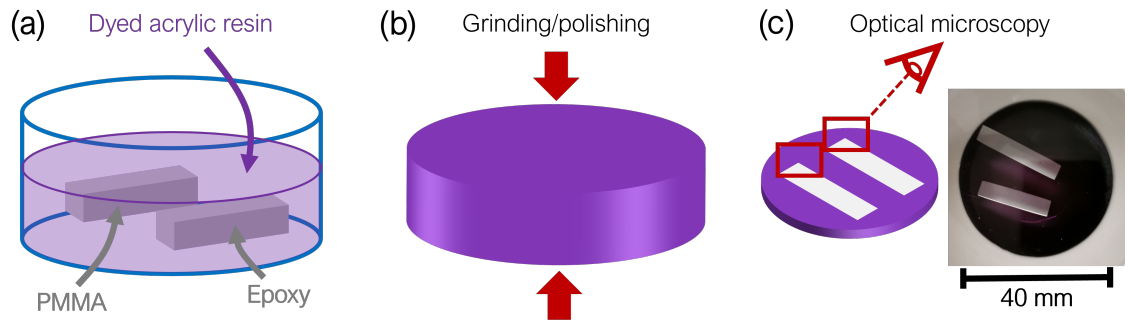

Figure 6.8: *Specimens were prepared for optical microscopy by (a) immersing PMMA and epoxy cuboids in dyed acrylic resin before polymerisation, then (b) grinding and polishing the demoulded cylinder. The finished coupon is depicted in (c), and the observed regions are highlighted.*

6.2.3 Ultrasonic Welding

Coupons were also ultrasonically welded as an initial trial by TWI, UK, to provide a comparison between resin welding and a traditional welding method using the same GF1-MCS/acrylic material. The adherends were GF1-MCS/acrylic coupons manufactured as detailed in Section 6.2.1.1, but with the addition of energy directors. This was achieved by machining a groove with a 90° triangular cross section into a flat aluminium plate, as in [9], lined with an adhesive release film (Figure 6.9a). The laminate was laid up and infused as normal, then cut to 100×25 mm, creating adherends with integrated energy directors (Figure 6.9b). Each adherend with an integrated energy director was welded to a flat adherend (Figures 6.9c and d) for a total of five single lap coupons.

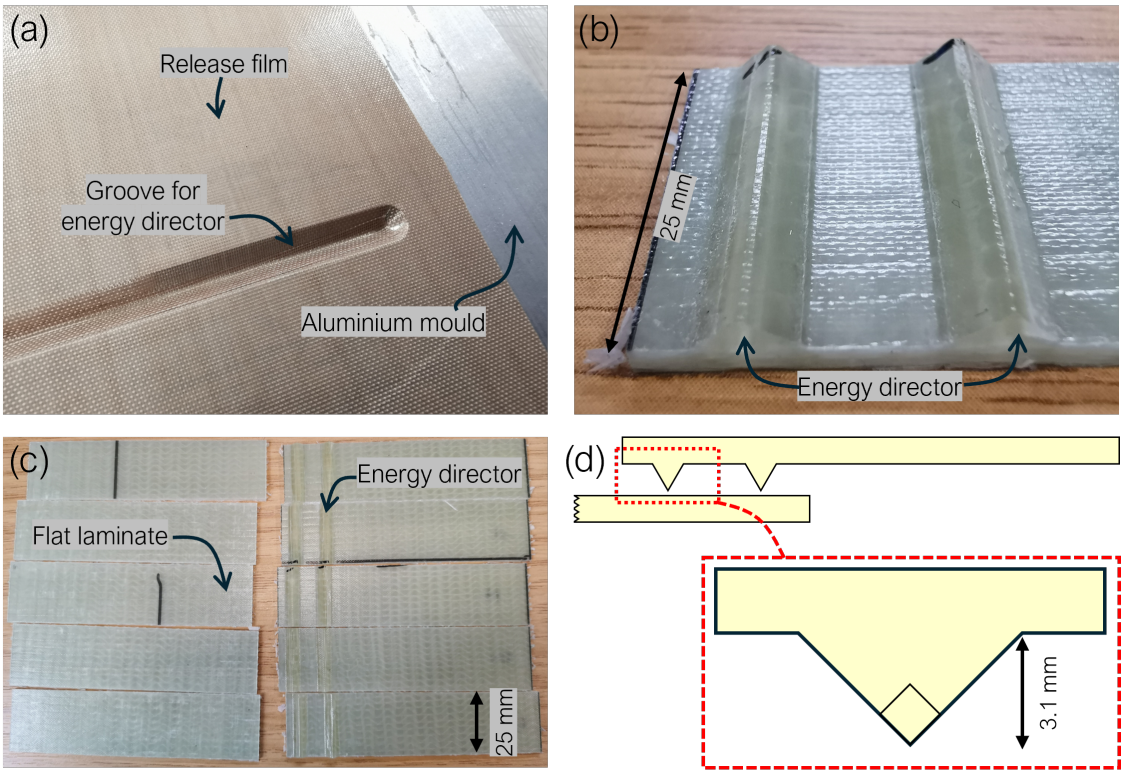

Figure 6.9: *Adherend manufacturing and geometry for ultrasonic welding. (a) An image of the groove machined into a flat aluminium plate covered with release film. (b) A side view of the energy directors. (c) Each adherend with an energy director (right) was welded to a flat coupon (left). (d) Side view of the energy director and welding geometry (not to scale).*

A 20 kHz, 2kW ultrasonic welding machine from Weber Ultrasonics was used with the parameters provided below:

- 100% amplitude
- Weld by distance mode, 1-3 mm range
- Weld pressure 800 N
- Hold pressure 1000N
- Hold time 1 s

The energy director is intended to melt and flow across the single lap joint, but the resin flow was much more localised than expected. This is discussed further

in Section 6.3.1.3, but meant that the overlap area, as specified in ASTM D5868, could not be used to calculate the strength. Instead, the force applied at failure was divided by the actual bonded area. This was measured using ImageJ [11] by taking the average damaged area of each side of the fractured coupons (Figure 6.10).

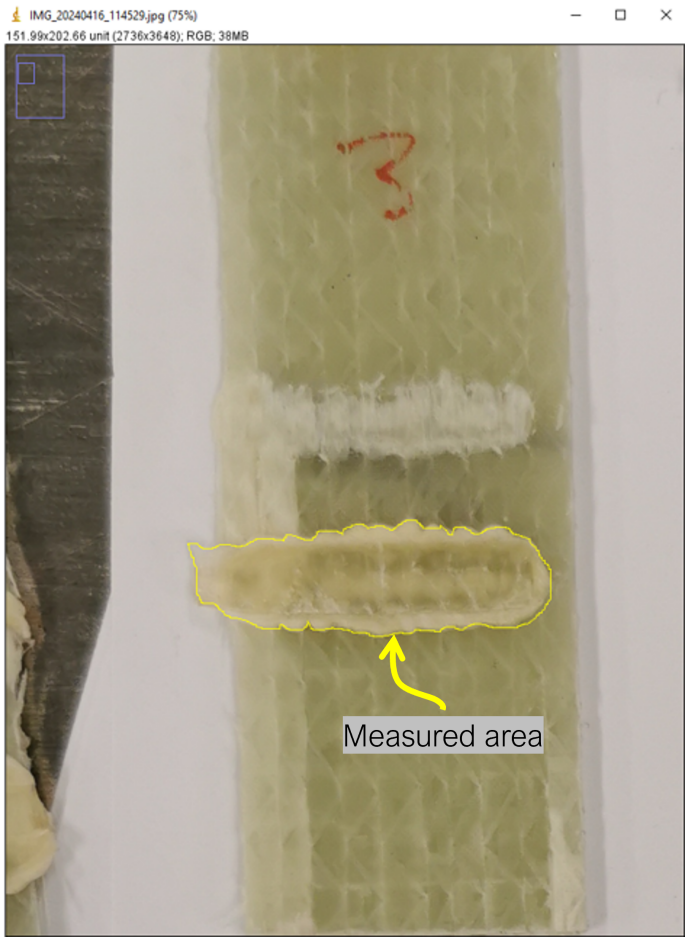

Figure 6.10: *Demonstration of bonded area measurement using ImageJ [11]. One half of a fractured coupon is shown, in which two areas of damage are visible. The area was manually measured as illustrated by the yellow boundary.*

6.2.4 Manufacture of Welded T-Section

To demonstrate resin welding in more complex geometries, a resin-welded T-section was manufactured. A flat GF2-AS/acrylic laminate (approximately 100 mm × 200 mm) was manufactured using a standard vacuum infusion method, and an L-shaped laminate was then manufactured on an aluminium mould and cut into two pieces (Figure 6.11a). The three pieces were assembled with dry glass fibre layers between them, and a rolled-up section of glass fibre was used to fill the noodle region

at the centre of the 'T' (Figure 6.11b–d). Spiral tubing was attached to the edges to improve resin flow, a resin inlet and outlet were attached, and the T-section was then sealed in a vacuum bag with sealant tape (Figure 6.11e). Acrylic resin was infused and left to polymerise for 24 hours, the bagging was removed and the edges of the T-section were trimmed (Figure 6.11f).

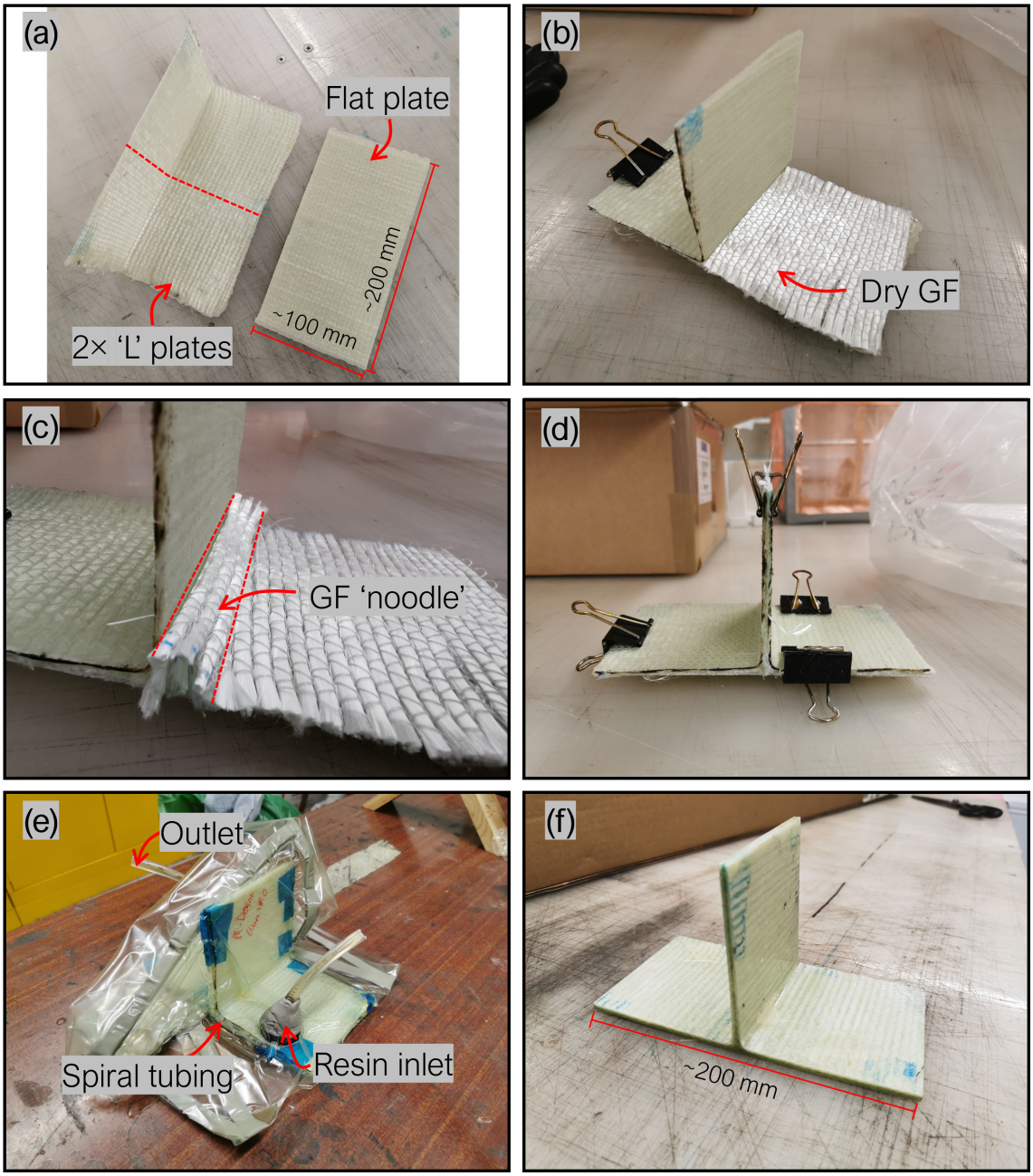

Figure 6.11: *The process of manufacturing a resin-welded T-section. (a) The L-shaped and flat GF2-AS/acrylic laminates used to manufacture the T-section. (b) A layer of GF2-AS glass fibre was placed between the laminates. (c) The noodle region was filled with glass fibre. (d) The final layer of glass fibre and the L-section were clipped in place. (e) Spiral tubing and a resin inlet and outlet were attached. The T-section was sealed in a vacuum bag and infused with acrylic resin. (f) The edges were trimmed after polymerisation.*

6.3 Results and Discussion

6.3.1 Single lap shear testing

6.3.1.1 Mechanical properties

The single lap shear strengths for each joint type and thickness are shown in Figure 6.12. The bond strength of the resin-welding method is promising overall as the highest average weld strength reached 27.9 MPa for the sample with 0.5 mm bondline thickness and with 0° fibre reinforcement. This is 24% higher than the strongest reported single lap weld of acrylic-matrix composites in the literature: resistance-welded GF/acrylic adherends ($[0°_4]$ layup of 1200 g m^{-2} fabric, 3.5 mm thickness) with a biaxial carbon fibre heating element [8]. It also far exceeds the minimum 12 MPa single lap shear strength required for type approval as a rigid adhesive according to DNV-CP-0086.

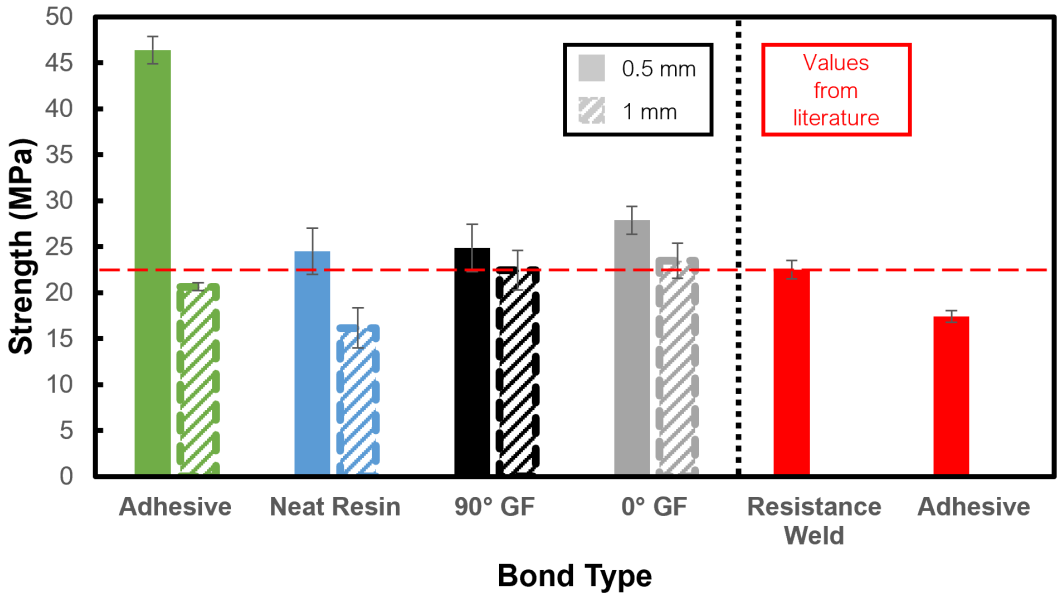

Figure 6.12: *The single lap shear strengths of each joint type. The values for 0.5 mm thick bonds are solidly coloured and the values for 1 mm thick bonds are hatched. Error bars represent ±1 standard deviation. A comparison with the highest published weld and adhesive strengths for acrylic-matrix composites [8] is included in red on the right.*

The effect of including fibres in the bondline can be found by comparing the strengths of the bonds with fibres to the bonds with neat resin. Considering first the 0.5 mm bondlines, the welds with 0° fibres, 90° fibres and neat resin had strengths which were not significantly different according to the statistical analysis. The highest strength of 46.4 MPa was obtained with adhesive and a bondline of 0.5 mm, 66.4% greater than the 0.5 mm weld with 0° fibres (P=0.000).

This study therefore measures no significant effect of fibre type, or if there is an effect it is too small in magnitude to observe under the parameters of the study. Other studies have measured a much greater effect on single lap shear strength from the inclusion of unidirectional reinforcement in adhesive bondlines. Khalili et al. tested the single lap shear strength of GF/polyester adherends bonded with epoxy adhesive reinforced with unidirectional 0° glass fibres, resulting in a 54% increase in strength (18.4 MPa vs. 11.9 MPa) over neat adhesive bonds [12]. Delzendehrooy et al. similarly compared the single lap shear strength of aluminium adherends bonded with epoxy adhesive, and date palm fibre reinforced epoxy adhesive. Bonds reinforced with 0° fibres reached a strength up to 98% greater than those with unreinforced adhesive [13]. Finally, Behera et al. tested both aluminium-to-composite (GF/epoxy) and aluminium-to-aluminium bonds with 0° glass fibre reinforced adhesive [14]. In comparison with neat adhesive, the reinforced adhesive increased single lap shear strength by 27.3% in aluminium-to-aluminium bonds and by 45.4% in aluminium-to-composite bonds.

The effect of heating element fibre orientation in the welding of thermoplastic composites has also been studied in the literature, although comparisons between fibre orientations may be complicated by the changes in welded area and thermal uniformity that different heating element fabrics create in resistance and induction welding [8, 15]. In one study by Tanabe et al. [15], CF/PPS composites were joined using resistance welding, with carbon fibre heating elements in either the 0° or 90° direction. Similar welded areas were achieved using each fibre direction but changing the heating element fibre orientation from 90° to 0° increased the single lap shear strength by 65%, from 16.5 MPa to 27.2 MPa.

The key difference between these published papers and the present work is the fracture behaviour of the coupons. In each of these studies there was at least partial

cohesive failure, and fracture occurred through the adhesive reinforcement or heating element fibres. The fibres therefore contributed to the single lap shear strength by resisting crack propagation. However, as will be discussed further in Section 6.3.1.2, crack propagation in the present study initiated via peeling at the edges and continued through the upper layer of the adherends for all coupons, rather than through the bondline. Therefore, the reinforcement in the bondline was unable to contribute significantly to an increase in strength.

The effect of increasing bondline thickness differs depending on the bond type. Although the Plexus MA310 adhesive had a high single lap shear strength (46.4 MPa) with a 0.5 mm bondline, the adhesive bond strength saw a large drop of 56% (P=0.000) as thickness increased to 1 mm. The neat-resin bonds also saw a large drop in strength of 34% (P=0.005) from 24.5 MPa to 16.2 MPa as the thickness was increased to 1 mm from 0.5 mm. Decreases in single lap shear strength with increasing bondline thickness have also been reported in the literature and have been attributed to greater peel and shear stresses, and an increased likelihood of voids and other imperfections in the bondline [16–18]. In contrast, the mean strength of bonds with 90° fibres and 0° fibres decreased by only 11% and 16% respectively with increasing thickness, which were therefore not found to be statistically significant changes (P=0.584 and P=0.238 respectively). The inclusion of fibres in the bond therefore appears to have benefits in thicker bondlines.

These results show that increasing bondline thickness has a significant detrimental effect on adhesive bond strength; indeed, Plexus MA310 has a maximum recommended thickness of just 3.2 mm according to its technical datasheet [19] and would therefore be unsuitable for use in the thick bondlines found in wind turbine blades. Other adhesives which are designed for use in thick bondlines are available, but their strengths are significantly lower [8, 20], and failure in adhesives is therefore common in wind turbine blades due to the relative weakness of these thick adhesive bonds, and the likelihood of them containing defects [21]. The presented results therefore suggest that resin welding could serve as a viable alternative to adhesives in acrylic-matrix composite wind turbine blades and other large structures. In resin welding, the bondlines are not constrained to the same maximum thickness as adhesives and could reach the same thickness as the thick-section composites being

joined.

There is a discrepancy between the adhesive single lap shear strengths measured in the current study (46.4 MPa at 0.5 mm and 20.4 MPa at 1 mm) and the strength of 17.4 MPa for GF/acrylic coupons joined by MA310 adhesive, as published by Murray et al. [8]. For comparison, the adhesive's technical datasheet suggests a single lap shear strength range of 20.7–24.1 MPa [19]. Differences in bondline thickness could have a contribution, as Murray et al. manufactured coupons with a bondline thickness of 0.76 mm. We would therefore expect a lower strength than the 0.5 mm adhesive bond in the present study, although it does not explain why Murray et al. measured a lower bond strength than the 1 mm adhesive bond in the current study. The edge quality of the specimens is likely to play a role, as Murray et al. allowed the adhesive to spill out the edges. On the other hand, in the present study the edges were smoothed, possibly reducing stress concentrations and increasing strength [22].

Representative load-extension curves for each bond type are provided in Figure 6.13a. A ductile failure of the adhesive bonds is evident compared to the brittle fractures of the weld specimens. It should also be noted that the 0.5 mm and 1 mm adhesive bonds reached similar average extensions before failure (4.6 ± 0.1 mm and 4.3 ± 0.2 mm respectively) despite the latter's significantly lower strength. The stiffness of the 1 mm adhesive bond is therefore lower than that of the 0.5 mm adhesive bond; however, comparisons between the bond stiffnesses is made difficult by the shapes of the load-extension curves.

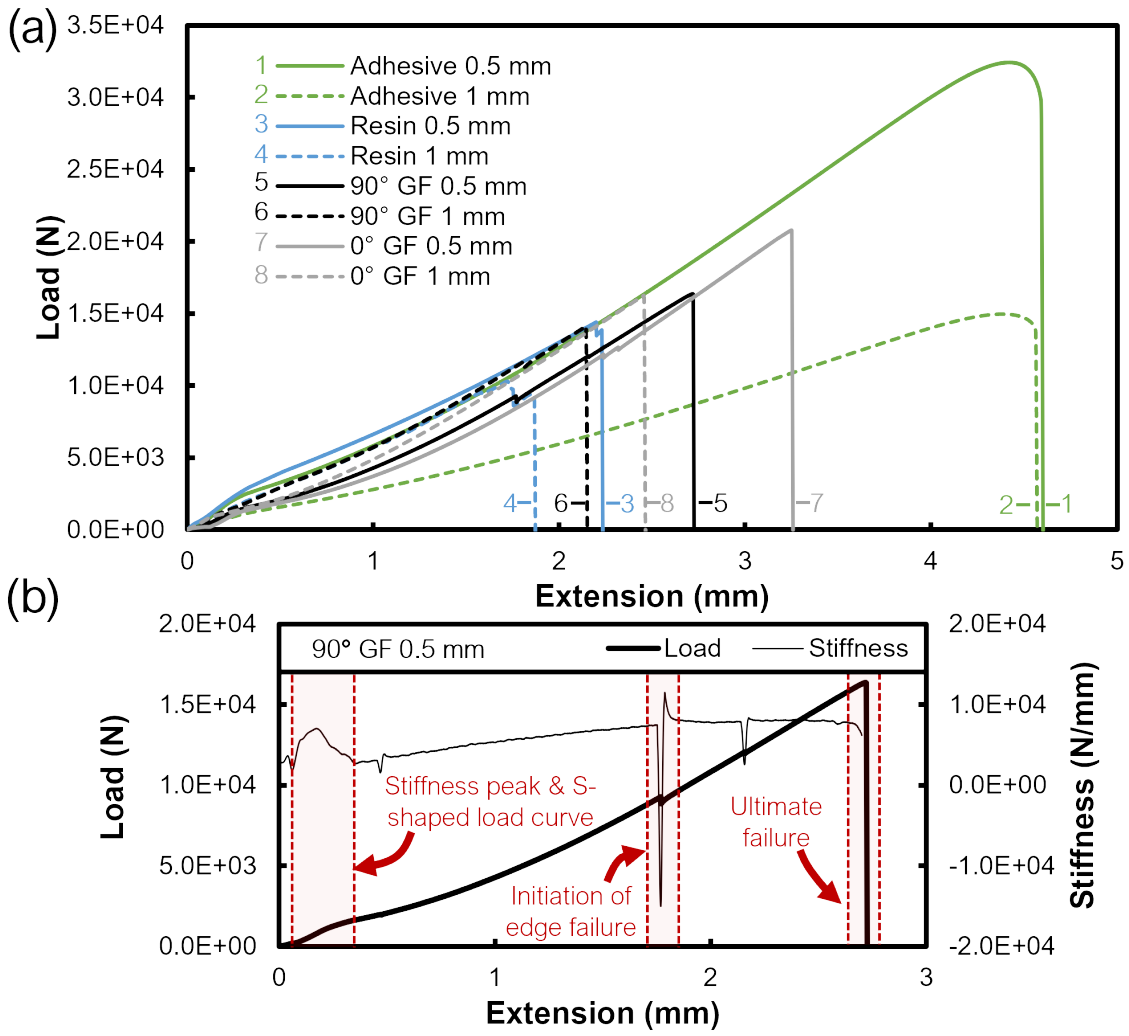

Figure 6.13: *(a) Representative load-extension curves for each type of single lap bond. Bonds of the same type are the same colour, with the 0.5 mm bond having a solid line and the 1 mm bond having a dashed line. (b) The representative load-extension curve of the 90° GF 0.5 mm coupon along with its derivative i.e. the variation in stiffness of the coupon throughout the test. Highlighted in red for both the load and stiffness curves are the initial peak in stiffness, corresponding to the S-shape in the load-extension curve; the initial edge failure, which is also visible as a small drop in the load-extension curve; and the ultimate failure.*

Although an initial linear load-extension response for composite single lap shear bonds is reported in some publications [23], allowing stiffnesses to be easily calculated, in this case the load-extension curves have an initial s-shape below approximately 0.5 mm extension followed by a gradually increasing gradient (Figure 6.13b). Therefore, in order to compare the stiffnesses of the single lap coupons, the load-

extension curves are differentiated. The resulting stiffness vs. extension curves have a shape similar to that in Figure 6.13b, in which there is an initial peak in stiffness. Loading in single lap joints is complex and is a mixture of shear and peel, which is accompanied by the bending of the adherends. The reason for the nonlinear curve shape was therefore investigated by measuring the bending angle of the coupons using DIC (Figure 6.14).

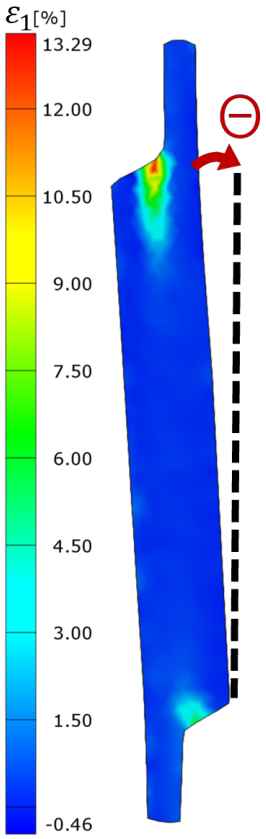

Figure 6.14: *A representative map of major strain in a single lap coupon close to failure, as measured using DIC. Stress concentrations are found at the edges of the overlap region. The rotation of the specimens during testing (Θ) is highlighted.*

Below 0.5 mm extension, there is a rapid increase then subsequent slowing in bending rate, therefore the initial peak in stiffness (Figure 6.13b) can be attributed to the bending of the adherends. The average peak in gradient before 0.5 mm extension for each joint is summarised in Figure 6.15. Only the 1 mm adhesive joint has a significantly lower peak stiffness of 4.2 kN/mm due to the low modulus and high ductility of the adhesive, which makes a greater contribution to coupon stiffness at higher bondline thicknesses.

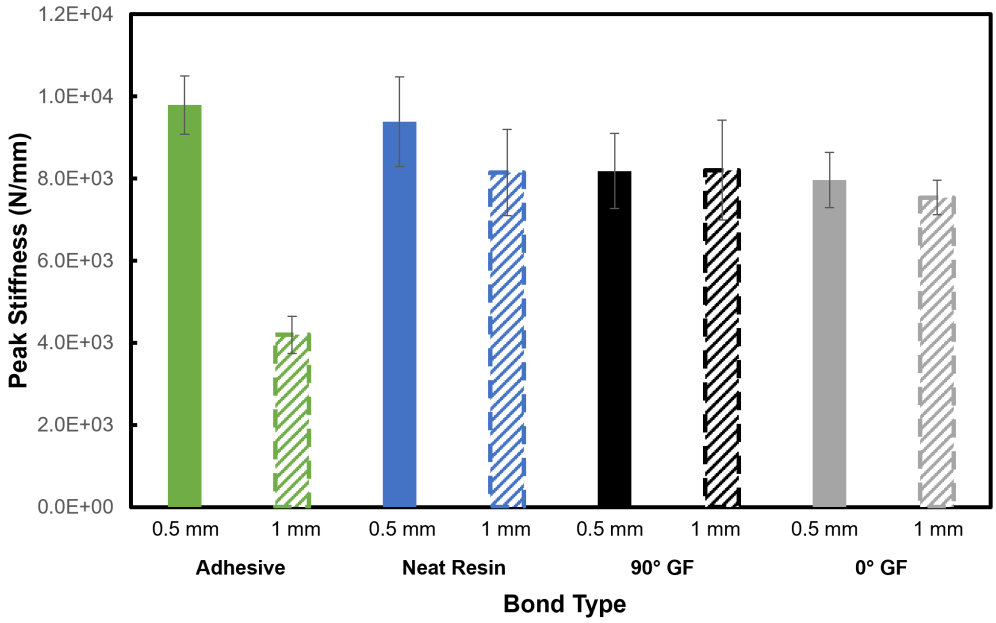

Figure 6.15: *The average peak gradient of the load-extension curves for each bond type below 0.5 mm extension. The 1 mm adhesive bond has a significantly lower stiffness than the rest.*

6.3.1.2 Failure modes and mechanisms

Images of the failed resin-welded and adhesively bonded coupons are shown in Figure 6.16.

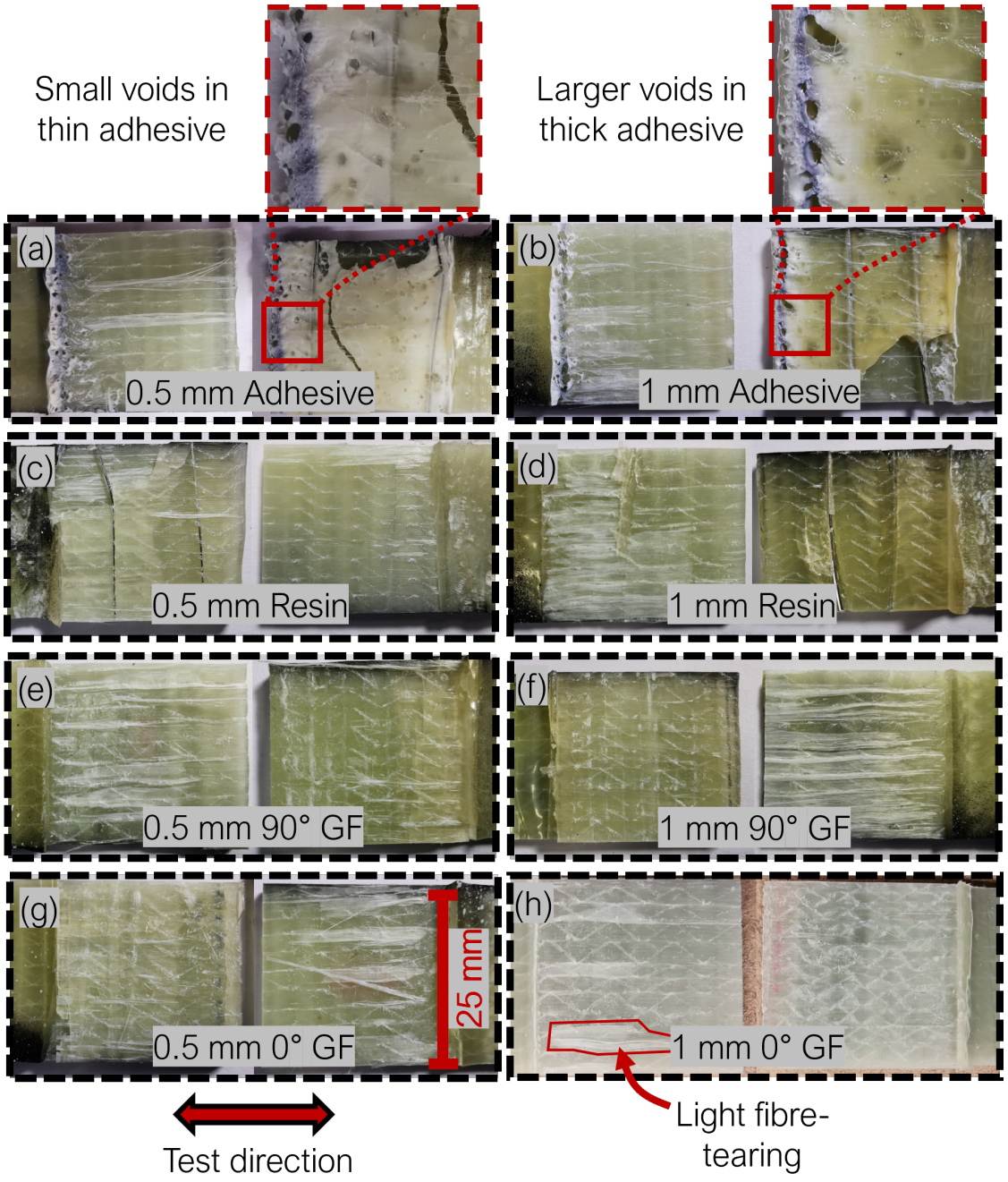

Figure 6.16: *Representative fracture surfaces of the tested single lap coupons. Each image is of both halves of a fractured coupon. The crack propagation direction (the testing direction) is shown. Light fibre tearing is highlighted in the 1 mm 0° GF coupon (h), but it is visible in all fracture surfaces. The voids present in both adhesive bonds—(a) and (b)—are shown at higher magnification, and larger voids are visible in the 1 mm thick adhesive (b). Voids were not visible in the resin welded coupons—(c) and (d).*

The failure modes of all the adhesively bonded and resin-welded coupons can be

classified as light fibre tear failure (ASTM D5573) as, rather than the more common adhesive or cohesive failure types, a small amount of resin and glass fibre is removed from the surface of the adherend. The clearest evidence of this is the fibre bridging in coupons with no fibres in the bondline (Figure 6.17a), indicating that these fibres must come from the adherend. It is therefore the adherend matrix that fails, rather than the bond between the infused resin and the adherend matrix (Figure 6.17b and c).

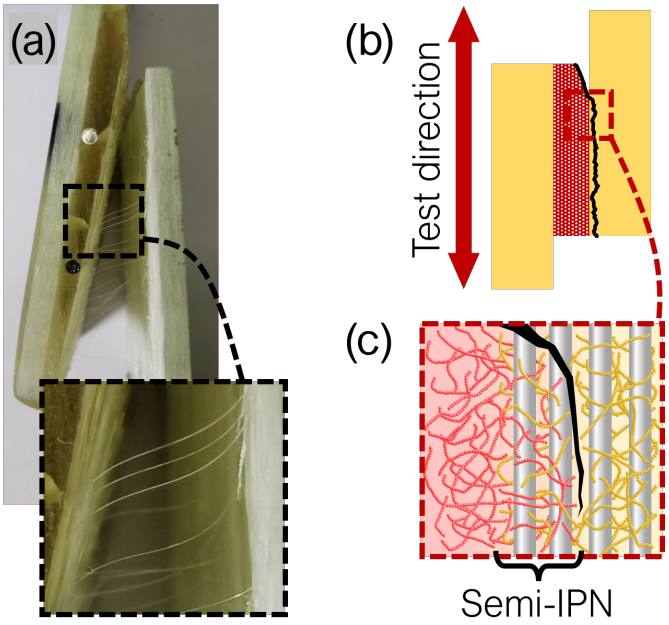

Figure 6.17: *The fracture behaviour of the coupons. (a) Fibre bridging in a coupon bonded with neat resin (no reinforcement). The bridging fibres therefore come from the surface of the adherend. (b) The failure mode of the welded coupons was light fibre tearing where a small amount of glass fibre is removed from the adherend surface (c) The fracture propagation was through the adherend matrix (yellow) rather than through the tougher semi-IPN.*

This is confirmed via the representative SEM images presented in Figure 6.18, which depict both halves of a single lap shear tested coupon bonded with 0.5 mm of neat acrylic resin. The presence of fibres on both sides—despite no fibres being included in the bondline—shows that the crack propagates within the first layer of the adherend fibres (light fibre tearing). These results suggest that the formation of a semi-IPN increases fracture toughness compared to the bulk polymer, leading to

failure in the adherend matrix rather than in the semi-IPN at the bonding interface, as shown previously in Figure 6.17b and c.

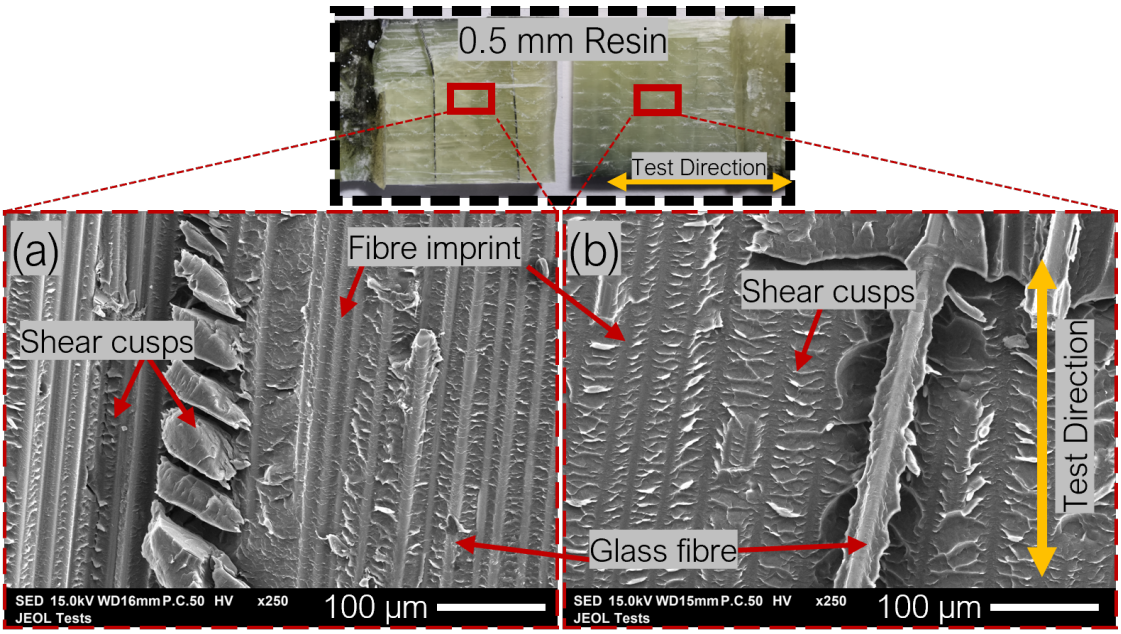

Figure 6.18: *SEM images of the fracture surfaces of GF1-MCS/acrylic bonded with 0.5 mm of neat acrylic resin. Photographs of the imaged fracture surfaces are provided above, with the imaged areas represented by red rectangles (not to scale). Image (a) is of one half of a fractured single lap shear coupon and image (b) is of the other half. Fibres and imprints are present in both halves indicating light fibre tearing of the adherend. Cusps indicate a shear failure.*

Further insight into the failure of the single lap coupons was gained using DIC. A map of the major strain across the profile of a single lap coupon just before failure was presented in Figure 6.14. As noted by Noble et al. [24], there are stress concentrations at the edges of the overlap region, and this is therefore where failure initiates. The rotation of the specimens during testing means that this is a concentration of both shear and peel forces [22, 25], but failure was observed to initiate via peeling at the edges. This is visible as sudden increases in bending angle in Figure 6.19. However, shear cusps are present in the SEM images in Figure 6.18a and b, therefore failure proceeds via a mixture of shear and peeling.

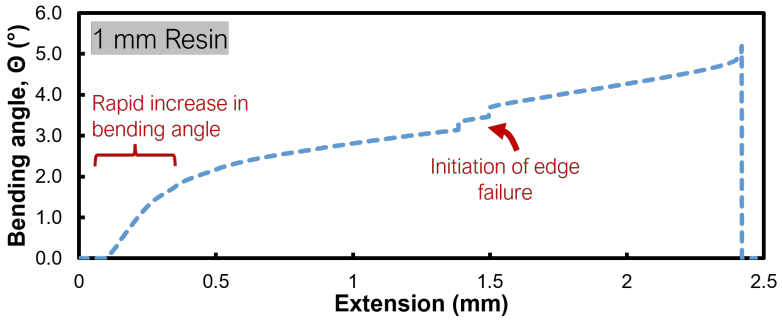

Figure 6.19: *A representative bending angle vs. extension curve for a 1 mm resin weld. The rapid increase in bending angle corresponding to the stiffness peak is highlighted.*

6.3.1.3 Ultrasonic welds

A representative ultrasonically welded coupon is shown in Figure 6.20. Ultrasonic welding was performed externally with the intention of providing comparative data for the resin welding process. However, the ultrasonic welding was not entirely successful as the energy directors did not flow across the bonded area as intended, as can be seen in Figure 6.20b. Additionally, the adherends were welded slightly off-angle, and the coupons had a total overlap of 50 mm, rather than the 25 mm overlap in the adhesively bonded and resin-welded coupons.

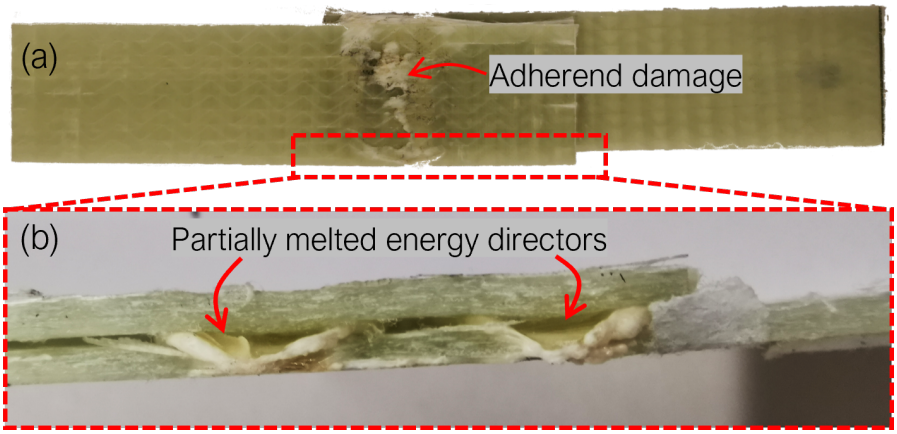

Figure 6.20: *A representative ultrasonically welded GF1-MCS/acrylic coupon. (a) A top view of the coupon, with adherend damage visible. (b) A side view showing that the energy directors did not fully melt and flow across the overlap region.*

The single lap shear strength was therefore calculated using the actual bonded area (an average of 414 ± 68 mm^2), and found to be 14.6 ± 0.8 MPa. This is on par

with the ultrasonic weld strengths measured by Bhudolia et al. [9] before proper optimisation of the process, and optimisation allowed ultrasonic weld strengths to reach 18.9 MPa [26]. Since the ultrasonic welds in the current study were from an initial trial, their strengths are understandably lower than the 27.9 MPa maximum strength of resin welds, and the maximum strength of around 22.5 MPa reported in the literature for a resistance weld, but increased strengths are expected with further optimisation of the process.

6.3.2 Bonding mechanism

Adhesives can bond adherends via several mechanisms, including the formation of chemical or physical bonds with the adherend surface, mechanical interlocking between the adhesive and a rough adherend surface, via electrostatic attraction or through diffusive bonding [27, 28]. Since PMMA is soluble in its monomer, the resin-welding method is expected to create a bond via dissolution, diffusion, and the subsequent formation of a semi-IPN. The experiment described in Section 6.2.2 allows us to visualise this bond.

Optical microscope images of the interfaces between dyed acrylic resin and clear cast coupons of epoxy and PMMA polymers can be found in Figure 6.21a and Figure 6.21b respectively. There are two visible differences between the interfaces of epoxy and PMMA with the acrylic resin. Firstly, there is a difference in colour, as in the epoxy there is a well-defined colour boundary with the dyed resin, whereas in the PMMA there is a colour gradient. The dye molecules therefore diffuse into the PMMA as it is dissolved by the acrylic monomeric resin and remain there once the resin polymerises.

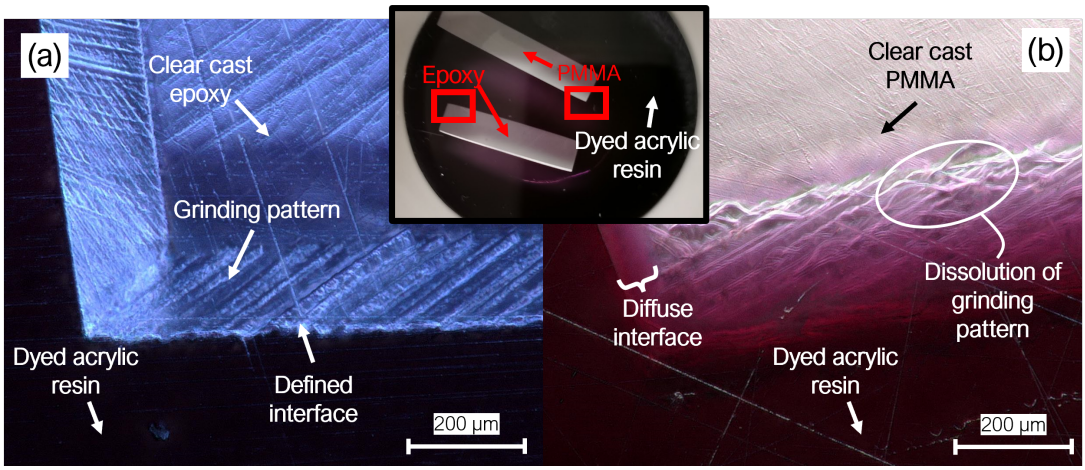

Figure 6.21: *Optical microscope images of the edges of (a) epoxy and (b) PMMA cuboids immersed in dyed acrylic resin. A lower magnification photograph of the epoxy and PMMA cuboids cast in dyed acrylic resin is shown in the centre of the figure. The optical microscopy imaging locations are highlighted with red rectangles.*

Secondly, there is a difference in morphology at the interface. There are ridges at the edges of the polymer coupons caused by grinding, and in the case of epoxy these are again well-defined and unaffected by the acrylic resin whereas signs of dissolution are evident in the PMMA specimen (Figure 6.21b). This is to be expected as epoxies are thermoset polymers, so they do not dissolve in solvents. This experiment therefore provides evidence for the formation of a semi-IPN as the bonding mechanism, which is only applicable when the polymer is soluble in the infused resin.

The low viscosity of the acrylic resin allows significant penetration of the monomer into the acrylic polymer; however, the same bonding mechanism may be expected to occur when bonding GF/acrylic with Plexus MA310 adhesive due to its MMA content. The similarity in failure mechanisms between the resin welds and the adhesive bonds—light fibre-tearing (Figure 6.17)—would support this, although the high viscosity and short working time of the adhesive (approximately 15 minutes vs. 90 minutes for the acrylic resin) may limit semi-IPN formation.

6.3.3 Element Level Manufacturing and Beyond

Resin welding is unlikely to be the best choice for making single lap coupons, especially considering the high strengths that can be obtained using methacrylate structural adhesives with thin bondlines. A resin-welded T-section was therefore

manufactured, which was used to observe the quality of more complex bondlines and to explore the use of resin welding in large structures. The bond quality was found to be very good, as shown by Figure 6.22 in which the bondline (the middle ply) is difficult to distinguish, and the part therefore looks as though it were infused as one piece.

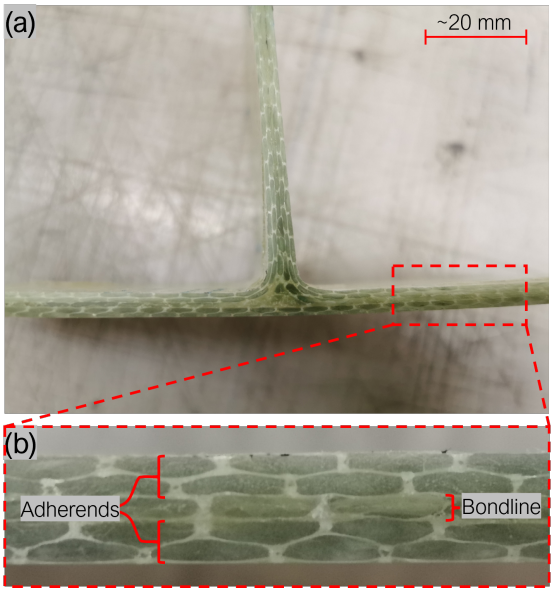

Figure 6.22: *A demonstration of the quality of the resin-welded T-section. (a) A side-view of the T-section. (b) A close-up view of the bondline (the centre ply). It is indistinguishable from the adherends.*

As an example of possible applications, T-joints such as these are often used in the building of composite ships [29, 30]. We also envisage that the method could be applied to wind and tidal turbine blades as shown in Figure 6.23, with the result expected to be similar to the Siemens IntegralBlade process [31].

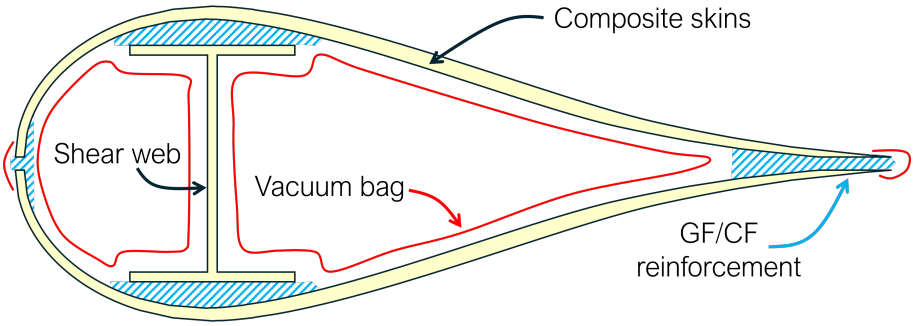

Figure 6.23: *Cross section of a possible method for resin welding an acrylic-matrix wind turbine blade. Glass or carbon fibre reinforcement would be placed in the gaps between the blade shells and the shear web, and the bondlines sealed with vacuum bagging (e.g. a vacuum bag film tube) before infusion of acrylic resin.*

These large structures would require the creation of thick bondlines, but the resin-welded bondlines discussed here are relatively thin at a maximum of 1 mm thickness. A key benefit of resin welding is the ability of the bondline to reach the thickness of any composite laminate made with acrylic resin, including the thick-section laminates already used in wind turbine blade manufacturing. For a demonstration of resin welding in thicker bondlines (∼6 mm thickness), see Appendix A.3. The principles underlying the resin welding process also allows injection-repaired acrylic-matrix composites to have excellent mechanical properties, as detailed in Appendix A.4, which is highly relevant to the repair of wind turbine blades.

A further benefit of resin welding may be found in the recycling of the blades. During recycling, the composite parts are separated from other components such as adhesives, core materials and lightning protection [32, 33]. Resin welding, in which a continuous material is created across the bondline, may therefore simplify blade recycling.

6.4 Chapter Summary

Welded bonds in acrylic-matrix composites have been shown in the literature to increase static strength and fatigue life over adhesive bonds, but improvements in manufacturing tolerances must be made if they are to be applied to large structures like wind turbine blades. The technique introduced in this work—resin welding—has

been shown to be a promising joining alternative for acrylic-matrix composites. As with traditional welding methods, resin welding also results in the entanglement of PMMA chains at the bonding interface. However, in resin welding, instead of heating and melting the polymer chains, acrylic monomer resin is infused into a bondline packed with reinforcement fibres. Here, the resin dissolves and diffuses into the acrylic matrix of the adherends, polymerising around the existing polymer and leading to the formation of a semi-IPN, as evidenced by the diffusion of dyed acrylic resin into clear cast PMMA.

The single lap shear strength of resin welded coupons reached a maximum of 27.9 MPa with a 0.5 mm bondline packed with 0° glass fibres, a strength 24% higher than the highest published value for welded acrylic-matrix composites, which was achieved via resistance welding [8]. Nevertheless, this strength was exceeded by bonds prepared with a commercially available methacrylate adhesive, which reached 46.4 MPa with a 0.5 mm bondline. Unlike the resin welded bonds, however, the adhesive strength and stiffness were highly affected by thickness, and the strength dropped by 56% and the stiffness by 57% when the bondline thickness was increased to 1 mm from 0.5 mm. Additionally, an initial trial of ultrasonic welding was performed, but further optimisation of the method is required as a relatively low average strength of 14.6 MPa was achieved.

Methacrylate adhesives may therefore be the most appropriate joining method for acrylic-matrix composites when bondlines are thin as they create strong bonds, but their strength quickly drops with increasing thickness. Welding methods like ultrasonic, resistance or induction welding can also result in high bond strengths, but they generally require intimate contact between the adherends. As a result, thicker bondlines like those found in wind turbine blades may benefit from resin welding. The first steps towards the application of resin welding of large structures was to demonstrate the method in the welding of a GF/acrylic T-section. The bonding was observed to be of good quality, although it had a bondline thickness of only 1 mm. Further investigation of resin welding in large structures is therefore warranted, especially given the continuing development of recyclable acrylic-matrix composite based wind turbine blades.

6.5 Chapter References

[1] Kit O'Rourke. Investigating repairability of in-situ polymerisable thermoplastic composites. Thesis submitted for the degree of Master of Engineering, University of Edinburgh, 2020.

[2] Winifred Obande, Kit O'Rourke, Danijela Stankovic, Anna Lykkeberg, Jennifer A. Garden, Conchúr Ó Brádaigh, and Dipa Ray. Multi-stage, in-situ polymerisation for low-exotherm, liquid resin infusion of thick thermoplastic laminates at room temperature. *Composites Communications*, 45:101788, 2024. ISSN 2452-2139. doi: https://doi.org/10.1016/j.coco.2023.101788.

[3] Michael J. Troughton, editor. *Chapter 16 - Solvent Welding*, pages 139–143. William Andrew Publishing, Boston, 2009. ISBN 978-0-8155-1581-4. doi: https://doi.org/10.1016/B978-0-8155-1581-4.50018-4.

[4] C. B. Lin, Sanboh Lee, and K. S. Liu. The microstructure of solvent-welding of pmma. *The Journal of Adhesion*, 34(1-4):221–240, 1991. ISSN 0021-8464 1545-5823. doi: 10.1080/00218469108026516.

[5] RS Pro. Anglosol 12: Sds no. cp1205 v1.11 rs 144-406, August 2023 2022. URL `https://docs.rs-online.com/3a29/0900766b80980339.pdf`.

[6] RS Pro. Anglosol 70 part a: Sds no. cp1187a v1.12 rs 144-399, August 2023 2022. URL `https://docs.rs-online.com/2e2b/0900766b809599ae.pdf`.

[7] Pierre Gerard, Michel Glotin, and Bernay Hochstetter. Composite material via in-situ polymerization of thermoplastic (meth) acrylic resins and its use, US Patent 9,777,140 B2, 2017.

[8] Robynne E. Murray, Jason Roadman, and Ryan Beach. Fusion joining of thermoplastic composite wind turbine blades: Lap-shear bond characterization. *Renewable Energy*, 140:501–512, 2019. doi: 10.1016/j.renene.2019.03.085.

[9] Somen K. Bhudolia, Goram Gohel, Leong Kah Fai, and Robert J. Barsotti. Investigation on ultrasonic welding attributes of novel carbon/elium® composites. *Materials*, 13(5):10–15, 2020. doi: 10.3390/ma13051117.

[10] H. Perrin, M. Bodaghi, V. Berthe, and R. Vaudemont. On the addition of multifunctional methacrylate monomers to an acrylic-based infusible resin for the weldability of acrylic-based glass fibre composites. *Polymers (Basel)*, 15 (5), 2023. ISSN 2073-4360 (Electronic) 2073-4360 (Linking). doi: 10.3390/polym15051250.

[11] Caroline A. Schneider, Wayne S. Rasband, and Kevin W. Eliceiri. Nih image to imagej: 25 years of image analysis. *Nature Methods*, 9(7):671–675, 2012. ISSN 1548-7105. doi: 10.1038/nmeth.2089.

[12] S. M. R. Khalili, A. Shokuhfar, S. D. Hoseini, M. Bidkhori, S. Khalili, and R. K. Mittal. Experimental study of the influence of adhesive reinforcement in lap joints for composite structures subjected to mechanical loads. *International Journal of Adhesion and Adhesives*, 28(8):436–444, 2008. ISSN 01437496. doi: 10.1016/j.ijadhadh.2008.04.009.

[13] F. Delzendehrooy, M. R. Ayatollahi, A. Akhavan-Safar, and L. F. M. da Silva. Strength improvement of adhesively bonded single lap joints with date palm fibers: Effect of type, size, treatment method and density of fibers. *Composites Part B: Engineering*, 188, 2020. ISSN 13598368. doi: 10.1016/j.compositesb.2020.107874.

[14] Ranjan K. Behera, S. K. Parida, and R. R. Das. Effect of using fibre reinforced epoxy adhesive on the strength of the adhesively bonded single lap joints. *Composites Part B: Engineering*, 248, 2023. ISSN 13598368. doi: 10.1016/j.compositesb.2022.110358.

[15] Daiki Tanabe, Kazuaki Nishiyabu, and Tetsusei Kurashiki. Electro fusion joining of carbon fiber reinforced thermoplastic composites using carbon fiber heating element. *16th European Conference on Composite Materials, ECCM 2014*, 2014.

[16] D. M. Gleich, M. J. L. Van Tooren, and A. Beukers. Analysis and evaluation of bondline thickness effects on failure load in adhesively bonded structures. *Journal of Adhesion Science and Technology*, 15(9):1091–1101, 2001. ISSN 0169-4243 1568-5616. doi: 10.1163/156856101317035503.

[17] Lucas F. M. da Silva, T. N. S. S. Rodrigues, M. A. V. Figueiredo, M. F. S. F. de Moura, and J. A. G. Chousal. Effect of adhesive type and thickness on the lap shear strength. *The Journal of Adhesion*, 82(11):1091–1115, 2006. ISSN 0021-8464 1545-5823. doi: 10.1080/00218460600948511.

[18] Lucas F. M. da Silva. *Design Rules and Methods to Improve Joint Strength*, pages 689–723. Springer Berlin Heidelberg, Berlin, Heidelberg, 2011. ISBN 978-3-642-01169-6. doi: 10.1007/978-3-642-01169-6_27.

[19] ITW Performance Polymers. Technical data sheet plexus ma310 rev 09, 2018. URL `https://itwperformancepolymers.com/wp-content/uploads/umb/10754/ma310-data-sheet_rev09.pdf`.

[20] ITW Performance Polymers. Plexus adhesive selector guide emea, 2023. URL `https://itwperformancepolymers.com/wp-content/uploads/Plexus-Selector-Chart-EMEA.pdf`.

[21] Jr. Mishnaevsky, L. Root causes and mechanisms of failure of wind turbine blades: Overview. *Materials (Basel)*, 15(9), 2022. ISSN 1996-1944 (Print) 1996-1944. doi: 10.3390/ma15092959.

[22] Alec Redmann, Vinay Damodaran, Felix Tischer, Pavana Prabhakar, and Tim A. Osswald. Evaluation of single-lap and block shear test methods in adhesively bonded composite joints. *Journal of Composites Science*, 5(1):27–27, 2021. doi: 10.3390/jcs5010027.

[23] D. V. Srinivasan, V. Ravichandran, and S. Idapalapati. Failure analysis of gfrp single lap joints tailored with a combination of tough epoxy and hyperelastic adhesives. *Composites Part B: Engineering*, 200, 2020. ISSN 13598368. doi: 10.1016/j.compositesb.2020.108255.

[24] Thomas Noble, James Davidson, Christophe Floreani, Ankur Bajpai, William Moses, Thomas Dooher, Alistair McIlhagger, Edward Archer, Conchur O'Bradaigh, and Colin Robert. Powder epoxy for one-shot cure, out-of-autoclave applications: Lap shear strength and z-pinning study. *Journal of Composites Science*, 5:225, 2021. doi: 10.3390/jcs5090225.

[25] Lucas F M da Silva and R. D Adams. Techniques to reduce the peel stresses in adhesive joints with composites. *International Journal of Adhesion and Adhesives*, 27(3):227–235, 2007. ISSN 01437496. doi: 10.1016/j.ijadhadh.2006.04.001.

[26] Somen K. Bhudolia, Goram Gohel, Leong Kah Fai, and Robert J. Barsotti. Fatigue response of ultrasonically welded carbon/elium® thermoplastic composites. *Materials Letters*, 264:127362–127362, 2020. doi: 10.1016/j.matlet.2020.127362.

[27] Michael J. Troughton, editor. *Chapter 17 - Adhesive Bonding*, pages 145–173. William Andrew Publishing, Boston, 2009. ISBN 978-0-8155-1581-4. doi: https://doi.org/10.1016/B978-0-8155-1581-4.50019-6.

[28] D. J. Gardner. *Wood: Surface Properties and Adhesion*, pages 9745–9748. Elsevier, Oxford, 2001. ISBN 978-0-08-043152-9. doi: https://doi.org/10.1016/B0-08-043152-6/01769-1.

[29] Ferry Dharmawan, Rodney S. Thomson, Henry Li, Israel Herszberg, and Evan Gellert. Geometry and damage effects in a composite marine t-joint. *Composite Structures*, 66(1-4):181–187, 2004. ISSN 02638223. doi: 10.1016/j.compstruct.2004.04.036.

[30] F. Delzendehrooy, A. Akhavan-Safar, A.Q. Barbosa, R. Beygi, D. Cardoso, R.J.C. Carbas, E.A.S. Marques, and L.F.M. da Silva. A comprehensive review on structural joining techniques in the marine industry. *Composite Structures*, 289:115490, 2022. ISSN 0263-8223. doi: https://doi.org/10.1016/j.compstruct.2022.115490.

[31] Siemens Wind Power. Siemens unveils 75 m wind turbine blade. *Reinforced Plastics*, 56(4):30–31, 2012. ISSN 0034-3617. doi: https://doi.org/10.1016/S0034-3617(12)70078-4.

[32] Jr. Mishnaevsky, L. Sustainable end-of-life management of wind turbine blades: Overview of current and coming solutions. *Materials (Basel)*, 14(5), 2021. ISSN 1996-1944 (Print) 1996-1944 (Linking). doi: 10.3390/ma14051124.

[33] Aubryn Cooperman, Annika Eberle, and Eric Lantz. Wind turbine blade material in the united states: Quantities, costs, and end-of-life options. *Resources, Conservation and Recycling*, 168, 2021. ISSN 09213449. doi: 10.1016/j.resconrec.2021.105439.

Chapter 7

Thesis Conclusions and Recommendations

7.1 Conclusions

In this thesis, the suitability of acrylic-matrix composites for use in the marine and renewable energy industries was investigated. The main aims of this thesis were:

1. To investigate water absorption and its effects on mechanical and thermomechanical properties in glass fibre reinforced acrylic (GF/acrylic) and glass fibre reinforced acrylic-PPE (GF/acrylic-PPE), in comparison with a thermoset glass fibre reinforced epoxy (GF/epoxy).

2. To investigate the effect of an acrylic-tailored sizing agent on the fatigue of GF/acrylic, before and after saturation with water.

3. To develop a novel joining method for acrylic-matrix composite structures.

Work conducted towards each of these aims is summarised in the following paragraphs.

1. Seawater ageing of GF/acrylic, GF/acrylic-PPE and GF/epoxy. Prior to the commencement of this work, data was not available on the diffusion of water in unidirectional GF/acrylic composites, nor the mechanical properties of unidirectional GF/acrylic composites after saturation with water. Additionally, though

some promising results had been observed in acrylic-PPE hybrid matrix composites, the effects of this hybridisation on water absorption and property retention were unknown. Hydrothermal ageing studies of unidirectional GF/acrylic, GF/acrylic-PPE and GF/epoxy were therefore performed, allowing for comparison between these novel thermoplastics and a traditional thermoset. A summary of the mechanical and thermomechanical properties of each composite, dry and aged, is presented in Figure 7.1.

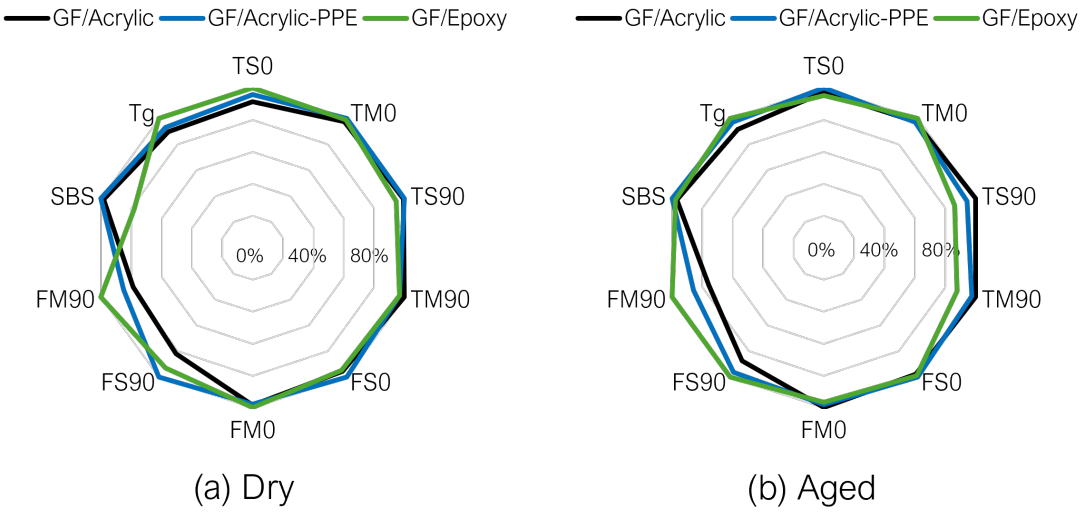

Figure 7.1: *Comparisons of the properties of (a) dry and (b) aged GF/acrylic, GF/acrylic-PPE and GF/epoxy, with axes normalised to a percentage of the largest value for each property. The short beam strength (SBS) and T_g are presented, and the other properties are labelled as follows: T= tensile, F= flexural, S = strength, M = modulus, 0 = 0° fibres, 90 = 90° fibres. For example, TS0 is the 0° tensile strength. The 0° properties were normalised to 50% FVF.*

From Figure 7.1, we can see that GF/acrylic and GF/acrylic-PPE are largely comparable with epoxy. The largest differences can be seen in the dry SBS, and dry and aged 90° flexural properties. GF/epoxy consistently had a higher T_g than GF/acrylic and GF/acrylic-PPE at 129°C, 116°C and 120°C when dry, and 108°C, 99°C and 105°C when aged, respectively. If a higher T_g or greater 90° flexural properties than GF/acrylic are required, this can be achieved via reactive hybridisation with PPE.

Although the composites are largely comparable after saturation, the diffu-

sion coefficient of water in GF/acrylic was an order of magnitude higher than in GF/epoxy (Figure 7.2a), meaning water will penetrate further into an acrylic-matrix tidal turbine blade or ship than its epoxy-matrix equivalent. This was attributed partly due to differences in void content (Figure 7.2a), but is largely due to higher hydrophilicity of epoxy, which slows the diffusion of water. It was further determined that, contrary to the hypothesised effect, hybridisation with PPE did not result in reduced moisture absorption. Indeed, water was absorbed faster and to a higher equilibrium content in GF/acrylic-PPE compared to GF/acrylic, despite the lower void content of the former, which may be due to changes in the polymer structure increasing the available free volume.

As illustrated in Figure 7.2b and c, however, approximate calculations showed that laminate thicknesses in these large structures are likely to result in limited penetration of water in reality. This is valuable information for tidal turbine manufacturers, and highlights that the results presented in Figure 7.1 are not the only consideration when selecting a resin. A balance must be struck between the effects of water on a composite and the speed at which it is absorbed, depending on the expected service life.

(a)	D_z [$\times 10^{-12}$ m^2 s^{-1}]	M_m [%]	Void Fraction [%]
GF/acrylic	1.81	0.81	1.43
GF/acrylic-PPE	3.4	0.91	0.95
GF/epoxy	0.15	0.63	0.45

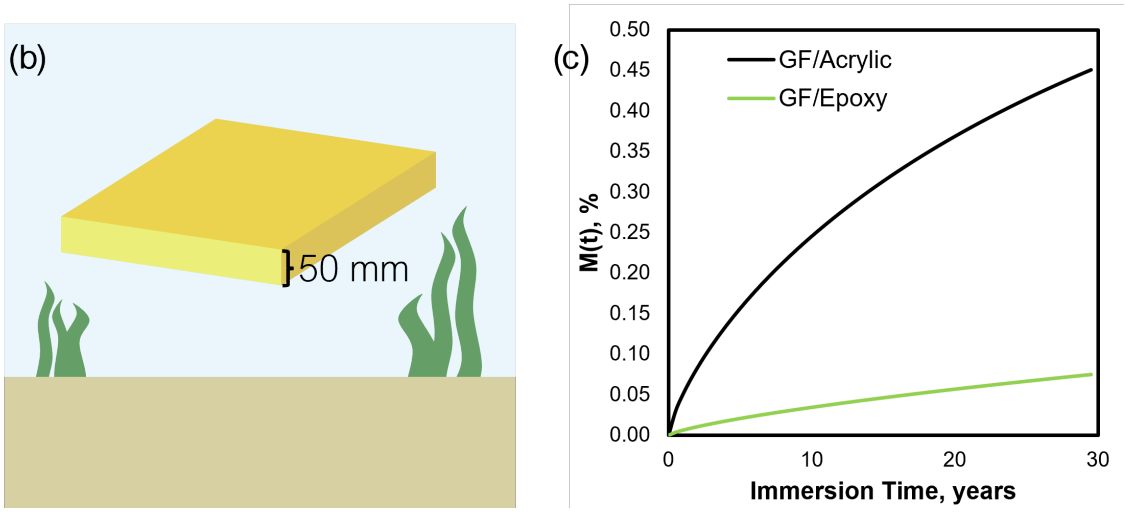

Figure 7.2: *An illustration of the differences in water absorption between GF/acrylic and GF/epoxy composites. (a) The diffusion coefficients and maximum water uptake of each material. (b) We can consider 50 mm thick GF/acrylic and GF/epoxy laminates immersed in 10°C seawater. (c) GF/acrylic would absorb more water than GF/epoxy over 30 years, but neither would saturate.*

2. The effect of a specialised sizing agent on fatigue. Data on the fatigue of unidirectional GF/acrylic composites, either dry or aged in water, was not available prior to the commencement of this project. Additionally, though speculation on the effects of a tailored sizing agent existed in the literature, there were few applicable comparisons between a tailored and multi-compatible sizing available for acrylic-matrix composites. GF/acrylic coupons with an acrylic-tailored sizing agent were therefore subject to tension-tension fatigue before and after ageing in water, and the results compared to multi-compatible GF/acrylic from the literature and Appendix A.1. The multi-compatible sized composite had superior low-cycle performance, but the performance of the two composites converged in high cycle fatigue. These differences are likely due to differences in the fibre volume fraction and fibre diameter between the two reinforcements, as supported by static testing

in Chapters 4 and 5, and Appendix A.2.

As discussed in Chapter 2.2, sizing formulations are complex and include various components such as a silane coupling agent and a film former. The formulations of the sizing agents used in this thesis are unknown, and so the effects of each component of the sizing agent cannot be determined. However, this work does provide further evidence that manufacturers wishing to use liquid acrylic resins may not need to seek out specialised fabrics. They are instead likely to achieve good results with a fabric which is compatible with polyester and vinylester, as recommended by the resin's manufacturer. Regardless of the sizing agent used, comparisons between this fatigue data and data from the literature showed that GF/acrylic can have performance on par with the thermoset composites used commercially in wind turbine blades.

3. Development of a novel joining method. Finally, a novel method of joining acrylic-matrix composite parts—termed *resin welding*—was introduced in Chapter 6. In this method, acrylic monomeric resin is infused between two acrylic-matrix parts, dissolving the top layer of the existing polymer. When the liquid resin polymerises, it entangles the dissolved polymer chains, creating a strong bond with the adherends. With the resin welding method, it was possible to achieve greater single lap shear strengths than the strongest weld (a resistance weld) in the literature [1], but without the need for intimate contact between the adherends. A surprising result was obtained with a methacrylate structural adhesive, which achieved much stronger bonds than expected, at 46 MPa, when the bondline was 0.5 mm thick. This may be due to the presence of methacrylate monomers in the adhesive, allowing for a similar bonding mechanism as in resin welding to occur. In thicker adhesive bondlines, large voids reduced bond strength. This therefore suggests that adhesive bonds may be the preferred joining method when low tolerances and thin bondlines can be achieved, but that resin welding could be beneficial when larger tolerances are involved—such as would be found in a wind or tidal turbine blade.

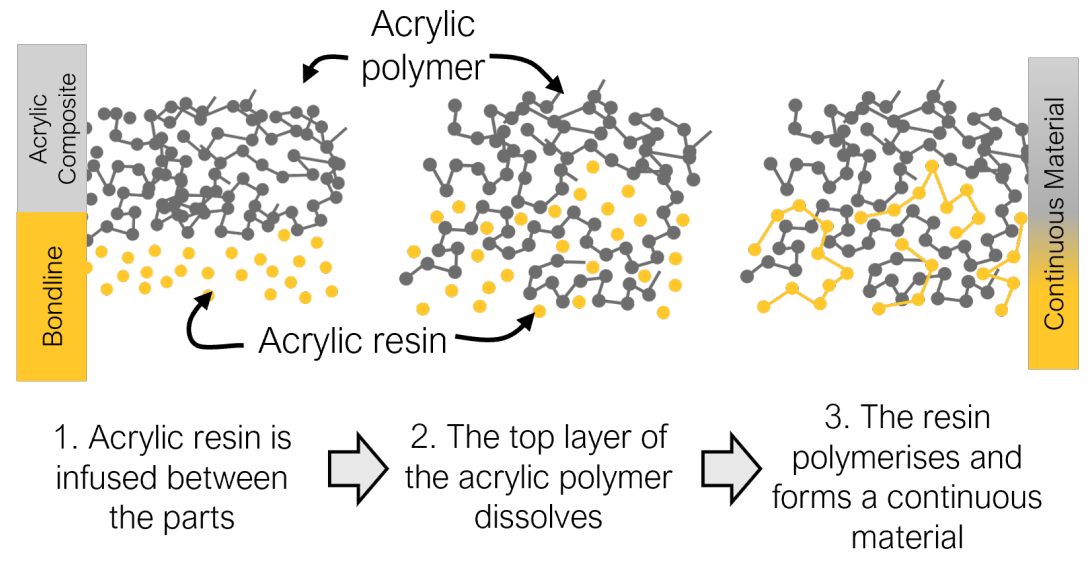

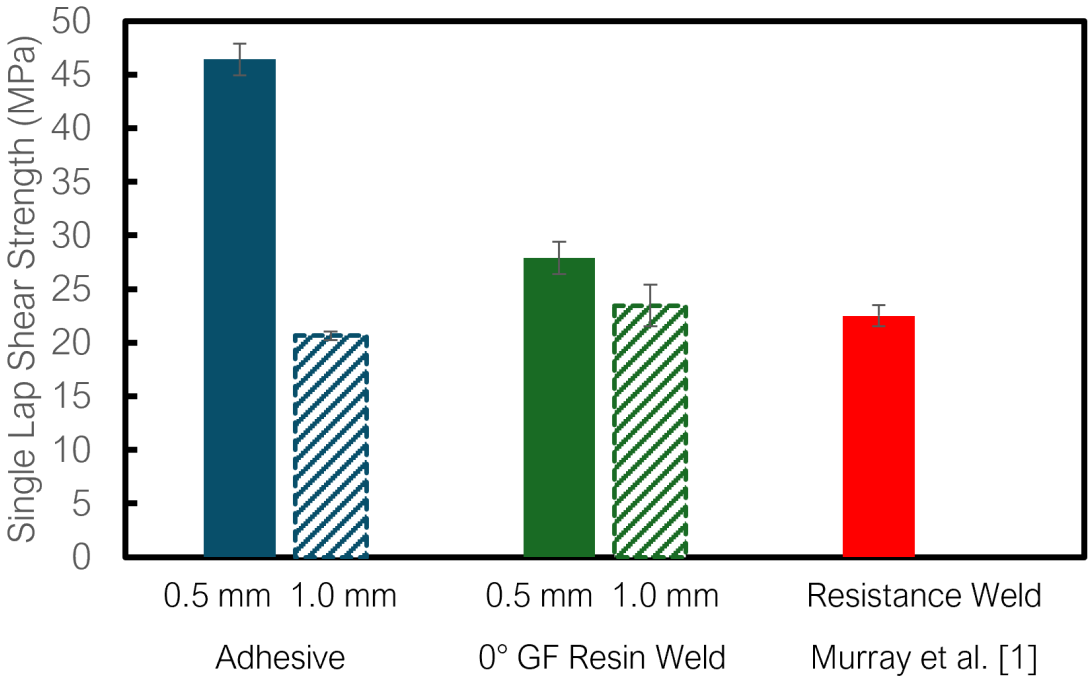

Figure 7.3: *An overview of the resin welding process, with a comparison between the strengths of adhesive bonds, resin welds with 0° glass fibres, and a resistance weld from Murray et al. [1].*

Overall, these three studies provide several assurances that acrylic-matrix composites may be an appropriate choice for use in the renewable energy and marine sectors. Understanding of the effects of water on the mechanical, thermomechanical and fatigue properties of these composites has been developed, with promising results in comparison to traditional thermosets. The role of the fibre sizing agent has

also been explored, with the conclusion that currently available multi-compatible fabrics may be sufficient. Finally, the resin welding method introduced here creates the possibility of achieving weld-like strengths with the thick bondlines currently found in wind and tidal turbine blades.

7.2 Recommendations

The research discussed in this thesis provides valuable insight into the use of GF/acrylic composites in the renewable energy and marine sectors, and highlights several areas for further investigation. The absorption of water into full-scale acrylic-matrix tidal turbine blades is poorly understood, and it is unclear if the faster diffusion of water in the acrylic matrix will pose a problem in practice. While full-scale GF/acrylic tidal turbine blades have been immersed in water and their mass increases tracked [2, 3], only a few months of experimental data is available, and it is complicated by osmotic blistering of the blade paint and absorption into the foam core. In combination with this experimental data, numerical simulations of water diffusion in full-scale blades would be helpful as the water penetration depth over time could be determined, rather than a single value of mass increase for the whole blade. This, together with data from coupon-scale tests, could allow the practical effects of water on the mechanical properties of an acrylic-matrix tidal turbine blade to be determined.

Coupon-scale comparisons between a multi-compatible reinforcement and an acrylic-tailored reinforcement have been presented in this thesis and in Appendix A.2, and have been used to infer the effect of the sizing agent on water absorption, mechanical properties, and fatigue. Direct measurements of the interfacial shear strengths would also be useful, but the volatility of acrylic resin makes fibre pullout tests difficult to achieve. Alternative tests such as single fibre fragmentation or fibre pushout could be employed, as coupons for these tests could be prepared without resin evaporation.

The conclusions drawn on the effect of sizing agent are complicated by the differences in fibre diameter and areal weight between the fabrics, and so a comparison of sizing agents on the same fibres may provide more certainty. This was not possible

in the current work due to the two fabrics being provided by different suppliers, however it may be useful to apply sizing agents in-house, for example after using a furnace to remove the sizing from commercial glass fabric. While the resulting properties may not be representative of a commercially applied sizing agent, the comparison would be useful. Additionally, this would allow for a deeper understanding of each component of the formulation, for example the role of the film former in water absorption in GF/acrylic composites.

Further investigation of the interfacial degradation process during water absorption would also provide valuable insight. In Chapters 4 and 5, it was proposed that hydrolysis of the silane coupling agent was the cause of the observed decreases in interfacial strength. This could be confirmed via infrared spectroscopy, or confocal Raman microscopy, which could detect any detachment of the silane coupling agent from the glass surface. This could be combined with the immersion of GF/acrylic coupons in room temperature seawater, to ensure that any degradation mechanisms observed would occur without thermal acceleration of the diffusion process.

The next logical step in the development of the resin welding method would be to manufacture a sub-component (an I-beam for example), or even a scale model of a tidal turbine blade. A method was proposed in Figure 6.23 for the application of resin welding to wind and tidal turbine blades, and could be used to determine the feasibility of the method, including the practicality of sealing the bondline and wetting out of bondline fibres with resin. Processing times and required manpower would be other important factors in the bonding method's practicality, and both could be explored in a demonstrator project. A comparison with an adhesively bonded equivalent would allow us to determine if the expected benefits to blade stiffness and bond strength are realised. Fatigue testing at the University of Edinburgh's FastBlade facility, for example, would allow such a comparison to be made.

7.3 Chapter References

[1] Robynne E. Murray, Jason Roadman, and Ryan Beach. Fusion joining of thermoplastic composite wind turbine blades: Lap-shear bond characterization. *Renewable Energy*, 140:501–512, 2019. doi: 10.1016/j.renene.2019.03.085.

[2] Robynne E. Murray, Ryan Beach, Paul Murdy, Scott Dana, and Scott Hughes. Structural characterization of deployed thermoplastic and thermoset composite tidal turbine blades. Report, 2024-04-08 2024.

[3] Paul Murdy, Ariel Lusty, Robynne Murray, Scott Hughes, and Ryan Beach. Post-deployment characterization of glass fiber-reinforced thermoset and thermoplastic composite tidal turbine blades: Preprint. 4 2024. URL https://www.osti.gov/biblio/2340123.

Appendix A

Collaborative Work

Work which was completed in collaboration with other researchers, for example as part of student projects, is presented here. Each of these studies was extended from the findings of the work previously presented in this thesis. In each of the following sections, the key information from each of these studies is presented. For further details, the reader is referred to the publications found in the List of Publications, and in Appendix C.

A.1 Fatigue of Acrylic-PPE

In Chapter 4, the static properties of GF/acrylic, GF/acrylic-PPE and GF/epoxy coupons were compared, both before and after saturation with seawater. Unidirectional 0° tensile coupons (1.5 × 15 × 250 mm), cut from the same laminates as in Chapter 4, were also tested in fatigue, as is discussed here. Half of the coupons were tested dry, and the other half were immersed in seawater at 50°C for 3 months before testing. The results of this study are published in Stankovic et al. [1].

During fatigue testing, maximum loads were applied at 80%, 60% and 40% of the coupons' ultimate tensile strengths, as measured in Chapter 4. The results of fatigue testing are presented in Figure A.1, in which curves of the form $f(x) = ae^{bx} + ce^{dx}$ have been fit to the data. The data from this study was discussed in Chapter 5, but a Basquin fit was applied to the data instead.

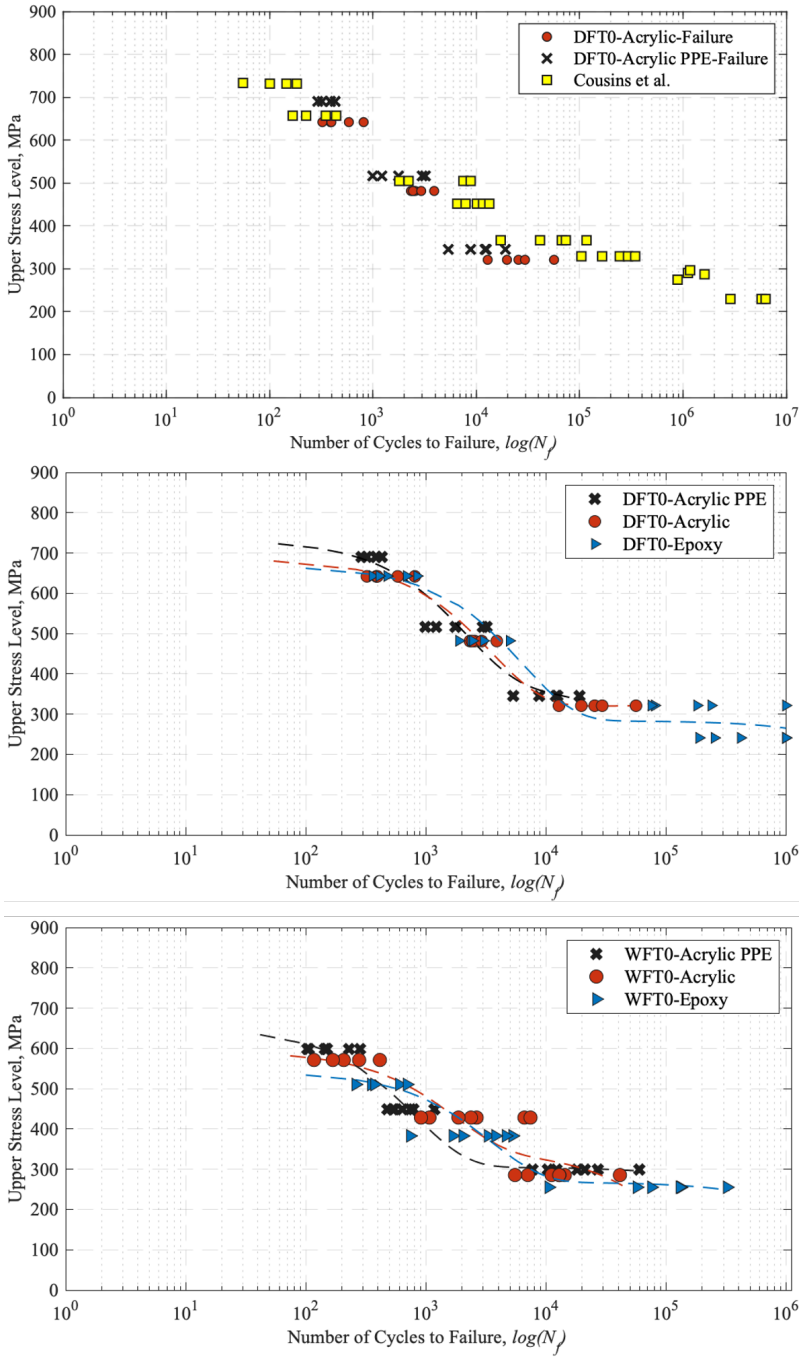

Figure A.1: *(a) Comparison of the dry S-N curves of GF/Acrylic and GF/Acrylic-PPE to the results from Cousins et al. [2]. (b) Comparison of all the dry coupons in this study. (c) Comparison of all the aged coupons in this study. DFT0 = 'dry fatigue tension 0°' and WFT0 = 'wet fatigue tension 0°'. Reproduced from Stankovic et al. [1].*

The performance of GF/acrylic and GF/acrylic-PPE is found to be similar overall. The performance of GF/acrylic and GF/acrylic-PPE is also similar to GF/epoxy

at high stresses, but GF/epoxy outperforms them both at lower stresses in the dry coupons. Fatigue data for 0° tensile GF/acrylic coupons from Cousins et al. [2] is included for comparison. The performance of GF/acrylic according to Cousins et al. is superior to those tested in the present study, and appears to be comparable to the GF/epoxy tested in the present study.

Testing was stopped once a coupon reached 10^6 cycles, which only occurred in one dry GF/epoxy coupon at 40% of its UTS, as well as two dry GF/epoxy coupons at 30% of their UTS. Post-fatigue tensile testing was applied to these coupons, and the results are presented in Table A.1. The strength decreased by between 13% and 37% of its initial value, but the modulus was largely unaffected, or even increased.

Table A.1: *Strength and modulus of dry GF/epoxy coupons after* 10^6 *load cycles at 30% and 40% of the UTS. Two coupons survived* 10^6 *cycles at 30% of the UTS, and one survived at 40%. The % changes with respect to the initial UTS and modulus are also presented.*

Max stress	$UTS_{post-fatigue}$, MPa	$\%\text{UTS}_{initial}$	$E_{post-fatigue}$	$\%E_{initial}$
30%	657.6	81.8	37.93	114.8
30%	505.9	63.0	32.82	99.4
40%	697.3	86.8	33.12	100.3

To conclude, the fatigue performance of GF/acrylic and GF/acrylic-PPE are similar, so there appears to be no significant benefit of acrylic-PPE in 0° tensile fatigue. However, the similar performance means that the mechanical and thermo-mechanical benefits of acrylic-PPE, as well as its enhanced solvent resistance, can be achieved without sacrificing fatigue performance. The fatigue results may be different with other test configurations—for example, the results of Chapter 4 suggest an improvement in 90° flexural strength. The performance of GF/epoxy was similar to the thermoplastics at high stresses, but outperformed GF/acrylic at low stresses. However, 0° tensile fatigue data of GF/acrylic coupons from the literature compared favourably to the GF/epoxy in this study. The use of GF/acrylic therefore seems promising.

A.2 Sizing Effects on Water Absorption

A study comparing the effects of multi-compatible (MCS) and acrylic-tailored (AS) sizing agents on the fatigue of GF/acrylic composites was presented in Chapter 5. Water absorption, retention in static properties and interfacial degradation were also compared between GF/acrylic composites made with the same two reinforcements (GF1-MCS and GF2-AS) as part of an MEng project [3], described in the following paragraphs. In this project, composite coupons were subject to 0° and 90° tension and flexure, as well as short beam strength tests, before and after immersion in 50°C seawater for 3 months.

In addition, coupons of GF1-MCS/acrylic, GF2-MCS/acrylic and unreinforced acrylic resin were subject to three absorption-desorption cycles by immersing them in 50°C seawater until saturation, drying them under vacuum and then repeating. The mass uptake of these coupons was monitored, and the effective diffusion coefficients of water in the composite (D_e) and the unreinforced resin (D_p) were calculated for each absorption cycle. These were used to determine the degree of interfacial loosening using Equation A.1, as per Tsenoglou et al. [4], in which f_i is the interfacial volume fraction, f_p is the polymer free volume fraction, and V_f is the fibre volume fraction.

$$f_i = \frac{f_p}{V_f}\left[\frac{1}{1 - f_p \ln\left(\frac{D_e}{D_p}\right)} - (1 - V_f)\right] \tag{A.1}$$

A plot of the mass uptake vs. time graphs for each material and absorption cycle is presented in Figure A.2.

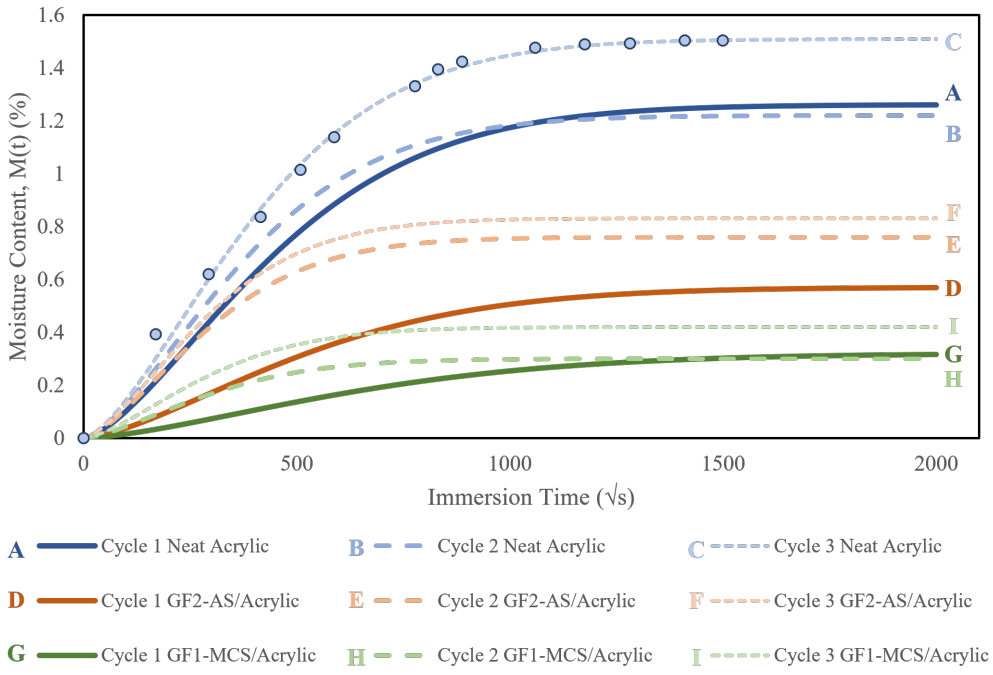

Figure A.2: *The fitted diffusion curves plotted against the square root of time. All three absorption cycles of neat acrylic resin (blue, A-C), GF2-AS/Acrylic (orange, D-F) and GF1-MCS/Acrylic (green, G-I) are presented. For clarity, only the experimental data (averages of 10 coupons) from the third neat acrylic cycle (C) have been included as blue circles and are indicative of the quality of fit.*

Applying Equation A.1, the values of f_i are calculated and presented in Figure A.3.

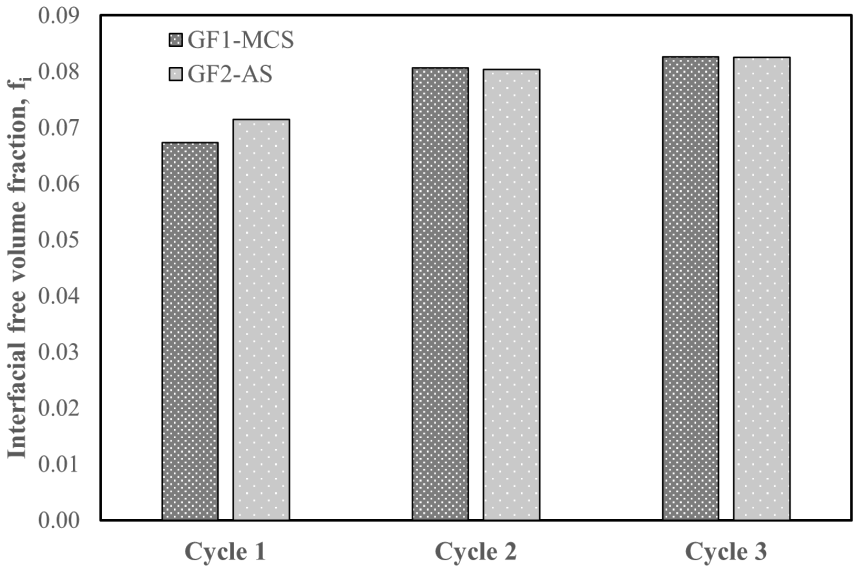

Figure A.3: *The calculated interfacial free volume fractions of the composites during each absorption cycle.*

The greater water absorption in unreinforced resin in Figure A.2 shows that water is mainly absorbed by the acrylic matrix. The increases in water uptake with subsequent cycles also shows that the matrix suffers permanent damage with each absorption-desorption cycle. Greater absorption in GF2-AS/acrylic is attributed to a greater void content at 1.37% vs. 0.22% in GF1-MCS/acrylic. Both composites experience similar degrees of interfacial loosening (Figure A.3), leading to wicking along the fibre-matrix interface, and water being absorbed faster and at greater percentages, in the second and third cycles.

A summary of the results of mechanical testing is presented in Table A.2, and compares the results of GF2-AS/acrylic from the current study with those of GF1-MCS/acrylic from Chapter 4. SEM images of the 0° tensile fracture surfaces of GF2-AS/acrylic before and after ageing are also presented in Figure A.4.

Table A.2: *A comparison between the mechanical properties of GF1-MCS/acrylic composites (from Chapter 4) with those of GF2-AS/acrylic (from the current study). The dry properties and change due to water absorption are presented for both composites. Note that the 0° properties have been normalised to 50% FVF for both reinforcements*

		GF2-AS/Acrylic			GF1-MCS/Acrylic		
Test	Property	Dry	Aged	% Change	Dry	Aged	% Change
0° Tension	Modulus (GPa)	35.3 ± 3.0	33.4 ± 3.2	-5%	33.2 ± 2.2	34.5 ± 2.8	+4%
	Strength (MPa)	683 ± 62	541 ± 25	-21%	750 ± 61	667 ± 64	-11%
90° Tension	Modulus (GPa)	10.5 ± 0.7	6.9 ± 1.0	-34%	9.3 ± 0.7	8.4 ± 0.4	-10%
	Strength (MPa)	37.1 ± 2.2	30.4 ± 1.6	-18%	37.1 ± 1.5	35.8 ± 4.5	-4%
0° Flexure	Modulus (GPa)	36.1 ± 3.6	36.3 ± 3.7	0%	31.6 ± 1.6	31.3 ± 0.8	-1%
	Strength (MPa)	789 ± 80	706 ± 34	-10%	810 ± 40	678 ± 53	-16%
90° Flexure	Modulus (GPa)	10.6 ± 0.7	8.4 ± 0.7	-21%	9.7 ± 0.6	8.0 ± 0.5	-17%
	Strength (MPa)	68.3 ± 5.2	55.3 ± 4.1	-19%	96.5 ± 8.7	74.4 ± 7.3	-23%
Short Beam	Strength (MPa)	46.6 ± 1.6	39.0 ± 1.6	-16%	57.3 ± 0.8	39.4 ± 2.3	-31%

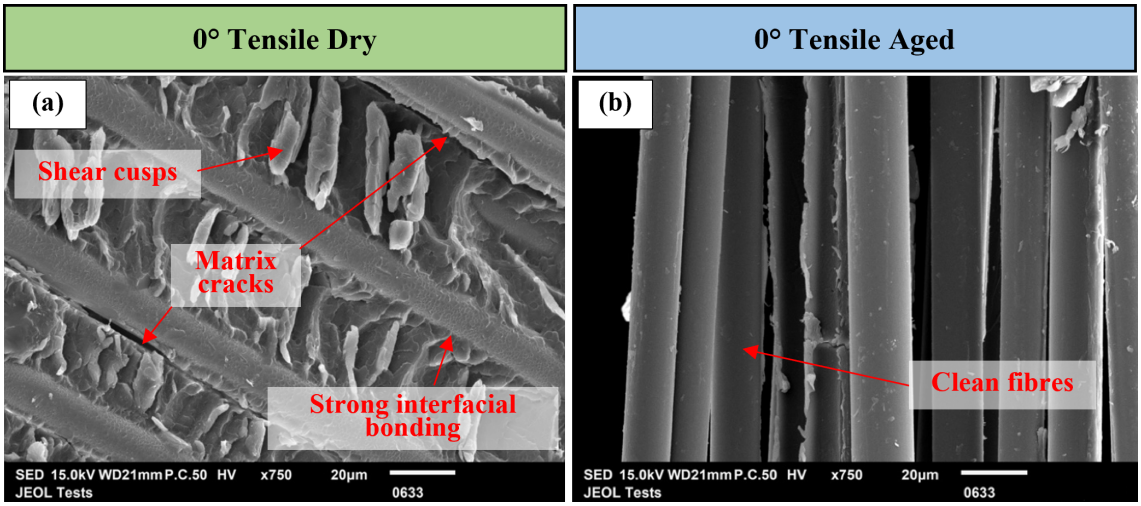

Figure A.4: *SEM images of the fracture surfaces of (a) dry and (b) aged 0° tensile GF2-AS/acrylic coupons. Crack propagation through the matrix in the dry coupon, instead of along the fibre-matrix interface, indicates strong interfacial bonding. The bare fibres in the aged coupon suggest that the fibre-matrix interface is weakened.*

From Table A.2, there were no consistent improvements in the retention of mechanical properties due to the specialised sizing agent. Additionally, from Fig-

ure A.4 it is clear that the same interfacial degradation mechanism reported for GF1-MCS/acrylic (Figure 4.15) occurs with the acrylic-tailored sizing agent.

The comparisons presented here therefore suggest that an acrylic-tailored sizing agent does not necessarily improve the water absorption properties of GF/acrylic, in agreement with the results of Chapter 5.

A.3 Thick resin welds vs. adhesive bonds

A T-section was manufactured in Chapter 6 to explore the use of resin welding in large structures. This was a more complex bondline than in the single lap shear coupons tested in Chapter 6, but the bondline thickness was only ∼1 mm. The practicality of resin welding with thicker bondlines was therefore investigated in a BEng project [5] through the bonding of flat ∼2 mm thick GF/acrylic laminates. These laminates were either adhesively bonded with ∼5 mm of Plexus MA 320 structural methacrylate adhesive, or resin welded with six plies of unidirectional glass fibre fabric (GF2-AS). Resin welding was performed by laying the fabric between the adherend laminates before vacuum bagging and infusing acrylic resin into the bondline. These processes are detailed in Figures A.5 and A.6.

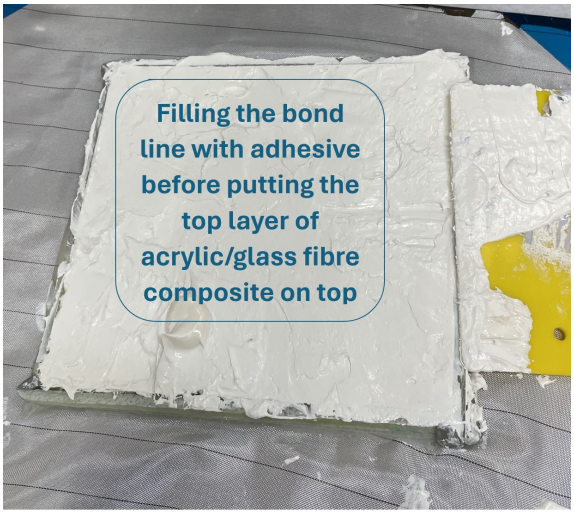

Figure A.5: *An image of the application of methacrylate adhesive on top of a GF/acrylic laminate. A second GF/acrylic laminate will be clamped on top. The bondline thickness is set with 5 mm PMMA blocks.*

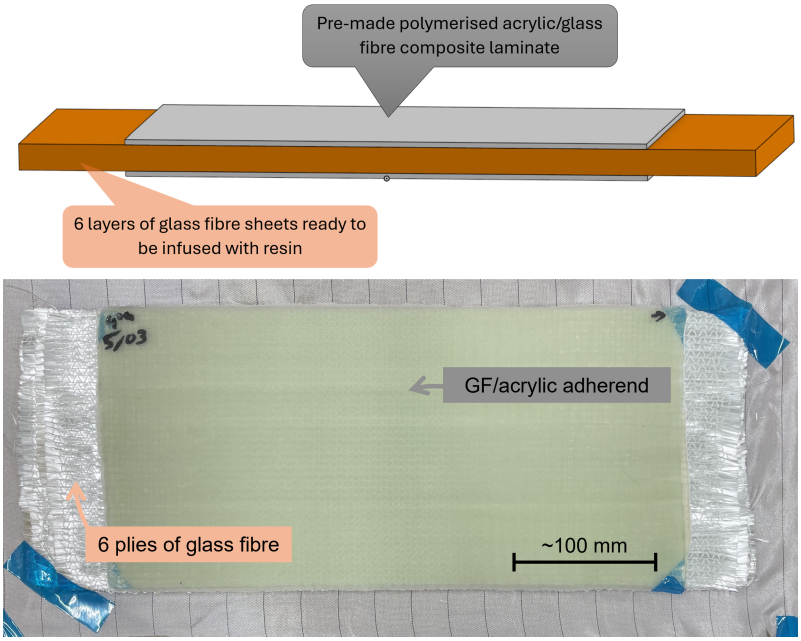

Figure A.6: *The resin welding process. (top) A side-view diagram , with six layers of dry glass fibre between two GF/acrylic composite adherends. (bottom) A photo of the setup before vacuum bagging and infusion of resin between the adherends.*

The bonded laminates were cut into 0° flexural coupons of nominal 173 × 13 × 9 mm dimensions, then tested in 3-point bending. A span of 144 mm was used, giving a nominal span-to-thickness ratio of 16:1, and the crosshead extension rate was 7 mm/min. Other coupons were immersed in seawater at 50°C for 10 days before testing. The seawater-immersed adhesive and resin-welded coupons absorbed 0.32% and 0.27% water respectively, and so the coupons had not reached the expected saturation value for GF/acrylic of ∼0.6-0.8% before testing.

The results of flexural testing are presented in Figure A.7, and images of the coupons are presented in Figure A.8.

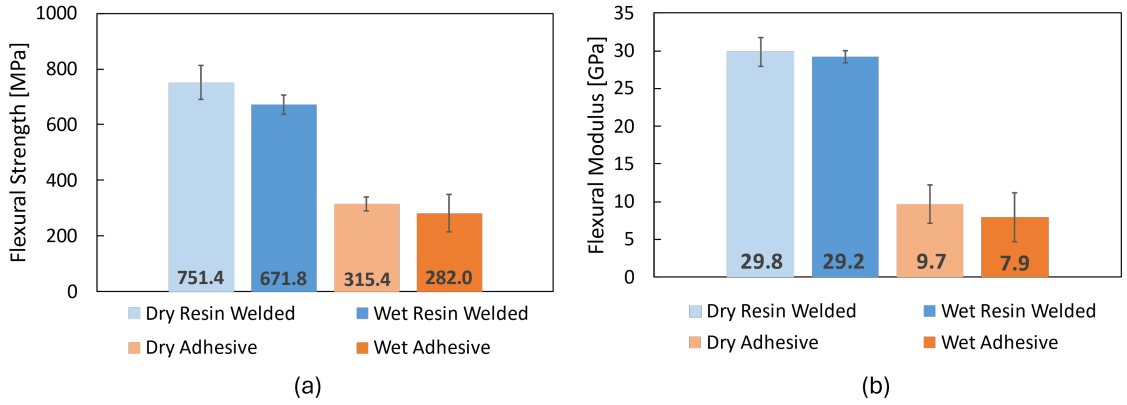

Figure A.7: *The (a) flexural strengths and (b) flexural moduli of dry and aged adhesively bonded and resin-welded coupons.*

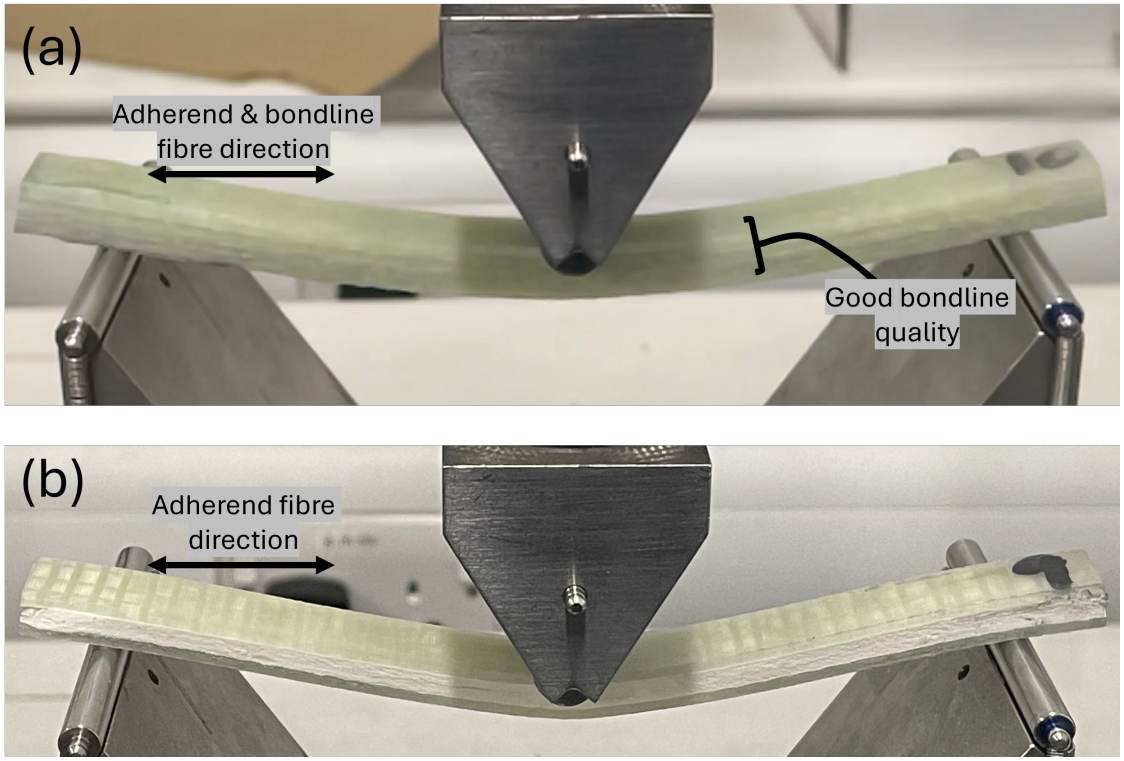

Figure A.8: *Images of (a) resin-welded and (b) adhesively bonded coupons during testing. The adherend and bondline fibre directions are labelled. Excellent wetting of the bondline plies is visible in the resin-welded coupon.*

The strengths and moduli of the resin-welded coupons were greatly increased over the adhesively bonded coupons. This is to be expected considering the inclusion of 0° glass fibres in the resin-welded bondline. Water immersion caused 11% decreases in both coupons' strengths, but caused a much greater decrease in the modulus of the

adhesively bonded coupons (-18%) than the resin-welded coupons (-2%). However, these differences should be interpreted with caution for several reasons. The large standard deviations in the adhesively bonded properties make comparisons difficult, and the coupons had not reached full saturation. Furthermore, the resin-welded coupons failed via interlaminar shearing, rather than tensile or compressive failure, due to the low span-to-thickness ratio.

The project therefore demonstrated that resin welding thicker bondlines is feasible, and excellent bond qualities can be achieved. The benefits to structural stiffness achieved by replacing adhesive bonds with resin welds were also demonstrated, though the bondline-to-adherend thickness ratio of ∼2.5:1 does not accurately represent an actual wind turbine blade. The effects of water absorption were less clear due to the large variance in coupon properties and the coupons not reaching saturation before testing. Initial results suggested a greater decrease in modulus for the adhesively bonded coupons due to water absorption, but this would need to be verified after a longer immersion time.

A.4 Injection vs. press repair of GF/acrylic

The mechanisms which allow resin-welded bonds to reach high strengths—the dissolution of acrylic polymer in its own monomeric resin, and the formation of a semi-IPN—also allow resin-injection repairs of acrylic-matrix composites to be highly effective. This was demonstrated as part of an MEng project, now published in Bolluk et al. [6], in which the effectiveness of resin injection repair was compared to that of heated press repairs via double cantilever beam (DCB) testing.

GF/acrylic DCB coupons were manufactured via the vacuum infusion of 4 plies of unidirectional E-glass fabric (GF2-AS). A polymer film of 13 µm thickness was placed between the two centre plies to form a pre-crack. Coupons were then cut to 175 × 25 mm dimensions, with a 63 mm pre-crack. Loading blocks were adhesively bonded to the coupons before testing.

DCB testing was carried out with a crosshead extension rate of 5 mm/min until the crack had propagated at least 50 mm, as measured by an Imetrum DIC video extensometer. The average mode-I fracture toughness during initiation $G_{IC,init}$ and

propagation $G_{IC,prop}$ was calculated via a modified beam theory method.

After testing, coupons were then repaired via resin injection or press repair. In both methods, the pre-crack film was left in place to ensure the pre-crack remained open after the repair. Resin injection repairs were carried out by injecting acrylic resin, mixed with a peroxide initiator, into the crack propagation region of the coupons. The coupons were then vacuum bagged to remove air (and therefore oxygen, which inhibits free radical polymerisation according to manufacturer guidance) and to apply pressure until the resin polymerised and the repair was complete. This process is detailed in Figure A.9.

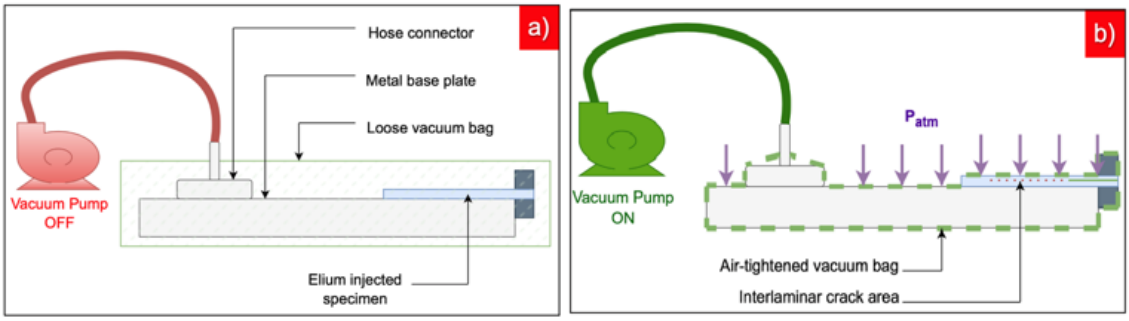

Figure A.9: *Schematic of resin injection repair, after resin has been injected into the repair area. (a) The coupon is placed on a base plate so the loading blocks overhang the edge, and the setup is vacuum bagged. (b) The bag is evacuated, applying pressure to the repair until the resin polymerises. Figure reproduced from [6].*

Heated press repairs were performed by subjecting each coupon to 3 bar of pressure at either 130°C or 160°C. The coupons were placed between steel plates such that pressure was not applied to the loading blocks (see Figure A.10), and were held at their target temperature for 30 minutes.

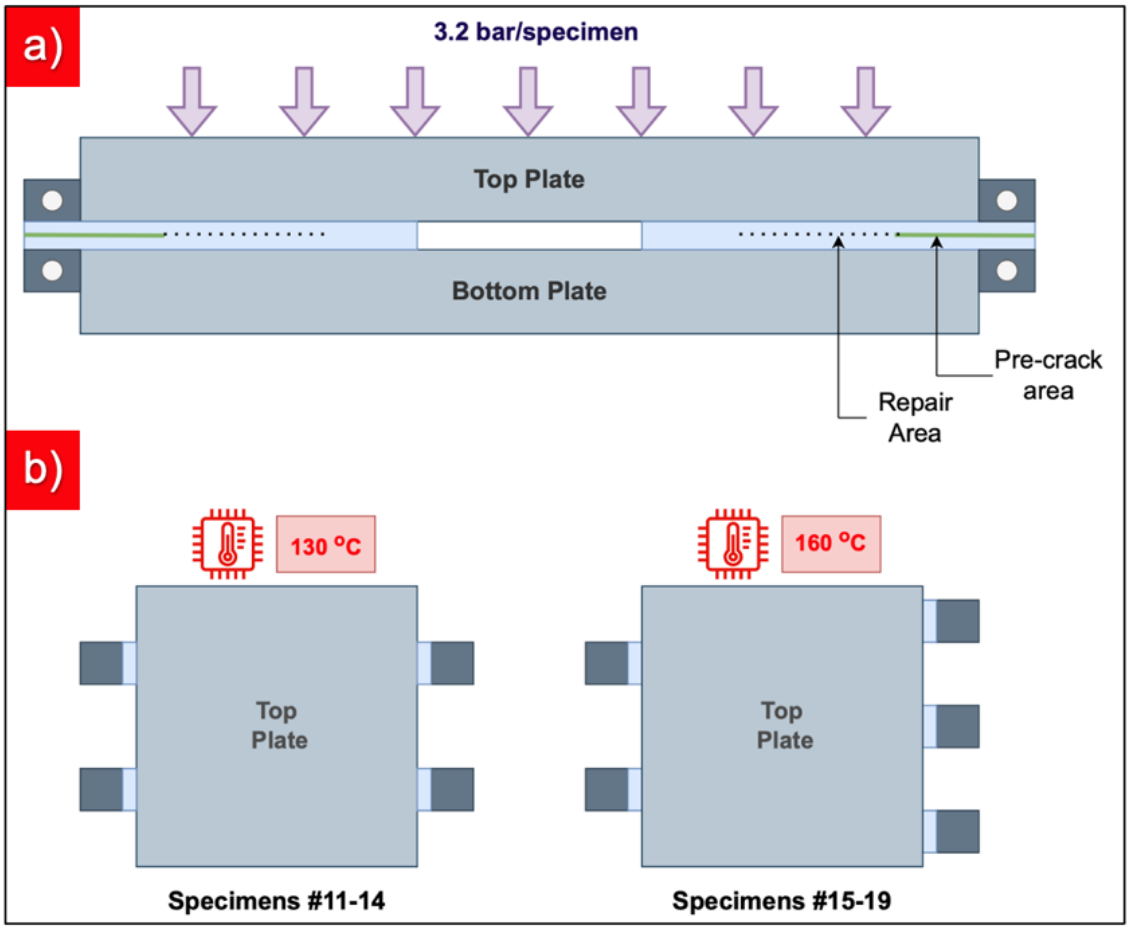

Figure A.10: *The press repair process. (a) Tested DCB coupons are placed between steel plates so that pressure is only applied to the repair area. (b) Pressure is applied at either 130°C or 160°C for 30 minutes. Figure reproduced from [6].*

The coupons were then re-tested as before, and the resulting G_{IC} values are compared to the virgin coupons' in Figure A.11.

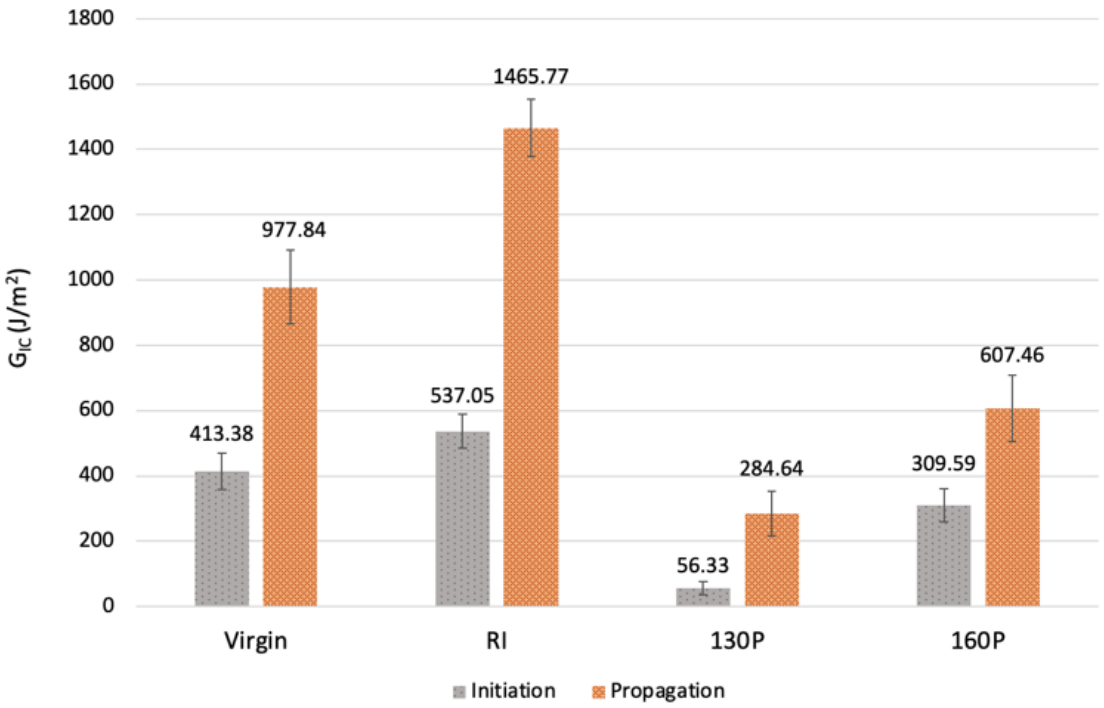

Figure A.11: *The mean $G_{IC,init}$ and $G_{IC,prop}$ values for the virgin coupons, as well as coupons repaired via resin injection (RI), 130°C press repair (130P) and 160°C press repair (160P). Figure reproduced from [6].*

From Figure A.11, the press repairs only partially restored the fracture toughness of the virgin coupons. The press repair at 130°C was inadequate, and led to rapid crack propagation. The press repair at 160°C was more successful, leading to 75% restoration of the coupons' $G_{IC,init}$ value compared to the virgin coupons. The $G_{IC,prop}$ value was restored to 62% of its original value, which is lower than the percentage $G_{IC,init}$ restoration, likely due to a lower contribution of fibre bridging in the press repaired coupons.

The resin injection repair was highly successful, leading to a 30% *increase* in $G_{IC,init}$ and a 50% increase in $G_{IC,prop}$ compared to the virgin coupons. This increase is attributed to a greater toughness of the semi-IPN which forms at the repair boundary, compared to the bulk acrylic matrix. This result is in accordance with Obande et al. [7], who measured increases in short beam strength in GF/acrylic laminates manufactured in multiple infusion steps compared to those manufactured in a single infusion.

Resin injection repair of acrylic-matrix composites is therefore highly effective

due to the solubility of the acrylic polymer in its monomeric resin. These repairs can be performed in situ without the need for heat or pressure beyond vacuum levels. This provides further incentive to use recyclable acrylic-matrix wind and tidal turbine blades, as effective repairs can significantly extend turbine lifetimes.

A.5 Chapter References

[1] Danijela Stankovic, Winifred Obande, Machar Devine, Ankur Bajpai, Conchúr M. Ó Brádaigh, and Dipa Ray. Accelerated seawater ageing and fatigue performance of glass fibre reinforced thermoplastic composites for marine and tidal energy applications. *Composites Part C: Open Access*, 14:100470, 2024. ISSN 2666-6820. doi: https://doi.org/10.1016/j.jcomc.2024.100470.

[2] Dylan S. Cousins, Zach Arwood, Stephen Young, Brandon Hinkle, David Snowberg, Dayakar Penumadu, and Aaron P. Stebner. Infusible thermoplastic composites for wind turbine blade manufacturing: Fatigue life of thermoplastic laminates under ambient and low-temperature conditions. *Advanced Engineering Materials*, 25(11), 2023. ISSN 1438-1656 1527-2648. doi: 10.1002/adem.202201941.

[3] Duncan Hornsby. Infusible thermoplastic composites for tidal blade and marine applications. Thesis submitted for the degree of Master of Engineering, University of Edinburgh, 2023.

[4] Christos J. Tsenoglou, Sylvia Pavlidou, and Constantine D. Papaspyrides. Evaluation of interfacial relaxation due to water absorption in fiber–polymer composites. *Composites Science and Technology*, 66(15):2855–2864, 2006. ISSN 02663538. doi: 10.1016/j.compscitech.2006.02.022.

[5] Jack Wright. A comparative analysis: Room temperature welding of acrylic resin/glass fibre composites and adhesive bonding for thick bond lines in wind turbine blades. Thesis submitted for the degree of Master of Engineering, University of Edinburgh, 2024.

[6] Alp Bolluk, Machar Devine, James A. Quinn, and Dipa Ray. Repair of acrylic/glass composites by liquid resin injection and press moulding. *Com-*

posites Part B: Engineering, 281:111513, 2024. ISSN 1359-8368. doi: https://doi.org/10.1016/j.compositesb.2024.111513.

[7] Winifred Obande, Kit O'Rourke, Danijela Stankovic, Anna Lykkeberg, Jennifer A. Garden, Conchúr Ó Brádaigh, and Dipa Ray. Multi-stage, in-situ polymerisation for low-exotherm, liquid resin infusion of thick thermoplastic laminates at room temperature. *Composites Communications*, 45:101788, 2024. ISSN 2452-2139. doi: https://doi.org/10.1016/j.coco.2023.101788.

Appendix B

Seawater Ageing—Stress-Strain Curves

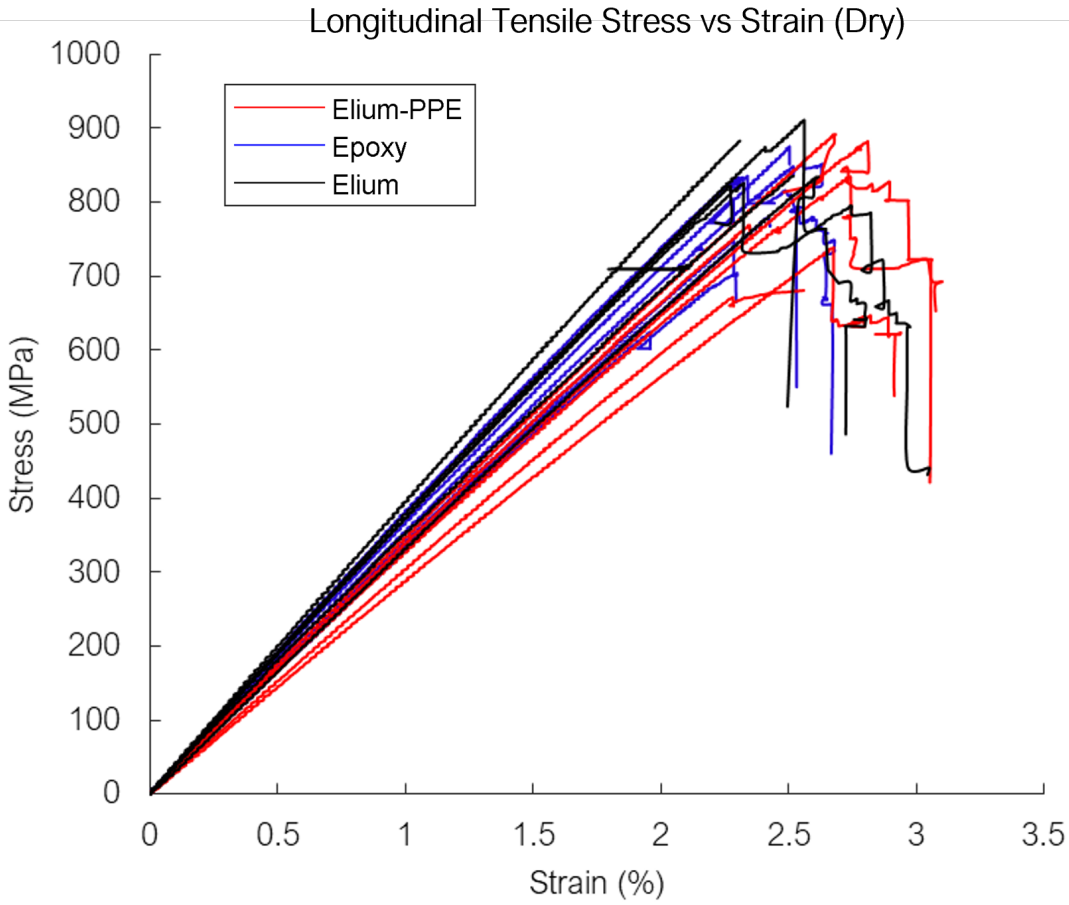

Figure B.1: *All stress-strain curves of dry 0° tensile coupons, manufactured with GF1-MCS reinforcement. Note that the stress values have not been normalised to the FVF.*

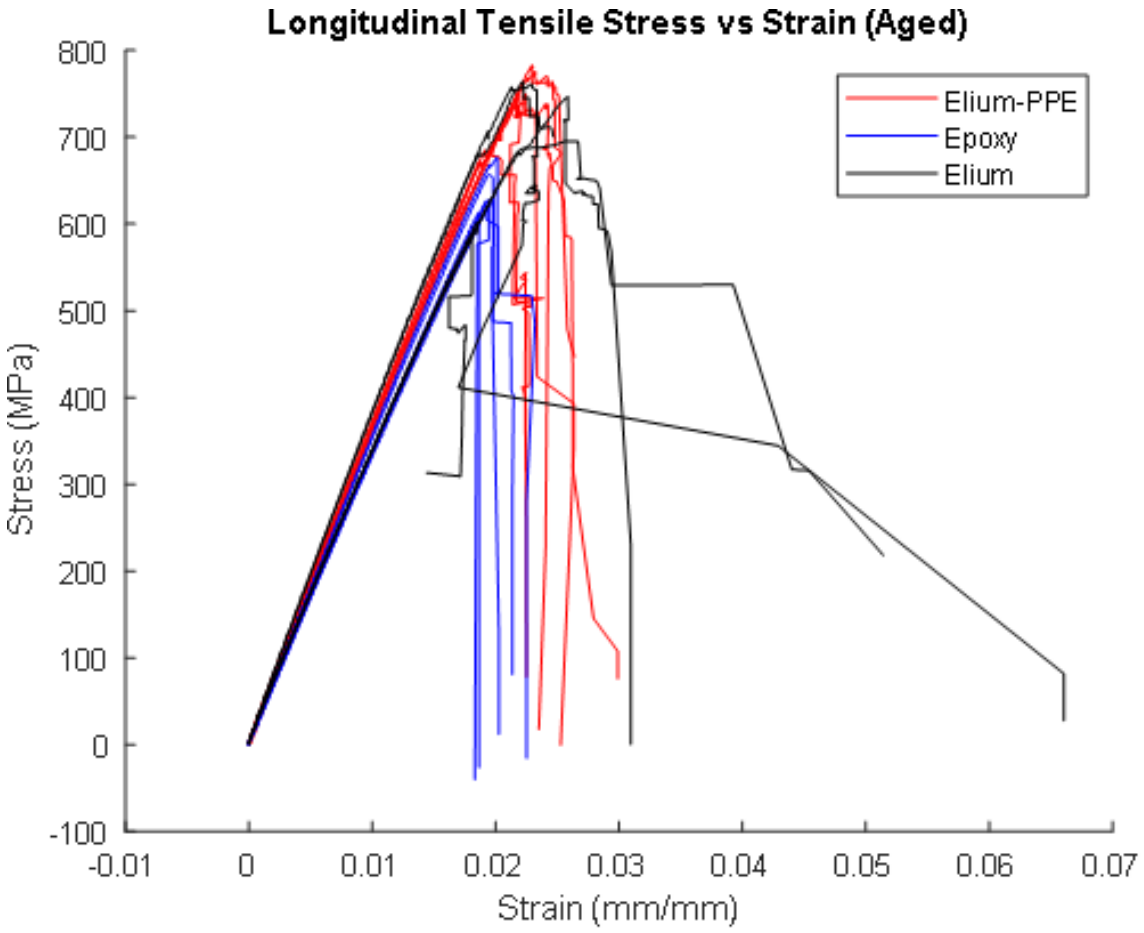

Figure B.2: *All stress-strain curves of aged 0° tensile coupons, manufactured with GF1-MCS reinforcement. Note that the stress values have not been normalised to the FVF.*

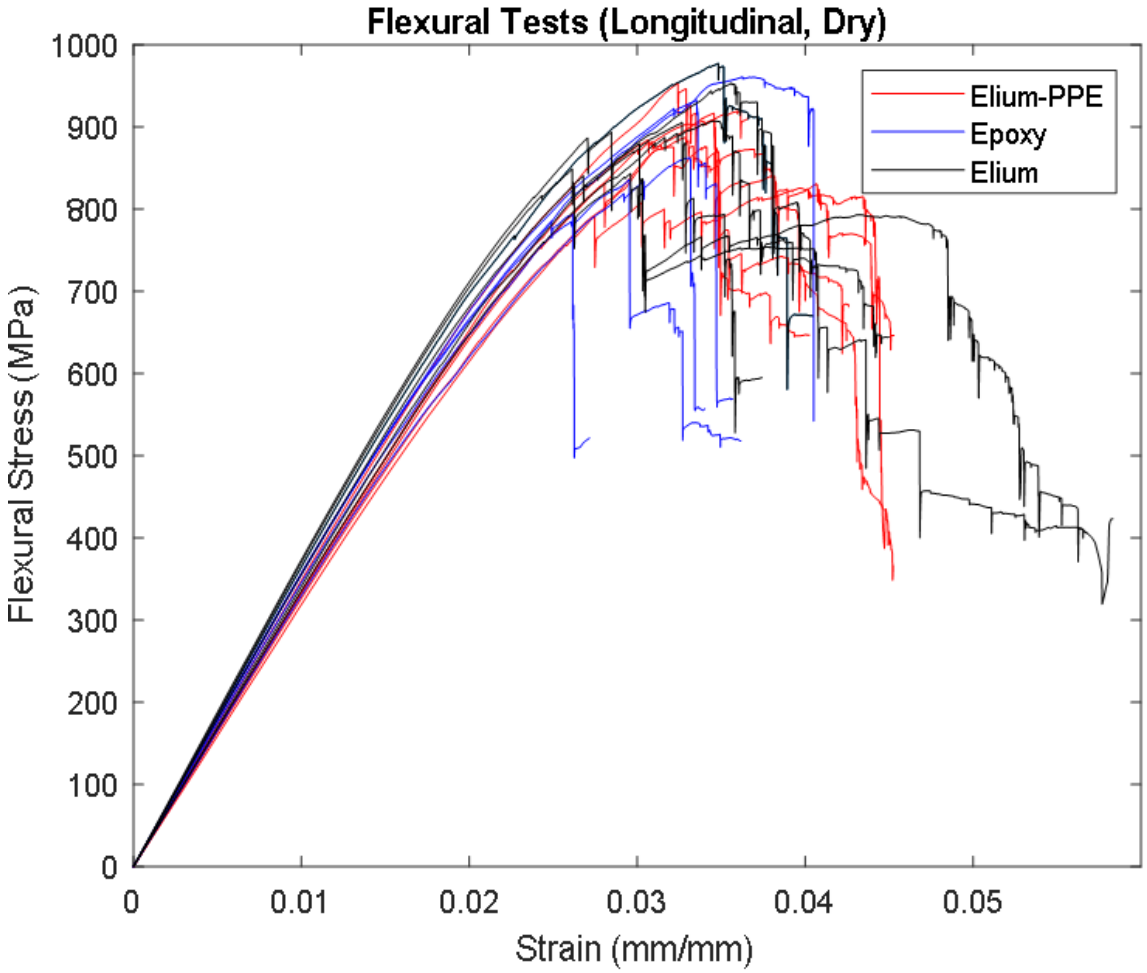

Figure B.3: *All stress-strain curves of dry 0° flexure coupons, manufactured with GF1-MCS reinforcement. Note that the stress values have not been normalised to the FVF.*

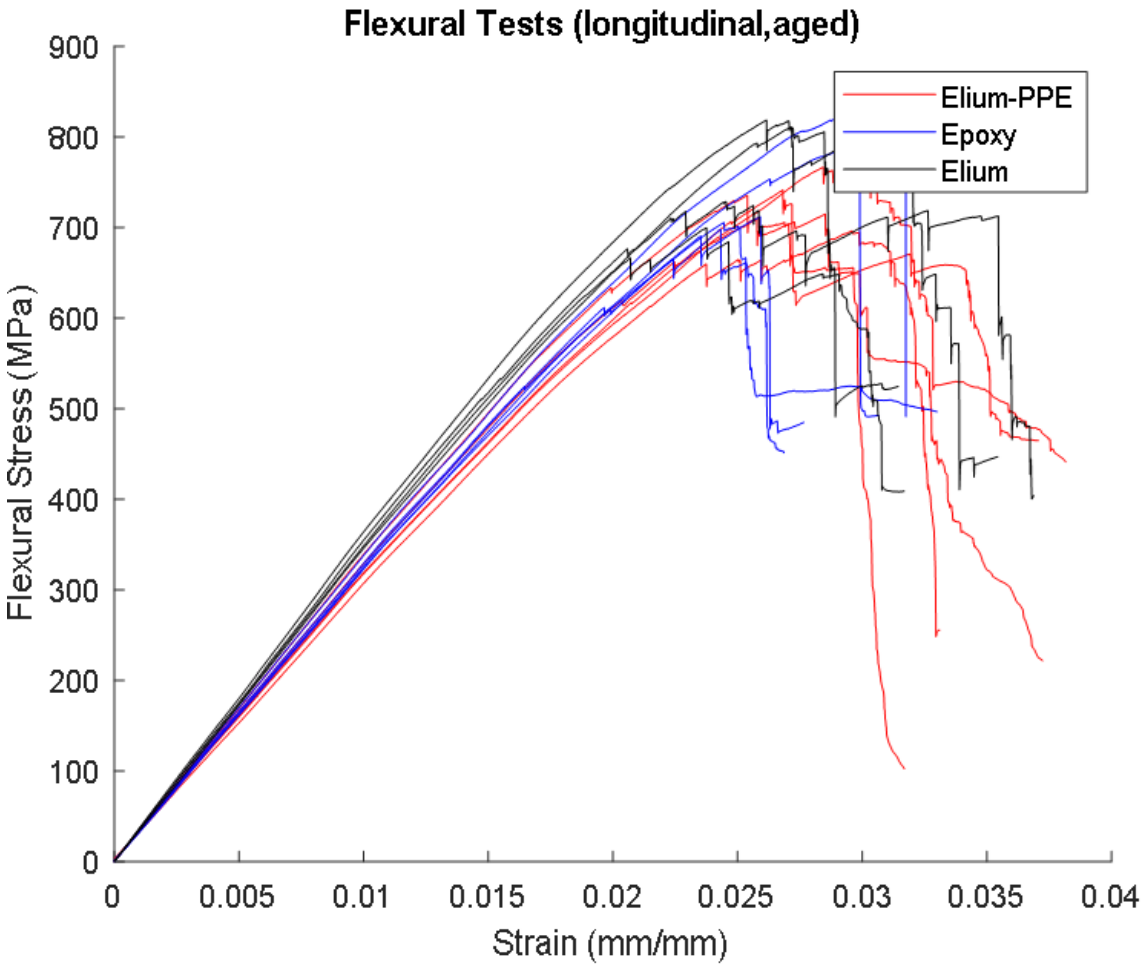

Figure B.4: *All stress-strain curves of aged 0° flexure coupons, manufactured with GF1-MCS reinforcement. Note that the stress values have not been normalised to the FVF.*

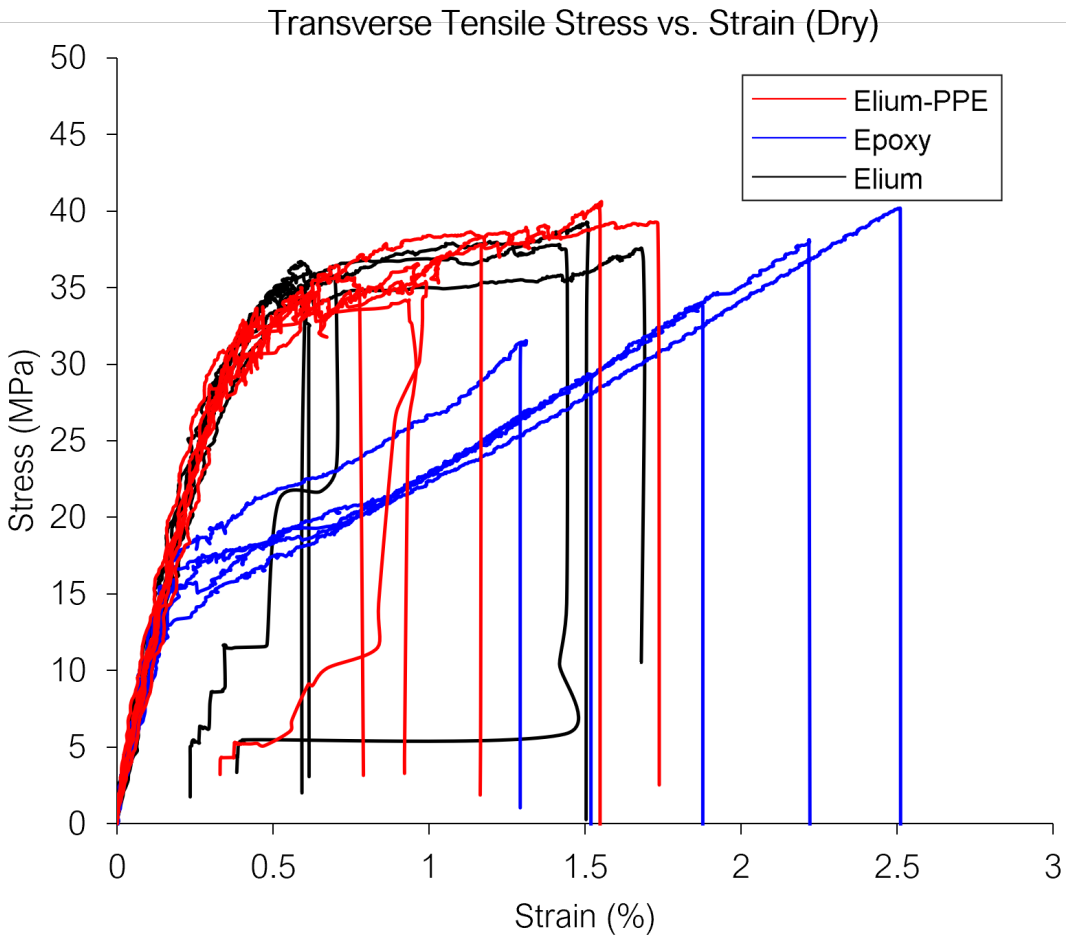

Figure B.5: *All stress-strain curves of dry 90° tensile coupons, manufactured with GF1-MCS reinforcement.*

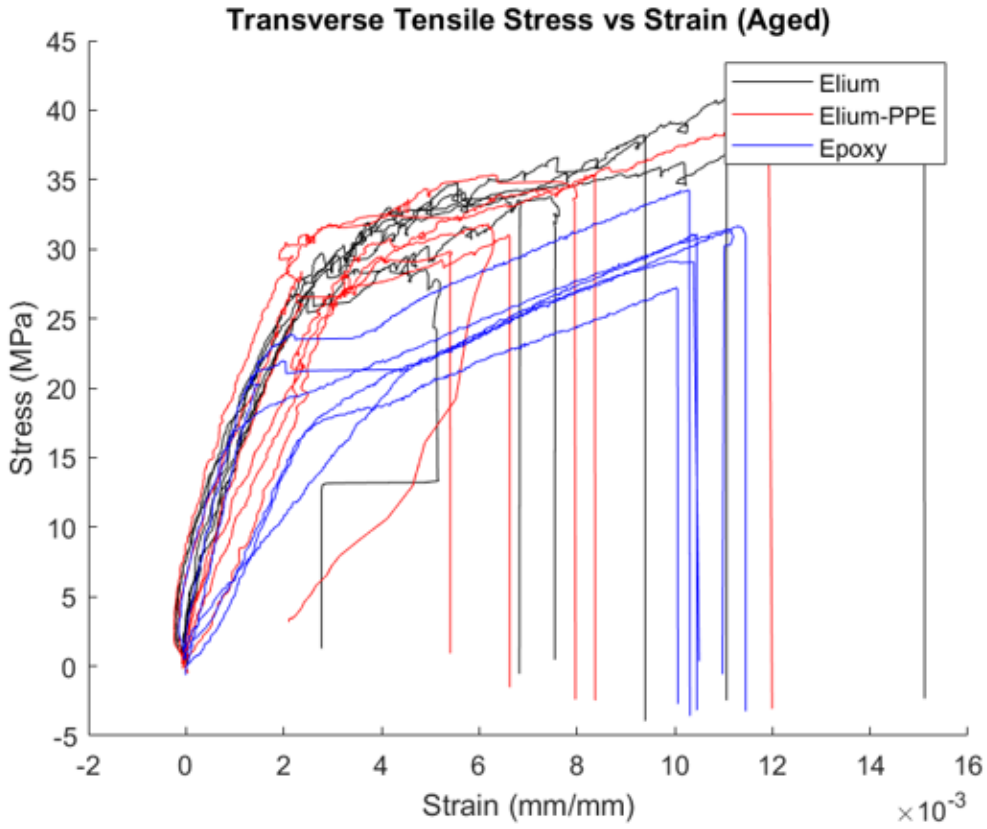

Figure B.6: *All stress-strain curves of aged 90° tensile coupons, manufactured with GF1-MCS reinforcement.*

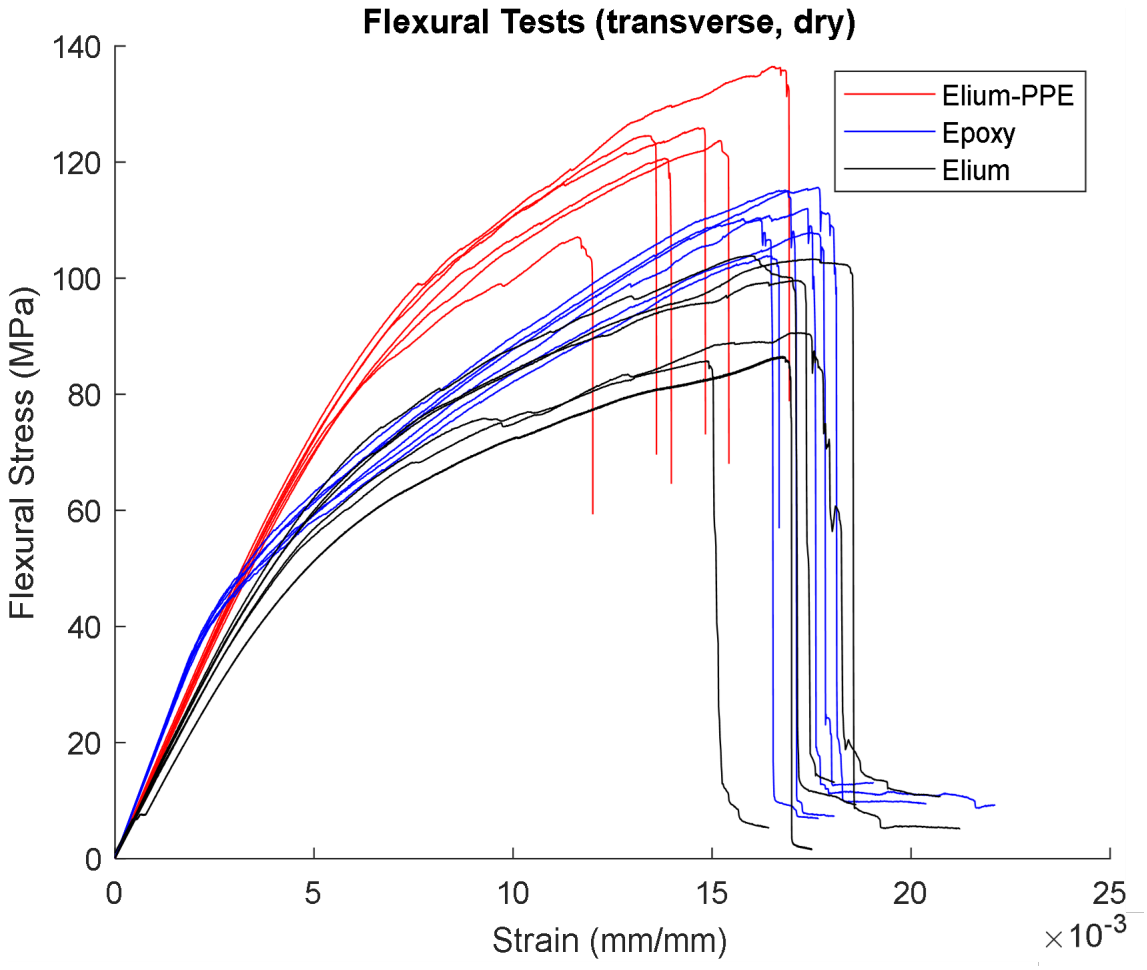

Figure B.7: *All stress-strain curves of dry 90° flexure coupons, manufactured with GF1-MCS reinforcement.*

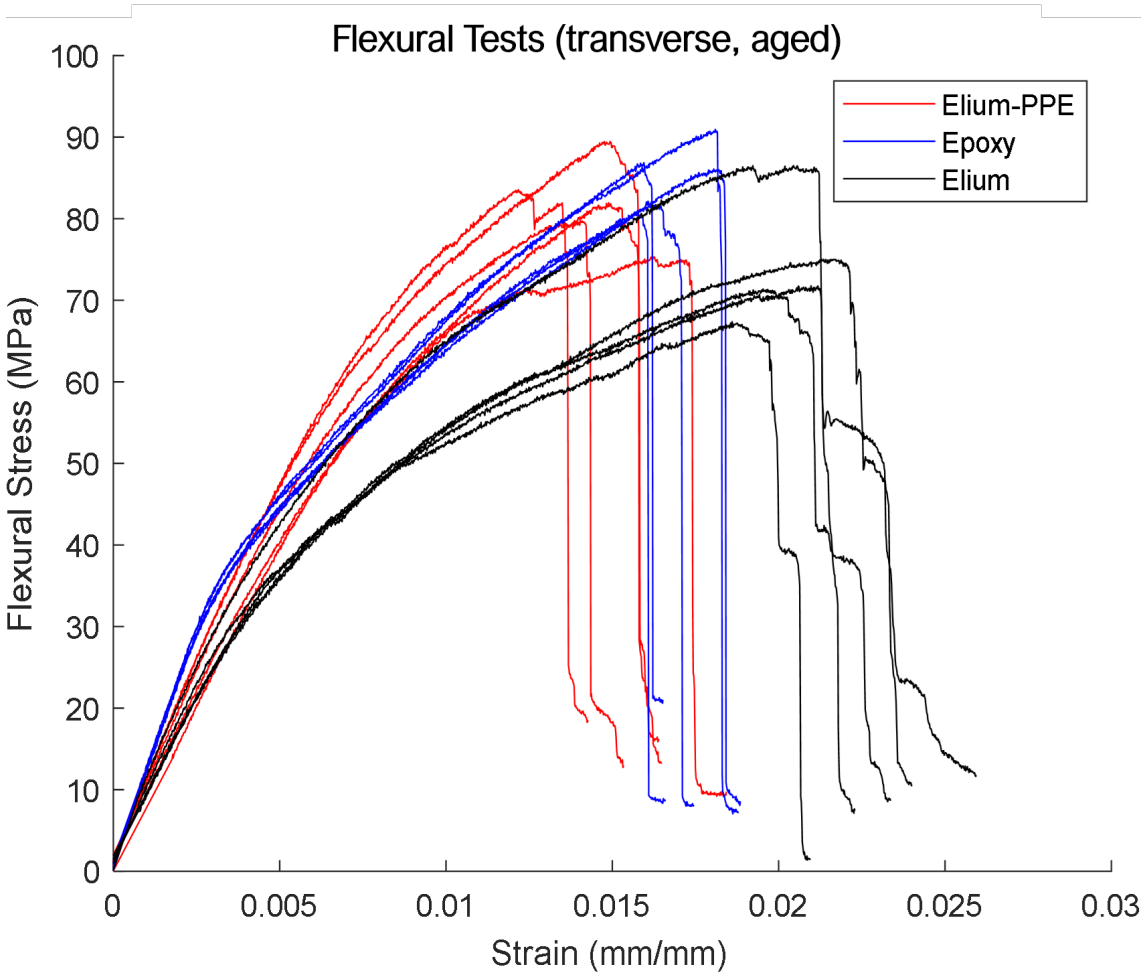

Figure B.8: *All stress-strain curves of aged 90° flexure coupons, manufactured with GF1-MCS reinforcement.*

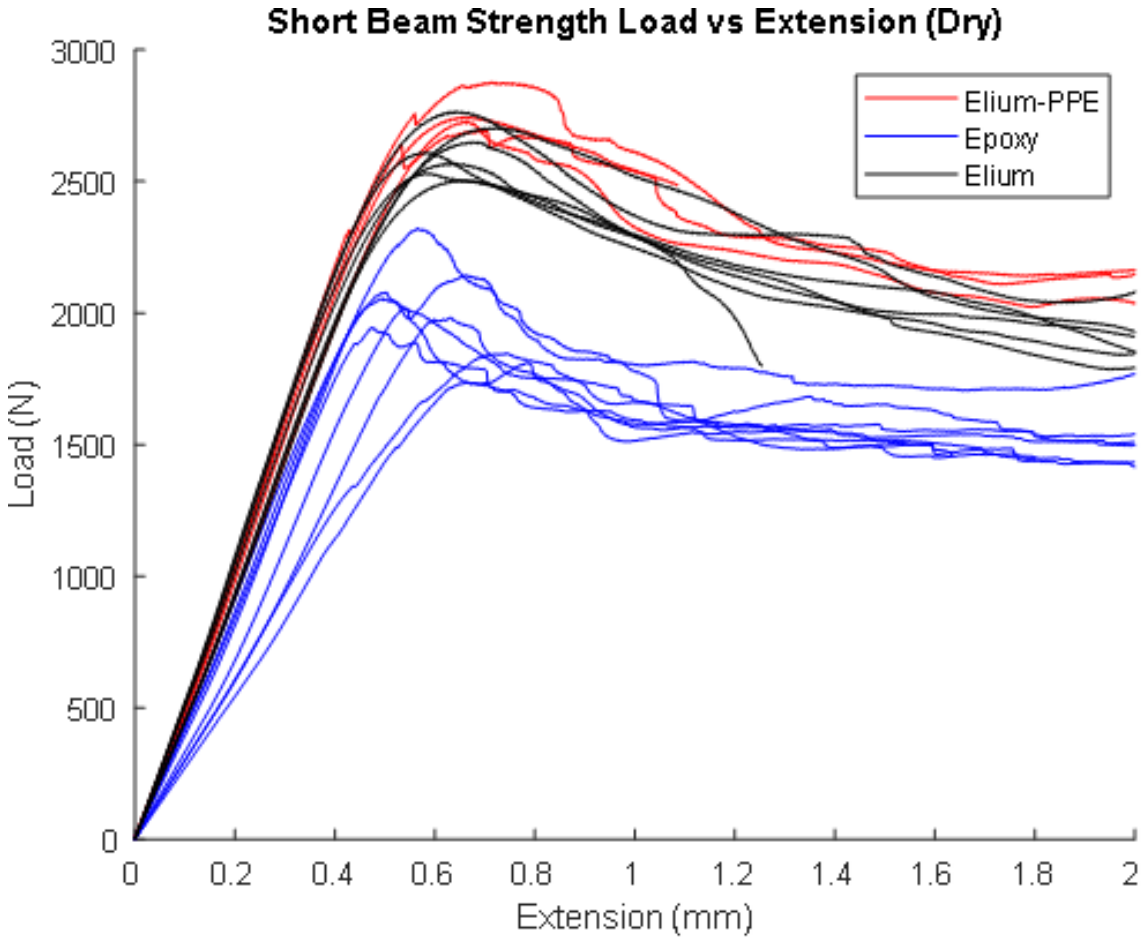

Figure B.9: *All stress-strain curves of dry SBS coupons, manufactured with GF1-MCS reinforcement.*

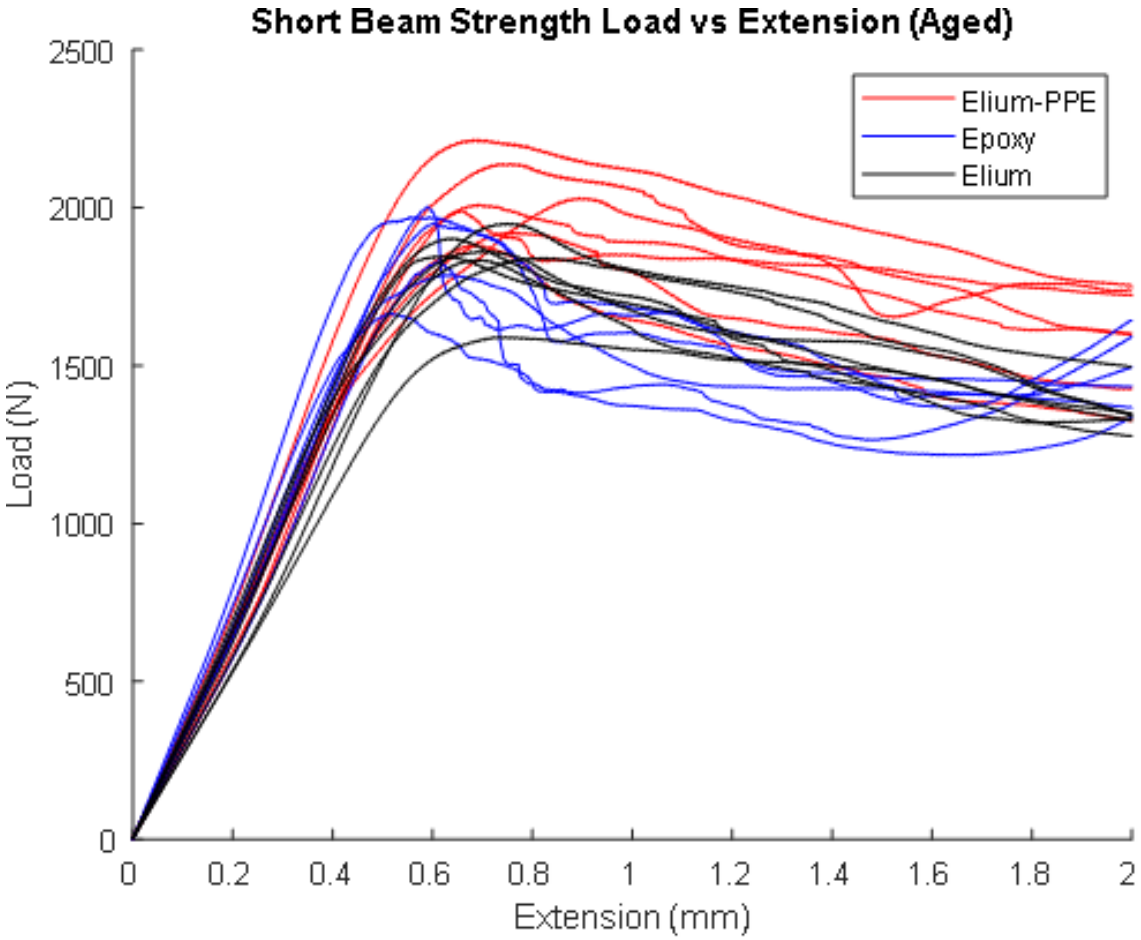

Figure B.10: *All stress-strain curves of aged SBS coupons, manufactured with GF1-MCS reinforcement.*

Appendix C

Published Papers

Composites Part B 263 (2023) 110879

Contents lists available at ScienceDirect

Composites Part B

journal homepage: www.elsevier.com/locate/compositesb

Seawater ageing of thermoplastic acrylic hybrid matrix composites for marine applications

Machar Devine, Ankur Bajpai, Winifred Obande, Conchúr M. Ó Brádaigh, Dipa Ray *

School of Engineering, Institute for Materials and Processes, The University of Edinburgh, Sanderson Building, Robert Stevenson Road, Edinburgh, EH9 3FB, Scotland, United Kingdom

ARTICLE INFO

Handling Editor: Dr Uday Vaidya

Keywords:
Thermoplastic resin
Environmental degradation
Fibre/matrix bond
Mechanical testing
Water ageing

ABSTRACT

Increasing usage of polymer composite materials necessitates the development of recyclable alternatives to traditional thermoset matrices or new techniques for recycling these materials. One family of promising recyclable matrices are the room temperature infusible acrylic resins, known commercially as Elium®. If these new materials are to be used in the tidal stream energy and shipping sectors, they must be able to withstand long-term immersion in seawater without significant losses in mechanical properties. In this study, accelerated seawater ageing is applied to acrylic/glass fibre and modified acrylic/glass fibre composites along with a traditional epoxy/glass fibre baseline. The mechanical properties (tensile, flexural, and short beam) are compared before and after ageing, and electron microscopy is used to examine fracture surfaces to determine the effects of water ingress on fracture propagation. In addition, the diffusion coefficients of the composites in seawater are compared and the changes in glass transition temperatures are used to determine the effects of plasticisation.

1. Introduction

The use of composite materials is rapidly growing, and as a result, so is the volume of composite waste. For example, it is estimated that onshore wind turbine blades alone will create over 43 million tonnes of composite waste by 2050 [1]. The usage of composites in marine sectors is also expected to grow to reach carbon neutrality targets; for example, the deployment of tidal stream turbines which use fibre-reinforced composite materials in their blades is required to expand fiftyfold [2], and decarbonisation of the shipping sector may include a switch to composite materials [3]. As these are generally large structures, they are currently manufactured with room-temperature infusible liquid thermoset resins via vacuum infusion. Such thermoset composites are non-recyclable and are therefore disposed of in landfill or through incineration with the possibility of energy recovery, for example in cement kilns. It is therefore important to find recyclable alternatives that will allow increased production of large structures at room temperature and that perform equally well under seawater.

Traditional thermoplastic composites are not suitable for manufacturing very large structures, as they typically need the application of positive pressures (more than atmospheric vacuum) for the production of void-free laminates, due to their elevated melt viscosity and melting temperature. These positive pressures are normally applied by a press or autoclave, which is not economically feasible for very large structures such as ship sections and tidal energy blades [4]. Liquid acrylic resins (Elium®) from Arkema have the ease of processing of a thermoset resin (low viscosity at room temperature), but since they are thermoplastics, they can be recycled via crushing and heating [4], separation of the fibres and matrix through dissolution [5–7] or pyrolysis [8], or by thermoforming of the continuous fibre composite [5,9]. The resins are largely composed of methyl-methacrylate monomers which are infused into reinforcement and polymerised in situ during composite manufacturing. Their room temperature processibility, low viscosity and promising mechanical properties [10] may make them a drop-in replacement for epoxy infusion resins.

A key consideration for the application of acrylic resins in the shipping and tidal sectors is their water absorption behaviour and retention of mechanical properties, even after a service life on the order of decades. The water ageing behaviour of acrylic composites reinforced with both glass fibres (GF) and carbon fibres (CF) has been reported by other researchers, but there is significant variation in the reported changes due to differences in materials, layup and ageing conditions. For example, Davies et al. [11] found that woven 0/90° GF/acrylic coupons exhibited a decrease in tensile modulus by 11% and tensile strength by

* Corresponding author.
E-mail address: dipa.roy@ed.ac.uk (D. Ray).

https://doi.org/10.1016/j.compositesb.2023.110879
Received 14 December 2022; Received in revised form 19 June 2023; Accepted 27 June 2023
Available online 28 June 2023

50% after 18 months of ageing in 60 °C saltwater. The reported decreases in 0/90° CF/acrylic laminates, however, are smaller. Bel Haj Frej et al. [12] measured losses of 6% in tensile modulus and 10% in tensile strength of non-woven 0/90° CF/acrylic coupons after 6 months of ageing in distilled water at 70 °C. Barbosa et al. [13] measured a decrease of only 4% in tensile modulus for woven 0/90° woven CF/acrylic coupons, and even a small increase of 3% in tensile strength, after ageing in distilled water at 80 °C for 8 weeks. Consistently large reductions in short beam (shear) strength (SBS) have been measured by several authors: Bel Haj Frej et al. [12] measured a 43% reduction in SBS for CF/acrylic composites and Nash et al. [3] saw a similar 38% reduction for GF/acrylic coupons.

Two main causes of degradation in mechanical properties of acrylic-matrix composites have been identified by several authors [3,12–14] as swelling and plasticisation of the matrix and degradation of the fibre-matrix interface. The selection of matrix and reinforcement is therefore crucial to a composite's performance under water.

Acrylics are not considered high-performance matrices in structural composites. There is therefore an opportunity to improve their performance as composite matrices by hybridising them with other higher-performing engineering thermoplastics. Papers on a hybrid matrix of acrylic resin modified with polyphenylene ether (PPE) have already been published by the current researchers [15,16]. These studies presented enhanced transverse flexural properties, initiation fracture toughness and solvent resistance of GF/acrylic-PPE composites compared to equivalent GF/acrylic composites, while retaining recyclability. This work is a continuation of the aforementioned work and investigates the seawater ageing behaviour of the GF/acrylic-PPE composites in comparison with GF/acrylic and an equivalent thermoset GF/epoxy composite. The diffusion of water in the composites is studied along with the drop in mechanical properties in the aged samples. The aged and dry samples are examined via scanning electron microscopy (SEM) to study the behaviour of the interface due to water ingress. The change in glass transition temperature due to seawater ageing is studied via dynamic mechanical analysis (DMA).

2. Materials and methods

2.1. Manufacturing and sample preparation

Three types of unidirectional (UD) GF-reinforced laminates were manufactured: GF/acrylic, GF/acrylic-PPE and GF/epoxy. GF/acrylic laminates were made with an acrylic resin (Elium® 188 O, Arkema) and peroxide initiator (BP-50-FT, United Initiators) in a 100:3 ratio by weight. GF/acrylic-PPE laminates were made using 5 wt% of PPE oligomer with methacrylate end functionality (NORYL™ SA9000 Resin, SABIC) in the same acrylic resin, again with the BP-50-FT peroxide initiator in a 100:3 ratio. GF/epoxy laminates were prepared using SR 1710 Injection epoxy resin and SD 7820 hardener (Sicomin) in a 100:36 ratio by weight. The same unidirectional non-crimp E-glass fibre fabric (TEST2594-125-50, Ahlstrom-Munksjö) with multi-compatible sizing was used for all matrix types, containing 600 g/m^2 of 0° fibres, 36 g/m^2 of 90° fibres and 10 g/m^2 of polyester stitching.

All laminates were prepared via a standard vacuum resin infusion route. Laminate thicknesses were 1.5 mm for tensile testing, 4 mm for flexural testing and SBS and 2 mm for diffusion coefficient measurement. After infusion, the laminates were left to polymerise at room temperature for 24 h. The GF/epoxy laminates were then subject to a freestanding post-cure at 60 °C for 8 h followed by 100 °C for 4 h according to the manufacturer's recommendations. The GF/acrylic and GF/acrylic-PPE laminates did not require any post-cure.

2.2. Seawater ageing

Composite specimens were subject to seawater ageing. Filtered natural seawater, collected from Gullane Beach in the Firth of Forth, Scotland, was maintained at 50 °C and samples for mechanical testing were immersed for 3 months. Evaporated water was topped up with fresh water to maintain a constant water level. Aged specimens were kept immersed in seawater at room temperature until testing to prevent them from drying. Each of the mechanical tests detailed in the following sections was conducted on dry specimens as well as on aged specimens. In addition to specimens for mechanical testing, three nominally 160 × 160 × 2 mm specimens each of GF/acrylic, GF/acrylic-PPE and GF/epoxy were used to determine the diffusion coefficient and maximum water uptake. They were first oven-dried at 50 °C for 5 days and then immersed in seawater at 50 °C for 5 months. The specimens were removed from the water bath at 24-h intervals, their surfaces were dried with a cloth and their weights were measured.

At each measurement interval, the percentage mass increase was calculated according to Equation (1) (ASTM D5229M) in which $M(t)$ is the percentage increase in mass caused by water uptake at time t, W_i is the measured specimen mass at time t and W_o is the oven-dry specimen mass.

$$M(t) = \frac{W_i - W_o}{W_o} \times 100 \tag{1}$$

A Fickian diffusion curve of the form in Equation (2) (ASTM D5229M) where h is the specimen thickness was then fitted, and values for the diffusion coefficient at 50 °C (D_z) and equilibrium water content (M_m) were taken from the fitted curve.

$$M(t) = M_m \left\{ 1 - exp\left[-7.3 \left(\frac{D_z t}{h^2} \right)^{0.75} \right] \right\} \tag{2}$$

2.3. Testing

2.3.1. Mechanical tests

Tensile testing (0° and 90°) was carried out according to ASTM D3039, using an MTS Criterion Model 45 300 kN test system. Specimens were spray-painted with a black and white speckle pattern to allow strain measurements to be taken with a video extensometer and the 0° tensile specimens were tabbed with an epoxy-glass composite. All tensile tests were conducted with a crosshead extension rate of 2 mm/min.

Flexural testing (0° and 90°) was carried out according to ASTM D7264 on an Instron 3369 test system using a span-to-thickness ratio of 32:1. The crosshead extension rate was set at 7 mm/min, and mid-span deflection was taken to be the crosshead extension. Short beam strength tests were performed in accordance with ASTM D2344, using a span-to-thickness ratio of 4:1. The crosshead extension rate was set at 1 mm/min.

2.3.2. Fibre volume fraction

Fibre volume fraction (FVF) and void fraction of the composites were measured using a matrix burn-off method according to ASTM D3171. The densities of the composite coupons, matrices and glass fibres were measured using a displacement method (ASTM D792).

2.3.3. Scanning electron microscopy

Scanning electron microscopy (SEM) was carried out using a JEOL JSM series microscope on fragments of 0° tensile specimens after fracture. Samples were sputter-coated with 30 nm of gold before imaging at 15 kV.

2.3.4. Dynamic mechanical analysis

The glass transition temperatures of both dry and aged specimens were measured using dynamic mechanical analysis (DMA). A TA Instruments Discovery DMA 850 was used in 3-point bend mode at a frequency of 1 Hz and an amplitude of 20 μm. Specimens were 50 × 13 × 1.5 mm with 0° fibres in the span direction. A ramp rate of 1 °C/min between ambient temperature and 180 °C was selected and 1 specimen

was tested for each composite type, both dry and saturated with water. Aged specimens were removed from the water bath, wiped to remove surface water and then immediately tested.

3. Results and discussion

3.1. Water absorption

A graph of percentage mass increase against the square root of time is presented in Fig. 1. The experimental data as well as the fitted diffusion curves are shown in Fig. 1 and the resulting M_m and D_z are given in Table 1. Each data point is the average increase of 3 specimens.

The GF/acrylic and GF/acrylic-PPE both exhibited Fickian behaviour—a linear increase in absorbed water when plotted against $\sqrt{t}$ which plateaus after reaching saturation (Fig. 1). Although a Fickian diffusion curve is also fitted to the GF/epoxy data, there is a slight deviation from purely Fickian behaviour as there was an initial period of more rapid absorption followed by a more gradual mass increase after approximately 4 days (600 $\sqrt{s}$). The diffusion coefficients of GF/acrylic, GF/acrylic-PPE and GF/epoxy composites are given in Table 1 along with diffusion coefficient values of acrylic-matrix composites and unreinforced acrylic resin reported in published literature. The diffusion in GF/epoxy was an order of magnitude slower than in GF/acrylic and GF/acrylic-PPE.

These differences may be explained by considering the differences in structure and chemistry between the polymers and relating these to theories of diffusion. The structure of the acrylic matrix is typical of an amorphous thermoplastic and the epoxy has the typical structure of a thermoset. The structure of acrylic-PPE (5 wt% PPE), depicted in Fig. 2 and Fig. S1, has been previously investigated by Obande et al. [15] and is believed to consist of PPE-rich cross-linked zones surrounded by acrylic-rich regions. The PPE with methacrylate end functionality reacts with the acrylic monomers during in-situ polymerisation to form crosslinks between acrylic chains.

Diffusion can be modelled using the free volume of the material, or by modelling the interaction between the polymer and the diffusant. In the *free volume theory*, the diffusant is assumed not to interact strongly with the material and instead diffuses through voids in the composite and the free volume in the matrix, to which the diffusion rate is highly sensitive [18,19]. In the *polar interaction theory,* the diffusant forms bonds with polar sites in the polymer and water diffuses by hopping between these sites [18].

Free-volume diffusion is expected to occur in all three composites in this study, but the extent of free volume is likely to be less in GF/epoxy due to its 3D crosslinked network. Fujii et al. [20] demonstrated via quasi-elastic neutron scattering studies that the majority of water in PMMA is *free-water,* which occupies matrix free-volume and interacts little with the polymer. We expect similar behaviour in acrylic and acrylic-PPE matrix composites, shown schematically in Fig. 2a(ii) and b (ii). Even if free-volume diffusion does not occur through the polymer, voids introduced by resin infusion and the presence of fibres also provide a route for water ingress. For example, in void-free epoxy, free-volume diffusion is not expected to be significant, but free water content increases as more voids are introduced [21].

Additionally, polar interactions occur in all three matrices. In PMMA around 28% of water molecules exist as *intermediate water* [20] which interacts through hydrogen bonding with carbonyl groups on the PMMA side chains (Fig. 2a(i) and b(i)). This interaction results in a slower motion of water molecules than in free water. In epoxy, water interacts with the hydroxyl groups attached to the polymer backbone and amine groups of the curing agents (Fig. 2c) [22]. Epoxy/amine resins such as the Sicomin SR1710/SD7820 system used in this study are regarded as hydrophilic due to these groups, and hence the interaction with water is stronger than in PMMA.

In this study, GF/acrylic and GF/acrylic-PPE diffusion coupons both had higher void contents than the GF/epoxy, as displayed in Fig. 1 and Table 2, which could explain the higher D_z values of the thermoplastic composites. In addition to a higher void content, the acrylic matrices are

Table 1
The diffusion coefficients measured in this study along with values from literature for comparison.

Material	Ageing Conditions	D_z ($\times 10^{-12}$ $m^2\ s^{-1}$)	M_m (%)	Source
GF/acrylic $[0°]_4$	50 °C seawater 5 months	1.81	0.81	Current work
GF/acrylic-PPE $[0°]_4$	50 °C seawater 5 months	3.40	0.91	Current work
GF/epoxy $[0°]_4$	50 °C seawater 5 months	0.15	0.63	Current work
Acrylic/Carbon fibre	70 °C deionised water 6 months	9.62/0.15[a]	1.7/ 5.2[a]	[12]
PMMA Cast resin	60 °C deionised water	4.54	–	[17]
Acrylic (Elium 190) Cast resin	60 °C seawater 365 days	4.23	1.90	[14]

[a] A dual Fickian model was fitted. Both diffusion coefficients and values for M_m are presented.

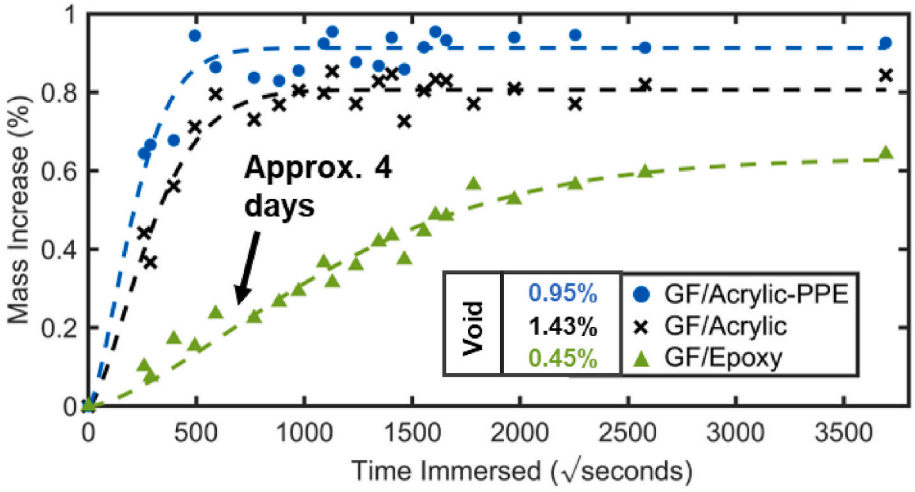

Fig. 1. The water absorption curves of the three composites with their corresponding void volume fractions. The experimental data are presented as points and the fitted Fickian diffusion curves as dotted lines. A decrease in the diffusion coefficient is visible in the GF/epoxy after approximately 4 days.

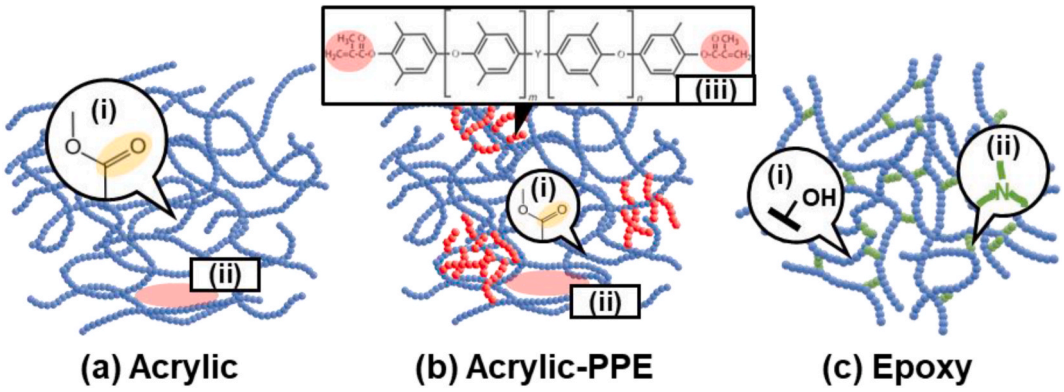

Fig. 2. A comparison of the polymer and composite structures as relevant to the diffusion of water. (a) Acrylic polymer with (i) polar carbonyl groups with the acrylic chains and (ii) free volume. (b) Acrylic-PPE with (i) carbonyl groups in the acrylic chains, (ii) free volume and (iii) PPE oligomers with methacrylate end groups highlighted in red. (c) Epoxy has (i) hydroxyl groups and (ii) amine groups from the hardener. (For interpretation of the references to colour in this figure legend, the reader is referred to the Web version of this article.)

Table 2
Fibre and void volume fractions of composites used for mechanical testing.

	Matrix	Fibre fraction (vol%)	Void fraction (vol%)
Diffusion Specimens	Acrylic	56.8 ± 0.4	1.4 ± 0.1
	Acrylic-PPE	55.8 ± 0.3	1.0 ± 0.3
	Epoxy	52.8 ± 0.2	0.5 ± 0.1
90° Tension Specimens	Acrylic	53.5 ± 0.5	2.1 ± 0.3
	Acrylic-PPE	53.5 ± 0.3	0.8 ± 0.4
	Epoxy	50.9 ± 0.7	1.7 ± 0.5
0° Tension Specimens (Average of 2 Laminates)	Acrylic	53.5 ± 0.8	1.9 ± 0.8
	Acrylic-PPE	54.7 ± 0.8	1.9 ± 0.7
	Epoxy	49.0 ± 1.2	0.4 ± 0.3
0/90° Flexure, Short Beam Strength Specimens	Acrylic	56.4 ± 0.3	1.9 ± 0.4
	Acrylic-PPE	52.7 ± 0.2	1.9 ± 0.3
	Epoxy	54.6 ± 0.3	1.1 ± 0.1

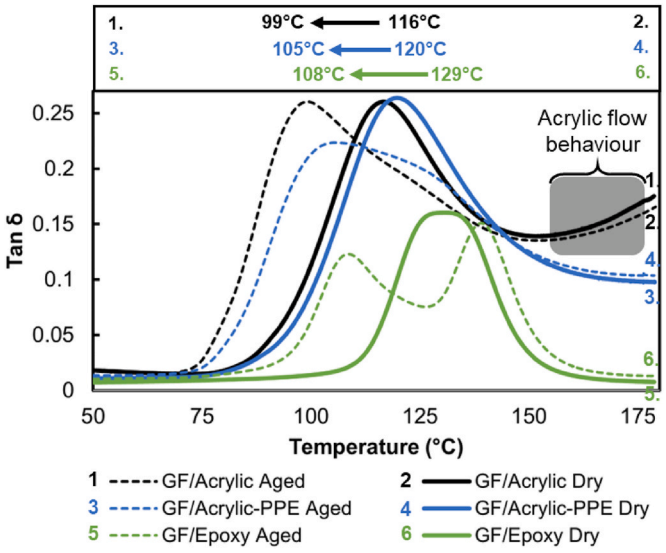

Fig. 3. (Top) The T_g of GF/acrylic, GF/acrylic-PPE and GF/epoxy before and after ageing as determined via DMA. (Bottom) Tan δ vs. temperature for the dry (solid lines) and aged (dotted lines) coupons. In the aged specimens, a shoulder or secondary peak is present due to drying. Flow behaviour of the acrylic matrix in the dry and aged GF/acrylic is highlighted (curves 1 and 2).

thermoplastic amorphous polymers and are therefore likely to have more free volume than the crosslinked epoxy matrix [17,22]. The GF/acrylic-PPE, however, shows a higher diffusion rate and final water content than the GF/acrylic, whereas the lower void fraction measured in the GF/acrylic-PPE would correspond to a lower diffusion rate under the free-volume theory. The differences in the polymer structure induced by the addition of PPE oligomers (Fig. 2b) could increase the free volume and explain this observation. Considering the polar interaction theory, an increase in hydrophilicity is associated with slower diffusion [22,23] and non-Fickian absorption behaviour, as noted in the GF/epoxy specimens in this study due to a mixture of free-volume and polar interaction diffusion [24,25]. The stronger interaction between the water and epoxy compared with the acrylic could therefore also contribute to the slower diffusion in GF/epoxy.

3.2. Dynamic mechanical analysis

DMA was used to determine the glass transition (T_g) of each composite specimen before and after ageing. Fig. 3 presents the T_g of each composite and the damping parameter (*tan δ*) vs temperature curves of each composite type from which the T_g is derived. The reductions in T_g indicate plasticisation of the matrices caused by the ingress of water [26,27], which is associated with a decrease in matrix modulus and strength. Secondary peaks or shoulders in the *tan δ* curves of the aged specimens are observed in Fig. 3 with the most prominent being in the case of GF/epoxy. This is attributed to drying of the specimens during DMA as observed in other studies [28]. After the drying peak, the *tan δ* curves closely follow the curves of the dry specimens.

The addition of PPE resulted in enhanced thermomechanical properties. Firstly, the T_g of GF/acrylic-PPE was 4 °C higher than that of GF/acrylic when dry (120 °C vs. 116 °C), and 6 °C higher when aged (105 °C vs. 99 °C). The GF/epoxy had a higher T_g of 129 °C when dry and 108 °C when aged, as was expected due to its highly crosslinked structure. Secondly, there is a clear difference in behaviour between the acrylic and the acrylic-PPE composites at temperatures above the T_g in Fig. 3. A rise in tan *δ* after the T_g peak is observed in GF/acrylic which is indicative of the beginning of flow behaviour, but this behaviour is absent in the GF/acrylic-PPE and the GF/epoxy. This difference in the behaviour of GF/acrylic-PPE is due to the presence of intermittent crosslinked regions as depicted in Fig. 2 and Fig. S1. The suppression of flow behaviour through the addition of PPE may have implications in its use at high temperatures and in the fire safety of acrylic-PPE over acrylic, as melting and dripping of thermoplastics during a fire is a known safety hazard [29].

3.3. Mechanical testing

Dry and aged specimens were tested in 0° and 90° tension, 0° and 90° flexure and for SBS. All 0° tensile and 0° flexural properties are normalised to 50% FVF. Representative stress-strain curves are available in Figs. S2–S6.

3.3.1. Fibre and void volume fractions

The densities of the acrylic, acrylic-PPE and epoxy matrices—as measured according to Section 2.3.2—used to calculate the fibre and void volume fractions were 1.18 g/cm^3, 1.15 g/cm^3, and 1.14 g/cm^3 respectively. The density of the glass fibres was similarly measured to be 2.60 g/cm^3. The fibre and void volume fractions of the laminates manufactured for each test are given in Table 2.

3.3.2. Tension

As shown in Fig. 4a, the 0° tensile moduli were not decreased by water ageing, and the marginal increases after ageing are considered within experimental error. The 0° modulus is dominated by the fibres which are not significantly affected by ageing; therefore, the moduli remain approximately constant. In the dry specimens, the GF/epoxy had a 9% and 4% higher strength than GF/acrylic and GF/acrylic-PPE respectively. The decrease due to ageing is highest in GF/epoxy, however—21% versus 11% and 13% drops in GF/acrylic and GF/acrylic-PPE respectively (Fig. 4b)—therefore the GF/epoxy has the lowest strength after ageing.

In contrast to 0° tension, there were drops in the 90° tensile modulus attributed to matrix plasticisation. The decrease in modulus was largest for GF/epoxy at 18%, nearly double the drop observed in the GF/acrylic and GF/acrylic-PPE (Fig. 4c). Before ageing, the moduli of the three composites were approximately equal, but the larger decrease in GF/epoxy modulus meant that after ageing the GF/acrylic and GF/acrylic-PPE had 14% and 11% higher moduli respectively.

The 90° tensile strengths of the GF/acrylic and GF/acrylic-PPE were higher than GF/epoxy when both dry and aged. Water ageing caused only a small decrease in GF/acrylic strength of 4%, but the decreases in GF/acrylic-PPE and GF/epoxy were larger at 10% and 13% respectively (Fig. 4d). After ageing, therefore, the GF/acrylic's strength was 16% higher than GF/epoxy and 10% higher than GF/acrylic-PPE.

As noted in Section 1, a large decrease in strength (−50%) was reported by Davies et al. [14] for 0/90° woven GF/acrylic composites. The differences in fabric weave, sizing agent, resin (Elium® RT300) and ageing conditions (18 months in 80 °C seawater) used by the authors may account for this discrepancy from the current results.

3.3.3. Flexure

Data from flexural testing is presented in Fig. 5. As was observed in the 0° tensile testing, there were no large decreases in 0° flexural modulus as this is a fibre-dominated property. Only the GF/epoxy saw an appreciable decrease of 6% (Fig. 5a). The 0° flexural strengths saw larger decreases due to ageing, but there weren't significant differences in the percentage drops between materials, which ranged between 15% and 18%.

In 90° flexure, all three composites were affected by ageing. Reductions in 90° flexural modulus were 17% for GF/acrylic, 13% for GF/acrylic-PPE, and 14% for GF/epoxy (Fig. 5c). Even larger drops of 23%, 30% and 22% were observed in the 90° flexural strengths of GF/acrylic, GF/acrylic-PPE, and GF/epoxy respectively (Fig. 5d). The GF/epoxy had the highest 90° flexural modulus when dry at 27% higher than GF/acrylic and 18% higher than GF/acrylic-PPE. Similar differences were seen after ageing when GF/epoxy had a 32% higher modulus than GF/acrylic and a 16% higher modulus than GF/acrylic-PPE. This can be attributed to the high degree of crosslinking present in the epoxy matrix adding rigidity.

Comparing the GF/acrylic and GF/acrylic-PPE, the addition of PPE enhanced 90° flexural properties. GF/acrylic-PPE had an 8% higher modulus when dry and a 13% higher modulus when aged (Fig. 5c). Strength was increased by 22% when dry and 10% when aged (Fig. 5d).

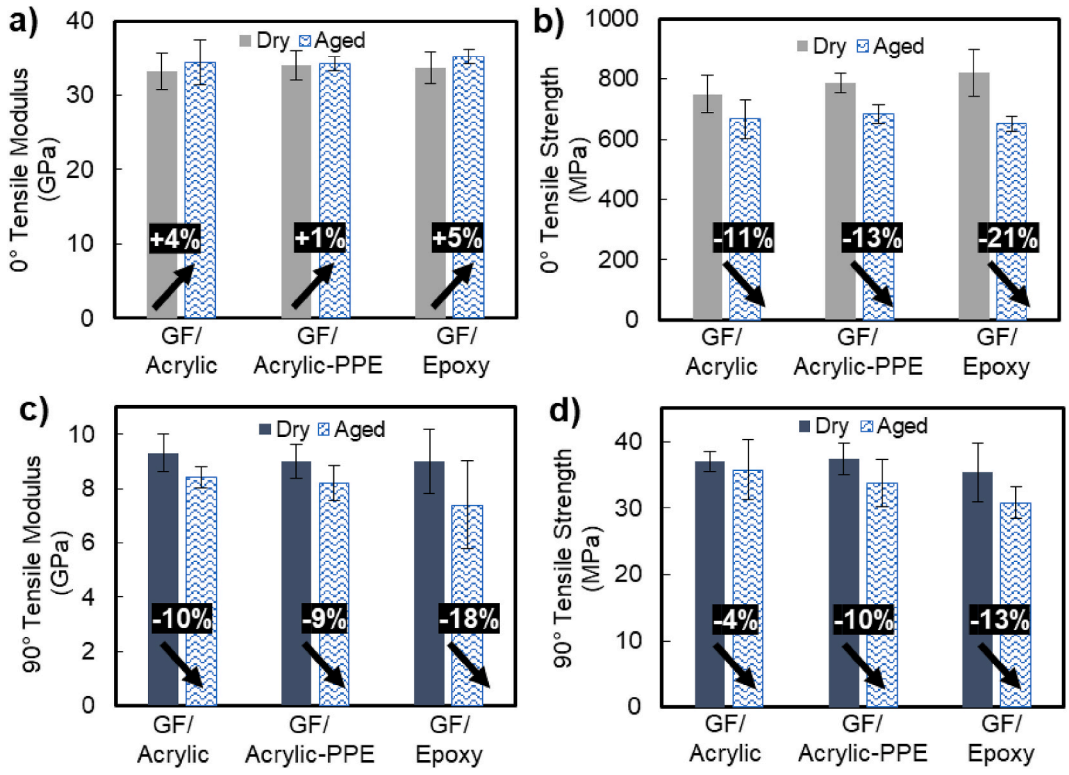

Fig. 4. The tensile properties of the composites are displayed before and after ageing with percentage changes. The 0° tensile properties are normalised to 50% FVF and found in (a) and (b). The 90° tensile properties are in (c) and (d). All error bars are ±1 standard deviation.

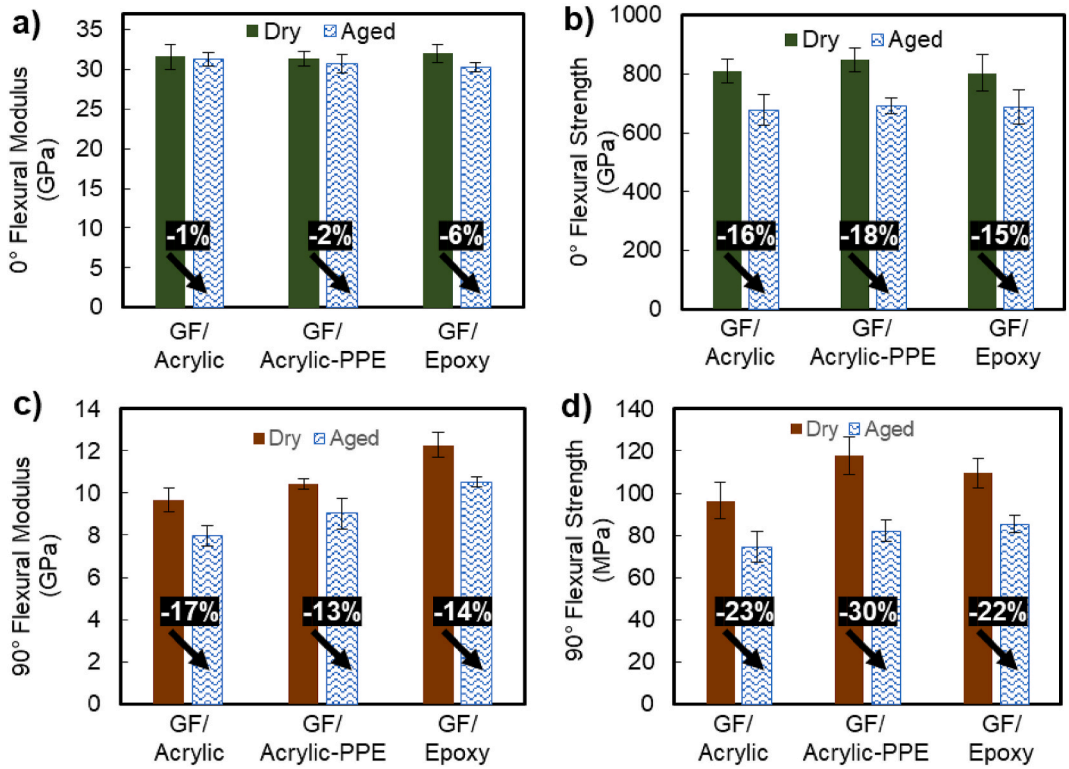

Fig. 5. The flexural properties of the composites are displayed before and after ageing with percentage changes. The 0° flexural properties are normalised to 50% FVF and are found in (a) and (b). The 90° flexural properties are in (c) and (d).

The localised crosslinked regions in the acrylic-PPE matrix therefore have a similar effect to the crosslinking in epoxy, increasing both strength and modulus, but thermoplasticity is retained as acrylic-PPE resin coupons can be reshaped upon heating [15].

3.3.4. Short beam strength

The short beam strength (Fig. 6) of GF/acrylic and GF/acrylic-PPE were equivalent when dry and 28% higher than GF/epoxy. During water ageing, however, GF/acrylic and GF/acrylic-PPE saw larger drops of approximately 30% vs. 13% for GF/epoxy. The strengths after ageing were equivalent for the three materials. The higher drop in SBS in the GF/acrylic and GF/acrylic-PPE can be attributed to both the plasticisation of the matrix and weakening of the fibre/matrix interface [12]. SEM investigations, however, revealed that interfacial debonding during failure played a dominant role, as reported in Section 3.4.

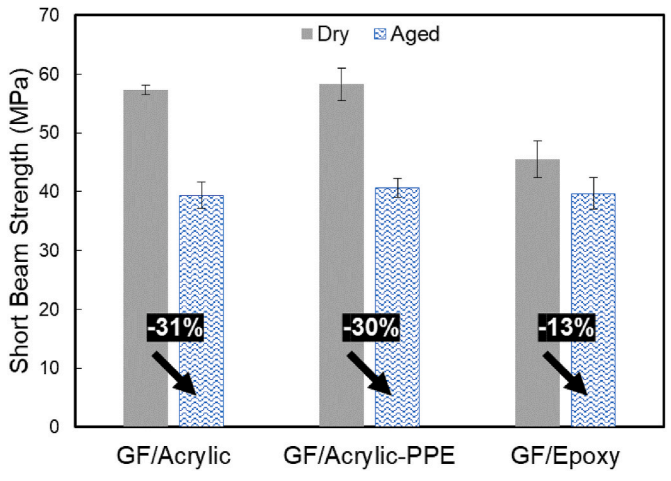

Fig. 6. The SBS of the composites when dry (grey) and aged (blue). The percentage drop in strength due to ageing is highlighted. (For interpretation of the references to colour in this figure legend, the reader is referred to the Web version of this article.)

3.4. SEM and fracture

In this section, the reasons for the observed differences in mechanical properties caused by ageing are explored using SEM. The 0° tensile specimens of all matrices, both dry and aged, failed via longitudinal splitting or *brooming*. The differences in crack propagation between the composites were determined via SEM imaging of failed 0° tensile specimens as shown schematically in Fig. S7. Representative images of 0° tensile fracture surfaces of dry and aged composites are compared in Fig. 7.

3.4.1. GF/acrylic and GF/acrylic-PPE

The images of GF/acrylic and GF/acrylic-PPE show similar fracture behaviour. In the dry state, there is a matrix layer covering the fibres after fracture (Fig. 7a and b). Evidence of the microductility of the thermoplastic matrices is also seen in Fig. 7a and b, as are cusps, which are formed by shear failure during longitudinal splitting. After ageing, however, the fibres appear bare, devoid of any adhered matrix layer.

This difference in behaviour can be explained through the Cook-Gordon mechanism [30–34], which describes the propagation of a crack through an anisotropic, inhomogeneous material as it reaches a weak plane—in this case, the fibre-matrix interface. Immediately at the crack tip in 0° tensile testing, the 0° tensile stress (σ_1) is at a maximum. In addition, shear (τ) and transverse tensile (σ_2) stresses are present, the latter of which reaches a maximum ahead of the crack tip. If the interface is weak relative to the matrix, σ_2 causes interfacial debonding ahead of the crack tip, and the crack propagates along the interface (adhesive failure in Fig. 8). If the interface is strong, shear forces cause longitudinal splitting through the matrix, parallel to the fibres, and the formation of shear cusps (cohesive failure in Fig. 8) [35].

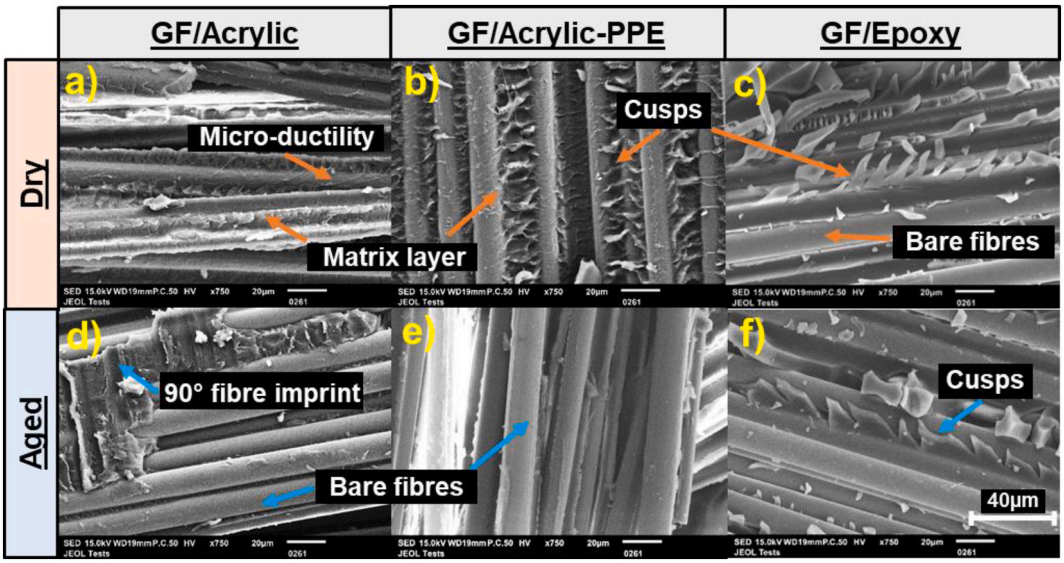

Fig. 7. SEM images of 0° tension specimen fracture surfaces with fractographic features annotated.

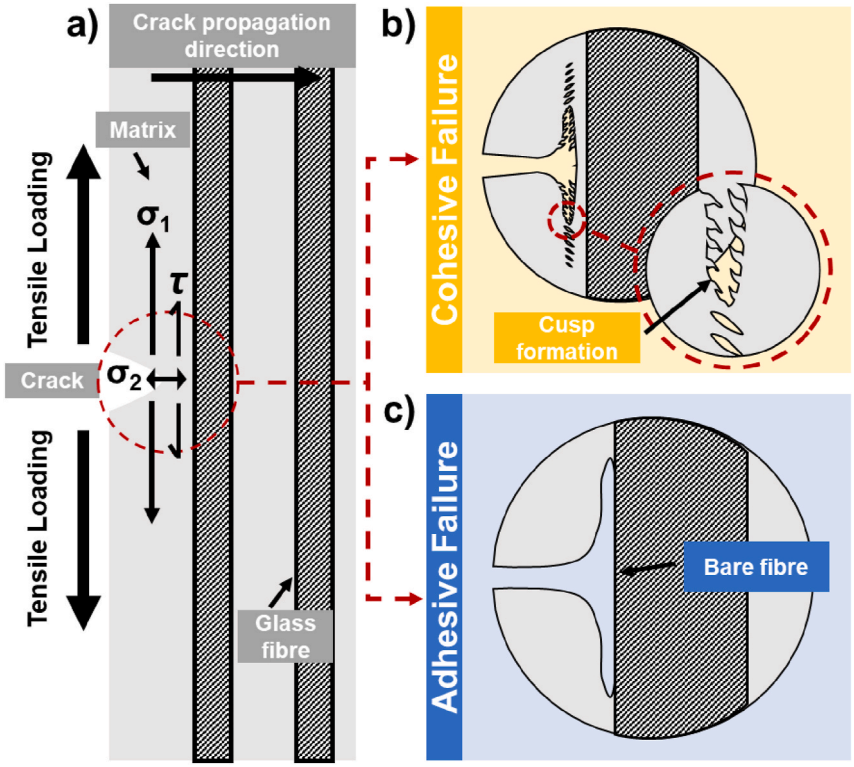

Fig. 8. Fracture propagation under 0° tension with 0° tensile stress (σ_1), 90° tensile stress (σ_2) and shear stress (τ) ahead of the crack tip labelled [30]. Cohesive failure indicates a strong interface and adhesive failure indicates a weak interface relative to the matrix.

Cohesive failure was detected in the dry GF/acrylic and GF/acrylic-PPE specimens (Fig. 7a and b) whereas adhesive failure was detected in the aged GF/acrylic, the aged GF/acrylic-PPE and both dry and aged GF/epoxy specimens (Fig. 7c–f). The GF/acrylic and GF/acrylic-PPE therefore have a strong interface when dry and a weak interface after ageing. This switch from cohesive to adhesive failure in GF/acrylic and GF/acrylic-PPE suggests the weakening of the interface must be more significant than any weakening of the acrylic and acrylic-PPE matrices from plasticisation. This is confirmed by the large drops in SBS measured in these specimens (Fig. 6).

The reduction in interfacial strength can be attributed to the hydrolysis of the sizing agent which, although proprietary, can be assumed to contain a silane coupling agent which is typical for glass-fibre composites [36]. The bond formed between the coupling agent and the GF is easily hydrolysed; for example, silane sizings can be removed from GF by simply boiling in water [36,37]. As depicted in Fig. 9, sizing hydrolysis in combination with matrix swelling causes debonding of the matrix from the fibres and therefore leads to interfacial degradation as observed in this study.

3.4.2. GF/epoxy

The SEM images in Fig. 7 show different failure behaviour between

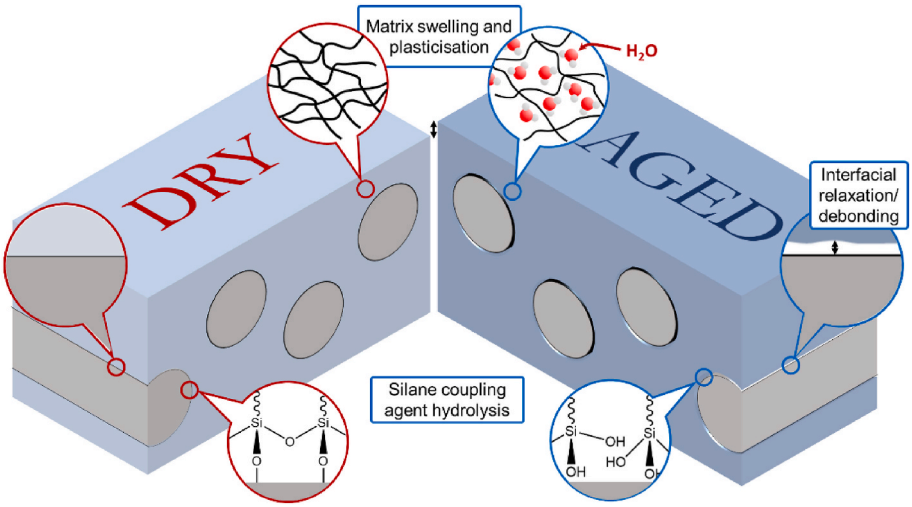

Fig. 9. A comparison of dry (left) and seawater aged (right) composites demonstrating some damage mechanisms of seawater ageing [25,38].

the thermoplastic composites and the thermoset GF/epoxy. In the former, crack propagation is through the matrix (cohesive failure) when dry but along the interface (adhesive failure) when aged. In contrast, crack propagation is along the interface in both dry and aged epoxy. This may indicate that the crosslinked epoxy matrix is stronger than the epoxy-GF interface both before and after ageing. This is likely, given that it is a crosslinked thermoset matrix rather than an amorphous thermoplastic like acrylic.

4. Conclusions

This study aimed to determine the behaviour of thermoplastic GF/acrylic and GF/acrylic-PPE composites during and after ageing in seawater at 50 °C, in comparison with an equivalent thermoset GF/epoxy composite.

The diffusion coefficients of the GF/acrylic (1.8×10^{-12} m^2 s^{-1}) and GF/acrylic-PPE (3.4×10^{-12} m^2 s^{-1}) were an order of magnitude larger than that of GF/epoxy (0.15×10^{-12} m^2 s^{-1}), and the final masses of absorbed water in GF/acrylic and GF/acrylic-PPE were also higher at 0.91% and 0.81% vs. 0.63% for GF/epoxy, respectively. This difference is likely due to a combination of higher void contents in the thermoplastic composite coupons used for water diffusion studies and a stronger interaction of the epoxy matrix with water in GF/epoxy. The faster water diffusion in the thermoplastic composites, however, did not correspond to greater reductions in mechanical properties due to ageing. In general, the GF/acrylic and GF/acrylic-PPE compared favourably and had similar or smaller reductions in mechanical properties due to seawater ageing compared to the GF/epoxy baseline. The effect of free water in voids and interstitial sites may therefore be less detrimental than bound water.

The 0° tensile and flexural moduli were approximately equal between matrices and not significantly affected by ageing. The strengths, however, saw larger decreases—up to 20% in the case of GF/epoxy in 0° tension. SEM imaging of these specimens, along with DMA studies, reveal that interfacial degradation and matrix plasticisation are the causes of deterioration in mechanical properties after seawater ageing. Future studies may therefore focus on determining the effects of acrylic-tailored sizings on the degradation of GF/acrylic composites in water.

The most significant mechanical benefits of GF/acrylic-PPE over GF/acrylic were found in 90° flexural testing. GF/acrylic-PPE had higher 90° flexural strength (+22%) and modulus (+8%) when dry, and also enhanced 90° flexural strength (+10%) and modulus (+13%) when aged, compared to GF/acrylic. In addition, the T_g of the GF/acrylic-PPE was 4 °C higher than the GF/acrylic before ageing and 6 °C after ageing. DMA revealed no evidence of melt-softening behaviour by 180 °C in the GF/acrylic-PPE, whereas the onset of softening was observed in GF/acrylic.

These results add further evidence that thermoplastic acrylic composites are a promising recyclable alternative to thermosets in marine applications, given their favourable material properties when compared to an epoxy baseline. In addition, acrylic-PPE allows for improved mechanical and thermomechanical properties while remaining recyclable.

Author statement

Machar Devine Conceptualization, Data curation, Formal analysis, Investigation, Methodology, Project administration, Resources, Visualization, Writing - original draft, Writing - review & editing.

Ankur Bajpai Conceptualization, Data curation, Formal analysis, Investigation, Methodology, Project administration, Resources, Visualization, Writing - review & editing.

Winifred Obande Conceptualization, Data curation, Formal analysis, Investigation, Methodology, Project administration, Resources, Visualization, Writing - review & editing.

Conchúr M. Ó Brádaigh Funding acquisition, Resources, Supervision, Validation, Writing - review & editing.

Dipa Ray Conceptualization, Funding acquisition, Methodology, Project administration, Resources, Supervision, Validation, Visualization, Writing - review & editing.

Declaration of competing interest

The authors declare that they have no known competing financial interests or personal relationships that could have appeared to influence the work reported in this paper.

Data availability

Data will be made available on request.

5 Acknowledgements

The authors are grateful for funding provided by the Wind and Marine Energy Systems and Structures Centre for Doctoral Training (CDT-WAMSS) and to Prof Andy Mount Dean of Research at CSE UoE and EPSRC IAA support team at Edinburgh Innovations. The authors gratefully acknowledge Arkema GRL, France and SABIC for the provision of materials towards this research. SABIC and brands marked with ™ are trademarks of SABIC or its subsidiaries or affiliates unless otherwise noted.

Appendix A. Supplementary data

Supplementary data to this article can be found online at https://doi.org/10.1016/j.compositesb.2023.110879.

References

[1] Liu P, Barlow CY. Wind turbine blade waste in 2050. Waste Manag 2017;62:229–40.
[2] IEA. Net. Zero by 2050 A roadmap for the global energy sector. 2021.
[3] Nash NH, Portela A, Bachour-Sirerol CI, Manolakis I, Comer AJ. Effect of environmental conditioning on the properties of thermosetting- and thermoplastic-matrix composite materials by resin infusion for marine applications. Compos B Eng 2019:177.
[4] Qin Y, Summerscales J, Graham-Jones J, Meng M, Pemberton R. Monomer selection for in situ polymerization infusion manufacture of natural-fiber reinforced thermoplastic-matrix marine composites. Polymers 2020;12(12).
[5] Cousins DS, Suzuki Y, Murray RE, Samaniuk JR, Stebner AP. Recycling glass fiber thermoplastic composites from wind turbine blades. J Clean Prod 2019;209:1252–63.
[6] Gebhardt M, Manolakis I, Chatterjee A, Kalinka G, Deubener J, Pfnür H, et al. Reducing the raw material usage for room temperature infusible and polymerisable thermoplastic CFRPs through reuse of recycled waste matrix material. Compos B Eng 2021:216.
[7] Meyer Zu Reckendorf I, Sahki A, Perrin D, Lacoste C, Bergeret A, Ohayon A, et al. Chemical recycling of vacuum-infused thermoplastic acrylate-based composites reinforced by basalt fabrics. Polymers 2022;14(6).
[8] Bel Haj Frej H, Léger R, Perrin D, Ienny P, Gérard P, Devaux J-F. Recovery and reuse of carbon fibre and acrylic resin from thermoplastic composites used in marine application. Resour Conserv Recycl 2021:173.
[9] Obande W, Stankovic D, Bajpai A, Devine M, Wurzer C, Lykkeberg A, et al. Thermal reshaping as a route for reuse of end-of-life glass fibre-reinforced acrylic composites. Compos B Eng 2023:257.
[10] Obande W, Mamalis D, Ray D, Yang L, Ó Brádaigh CM. Mechanical and thermomechanical characterisation of vacuum-infused thermoplastic- and thermoset-based composites. Mater Des 2019:175.
[11] Davies P, Arhant M. Fatigue behaviour of acrylic matrix composites: influence of seawater. Appl Compos Mater 2018;26(2):507–18.
[12] Bel Haj Frej H, Léger R, Perrin D, Ienny P. A novel thermoplastic composite for marine applications: comparison of the effects of aging on mechanical properties and diffusion mechanisms. Appl Compos Mater 2021;28:899–922.
[13] Barbosa LCM, Santos M, Oliveira TLL, Gomes GF, Ancelotti Junior AC. Effects of moisture absorption on mechanical and viscoelastic properties in liquid thermoplastic resin/carbon fiber composites. Polym Eng Sci 2019;59(11):2185–94.
[14] Davies P, Le Gac PY, Le Gall M. Influence of sea water aging on the mechanical behaviour of acrylic matrix composites. Appl Compos Mater 2016;24(1):97–111.
[15] Obande W, Gruszka W, Garden JA, Wurzer C, Ó Brádaigh CM, Ray D. Enhancing the solvent resistance and thermomechanical properties of thermoplastic acrylic polymers and composites via reactive hybridisation. Mater Des 2021:206.
[16] Obande W, Ó Brádaigh CM, Ray D. Thermoplastic hybrid-matrix composite prepared by a room-temperature vacuum infusion and in-situ polymerisation process. Compos Commun 2020:22–7.
[17] Unemori M, Matsuya Y, Matsuya S, Akashi A, Akamine A. Water absorption of poly (methyl methacrylate) containing 4-methacryloxyethyl trimellitic anhydride. Biomaterials 2003;24(8):1381–7.
[18] Moghbelli E, Banyay R, Sue H-J. Effect of moisture exposure on scratch resistance of PMMA. Tribol Int 2014;69:46–51.
[19] Tsenoglou CJ, Pavlidou S, Papaspyrides CD. Evaluation of interfacial relaxation due to water absorption in fiber–polymer composites. Compos Sci Technol 2006;66(15):2855–64.
[20] Fujii Y, Tominaga T, Murakami D, Tanaka M, Seto H. Local dynamics of the hydration water and poly(methyl methacrylate) chains in PMMA networks. Front Chem 2021;9:728738.
[21] Abdelmola F, Carlsson LA. State of water in void-free and void-containing epoxy specimens. J Reinforc Plast Compos 2019;38(12):556–66.
[22] Bellenger V, Verdu J, Morel E. Structure-properties relationships for densely cross-linked epoxide-amine systems based on epoxide or amine mixtures. J Mater Sci 1989;24(1):63–8.
[23] Thominette F, Gaudichet-Maurin E, Verdu J. Effect of structure on water diffusion in hydrophilic polymers. Defect Diffusion Forum 2006;258–260:442–6.
[24] Bel Haj Frej H, Léger R, Perrin D, Ienny P. Effect of aging temperature on a thermoset-like novel acrylic thermoplastic composite for marine vessels. J Compos Mater 2021;55(19):2673–91.
[25] Bond DA, Smith PA. Modeling the transport of low-molecular-weight penetrants within polymer matrix composites. Appl Mech Rev 2006;59(5):249–68.
[26] Smith LSA, Schmitz V. The effect of water on the glass transition temperature of poly(methyl methacrylate). Polymer 1988;29(10):1871–8.
[27] Wright WW. The effect of diffusion of water into epoxy resins and their carbon-fibre reinforced composites. Composites 1981;12(3):201–5.
[28] Chateauminois A, Chabert B, Soulier JP, Vincent L. Dynamic mechanical analysis of epoxy composites plasticized by water: artifact and reality. Polym Compos 1995;16(4):288–96.
[29] Joseph P, Tretsiakova-McNally S. Melt-flow behaviours of thermoplastic materials under fire conditions: recent experimental studies and some theoretical approaches. Materials 2015;8(12):8793–803.
[30] Cook J, Gordon JE. A mechanism for the control of crack propagation in all-brittle systems. Proceedings of the Royal Society of London Series A Mathematical and Physical Sciences 1964;282(1391):508–20.
[31] Ma Y, Yang Y, Sugahara T, Hamada H. A study on the failure behavior and mechanical properties of unidirectional fiber reinforced thermosetting and thermoplastic composites. Compos B Eng 2016;99:162–72.
[32] Thouless M, Parmigiani J. Mixed-mode cohesive-zone models for delamination and deflection in composites. In: Proceedings of the 28th risø international symposium on material science: interface design of polymer matrix composites; 2007.
[33] Raab M, Schulz E, Sova M. The cook-gordon mechanism in polymeric materials. Polym Eng Sci 1993;33(21):1438–43.
[34] Fibre-dominated failures of polymer composites. In: Greenhalgh ES, editor. Failure analysis and fractography of polymer composites. Woodhead Publishing; 2009. p. 107–63.
[35] Delamination-dominated failures in polymer composites. In: Greenhalgh ES, editor. Failure analysis and fractography of polymer composites. Woodhead Publishing; 2009. p. 164–237.
[36] Thomason JL. Glass fibre sizing: a review. Compos Appl Sci Manuf 2019;127.
[37] Ishai O. Environmental effects on deformation, strength, and degradation of unidirectional glass-fiber reinforced plastics. II. Experimental study. Polym Eng Sci 1975;15(7):491–9.
[38] Nihei T. Dental applications for silane coupling agents. J Oral Sci 2016;58(2):151–5.

Composites Part B 272 (2024) 111212

Contents lists available at ScienceDirect

Composites Part B

journal homepage: www.elsevier.com/locate/compositesb

‘Resin welding’: A novel route to joining acrylic composite components at room temperature

Machar Devine [a], Ankur Bajpai [a], Conchúr M. Ó Brádaigh [b], Dipa Ray [a,*]

[a] School of Engineering, Institute for Materials and Processes, The University of Edinburgh, Sanderson Building, Robert Stevenson Road, Edinburgh, EH9 3FB, Scotland, United Kingdom

[b] Department of Materials Science & Engineering, Faculty of Engineering, University of Sheffield, Sir Robert Hadfield Building, Mappin Street, Sheffield S1 3JD, United Kingdom

ARTICLE INFO

Handling Editor: Prof. Ole Thomsen

Keywords:
Thermoplastic resin
Adhesion
Mechanical testing
Joints/joining
Thermoplastic welding

ABSTRACT

The solubility of acrylic polymer in its own liquid monomer creates the opportunity to ‘weld’ acrylic-matrix (Elium®) composites without the application of heat. In this method, termed *resin welding*, acrylic monomeric resin is infused between acrylic-matrix composite parts. The resin dissolves and diffuses into the acrylic matrix and creates a continuous material, and a strong bond, when it polymerises, without the sensitivities of traditional welding methods to adherend or bondline thickness. Single lap shear testing was conducted on resin-welded and adhesively-bonded coupons with varying bondline thicknesses and filling fibres, and the bonding and fracture mechanisms were investigated using SEM and the diffusion of dyed acrylic resin. The highest bond strength of resin-welded coupons reached 27.9 MPa, which is 24 % higher than the strongest weld reported in the literature, indicating that resin welding is a promising alternative to traditional bonding and welding methods for acrylic-matrix composites.

1. Introduction

Recyclable acrylic-matrix composites produced using infusible acrylic resins are a possible route towards creating a circular economy in the composites industry. They have been shown to have excellent mechanical properties on par with or even exceeding the properties of non-recyclable, but widely used, epoxy composites [1,2]. These resins are largely composed of methyl methacrylate (MMA) monomers which polymerise in-situ to form a poly-methyl methacrylate (PMMA) based copolymer during composite manufacturing. The resin therefore has a low viscosity, enabling its use in the manufacture of large composite structures such as the 62 m long acrylic-matrix wind turbine blade recently manufactured as part of the ZEBRA project, led by IRT Jules Verne [3].

These large structures are often manufactured in multiple sections which then require joining together. A common method of manufacturing wind turbine blades, for example, is to infuse two shells separately and join them together with a shear web or spar in the centre [4]. The current method of joining these parts is to use adhesives, however the use of thermoplastic matrices such as acrylic provides the opportunity to use welded joints instead. It has been suggested that higher joint strengths, greater fatigue life and faster processing times could be achieved through welding [5].

There are several types of welding which can be used for thermoplastic polymer matrix composites. Literature on the welding of acrylic-matrix composites has concentrated on fusion welding in which heat is applied to the adherends and the polymer matrix melts and interdiffuses when pressure is applied to the joint. Heat can be applied in several ways: for example, via a heating element in the joint (resistive and inductive welding), through frictional heating (ultrasonic, vibrational or spin welding), or via the direct heating of the adherends (e.g. with infrared or other radiation, a hot-plate, or hot gas) [6].

Four methods of welding acrylic-matrix composites are discussed in the literature: resistance, induction, ultrasonic and infra-red welding [5,7–10]. Resistance and induction welding in glass fibre reinforced acrylic composites have been explored by Murray et al. using single lap shear testing [5]. In this study, single lap resistance welds had average single lap strengths ranging between 19.1 MPa and 22.4 MPa depending on the heating element used. The fatigue limit, defined by the authors as the stress at which a coupon survived 10 million cycles at a stress ratio R of 0.1 and frequency of 10 Hz, was reported to be 5 MPa for resistance welds joined using a carbon fibre heating element [5]. Coupons joined

* Corresponding author.
E-mail address: dipa.roy@ed.ac.uk (D. Ray).

https://doi.org/10.1016/j.compositesb.2024.111212
Received 12 October 2023; Received in revised form 18 December 2023; Accepted 8 January 2024
Available online 9 January 2024

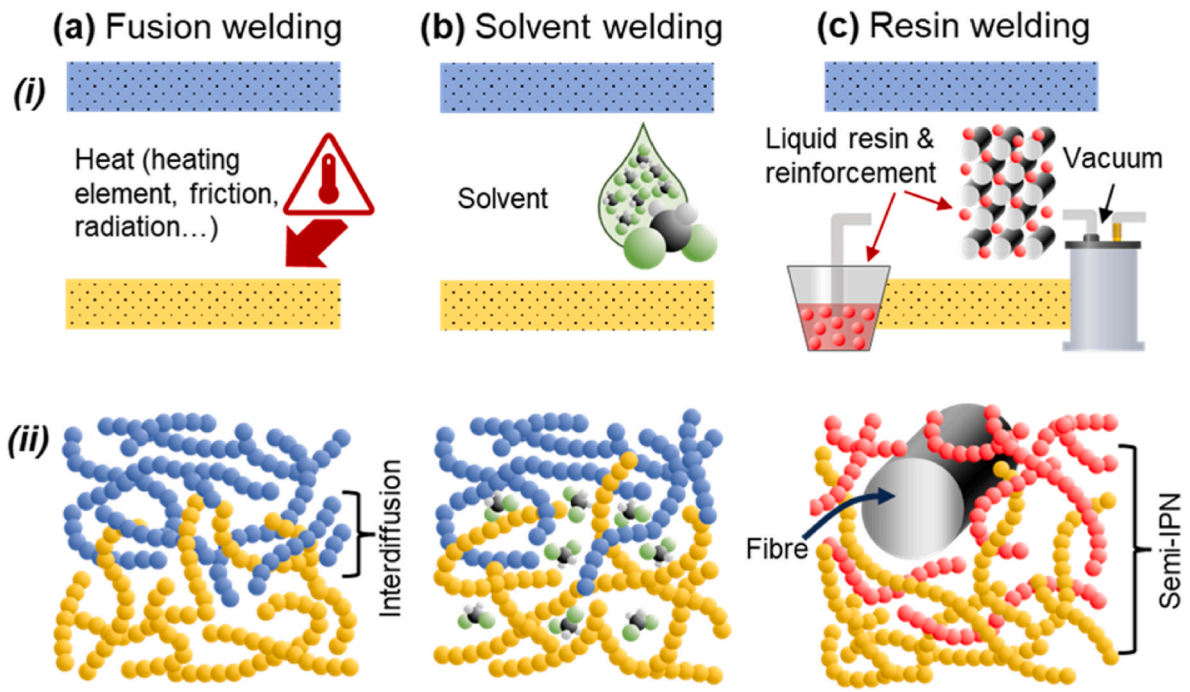

Fig. 1. Illustrations of the welding methods for thermoplastic polymers and composites. (a) Fusion bonding increases polymer mobility by heating. Applying pressure allows the polymer to interdiffuse. (b) Solvent welding increases polymer mobility by dissolution at room temperature, but solvent remains trapped in the polymer. (c) In the resin welding method, the acrylic monomer acts as a reactive solvent and polymerises around the adherend matrix. The same mechanism is applicable to reactive solvent cements.

via induction welding with a carbon fibre heating element reached a lower average single lap shear strength of 20.4 MPa. For comparison, several adhesive joints were also tested, although the highest adhesive single lap strength and fatigue limit—achieved using Plexus MA310 methacrylate adhesive—were only 17.4 MPa and 3 MPa respectively.

In another study, ultrasonic welding of carbon fibre reinforced acrylic has also been studied by Bhudolia et al. [7,9]. Similar results were achieved to Ref. [5], with welded single lap joints reaching a strength of 18.9 MPa with proper optimisation, which was 33 % higher than the strength of adhesive bonds (14.2 MPa) made with Bostik SAF 30-5 methacrylate adhesive. The fatigue strength of ultrasonically welded single lap coupons at 10^5 cycles ($R = 0.1$, frequency = 5 Hz) was also 12 % higher than that of adhesive bonds (7.26 MPa and 6.48 MPa respectively), although this reduced to a 7 % difference at 10^7 cycles.

The fourth welding method demonstrated for acrylic-matrix composites in the literature is infrared welding. Perrin et al. [10] obtained single lap shear strengths of 12.3 MPa using this method, although this was improved up to 19.1 MPa by the addition of a small amount of crosslinker to the acrylic matrix of the adherends.

Although each welding method has its advantages and disadvantages, a common requirement for all three is intimate contact between the adherends while pressure is applied, which may not be possible when manufacturing large and complex parts. In wind turbine blades, for example, adhesive bondlines of up to 30 mm may be required due to large manufacturing tolerances [4,11]. In addition, ultrasonic welding may not be suitable for joining thick sections as vibrations are attenuated through the adherend thickness [12,13]. There is therefore uncertainty about the commercial application of polymer welding in the wind power industry, and to the best of our knowledge there has not been a published demonstration of welding applied to wind turbine blades.

An alternative method of joining acrylic composite parts termed ‘resin welding’ is proposed in this paper. Thermoplastics like acrylics can not only melt but can also dissolve in appropriate solvents. This property has been used to join thermoplastics via *solvent welding* and *solvent cementing*, in which the application of a solvent, rather than heat as in fusion welding, allows for polymer chain mobility and subsequent interdiffusion and bonding of the thermoplastic polymer. However, residual solvent remains in the polymer and weakens the joint [14,15]. Interestingly, methyl methacrylate monomer is also a solvent for acrylic polymer and is available in commercial formulations to solvent weld PMMA [16]. This provides an opportunity to avoid the weakening effects of solvent welding as, if the acrylic monomer is mixed with an initiator as in some commercial formulations [17], the monomer will act as a reactive solvent and polymerise around the existing polymer network, forming a semi-interpenetrating polymer network (semi-IPN) rather than remaining as a monomer and weakening the joint. A comparison of the different methods is provided in Fig. 1.

In this work, the concept of solvent welding is extended to the joining of acrylic-matrix composite parts by the vacuum infusion of acrylic monomer resin (Elium®) into a joint packed with reinforcement fibre, followed by room temperature polymerisation, allowing for joining with large and varying bondlines with no requirement for heat input. The resin is believed to partially dissolve the matrix at the joining interface and form a semi-IPN after polymerisation, as described previously, creating a continuous, homogeneous material across the joint. This joining method has been termed ‘resin welding’.

In the following sections, the resin welding method is introduced, and the strengths of resin-welded single lap shear specimens are reported and compared with adhesively bonded coupons and welded coupons from the literature. The effect of including filler glass fibres between the adherends with 0° and 90° orientations is explored, as is the effect of changing the bondline thickness from 0.5 mm to 1 mm. The bonding mechanisms are then investigated, firstly through fractographic analysis of the single lap shear coupons’ fracture surfaces, and then by examining the interface between dyed acrylic resin and clear cast acrylic polymer for signs of dissolution of the polymer and formation of a semi-IPN.

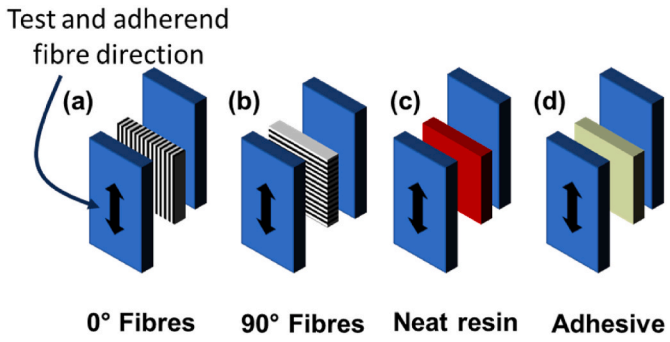

Fig. 2. The four types of single lap joint which were manufactured. Specimens were made with: (a) 0° fibres in the bondline, oriented in the same direction as testing and the fibre direction of the adherends; (b) 90° fibres which were placed perpendicular to the test direction; (c) neat acrylic resin with no fibres in the joint; and (d) an adhesive rather than acrylic resin.

2. Materials and methods

2.1. Single lap coupon manufacturing and testing

2.1.1. Laminate preparation

Glass fibre reinforced acrylic (GF/acrylic) laminates were prepared using a [0°$_4$] layup of 646 g/m^2 unidirectional non-crimp E-glass fibre fabric (TEST2594-125-50, Ahlstrom-Munksjö) with multi-compatible sizing for a total thickness of 2 mm. Laminates were prepared through the vacuum infusion of Elium® 188 O acrylic monomer resin (Arkema) mixed in a 100:3 wt ratio with BP-50-FT peroxide initiator (United Initiators). The resin polymerised at room temperature for 24 h before cutting with a water-cooled diamond-tipped saw.

2.1.2. Bonding methodology

Single lap shear coupons are commonly used to characterise adhesive strengths, and previous work published on welding acrylic-matrix composites uses single lap shear geometry [5,7,10]. The single lap geometry specified by ASTM D5868 was therefore chosen to allow for comparisons with published values. This was achieved by bonding two GF/acrylic adherend laminates with a 25 mm overlap from which 5 single lap coupons of 25 mm width (and therefore 25 × 25 mm joint area) were cut. The coupons were prepared so that the adherend reinforcement was parallel to the test direction.

Four types of bonds were prepared: resin-welded joints with neat resin, 0° fibres or 90° fibres in the bondline, and adhesive joints (Fig. 2). Two bond line thicknesses (0.5 mm and 1 mm) were manufactured for each bond type to match the thickness of 1 and 2 plies of GF fabric.

Adhesively joined specimens were prepared using Plexus MA310 two-part methacrylate adhesive, which has been previously shown to have good compatibility with acrylic-matrix composites [5]. The adhesive was applied between the adherends using a mixer nozzle and the bondline thickness was set using wire spacers of either 0.5 mm or 1 mm diameter. Pressure was applied using binder clips and the adhesive was left to cure at room temperature.

Resin-welded joints with reinforcement in the weld were prepared by placing glass fabric in the bondline between two adherend laminates (Figs. 2 and 3). Vacuum bagging, a resin inlet and a vacuum outlet were then attached using an epoxy adhesive to seal the weld region. Vacuum was applied and acrylic resin mixed with initiator was infused and left to polymerise for 24 h to allow the adherends to bond. Joints with neat resin in the bondline were prepared in a similar manner but using wire spacers instead of fabric to set the thickness.

The vacuum bagging, epoxy adhesive and tubing were then removed, and single lap coupons were cut with a diamond-tipped water-cooled saw (Fig. 4a). Composite tabs were applied to reduce loading eccentricities during testing (Fig. 4b). Five coupons were cut for each weld type and thickness, and the 90° and neat resin welds at 1 mm thickness were repeated to give a total of ten coupons for each. Out of the samples cut, only 3 samples each were successfully tested from the 0° fibre welds.

2.1.3. Mechanical testing

Single lap shear coupons were tested in tension according to ASTM D5868 using an Instron 3369 test machine with a 50 kN load cell. A crosshead extension rate of 1 mm/min was selected due to the lower ductility of acrylic resin compared to typical adhesives. The sides of the coupons were speckled with spray paint so that deformations could be tracked using the GOM Correlate Digital Image Correlation (DIC) software.

2.1.4. Statistical analysis

Statistical analysis of the weld strengths was performed using Minitab® 20 statistical software. A Welch's ANOVA test ($\alpha = 0.05$) was employed, followed by a Games-Howell post-hoc test.

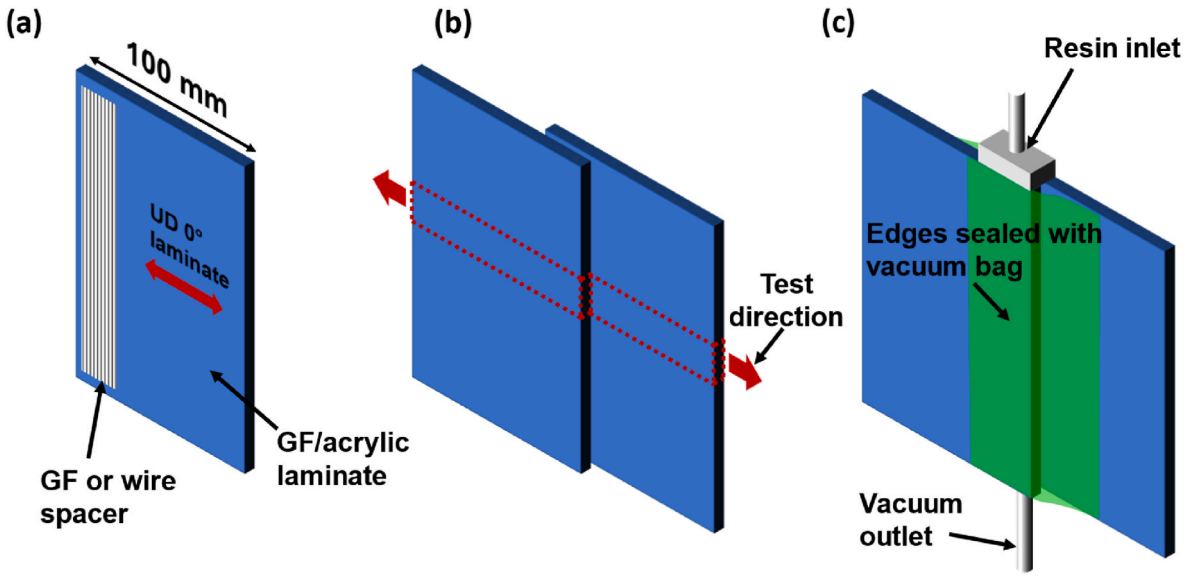

Fig. 3. Details of the resin-welding process. (a) Glass reinforcement, or a wire spacer for adhesive and neat-resin bonds, is placed on the adherend then (b) a second adherend is placed on top—the coupon outline and test direction are highlighted—and (c) the weld region is sealed with vacuum bagging and a resin inlet and outlet.

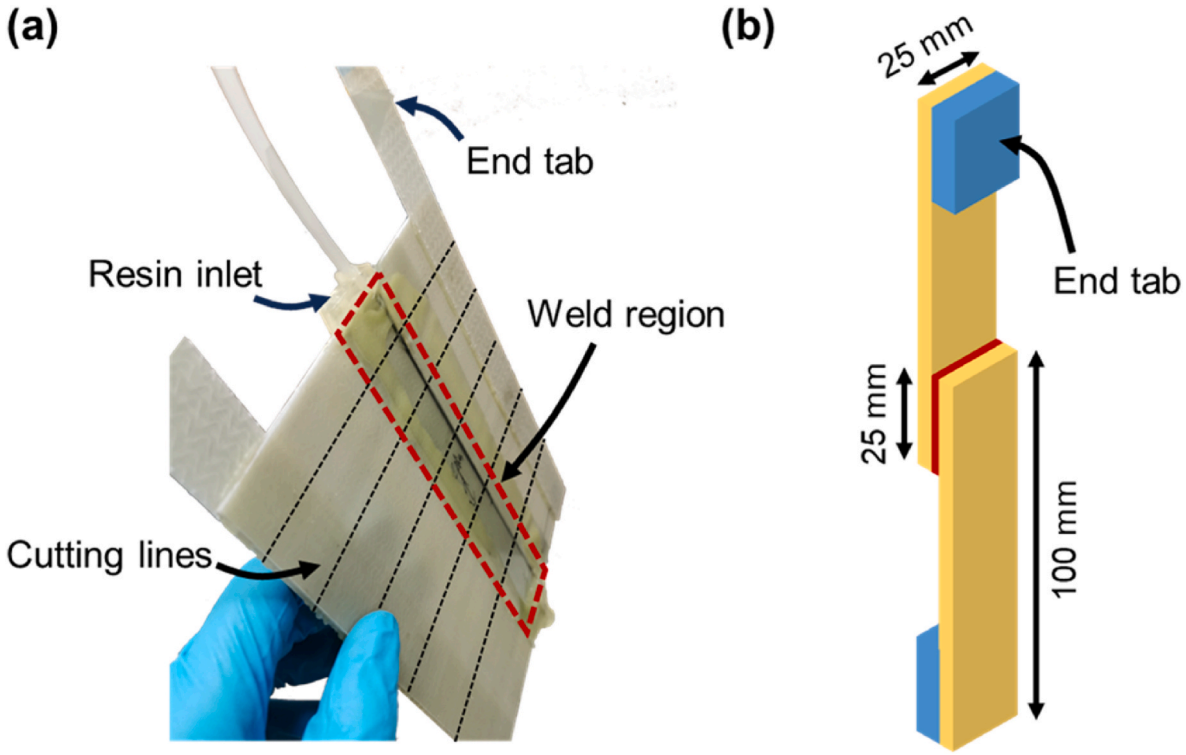

Fig. 4. (a) A prepared weld with lines depicting where coupons are cut in black, and the weld region highlighted in red. (b) The single lap coupon geometry with tabs applied. (For interpretation of the references to colour in this figure legend, the reader is referred to the Web version of this article.)

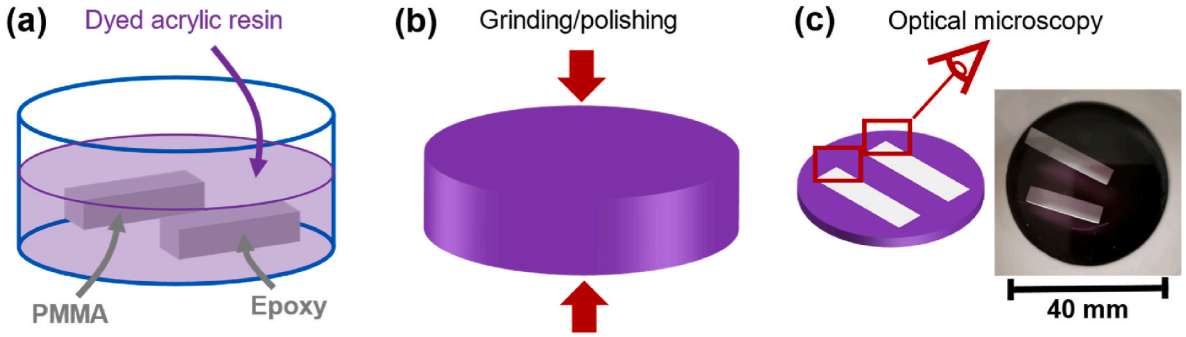

Fig. 5. Specimens were prepared for optical microscopy by (a) immersing PMMA and epoxy coupons in dyed acrylic resin then (b) grinding and polishing the demoulded cylinder. The finished coupon is depicted in (c), and the observed regions are highlighted.

2.1.5. Fractography

Scanning electron microscopy (SEM) was used to observe the fracture surfaces of the single lap shear coupons after testing. The fracture surfaces were sputter-coated with 30 nm of gold and were imaged at 15 kV using a JEOL JSM series electron microscope.

2.2. Investigation of the proposed bonding mechanism

The bonding mechanism that occurs during resin welding was investigated by comparing the diffusion of acrylic resin in PMMA and epoxy polymers using optical microscopy. Epoxy was included for comparison since thermosets do not dissolve in solvents and should therefore not bond via extensive semi-IPN formation, resulting in a difference between the acrylic-acrylic and acrylic-epoxy interfaces.

Cuboids of clear cast PMMA and epoxy were cut and placed into a sample cup of 40 mm diameter which was coated in release agent. Elium® 188 O acrylic resin was dyed with Bestoil Blue 2 N (FastColours Ltd.)—a solvent/oil soluble dye—then mixed in a 100:3 ratio with BP-50-FT peroxide initiator. The resin was then poured into the sample cup to immerse the polymer cuboids (Fig. 5a). The dye allowed diffusion of the resin to be observed visually, and Bestoil Blue 2 N was chosen for its resistance to bleaching during the free-radical polymerisation of the acrylic. The resin was left to polymerise for 24 h, and the resulting cylinder was demoulded then ground and polished (Fig. 5b) to a thin disc to reveal the immersed polymers for optical microscopy (Fig. 5c).

Grinding and polishing were performed using a water-cooled ATA Saphir 520 polisher. The coupon was first ground to the correct thickness using a P180 grinding disc, and was then polished using a force of 30 N with increasingly fine polishing discs (P400, P800, P1200, P2500, 3 μm and 1 μm) for approximately 3 minutes on each side.

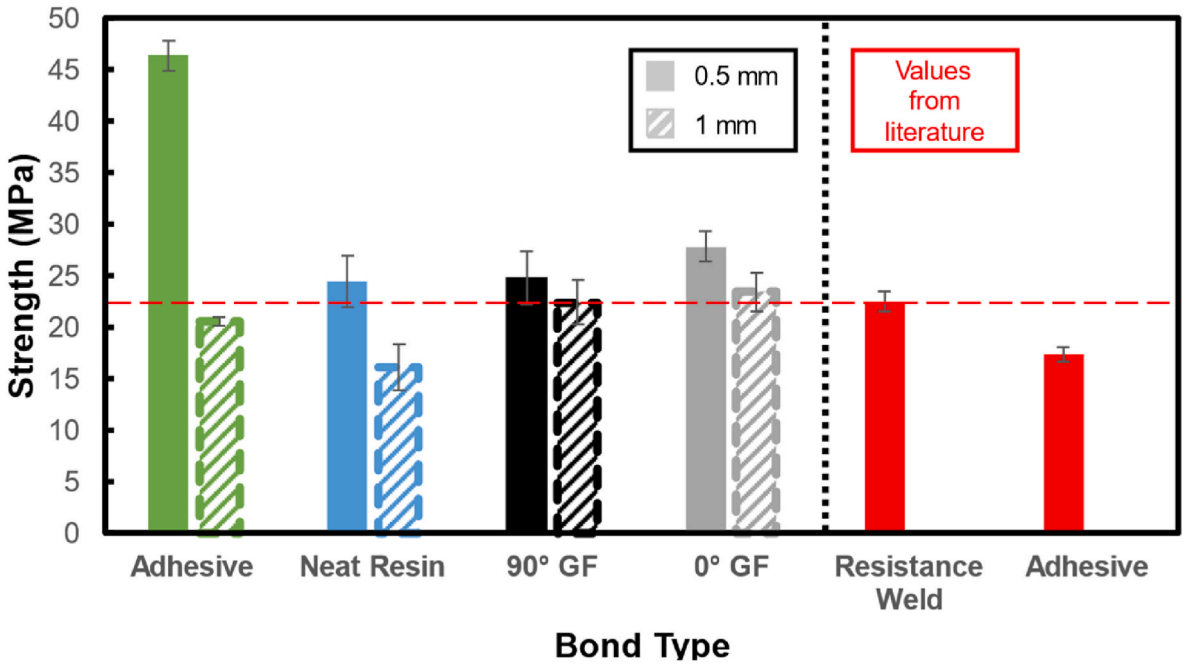

Fig. 6. The single lap shear strengths of each joint type. The values for 0.5 mm thick bonds are solidly coloured and the values for 1 mm thick bonds are hatched. Error bars represent ±1 standard deviation. A comparison with the highest published weld and adhesive strengths for acrylic-matrix composites [5] is included in red on the right. (For interpretation of the references to colour in this figure legend, the reader is referred to the Web version of this article.)

3. Results and discussion

3.1. Single lap shear testing

3.1.1. Mechanical properties

The single lap shear strengths for each joint type and thickness are shown in Fig. 6. The bond strength of the resin-welding method is promising overall as the highest average weld strength obtained—0.5 mm of 0° fibre reinforcement—reached 27.9 MPa. This is 24 % higher than the strongest reported single lap weld of acrylic-matrix composites in the literature: resistance-welded GF/acrylic adherends ($[0°_4]$ layup of 1200 g/m2 fabric, 3.5 mm thickness) with a biaxial carbon fibre heating element [5].

The effect of including fibres in the bondline can be found by comparing the strengths of the bonds with fibres to the bonds with neat resin. Considering first the 0.5 mm bondlines, the welds with 0° fibres, 90° fibres and neat resin had strengths which were not significantly different according to the statistical analysis. The highest strength of 46.4 MPa was obtained with adhesive and a bondline of 0.5 mm, 66.4 % greater than the 0.5 mm weld with 0° fibres ($P = 0.000$).

This study therefore measures no significant effect of fibre type, or if there is an effect it is too small in magnitude to observe under the parameters of the study. Other studies have measured a much greater effect on single lap shear strength of including unidirectional reinforcement in adhesive bondlines. Khalili et al. tested the single lap shear strength of GF/polyester adherends bonded with epoxy adhesive reinforced with unidirectional 0° glass fibres, resulting in a 54 % increase in strength (18.4 MPa vs. 11.9 MPa) over neat adhesive bonds [18]. Delzendehrooy et al. similarly compared the single lap shear strength of aluminium adherends bonded with epoxy adhesive and date palm fibre reinforced epoxy adhesive. Bonds reinforced with 0° fibres reached a strength up to 98 % greater than those with unreinforced adhesive [19]. Finally, Behera et al. tested both aluminium-to-composite (GF/epoxy) and aluminium-to-aluminium bonds with 0° glass fibre reinforced adhesive [20]. In comparison with neat adhesive, the reinforced adhesive increased single lap shear strength by 27.3 % in aluminium-to-aluminium bonds and by 45.4 % in aluminium-to-composite bonds.

The effect of heating element fibre orientation in the welding of thermoplastic composites has also been studied in the literature, although comparisons between fibre orientations may be complicated by the changes in welded area and thermal uniformity that different heating element fabrics create in resistance and induction welding [5,21]. In one study by Tanabe et al. [21], CF/PPS composites were joined using resistance welding, with carbon fibre heating elements in either the 0° or 90° direction. Similar welded areas were achieved using each fibre direction but changing the heating element fibre orientation from 90° to 0° increased the single lap shear strength by 65 %, from 16.5 MPa to 27.2 MPa.

The key difference between these studies and the present work is the fracture behaviour of the coupons. In each of these studies there was at least partial cohesive failure, and fracture occurred through the adhesive reinforcement or heating element fibres. The fibres therefore contributed to the single lap shear strength by resisting crack propagation. However, as will be discussed further in Section 4.1.2, crack propagation in the present study initiated via peeling at the edges and continued through the upper layer of the adherends for all coupons, rather than through the bondline. Therefore, the reinforcement in the bondline was unable to contribute significantly to an increase in strength.

The effect of increasing thickness differs depending on the bond type. Although the Plexus MA310 adhesive had a high single lap shear strength (46.4 MPa) with a 0.5 mm bondline the adhesive bond strength saw a large drop of 56 % ($P = 0.000$) as thickness increased to 1 mm. The neat-resin bonds also saw a large drop in strength of 34 % ($P = 0.005$) from 24.5 MPa to 16.2 MPa as the thickness was increased. Decreases in single lap shear strength with increasing bondline thickness have also been reported in the literature and have been attributed to greater peel and shear stresses and an increased likelihood of voids and other imperfections [22–24]. In contrast, the mean strength of bonds with 90° fibres and 0° fibres decreased by only 11 % and 16 % respectively with increasing thickness, which were therefore not found to be statistically significant changes ($P = 0.584$ and $P = 0.238$ respectively). The inclusion of fibres in the bond therefore appears to have benefits in thicker bondlines.

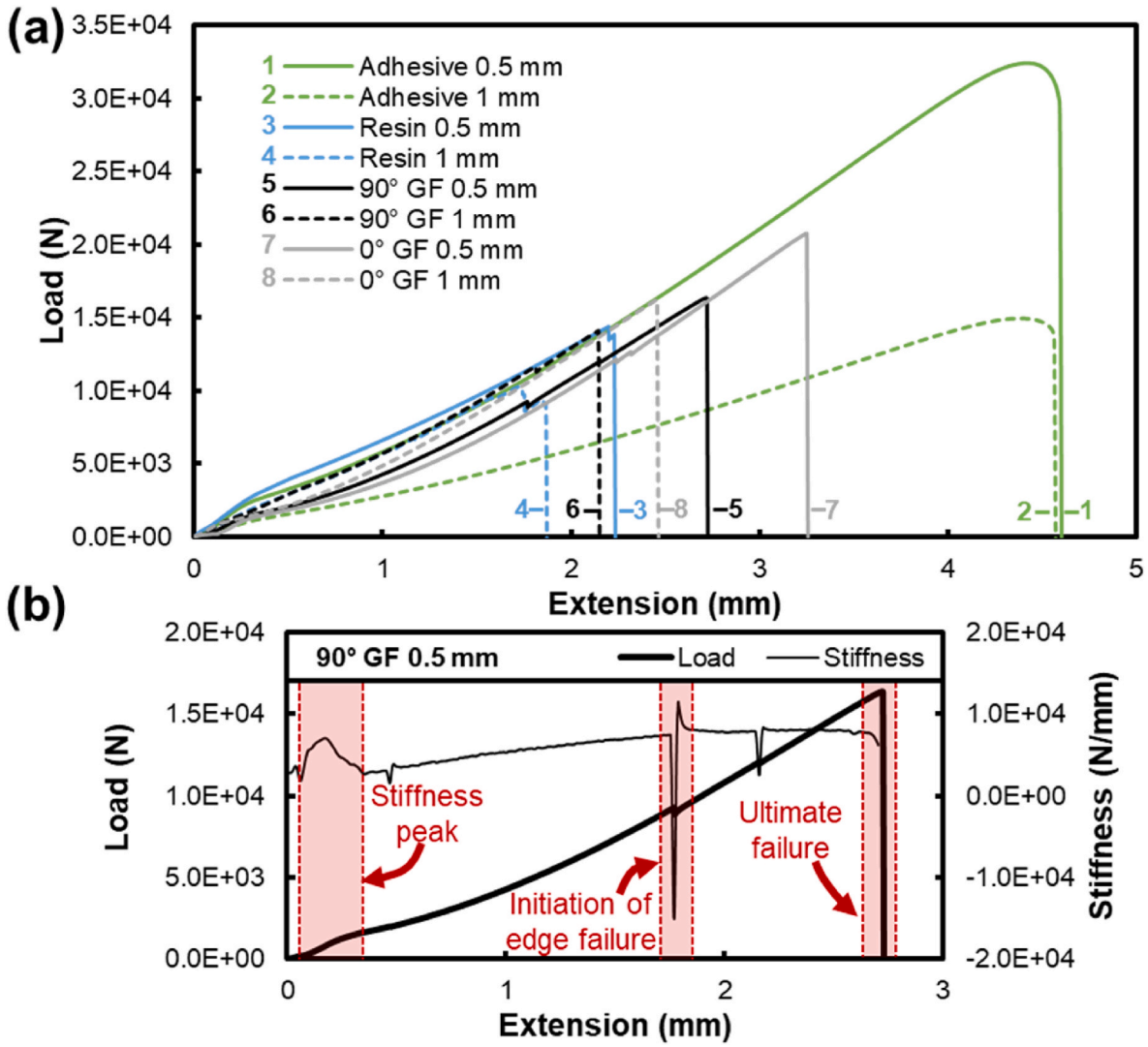

Fig. 7. (a) Representative load-extension curves for each type of single lap bond. Bonds of the same type are the same colour, with the 0.5 mm bond having a solid line and the 1 mm bond having a dashed line. (b) The representative load-extension curve of the 90° GF 0.5 mm coupon along with its derivative i.e. the variation in stiffness of the coupon throughout the test. The initial peak in stiffness, the initial edge failure—which is also visible as a small drop in the load-extension curve—and the ultimate failure are highlighted in red for both the load and stiffness curves. (For interpretation of the references to colour in this figure legend, the reader is referred to the Web version of this article.)

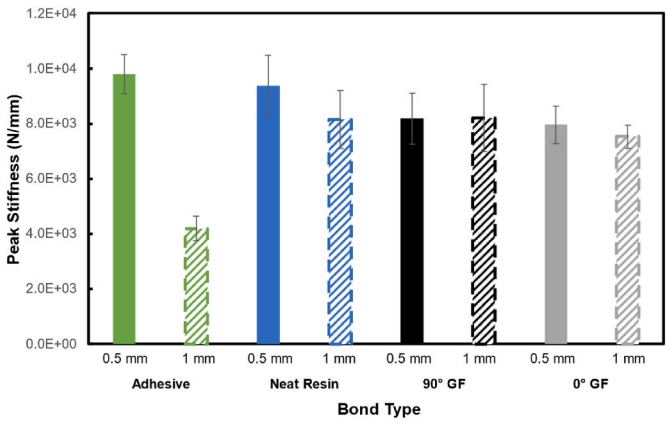

Fig. 8. The average peak gradient of the load-extension curves for each bond type below 0.5 mm extension. The 1 mm adhesive bond has a significantly lower stiffness than the rest.

These results show that increasing bondline thickness has a significant detrimental effect on adhesive bond strength; indeed, Plexus MA310 has a maximum recommended thickness of just 3.2 mm according to its technical datasheet [25] and would therefore be unsuitable for use in the thick bondlines found in wind turbine blades. Other adhesives which are designed for use in thick bondlines are available, but their strengths are significantly lower [5,26], and failure in adhesives is therefore common in wind turbine blades due to the relative weakness of these thick adhesive bonds, and the likelihood of them containing defects [27]. The presented results therefore suggest that resin welding could serve as a viable alternative to adhesives in wind turbine blades and other large structures. In resin welding, the bondlines are not constrained to the same maximum thickness as adhesives and could reach the same thickness as the thick-section composites being joined.

This effect of bondline thickness would partly explain discrepancies with the published single lap shear strength of 17.4 MPa for GF/acrylic coupons joined by MA310 adhesive published by Murray et al. [5], which was conducted with a bondline thickness of 0.76 mm. For comparison, the adhesive's technical datasheet suggests a single lap shear

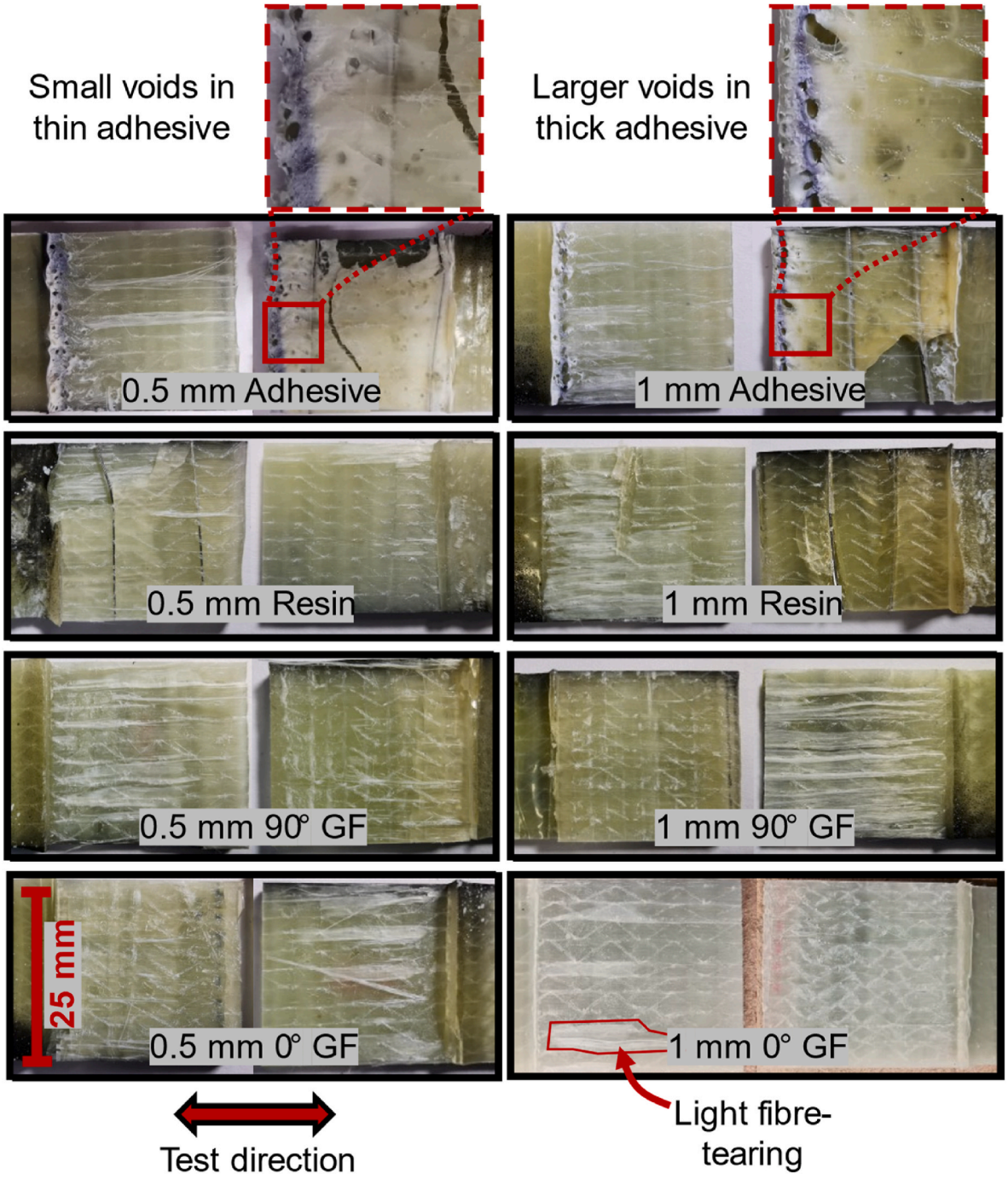

Fig. 9. Representative fracture surfaces of the tested single lap coupons. Each image is of both halves of a fractured coupon. The crack propagation direction (the testing direction) is shown. Light fibre tearing is highlighted in the 1 mm 0 GF coupon, but it is visible in all fracture surfaces. The voids present in both adhesive bonds are shown at higher magnification, and larger voids are visible in the 1 mm thick adhesive. Voids were not visible in the resin welded coupons.

strength range of 20.7–24.1 MPa [25]. The edge quality of the specimens could also play a role as Murray et al. allowed the adhesive to spill out the edges, whereas in the present study the edges were shaped to match the edges of the resin-welded specimens more closely, possibly reducing stress concentrations and increasing strength [28].

Representative load-extension curves for each bond type are provided in Fig. 7. A ductile failure of the adhesive bonds is evident compared to the brittle fractures of the weld specimens. It should also be noted that the 0.5 mm and 1 mm adhesive bonds reached similar average extensions before failure (4.6 ± 0.1 mm and 4.3 ± 0.2 mm respectively) despite the latter's significantly lower strength. The stiffness of the 1 mm adhesive bond is therefore lower than that of the 0.5 mm adhesive bond, however comparisons between the bond stiffnesses is made difficult by the shapes of the load-extension curves.

Although an initial linear load-extension response for composite single lap shear bonds is reported in some publications [29], allowing stiffnesses to be easily calculated, in this case the load-extension curves have an initial s-shape below approximately 0.5 mm extension followed by a gradually increasing gradient. Therefore, in order to compare the stiffnesses of the single lap coupons, the load-extension curves are differentiated. The resulting stiffness vs. extension curves have a shape similar to that in Fig. 7b in which there is an initial peak in stiffness. Loading in single lap joints is complex and is a mixture of shear and peel which is accompanied by the bending of the adherends. The reason for

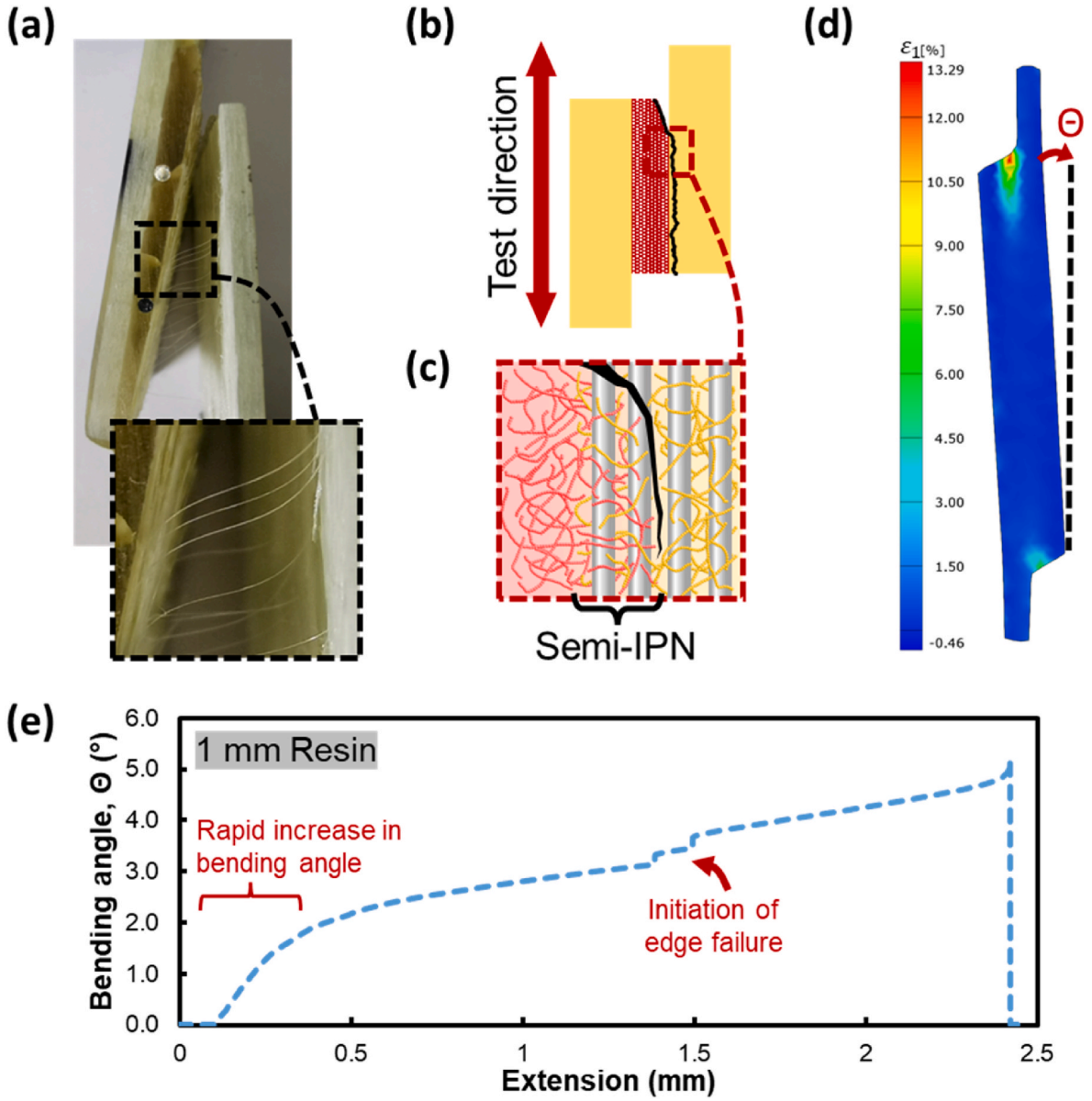

Fig. 10. Fibre bridging in a coupon bonded with neat resin (no reinforcement). The bridging fibres therefore come from the surface of the adherend. (b) The failure mode of the welded coupons was light fibre tearing where a small amount of glass fibre is removed from the adherend surface (c) The fracture propagation was through the adherend matrix (yellow) rather than through the tougher semi-IPN. (d) A representative map of major strain in a single lap coupon close to failure. Stress concentrations are found at the edges of the overlap region. The rotation of the specimens during testing (Θ) is highlighted. (e) A representative bending angle vs. extension curve for a 1 mm resin weld. The rapid increase in bending angle corresponding to the stiffness peak is highlighted. (For interpretation of the references to colour in this figure legend, the reader is referred to the Web version of this article.)

the nonlinear curve shape was therefore investigated by measuring the bending angle of the coupons using DIC (Fig. 10e). Below 0.5 mm extension, there is a rapid increase then subsequent slowing in bending rate, therefore the initial peak in stiffness (Fig. 7b) can be attributed to the bending of the adherends. The average peak in gradient before 0.5 mm extension for each joint is summarised in Fig. 8. Only the 1 mm adhesive joint has a significantly lower peak stiffness of 4.2 kN/mm due to the low modulus and high ductility of the adhesive, which makes a greater contribution to stiffness at higher bondline thicknesses.

3.1.2. *Failure modes and mechanisms*

Images of the failed coupons are shown in Fig. 9.

The failure modes of the adhesive and resin-welded coupons can be classified as light fibre tear failure (ASTM D5573) as, rather than the more common adhesive or cohesive failure types, a small amount of resin and glass fibre is removed from the surface of the adherend. The clearest evidence of this is the fibre bridging in coupons with no fibres in the bondline (Fig. 10a), indicating that these fibres must come from the adherend. It is therefore the adherend matrix that fails rather than the bond between the infused resin and the adherend matrix (Fig. 10b and c). This is confirmed via SEM imaging which showed that 0° fibres were present in the fracture surfaces of all coupons, regardless of whether or not 0° fibres were placed in the bondline.

Representative SEM images are presented in Fig. 11 and depict both halves of a coupon bonded with 0.5 mm of neat acrylic resin. The presence of fibres on both sides—despite no fibres being included in the bondline—shows that the crack propagates within the first layer of the adherend fibres (light fibre tearing). These results suggest that the formation of a semi-IPN increases fracture toughness compared to the bulk polymer, leading to failure in the adherend matrix rather than in the

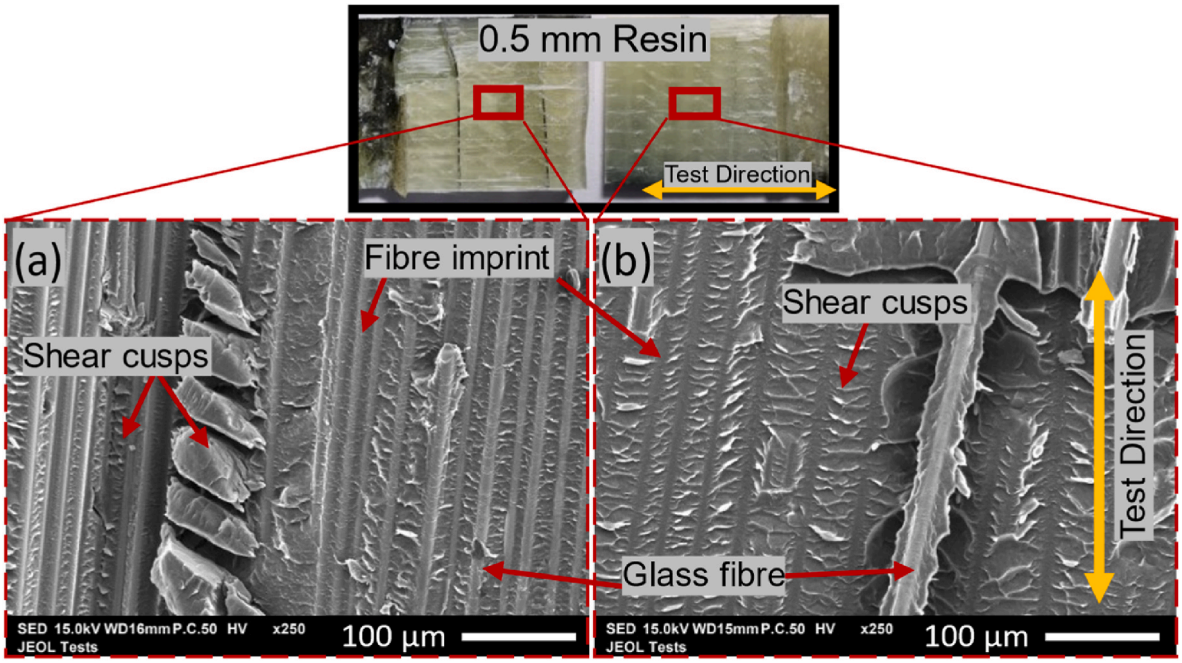

Fig. 11. SEM images of the fracture surfaces of GF/acrylic bonded with 0.5 mm of neat acrylic resin. Photographs of the imaged fracture surfaces are provided above, with the imaged areas represented by red rectangles (not to scale). Image (a) is of one half of a fractured single lap shear coupon and image (b) is of the other half. Fibres and imprints are present in both halves indicating light fibre tearing of the adherend. Cusps indicate a shear failure. (For interpretation of the references to colour in this figure legend, the reader is referred to the Web version of this article.)

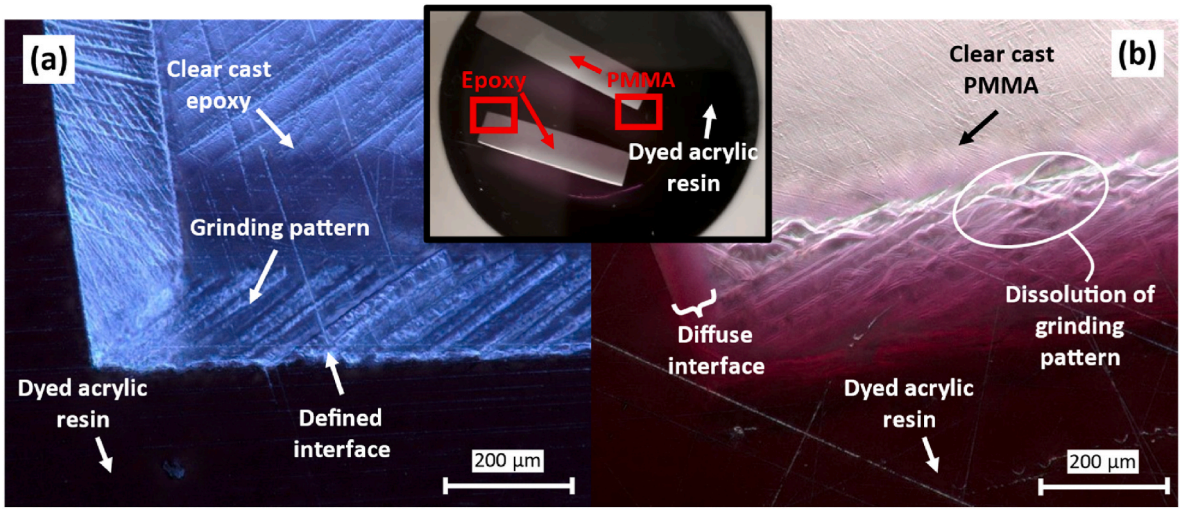

Fig. 12. Optical microscope images of the edges of (a) epoxy and (b) PMMA cuboids immersed in dyed acrylic resin. A lower magnification photograph of the epoxy and PMMA cuboids cast in dyed acrylic resin is shown in the centre of the figure. The optical microscopy imaging locations are highlighted with red rectangles. (For interpretation of the references to colour in this figure legend, the reader is referred to the Web version of this article.)

semi-IPN at the bonding interface, as shown schematically in Fig. 10b and c.

Further insight into the failure of the coupons was gained using DIC. A map of the major strain across the profile of a single lap coupon just before failure is presented in Fig. 10d. As noted in the literature [30], there are stress concentrations at the edges of the overlap region, and this is therefore where failure initiates. The rotation of the specimens during testing means that this is a concentration of both shear and peel forces [28,31], but failure was observed to initiate via peeling at the edges. However, shear cusps are present in the SEM images in Fig. 11a and b, therefore failure proceeds via a mixture of shear and peeling.

3.2. Bonding mechanism

Adhesives can bond via several mechanisms, including the formation of chemical or physical bonds with the adherend surface, mechanical interlocking between the adhesive and a rough adherend surface, via electrostatic attraction or through diffusive bonding [32,33]. Since PMMA is soluble in its monomer, the resin-welding method is expected to create a bond via dissolution, diffusion, and the subsequent formation of a semi-IPN. The experiment described in Section 3.2 allows us to visualise this bond.

Optical microscope images of the interfaces between dyed acrylic resin and clear cast coupons of epoxy and PMMA polymers can be found in Fig. 12a and b respectively. There are two visible differences between

the interfaces of epoxy and PMMA with the acrylic resin. Firstly, there is a difference in colour, as in the epoxy there is a well-defined colour boundary with the dyed resin, whereas in the PMMA there is a colour gradient. The dye molecules therefore diffuse into the PMMA as it is dissolved by the acrylic monomeric resin and remain there once the resin polymerises.

Secondly, there is a difference in morphology at the interface. There are ridges at the edges of the polymer coupons caused by grinding, and in the case of epoxy these are again well-defined and unaffected by the acrylic resin, whereas signs of dissolution are evident in the PMMA specimen (Fig. 12b). This is to be expected as epoxies are thermoset polymers, so they do not dissolve in solvents. This experiment therefore provides evidence for the formation of a semi-IPN as the bonding mechanism, which is only applicable when the polymer is soluble in the infused resin.

The low viscosity of the acrylic resin allows significant penetration of the monomer into the polymer; however, the same bonding mechanism may be expected to occur when bonding GF/acrylic with Plexus MA310 due to its MMA content. The similarity in failure mechanisms between the resin welds and the adhesive bonds—light fibre-tearing (Fig. 10)—would support this, although the high viscosity and short working time of the adhesive (approximately 15 min vs. 90 min for the acrylic resin) may limit semi-IPN formation.

4. Conclusions

Welded bonds in acrylic-matrix composites have been shown in the literature to increase static strength and fatigue life over adhesive bonds, but improvements in manufacturing tolerances must be made if they are to be applied to large structures like wind turbine blades. The technique introduced in this work—*resin welding*—has been shown to be a promising joining alternative for acrylic-matrix composites. As with traditional welding methods, resin welding also results in the entanglement of PMMA chains at the bonding interface. However, in resin welding, instead of heating and melting the polymer chains, acrylic monomer resin is infused into a bondline packed with reinforcement fibres. Here, the resin dissolves and diffuses into the acrylic matrix of the adherends, polymerising around the existing polymer and leading to the formation of a semi-IPN, as evidenced by the diffusion of dyed acrylic resin into clear cast PMMA.

The single lap shear strength of resin welded coupons reached a maximum of 27.9 MPa with a 0.5 mm bondline packed with 0° glass fibres, a strength 24 % higher than the highest published value for welded acrylic-matrix composites [5]. Nevertheless, this strength was exceeded by bonds prepared with a methacrylate adhesive, which reached 46.4 MPa with a 0.5 mm bondline. Unlike the resin welded bonds, however, the adhesive strength and stiffness were highly affected by thickness, and the strength dropped by 56 % and the stiffness by 57 % when thickness was increased to 1 mm.

Methacrylate adhesives may therefore be the most appropriate joining method for acrylic-matrix composites when bondlines are thin as they create strong bonds, but their strength quickly drops with increasing thickness. Welding methods like ultrasonic, resistance or induction welding also result in high bond strengths, but they generally require intimate contact between the adherends. As a result, thicker bondlines like those found in wind turbine blades may benefit from resin welding, and further investigation of the method in large structures is therefore warranted with the continuing development of recyclable acrylic-matrix wind turbine blades.

CRediT authorship contribution statement

Machar Devine: Conceptualization, Data curation, Formal analysis, Investigation, Methodology, Project administration, Resources, Visualization, Writing – original draft, Writing – review & editing. **Ankur Bajpai:** Conceptualization, Data curation, Formal analysis, Investigation, Methodology, Project administration, Resources, Visualization, Writing – review & editing. **Conchúr M. Ó Brádaigh:** Funding acquisition, Resources, Supervision, Validation, Writing – review & editing. **Dipa Ray:** Conceptualization, Funding acquisition, Methodology, Project administration, Resources, Supervision, Validation, Visualization, Writing – review & editing.

Declaration of competing interest

The authors declare that they have no known competing financial interests or personal relationships that could have appeared to influence the work reported in this paper.

Data availability

Data will be made available on request.

Acknowledgements

The authors are grateful for funding provided by the Wind and Marine Energy Systems and Structures Centre for Doctoral Training (CDT-WAMSS), to the University of Edinburgh EPSRC IAA for funding received through block grant EP/R511687/1, and to the Supergen ORE Hub for funding received through the Flexible Fund Award FF2021-1014. The authors gratefully acknowledge Arkema GRL, France for the provision of materials towards this research.

References

[1] Obande W, Ó Brádaigh CM, Ray D. Continuous fibre-reinforced thermoplastic acrylic-matrix composites prepared by liquid resin infusion – a review. Compos B Eng 2021:215.
[2] Obande W, Mamalis D, Ray D, Yang L, Ó Brádaigh CM. Mechanical and thermomechanical characterisation of vacuum-infused thermoplastic- and thermoset-based composites. Mater Des 2019:175.
[3] Denis Y, Siddig N, Guitton R, Le Bot P, De Fongalland A, Lecointe D. Thermo-chemical modeling and simulation of glass/elium® acrylic thermoplastic resin composites. Materials Research Proceedings 2023;28:313–20.
[4] Subrahmanian KP, Dubouloz F. Adhesives for bonding wind turbine blades. Reinforc Plast 2009;53(1):26–9.
[5] Murray RE, Roadman J, Beach R. Fusion joining of thermoplastic composite wind turbine blades: lap-shear bond characterization. Renew Energy 2019;140:501–12.
[6] Ageorges C, Ye L, Hou M. Advances in fusion bonding techniques for joining thermoplastic matrix composites: a review. Compos Appl Sci Manuf 2001;32(6):839–57.
[7] Bhudolia SK, Gohel G, Fai LK, Barsotti RJ. Investigation on ultrasonic welding attributes of novel carbon/Elium® composites. Materials 2020;13(5):10–5.
[8] Bhudolia SK, Gohel G, Kantipudi J, Leong KF, Barsotti Jr RJ. Ultrasonic welding of novel carbon/elium((R)) thermoplastic composites with Flat and integrated Energy directors: lap shear characterisation and fractographic investigation. Materials 2020;13(7).
[9] Bhudolia SK, Gohel G, Kah Fai L, Barsotti RJ. Fatigue response of ultrasonically welded carbon/Elium® thermoplastic composites. Mater Lett 2020;264:127362.
[10] Perrin H, Bodaghi M, Berthe V, Vaudemont R. On the addition of multifunctional methacrylate monomers to an acrylic-based infusible resin for the weldability of acrylic-based glass fibre composites. Polymers 2023;15(5).
[11] Zarouchas D, Nijssen R. Mechanical behaviour of thick structural adhesives in wind turbine blades under multi-axial loading. J Adhes Sci Technol 2016;30(13):1413–29.
[12] Bhudolia SK, Gohel G, Leong KF. Advances in ultrasonic welding of thermoplastic composites : a review. 2020.
[13] Benatar A, Cheng Z. Ultrasonic welding of thermoplastics in the far-field. Polym Eng Sci 1989;29(23):1699–704.
[14] Chapter 16 - solvent welding. In: Troughton MJ, editor. Handbook of plastics joining. second ed. Boston: William Andrew Publishing; 2009. p. 139–43.
[15] Lin CB, Lee S, Liu KS. The microstructure of solvent-welding of PMMA. J Adhes 1991;34(1–4):221–40.
[16] RS Pro. Anglosol 12: SDS No. CP1205 v1.11 RS 144-406 2022 [Online]. Available: https://docs.rs-online.com/3a29/0900766b80980339.pdf.
[17] RS Pro. Anglosol 70 Part A: SDS No. CP1187A v1.12 RS 144-399 2022 [Online]. Available: https://docs.rs-online.com/2e2b/0900766b809599ae.pdf.
[18] Khalili SMR, Shokuhfar A, Hoseini SD, Bidkhori M, Khalili S, Mittal RK. Experimental study of the influence of adhesive reinforcement in lap joints for composite structures subjected to mechanical loads. Int J Adhesion Adhes 2008;28(8):436–44.

[19] Delzendehrooy F, Ayatollahi MR, Akhavan-Safar A, da Silva LFM. Strength improvement of adhesively bonded single lap joints with date palm fibers: effect of type, size, treatment method and density of fibers. Compos B Eng 2020:188.
[20] Behera RK, Parida SK, Das RR. Effect of using fibre reinforced epoxy adhesive on the strength of the adhesively bonded Single Lap Joints. Compos B Eng 2023:248.
[21] Tanabe D, Nishiyabu K, Kurashiki T. Electro fusion joining of carbon fiber reinforced thermoplastic composites using carbon fiber heating element. In: 16th European conference on composite materials, ECCM 2014; 2014.
[22] Gleich DM, Van Tooren MJL, Beukers A. Analysis and evaluation of bondline thickness effects on failure load in adhesively bonded structures. J Adhes Sci Technol 2001;15(9):1091–101.
[23] da Silva LFM, Rodrigues TNSS, Figueiredo MAV, de Moura MFSF, Chousal JAG. Effect of adhesive type and thickness on the lap shear strength. J Adhes 2006;82 (11):1091–115.
[24] da Silva LFM. Design rules and methods to improve joint strength. In: da Silva LFM, Öchsner A, Adams RD, editors. Handbook of adhesion technology. Berlin, Heidelberg: Springer Berlin Heidelberg; 2011. p. 689–723.
[25] ITW Performance Polymers. Technical Data Sheet Plexus MA310 Rev 09 2018 [Online]. Available: https://itwperformancepolymers.com/wp-content/uploads/umb/10754/ma310-data-sheet_rev09.pdf.
[26] ITW Performance Polymers. Plexus Adhesive Selector Guide EMEA 2023 [Online]. Available: https://itwperformancepolymers.com/wp-content/uploads/Plexus-Selector-Chart-EMEA.pdf.
[27] Mishnaevsky Jr L. Root causes and mechanisms of failure of wind turbine blades: overview. Materials 2022;15(9).
[28] Redmann A, Damodaran V, Tischer F, Prabhakar P, Osswald TA. Evaluation of single-lap and block shear test methods in adhesively bonded composite joints. Journal of Composites Science 2021;5(1):27.
[29] Srinivasan DV, Ravichandran V, Idapalapati S. Failure analysis of GFRP single lap joints tailored with a combination of tough epoxy and hyperelastic adhesives. Compos B Eng 2020:200.
[30] Noble T, Davidson J, Floreani C, Bajpai A, Moses W, Dooher T, et al. Powder epoxy for one-shot cure, out-of-autoclave applications: lap shear strength and Z-pinning study. Journal of Composites Science 2021;5:225.
[31] da Silva L FM, Adams R D. Techniques to reduce the peel stresses in adhesive joints with composites. Int J Adhesion Adhes 2007;27(3):227–35.
[32] Chapter 17 - adhesive bonding. In: Troughton MJ, editor. Handbook of plastics joining. second ed. Boston: William Andrew Publishing; 2009. p. 145–73.
[33] Gardner DJ. Wood: surface properties and adhesion. In: Buschow KHJ, Cahn RW, Flemings MC, Ilschner B, Kramer EJ, Mahajan S, et al., editors. Encyclopedia of materials: science and technology. Oxford: Elsevier; 2001. p. 9745–8.